

The Development of Calcium Aluminate Phosphate Cement for Radioactive Waste Encapsulation

Paul David Swift

A thesis presented for the degree of Doctor of Philosophy

October 2013

Department of Materials Science and Engineering

Faculty of Engineering

The University of Sheffield

Abstract

Reactive metals such as aluminium metal make up a significant proportion of the UK's legacy radioactive waste. Current treatment methods – encapsulation in PC-based cementitious systems – do not perform optimally when applied to reactive metals. Corrosion of encapsulated aluminium, caused by the availability of free-water and highly alkaline pore solution, results in expansive corrosion products and the generation of significant quantities of hydrogen gas, which compromises the long-term performance of waste packages.

Calcium Aluminate Phosphate cements (CAP), formed from acid-base reaction between Calcium Aluminate Cements (CAC) and an acidic phosphate-based solution, were identified as alternative encapsulants that provide different internal chemistry i.e. pore solution of lower pH which may be advantageous when applied to the encapsulation of reactive metals. Various types of phosphates, monophosphates and polyphosphates, were assessed to identify suitable pre-cursor materials for producing a cementitious matrix when mixed with CAC, and a CAP formulation envelope suitable for the industry-defined processing and operational property requirements, was identified.

The corrosion behaviour of aluminium encapsulated in the CAP system was characterised by a dormant period, during which the corrosion and gas generation rates were very low, and a significant increase after the dormant period. The phase evolution of the CAP system altered not only the physico-mechanical properties of the system in longer-term but was also responsible for the latent corrosion behaviour of aluminium encapsulated in the CAP system.

Acknowledgements

I would like to thank my partner and best friend, Marianne, and my family, especially my mum, Elizabeth, and sisters, Megan and Rebecca, whose support and encouragement has been, at times, essential and always greatly appreciated.

I would like to express my appreciation and thanks to my supervisor Dr Hajime Kinoshita whose advice, support and commitment has been greatly appreciated throughout this project. I would also like to thank Dr Neil Milestone for first suggesting that I undertake this project and his continued support and guidance throughout.

I would also like to express my gratitude to my industrial supervisors, Dr Nick Collier, Dr Martin Hayes and Ed Butcher of the National Nuclear Laboratory for their support and helpful advice and input.

I would like to thank all the members of the Immobilisation Science Laboratory, with special thanks to Dr Claire Utton, Dr Oday Hussein, Dr Claire Corkhill, Dr Martin Stennett, Dr Susan Bernal López and Professor Neil Hyatt. I would also like to thank the technical staff of the Department of Materials Science and Engineering, in particular Andrew Mould, Bev Lane and Ian Watts for their help and support throughout this project.

Finally, I would like to acknowledge the EPSRC and the NDA for funding.

Contents

Abstract.....	i
Acknowledgements.....	ii
Contents	iii
Nomenclature and Acronyms	ix
1. Introduction.....	1
1.1. Nuclear Power in the UK.....	1
1.2. UK Legacy Wastes	1
1.3. Aims and Objectives.....	2
2. Literature Review	3
2.1. Introduction.....	3
2.2. Radioactive Waste in the UK	3
2.3. Radioactive Waste Management	5
2.3.1. Encapsulation and Immobilisation	6
2.3.2. Cementation.....	7
2.4. Cementation of Radioactive Waste	8
2.4.1. Important Cementing System Properties	8
2.4.2. Current Cementing Systems for Radioactive Waste Treatment.....	11
2.4.3. Limitations of Current Cementitious Systems.....	13
2.4.4. Corrosion of Aluminium in Cement.....	14
2.4.5. Alternative Cementitious Systems.....	17
2.5. Calcium Aluminate Cements	18
2.5.1. History	18
2.5.2. Chemical and Phase Composition	19
2.5.3. Hydration and Conversion Reactions	23
2.5.4. Setting Retarders.....	25

2.5.5. Applications in Radioactive Waste Treatment	25
2.6. Chemically Bonded Cements.....	26
2.6.1. Acid-Base Cements.....	26
2.6.2. Chemically Bonded Materials - Cements or Ceramics?	27
2.6.3. Chemically Bonded Phosphate Cements	28
2.6.4. Magnesium Phosphate Cements	29
2.6.5. Calcium Phosphate Cements	31
2.7. Phosphate-modified Calcium Aluminate Cements	32
2.7.1. Introduction.....	32
2.7.2. Development of PMCs.....	33
2.7.3. Hydration Reactions and Reaction Products	34
2.7.4. Physico-mechanical Properties	40
2.7.5. Microstructure and Morphology	41
2.8. Summary	42
3. Experimental.....	44
3.1. Introduction.....	44
3.2. Materials	44
3.2.1. Calcium Aluminate Cement.....	44
3.2.2. Phosphate-based Powders	47
3.2.3. Pulverised Fuel Ash	47
3.2.4. Boric Acid.....	49
3.2.5. Portland Cement	49
3.2.6. Blast Furnace Slag	49
3.2.7. Aluminium	50
3.3. Formulations	50
3.4. Sample Mixing and Curing.....	52

3.4.1. Small-Scale Mixing	52
3.4.2. Large-Scale Mixing	52
3.5. Plant Acceptance Tests	53
3.5.1. Colflow Test	53
3.5.2. Vicat Setting Time	54
3.5.3. Bleed Water Evaluation.....	54
3.6. Physico-mechanical Properties	55
3.6.1. Compressive Strength.....	55
3.6.2. Dimensional Stability	55
3.6.3. Mercury Intrusion Porosimetry	55
3.7. Phase Analysis	56
3.7.1. X-ray Diffraction	56
3.7.2. Thermogravimetric Analysis	59
3.8. Microstructure Analysis.....	59
3.8.1. Scanning Electron Microscopy.....	59
3.8.2. Energy Dispersive X-ray Spectroscopy.....	61
3.9. Hydrogen Generation Measurements	62
3.10. Pore Solution Expression.....	63
3.11. pH measurements.....	64
4. Results - Identification of Suitable Precursor Materials.....	66
4.1. Introduction.....	66
4.2. Formulations	66
4.3. Setting and Physico-mechanical Properties.....	67
4.4. Phase Analysis	70
4.4.1. XRD.....	70
4.4.2. TG.....	73

4.5. Microstructure.....	76
4.6. Discussion.....	79
4.7. Summary.....	83
5. Results – Development of CAP Formulation Envelope	85
5.1. Introduction.....	85
5.2. Formulations	86
5.3. Preliminary Vicat Setting Time Measurements	91
5.4. Effect of Formulation on Plant Acceptance Tests	94
5.4.1. Effect of H ₃ BO ₃ Content.....	94
5.4.2. Effect of Water Content.....	96
5.4.3. Effect of PFA Content	98
5.5. Materials Properties of Selected Formulations	100
5.5.1. Phase Characterisation.....	100
5.5.2. Microstructure.....	106
5.5.3. Physico-mechanical Properties	110
5.5.4. pH.....	114
5.6. Summary.....	116
6. Results – Encapsulation of Aluminium in CAP	118
6.1. Introduction.....	118
6.2. Formulations	118
6.3. Initial Corrosion of Aluminium in Cement Matrices.....	121
6.3.1. Hydrogen Gas Generation up to 28 days	121
6.3.2. Initial pH of Cement Pastes	125
6.4. Corrosion of Aluminium in the Longer-Term	128
6.4.1. Hydrogen Gas Generation up to 175 days	128
6.4.2. Examination of Specimens for BFS/PC System.....	131

6.4.3. Examination of Specimens for PFA/CAC System	134
6.4.4. Examination of Specimens for CAP System	136
6.5. Aluminium-Cement Interface	139
6.5.1. BFS/PC system	139
6.5.2. PFA/CAC system	144
6.5.3. CAP Systems	147
6.6. Corrosion Products	152
6.6.1. Corrosion Product in BFS/PC System	152
6.6.2. Corrosion Product in PFA/CAC System	153
6.6.3. Corrosion Product in CAP Systems.....	154
6.7. Discussion.....	162
6.8. Summary.....	163
7. Results – Characterisation of the CAP System.....	165
7.1. Introduction.....	165
7.2. Formulations	166
7.3. Physico-mechanical Properties	166
7.3.1. Compressive Strength.....	166
7.3.2. Porosity.....	169
7.3.3. Dimensional Stability	175
7.4. Phase Evolution of CAP Systems.....	177
7.5. Phase Evolution of PFA/CAC System	187
7.6. Microstructure of CAP Systems	192
7.7. Elemental Composition of CAP Matrix	199
7.8. Plant Acceptance Tests	205
7.9. Discussion.....	206
7.10. Summary.....	209

8. Conclusions.....	210
8.1. Overview.....	210
8.2. Identification of Suitable Precursor Materials	210
8.3. Development of CAP Formulation Envelope	211
8.4. Encapsulation of Aluminium in CAP	212
8.5. Characterisation of CAP	213
8.6. Summary	214
9. Recommendations for Further Work	216
10. References.....	217
Appendix 1 – XRD Data.....	228
Appendix 2 – TG Data.....	229
Appendix 3 – Supporting SEM and EDX.....	230
Appendix 4 – Relevant Publications.....	256

Nomenclature and Acronyms

Cement Chemistry Nomenclature

C	CaO	Calcium oxide
A	Al ₂ O ₃	Aluminum oxide
S	SiO ₂	Silicon dioxide
F	Fe ₂ O ₃	Iron(III) oxide
f	FeO	Iron(II) oxide
M	MgO	Magnesium oxide
T	TiO ₂	Titanium dioxide
Ŝ	SO ₃	Sulphate
N	Na ₂ O	Disodium oxide
K	K ₂ O	Dipotassium oxide
Ĉ	CO ₂	Carbon dioxide
H	H ₂ O	Water

Anhydrous Cement Phases

CA	CaO·Al ₂ O ₃	
CA ₂	CaO·2Al ₂ O ₃	
C ₂ AS	2CaO·Al ₂ O ₃ ·SiO ₂	Gehlenite
C ₃ A	3CaO·Al ₂ O ₃	
C ₁₂ A ₇	12CaO·7Al ₂ O ₃	
CT	CaO·TiO ₂	Perovskite

Hydration Products

CAH ₁₀	CaO·Al ₂ O ₃ ·10H ₂ O	
C ₂ AH ₈	2CaO·Al ₂ O ₃ ·8H ₂ O	
C ₃ AH ₆	3CaO·Al ₂ O ₃ ·6H ₂ O	
γ-AH ₃	Al(OH) ₃	Gibbsite
α-AH ₃	Al(OH) ₃	Bayerite
C-A-H	CaO·Al ₂ O ₃ ·H ₂ O (undefined stoichiometry)	Amorphous calcium aluminate hydrate
C ₂ ASH ₈	2CaO·Al ₂ O ₃ ·SiO ₂ ·8H ₂ O	Strätlingite, Gehlenite hydrate

Other

Amorphous Calcium Phosphate	ACP	$\text{Ca}_x\text{H}_y(\text{PO}_4)_z \cdot n\text{H}_2\text{O}$
Hydroxyapatite	HAp	$\text{Ca}_5(\text{PO}_4)_3(\text{OH})$ or $\text{Ca}_{10}(\text{PO}_4)_6(\text{OH})_2$
Alumina gel		$\text{Al}_2\text{O}_3 \cdot x\text{H}_2\text{O}$
Sodium LTA zeolite phase	[Na] [Al-Si-O]-LTA)	$([\text{Na}^+_{12}(\text{H}_2\text{O})_{27}]_8 [\text{Al}_{12}\text{Si}_{12}\text{O}_{48}]_8\text{-LTA}$
Quartz		SiO_2
Mullite		$\text{Al}_6\text{Si}_2\text{O}_{13}$
Hematite		Fe_2O_3

Experimental Techniques

BEI	Backscattered Electron Imaging
DTG	Derivative Thermogravimetric Analysis
EDX	Energy Dispersive X-ray spectroscopy
MIP	Mercury Intrusion Porosimetry
SEI	Secondary Electron Imaging
SEM	Scanning Electron Microscopy
TG	Thermogravimetric Analysis
XRD	X-Ray Diffraction

Other Acronyms

ABC	Acid-Base Cements
BFS	Blast Furnace Slag
CAC	Calcium Aluminate Cement
CAP	Calcium Aluminate Phosphate cement
CBC	Chemically Bonded Ceramic
CBPC	Chemically Bonded Phosphate Cement
CoRWM	Committee on Radioactive Waste Management
CPC	Calcium Phosphate Cements
FGMSP	First Generation Magnox Storage Pond
GDF	Geological Repository Facility

GWPS	Generic Waste Package Specification
HLW	High Level Waste
IAEA	International Atomic Energy Agency
ICP-OES	Inductively Coupled Plasma Optical Emission Spectrometry
ILW	Intermediate Level Waste
LLW	Low Level Waste
MPC	Magnesium Phosphate Cements
MSSS	Magnox Swarf Storage Silos
NDA	Nuclear Decommissioning Authority
PC	Ordinary Portland Cement
PFA	Pulverised Fuel Ash
PFCS	Pile Fuel Cladding Silo
PFSP	Pile Fuel Storage Pond
PGRC	Phased Geological Repository Concept
PMC	Phosphate-Modified Calcium aluminate cements
RH	Relative Humidity
RWMD	Radioactive Waste Management Directorate
SCM	Supplementary Cementitious Material
SLPS	Sellafield Legacy Ponds And Silos
WPSGD	Waste Package Specification and Guidance Documentation

1. Introduction

1.1. Nuclear Power in the UK

The nuclear power industry has long been tainted by controversy and as such has experienced stigma. The explosion at Chernobyl's number four reactor on 26th April 1986 was one of the biggest man-made disasters of all time. More recently, the disaster at the Fukushima Daiichi nuclear power plant has caused governments around the world to reconsider the use of nuclear power in their energy mix. There are also concerns associated with radioactive waste and long-term radioactive waste management. Before nuclear power is fully accepted by the general public, the nuclear power industry must demonstrate its ability to manage radioactive waste safely and securely.

1.2. UK Legacy Wastes

In the UK, the development and operation of the nuclear industry has resulted in so-called legacy wastes, the clean-up costs for which have been estimated to be up to £50 billion [1]. Along with other reactive metals such as magnesium and uranium, aluminium arises from the Magnox and other legacy waste streams, which contribute significantly to the UK's Low Level radioactive Waste (LLW) and Intermediate Level radioactive Waste (ILW). According to the 2010 UK Radioactive Waste Inventory [2], 1,200 tonnes and 17,000 tonnes of aluminium was classified as ILW and LLW, respectively. Although the ILW and LLW are usually encapsulated by cementitious matrices, the high internal pH of conventional cementing system along with the availability of free-water causes corrosion of reactive metals such as aluminium. The corrosion reactions of aluminium in cement result in expansive reaction products and the generation of considerable amounts of hydrogen gas, which can be detrimental to the long term durability of the wasteforms [3, 4]. There is

therefore an impetus to develop alternative and novel encapsulants in order to facilitate the conditioning of these problematic legacy wastes and decommissioning of aging facilities.

1.3. Aims and Objectives

The aim of the work presented here is to develop an alternative cementitious system with a lower pH environment, for the encapsulation of aluminium metal. In the first part, candidate materials have been tested to identify the suitable precursor materials. In the second part, the formulation of the cement matrix has been developed to fulfil certain processing and operational properties requirements, as defined by industry, in order to demonstrate it is practicable for application. In the third part, the reaction of the developed formulation with aluminium has been studied, and the fourth part further investigated the long-term phase evolution of the developed system to obtain insight into the reaction with aluminium and the long-term behaviour of the materials.

2. Literature Review

2.1. Introduction

This chapter will explore the relevant literature and give an account of the current state of research on cementation of radioactive waste in the UK, the issues arising from problematic wastes, the development of alternative cementing systems, and the research related to calcium phosphate cements. The aim is to provide a summary of the information and knowledge relevant to this research, as well as giving a critical review of the literature.

2.2. Radioactive Waste in the UK

Radioactive wastes in the UK arise largely from current operational and decommissioning nuclear programmes, with a smaller amount of additional wastes coming from the use of radioactive materials in medical applications, research and military applications. In the UK, these radioactive wastes are organised into the following categories according to its activity level, half-life and the amount of heat it evolves [2]:

- Low-Level Waste (LLW) - Waste that is slightly radioactive and as such cannot be disposed of with normal refuse. It should not exceed 4 Gbq tonne⁻¹ of alpha or 12 Gbq tonne⁻¹ of beta/gamma activity [2]. LLW is produced in the operation and decommissioning of nuclear facilities and currently consists of 66,000 m³ or 76,000 tonne in the UK. A further 4,360,000 m³ or 4,600,000 tonne of LLW is expected to arise as a result of current and future operational and decommissioning programmes [2].
- Intermediate-Level Waste (ILW) - Waste that exceeds the upper limit of LLW in terms of activity but does not require heat evolution to be taken into

account in the design of storage or disposal facilities. ILW arises from reactor operation, waste or components from the decommissioning of nuclear facilities, and spent fuel reprocessing. There are also ILW waste streams from the use of radioactive material in medical applications, research and military applications. There is 94,300 m³ or 110,000 tonne of ILW currently being stored in the UK [2]. It is expected that a further 192,000 m³ or 190,000 tonne of ILW will arise from current and future operational and decommissioning programmes. The proposed long-term management strategy for ILW involves geological disposal [5].

- High-Level Waste (HLW) - HLW is highly radioactive and as a result evolves considerable heat, which must be considered in the design of storage and disposal facilities. HLW is generated by the reprocessing of spent nuclear fuel and at present constitutes 1,620 m³ or 3,300 tonne of the nuclear waste currently being stored in the UK [2]. The volume of HLW is expected to fall due to the foreseen vitrification of liquid HLW. In 2006 the independent Committee on Radioactive Waste Management (CoRWM) recommended that geological disposal, preceded by safe and secure storage was the best option for the management of HLW [5].

As well as waste which arises from current and future operational and decommissioning programmes, there remains a considerable amount of legacy waste, which is often poorly characterised and stored in less than desirable conditions. Legacy wastes are derived from historical civil and military nuclear operations and have been stored for up to 50 years in aging facilities such as the Sellafield Pile Fuel Storage Pond (PFSP), First Generation Magnox Storage Pond (FGMSP), Magnox

Swarf Storage Silos (MSSS), Pile Fuel Cladding Silo (PFCS); collectively known as the Sellafield Legacy Ponds and Silos (SLPS). These facilities were not originally designed or commissioned for the long-term storage of radioactive wastes. However, various factors i.e. industrial accidents, unexpected downstream plant shutdowns, plant operator industrial action etc., necessitated their use as long-term storage facilities for a range of waste items and materials. These wastes include a variety of reactive metals (aluminium, Magnox, uranium) in the form of fuels, fuel element cladding, reactor components and miscellaneous operational wastes. Over the past 50 years the plant conditions have deteriorated significantly. Management of this legacy waste remains a major concern for the UK's nuclear industry [4, 6]. The risk posed by the SLPS has been defined as 'intolerable' and as such the decommissioning of the SLPS has been identified as a priority of the Nuclear Decommissioning Authority's (NDA) strategy [7].

2.3. Radioactive Waste Management

In the UK, the current preferred strategy for long-term management of ILW, and certain LLW, is for consignment to a Geological Repository Facility (GDF) based on the Phased Geological Repository Concept (PGRC). The Radioactive Waste Management Directorate (RWMD) of the NDA is ultimately responsible for the delivery of the GDF. Therefore, as the ultimate receiver of wastes, the RWMD has developed a suite of waste packaging standards and specifications to enable waste package producers to condition ILW into a form that is compatible with the PGRC. Various standards, specifications and performance criteria are presented in Generic Waste Package Specification (GWPS) and Waste Package Specification and Guidance Documentation (WPSGD) [8, 9]. The GWPS stipulates that waste packages should behave in a predictable manner during normal and unexpected

conditions. This is achieved by making them passively safe by encapsulation and immobilisation within an appropriate wastefrom matrix. The ‘passive safety’ is defined in the document as *‘the waste is chemically and physically stable, and is stored in containment and a manner that minimises the need for safety mechanisms maintenance, monitoring and human intervention, and that facilitates retrieval for final disposal.’*

2.3.1. Encapsulation and Immobilisation

The principle aim of radioactive waste management is to mitigate the potential risk from radioactive waste; thereby protecting both human health and the environment [1]. This can be achieved by a process known as immobilisation. The International Atomic Energy Agency (IAEA) defines immobilisation as *‘Conversion of waste into a waste form by solidification, embedding or encapsulation. The aim is to reduce the potential for migration or dispersion of radionuclides during handling, transport, storage and/or disposal.’* [10]. Immobilisation is widely considered to occur through both chemical and physical mechanisms [11-14]; distinguishing between chemical and physical mechanisms is difficult as they occur contiguously. An appropriate distinction would be on the basis of scale; chemical mechanisms occurring on the atomic scale, and physical occurring on the micro scale and above [11]. Chemical mechanisms render radionuclides insoluble, or incorporate them into the structure of a matrix. Encapsulation can be thought of as the physical aspect of immobilisation, and is the process of surrounding the waste within a matrix, thus rendering potentially hazardous radionuclides immobile.

In the UK, the majority of radioactive waste which currently arises from the operation of nuclear power stations and reprocessing facilities is treated by either

vitrification or cementation. Each immobilisation technology is waste dependent, and should ensure that the wasteform can be handled, transported, stored and finally disposed of safely. They should also reduce the potential release of radionuclides into the environment. Waste packages must maintain integrity during all phases of their management, which include interim storage, transport, emplacement, and repository operations.

2.3.2. Cementation

Cement is used in many applications within radioactive waste management; as an encapsulation matrix, but also as a structural material for storage and disposal facilities. Cementation has been accepted as the most suitable technology for the immobilisation of LLW and ILW in the UK [3, 4, 6, 11-21]. Cement has many attributes which have made it the matrix of choice for the immobilisation of LLW and ILW [3, 4, 19, 22-24]:

- High pH renders many radionuclides insoluble, precipitating them out of solution;
- High surface area of hydrates allows sorption;
- Ability to incorporate waste species into cement structure;
- Good long-term durability, both chemically and physically;
- Good mechanical properties;
- Act as a diffusion barrier;
- Low liquid and gas permeability;
- Provide radiation shielding;
- Fluid nature of cement grouts is advantageous in penetrating wastes with complex shapes;

- Ability to tailor formulations for specific wastes;
- Relatively cheap and readily available;
- Relatively simple processing, ease of preparation and possibility of use in remote operations;
- The material and associated technologies are well known.

2.4. Cementation of Radioactive Waste

2.4.1. Important Cementing System Properties

The research and development of cement has been driven by its use in civil engineering applications. Decades of experience have resulted in optimisation of cement properties, which have significant relevance to engineering applications. These properties are as follows [14, 25, 26]:

- Initial set time: Setting is the term denoting a sudden loss in plasticity, and conversion to a solid material without the development of significant strength. The initial set is the period of fluidity, where the rheology of the fresh cement paste is such that it can be worked and placed.
- Final set and strength development: This can be thought of as hardening of the cement paste, and the associated strength development.
- Ultimate strength and dimensional stability: ‘Strength’ is assumed to mean compressive strength. Strength development should continue to increase beyond 28 days. Strength regression should not occur, and the hydrates formed should exhibit dimensional stability.

As discussed previously, a suitable matrix for radioactive wastes should have both chemical and physical potential for immobilisation, and the properties above are also applicable to cement formulations for radioactive waste encapsulation and

immobilisation applications. For the wasteform matrix, additional optimisation and control of cement properties should also be considered [5, 6, 14]:

- Good mix fluidity: The fresh cement paste must be able to penetrate complex shapes, which may occur in drums filled with mixed solid wastes, to avoid void formation.
- Setting time: The initial setting time should be such that mixing and placement programmes can be completed before the system sets; industry has defined a requirement of initial setting time > 4 h. The final setting time should be such as to facilitate the throughput operations of the encapsulation plant, allowing movement and transportation of cemented waste packages after 24 h, hence a final setting time requirement of < 24 h.
- Low heat of hydration or low rate of heat evolution: Large cement-based monoliths will have a large heat of hydration, which may alter the mineralogy and microstructure of the cement. Excessive heat evolution can cause evaporation of mix water and thermal expansion, resulting in internal stresses and potential formation of cracks, which may compromise the integrity of the resulting wasteform.
- Control organic content: Organics and their reaction products can facilitate solubilisation of radionuclides.
- Tolerance to unusual environments: Cementing systems should be resistant to radiation-induced degradation.

Cementing systems used as encapsulating and immobilisation matrices for LLW and ILW in the UK are required to fulfil certain processing and property criteria, which have been referred to as plant acceptance tests [27, 28]. These are defined to demonstrate the suitability of the cementitious system for industrial application. These plant acceptance tests include assessment of setting time, grout fluidity, heat generated during hydration, and the amount of bleed water. The criteria for each of these tests are as follows:

- Flow > 200 mm after 150 min;
- Initial setting time > 4 h;
- Final setting time < 24 h;
- Heat of hydration < 180 kJ kg⁻¹ after 24 h;
- Bleed water < 2 % by volume.

The plant acceptance tests do not specify criteria for mechanical and physical properties of the hardened cement pastes. According to the GWPS [8, 9], potential wasteforms should ‘...provide sufficient mechanical strength to allow the waste package to be transported and handled without compromising the ability of the waste package to meet any aspect of this specification’. This is somewhat vague, but the lack of well-defined criteria is due to the fact that, in practice the physical and mechanical properties of the wasteform itself are to some extent irrelevant due to the composite nature of the overall waste package [9, 29]; the majority of the waste package ‘strength’ will come from the waste container. Also, the mechanical and physical properties of the wasteform will be a function of the particular waste which is being conditioned, the waste loading and the orientation of waste components within the wasteform. As a generic guide, the UK nuclear industry uses compressive strength of 7 MPa after 90 days curing as the minimum value for the hardened cementitious wasteforms [27, 28, 30]. NDA suggests that a compressive strength between 4 MPa and 40 MPa¹ should be sufficient to ensure waste package performance under accident conditions in the WPSGD [29].

¹ It should be noted that the WPSGD does not specify an age at which the wasteform should have developed such compressive strength.

Cementing systems for radioactive waste immobilisation are required to have a relatively high fluidity to allow successful processing in the encapsulation plant and full penetration of complex waste shapes which arise from a variety of waste streams. In order to achieve high fluidity, an excess of water is used in the composite cement formulations a proportion of which remains unreacted, existing as ‘free-water’ within the pores of the hardened cementitious matrix [19]. This free-water is then available to facilitate the corrosion of encapsulated metals. In cementitious materials, there is a relationship between the water:cement ratio (w/c) and the porosity of the resulting hardened cementitious matrix; porosity, and subsequently permeability, increases with increasing w/c [11, 25]. Therefore, when cementitious systems are designed for the encapsulation of reactive metals there is a compromise between achieving suitable fluidity and limiting free-water and controlling porosity and permeability.

2.4.2. Current Cementing Systems for Radioactive Waste Treatment

Current cementation systems for the treatment of ILW are composite cements based on Portland cement (PC). PC and its hydration reactions have been covered extensively in the literature [25, 26, 31]. When mixed with water, PC undergoes reactions which cause the cement to set and harden. These reactions and reaction products are known as hydration reactions and hydrates, respectively, and are responsible for setting and strength development. The principle hydration products for PC-based cementing systems are poorly crystalline calcium silicate hydrate (C-S-H) and calcium hydroxide ($\text{Ca}(\text{OH})_2$).

Hardened cement pastes are actually porous materials with a complex and continuous pore structure [25], which contains a highly alkaline solution, known as the pore solution. The pore solution can be considered to be an alkali hydroxide solution

which contains sodium, potassium, and hydroxide ions with trace amount of calcium, sulphate and silica ions [32]. This high alkalinity (*ca.* pH 13.5 [4]) is advantageous in limiting the solubility of many radionuclides; rendering them immobile.

Composite cements have been developed where Supplementary Cementitious Materials (SCMs), such as Blast Furnace Slag (BFS) and Pulverised Fuel Ash (PFA, or 'fly ash'), are used in large proportions; up to 95% and 80% for BFS and PFA composite systems, respectively [15]. BFS is an industrial by-product from the production of iron and is the most common material used in composite cements for radioactive waste immobilisation. PFA is used to a lesser extent, mainly in the cement formulations for capping grout or where high fluidity is required. These SCMs reduce the rate of hydration and so lower the heat of hydration, thus negating any detrimental thermally induced issues. The hydration reactions of PC are exothermic and evolve significant amounts of heat; known as the heat of hydration. For pure PC, the heat of hydration is typically *ca.* 230 kJ kg⁻¹, which can lead to temperatures in excess of 100 °C in the centre of a 500 L drum [4]. Such temperatures would lead to the evaporation of mix water, and thermally induced stress which could lead to cracking of the wasteform. Such events would compromise the integrity and long-term durability of the wasteform, and may facilitate the release of radionuclides.

There are other advantages to using SCMs in cement formulations; they participate in hydration reactions, thus contributing to the overall strength of the cementing systems; they result in improved microstructural properties, with reduced porosity and permeability [15, 32]; they improve the immobilisation capabilities by increasing the proportion of fine pores and increasing resistance to chemical attack [19, 33];

BFS and PFA are by-products from industrial processes, so they are cheap and their use has environmental advantages, as they would otherwise require disposal. The pH of composite cementing systems, typically *ca.* pH 12.0-12.5 [4], is lower than that of pure PC, but remains high enough to still render many radionuclides insoluble.

2.4.3. Limitations of Current Cementitious Systems

It has been recognised that current immobilisation technologies are not suitable for some radioactive wastes. The high pH and availability of free-water in current composite cementing systems raises issues of compatibility with some legacy LLW and ILW [3-6, 34]. Reactive metals such as aluminium, magnesium and uranium corrode in current composite cementing systems used to immobilise radioactive wastes in the UK. These reactive metals arise from the Magnox and other legacy waste streams, and make up a significant proportion of the UK's legacy radioactive waste [2].

The issues arising from the corrosion of aluminium, magnesium, uranium, and other metals such as lead, in current composite cementing systems, has been summarised by the NDA [5]. The corrosion of reactive metals results in volumetric changes and the generation of significant amounts of hydrogen gas [5]. The formation of expansive reaction products causes internal stresses within the monoliths, which may cause cracking of the cementitious matrix and deformation of the wasteform, and eventual failure of the waste package [35]. The generation of hydrogen gas can cause pressurisation of drums and poses a real risk of fire, or even the possibility of an explosion.

Aluminium metal makes up a significant proportion of the UK's legacy LLW and ILW. According to the 2010 UK Radioactive Waste Inventory [2], 1,200 tonnes and

17,000 tonnes of aluminium was classified as ILW and LLW, respectively. Aluminium metal was used as a cladding material and for components of various types of fuel element designs, including the cladding and other components of the fuel rod assemblages for Magnox nuclear power reactors. Aluminium was used as a cladding material for isotope cartridges used to produce various radioactive isotope sources in the Windscale Piles. Aluminium is also present in a variety of operational wastes such as High-Efficiency Particulate Air (HEPA) filters, which have high surface areas.

During the reprocessing of spent nuclear fuel, the cladding and other components were stripped and then stored in dry silos at Sellafield. The majority of metallic aluminium wastes remain in dry storage, although a small amount is stored in wet storage. At present, there is no strategy for the treatment of metallic aluminium wastes [36].

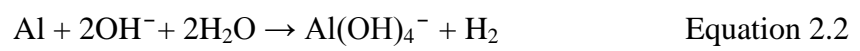
2.4.4. Corrosion of Aluminium in Cement

Studies related to the corrosion of aluminium in cement in the open literature are limited, although the subject has received much attention from the nuclear industry.

Aluminium is a reactive metal which, at ambient temperatures, will react in air to form an oxide surface layer. The oxide layer is very thin, *ca.* 0.01 μm , but is sufficient to act as a protective layer, preventing further corrosion [37]. The nature and thickness of this layer depends on the conditions under which it forms. For example, at elevated temperature (*ca.* 600 $^{\circ}\text{C}$) the oxide layer can be as thick as 0.1-1 μm . According to the Pourbaix diagram for aluminium in water at 25 $^{\circ}\text{C}$, aluminium is passive in the range pH 4-8.5 [38]. In this pH region, the oxide layer is stable and acts as a protective layer, preventing further corrosion. However, it should

be noted that the Pourbaix diagram does not consider the kinetics of the reactions, as it is based purely on thermodynamics. As such, aluminium could be considered to be passive at $\text{pH} > 8.5$ depending on the conditions [39].

In alkaline solutions, with $\text{pH} > 8.5$, the oxide layer undergoes dissolution to form hydroxy-aluminate ($\text{Al}(\text{OH})_4^-$) ions and expose the aluminium surface layer (Equation 2.1) [40]. The exposed aluminium surface undergoes further attack by hydroxyl ions to form more hydroxy-aluminate ions and hydrogen gas (Equation 2.2). The hydroxy-aluminate ions precipitate to form aluminium hydroxide, the nature of which is pH dependent; bayerite ($\alpha\text{-Al}(\text{OH})_3$) forms initially, then as pH increases, gibbsite ($\gamma\text{-Al}(\text{OH})_3$) is more likely to form.



The pore solution of PC is considered to be a highly alkaline solution; therefore the corrosion of aluminium in PC is analogous to that in alkaline solutions. The corrosion of aluminium in PC has been described by the following mechanism (Figure 2.1) [3, 40]:

1. Firstly, hydroxide ions attack the oxide layer producing hydroxy-aluminate ions and exposing the aluminium surface. The aluminium surface is then attacked by more hydroxide ions to produce yet more hydroxy-aluminate ions and hydrogen gas. The release of hydrogen from the initial corrosion causes a porous layer to form at the metal/cement interface, which allows the migration of soluble aluminium species.
2. The second stage of the mechanism involves these aluminium species interacting with hydrates from the silicate phases of the cement and producing Strätlingite (C_2ASH_8). It should be noted that the corrosion of aluminium does not affect the overall hydration of the bulk cement.

3. The final stage of the mechanism happens, as the diffusion rate of ions and water in the cement decreases, due to the cement hardening. As the concentration of hydroxide ions diminishes in the area surrounding the aluminium, the remaining hydroxy-aluminate ions decompose, liberating OH^- ions for further corrosion. Aluminium hydroxide precipitates around the aluminium surface, in the form of bayerite. Over time, bayerite converts to the more stable gibbsite phase.

Setiadi *et al.* [3] and Setiadi [40] reported that the use of high replacements levels of BFS and PFA resulted in cement with a pore solution *ca.* pH 12-12.5 and reduced aluminium corrosion compared to pure PC. However, reduction in pH was not sufficient to arrest corrosion completely. Results from studies on 9:1 BFS:PC composite cementing systems suggested that the mechanism of aluminium corrosion is very similar to that found in pure PC systems; aluminium corrodes and forms the porous structure at the cement-metal interface. Corrosion products, which grow into this porous interfacial zone, formed from the interaction of aluminium species and the calcium silicate hydrates. This was observed as a white corrosion layer between the bulk cement and the metal. This layer grows with time and has been observed to reach a thickness of 1-2mm after 28 days hydration.

Corrosion of aluminium is highly dependent not only on the pH of the environment but also the purity of the aluminium [41]. Impurities provide sites where pitting corrosion can initiate, thus impure aluminium (Al grade 1050, 99.5% Al) corrodes at a much higher rate than a high purity aluminium (99.999% Al) [3]. The development of the corrosion layer observed by Setiadi *et al.* [3, 40] was also dependent on the purity of the aluminium, as well as the composition of the cement system and the curing temperature.

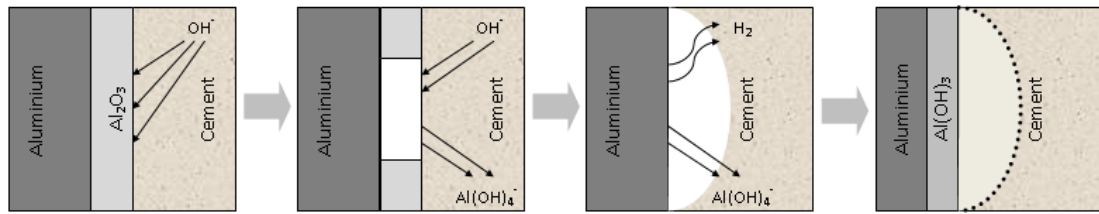


Figure 2.1 Schematic of the mechanism of aluminium corrosion in cement, adapted from [3, 40]

2.4.5. Alternative Cementitious Systems

As discussed previously, due to the incompatibility of some wastes with current cementing systems, it is necessary to develop alternative immobilisation technologies [5]. It has been suggested that alternative cementing systems, where the pore solution pH is lower than that of conventional PC-based cementing systems, may be advantageous for the encapsulation of reactive metals, such as aluminium [4, 6]. Also, because free-water plays a significant role in facilitating the corrosion of reactive metals in cementitious matrices, alternative cementing systems which limit the availability of free-water may be beneficial in reducing the corrosion of reactive metals [19, 34]. Several cementing systems have been identified for potential use as alternatives to PC-based cementing systems for the encapsulation of problematic reactive metals:

- Calcium aluminate cement [4, 42, 43];
- Calcium sulfoaluminate cement [4, 6, 44-46];
- Alkali-activated binders [4, 47-49];
- Sulphate activated composite cement [21, 50-52];
- Magnesium silicate hydrate [53];
- Acid-base cements [4];
- Chemically bonded phosphate materials [54, 55];
 - Magnesium phosphate cement [27, 30, 34, 44, 55-58];
 - Calcium phosphate cement [4, 27, 28, 59].

Literature related to these alternative cementing systems remains limited, especially that related to the application of these systems to radioactive waste immobilisation. This is especially apparent when compared to the amount of literature related to PC-based cementing systems for radioactive waste immobilisation. In general, the use of these alternative cementing systems has been limited to niche applications, where PC is not suitable; e.g. in highly acidic environments, in the presence of high sulphate concentrations, in high temperature applications, or where rapid-hardening is required [60].

2.5. Calcium Aluminate Cements

2.5.1. History

The history, manufacture, properties, applications and hydration mechanisms of calcium aluminate cements are discussed in detail by Robson [61, 62], Bensted [63], Taylor [64] and Scrivener [65]. Calcium Aluminate Cements (CACs) are characterised by a high alumina content; calcium aluminate phases are the principle reactive phases, rather than calcium silicates, as is the case in PC-based cementing systems.

The first documented examples of CACs originated in France in the mid-19th century under the observations of Ebelman and Saint-Claire Deville [61, 65-68]. Their experiments were the first to produce calcium aluminate species, by heating a mixture of alumina and lime or marble. Further work conducted in France and Germany studied the reactions of calcium aluminate species with water [68]. Though there was now awareness of calcium aluminate phases and their cementitious properties, there was little further work done until the turn of the 20th century. The corrosion of concrete on the Paris, Lyon & Mediterranean Railway and elsewhere in seawater defences initiated research on corrosion resistant cements [61]. ‘High-

alumina cement' (HAC) was the name given to the cement, patented by Bied in France [69] and the UK [70], developed as a sulphate resistant cementing system [63]. Bied fused a mixture of limestone and bauxite at high temperatures in the presence of coke, and ground the resulting clinker to a fine powder. The resulting cement exhibited sulphate resistance, as well as rapid hardening compared to PC.

Though the terms HAC and CAC can be used interchangeably, the latter is more commonly accepted as the collective term for cement with high alumina content; where calcium aluminate phases dominate the chemistry of the cement systems [4, 63, 65]. Therefore, these systems will be referred to as CACs throughout this work.

2.5.2. Chemical and Phase Composition

Table 2.1 gives the chemical composition of several CAC grades, with varying alumina content ranging from *ca.* 35 % to over 80 %. 'Standard' CAC is dark grey or black, with alumina content *ca.* 35-40 %, and can be used over a broad temperature range [63, 65]. Other constituents include oxides of calcium, iron, silicon, titanium, magnesium, sodium and potassium. Higher alumina grades, sometimes referred to as 'white' CACs, have alumina content *ca.* 50-80 % and are used for refractory purposes at high temperatures [63, 65]. These cements contain *ca.* 20 % CaO, with trace amount of other metals oxides.

Table 2.2 gives typical phase compositions for a range of CACs. The main hydraulic phase in all CACs is monocalcium aluminate (CA) [61, 65]. Occurring in varying amounts from 40 % upwards, CA reacts rapidly with water and is responsible for strength development in CACs. Secondary phases, such as calcium dialuminate (CA₂), dodecacalcium heptaaluminate (C₁₂A₇), gehlenite (C₂AS), dicalcium silicate

(belite, C_2S), ferrite solid solution (C_4AF) and/or perovskite (CT), may also be present [65].

The exact phase composition of any given CAC depends on its chemical composition, but is also highly dependent on the method of manufacture [65]. White CACs essentially exists in the $CaO-Al_2O_3$ binary system, which makes determining their phase composition relatively simple. Understanding the phase compositions of standard CACs is made more complex by the presence of relatively high amounts of iron oxides and silica. Silica usually exists as C_2S or C_2AS [61, 65]. It is the potential formation of C_2AS which necessitates the need to keep the silica content low; alumina, which would otherwise form CA combines to form C_2AS . Pure C_2AS has no hydraulic properties, but the phase present in CACs exists as a solid solution with a relatively high proportion of alumina and low silica content, resulting in this phase exhibiting some hydraulic properties [61, 63, 65]. The majority of iron oxides exist as ferrite solid solution, often given as C_4AF . However, the A/F ratio is highly variable and, coupled with the incorporation of TiO_2 , SiO_2 and MgO , the exact composition of this phase varies between cements and even from grain to grain within the same cement [65].

Table 2.1 Typical composition of various CACs, adapted from [65]

Grade	Colour	Chemical Composition (wt%)							
		Al ₂ O ₃	CaO	SiO ₂	Fe ₂ O ₃	TiO ₂	MgO	Na ₂ O	K ₂ O
'Standard' low alumina	Grey or buff to black	36-42	36-42	3-8	12-20	< 2	~ 1	~ 0.1	~ 0.15
Low alumina, low iron	Light buff or grey to white	48-60	36-42	3-8	1-3	< 2	~ 0.1	~ 0.1	~ 0.05
Medium alumina	White	65-75	25-35	< 0.5	< 0.5	< 0.05	~ 0.1	< 0.3	~ 0.05
High Alumina	White	≥ 80	< 20	< 0.2	< 0.2	< 0.05	< 0.1	< 0.2	~ 0.05

Table 2.2 Typical phase composition of various CACs [71]

Grade	Example	Typical phase composition	
		Major phase(s)	Minor phase(s)
'Standard' low alumina	Ciment Fondu	CA	$C_{12}A_7$, C_2S , C_2AS , C_4AF
Low alumina, low iron	Secar 51	CA	$C_{12}A_7$, C_2AS , CT
Medium alumina	Secar 71	CA, CA_2	$C_{12}A_7$, α -A
High Alumina	Secar 80	CA, CA_2 , α -A	$C_{12}A_7$

2.5.3. Hydration and Conversion Reactions

When mixed with water, CAC undergoes congruent dissolution of anhydrous hydraulic phases, followed by precipitation of hydrates [63, 65]. At temperatures above *ca.* 5 °C, C₃AH₆ and AH₃ (gibbsite) are the thermodynamically stable hydrate phases. However, other metastable phases - CAH₁₀, C₂AH₈ and amorphous hydrate phases - usually form as precursor phases, which undergo further reactions to form the stable CAC hydrate phases, C₃AH₆ and gibbsite.

The overall hydration of CACs is largely influenced by that of CA, as CA is the principle hydraulic phase in CACs [65, 72-75]. The formation of hydrates during CAC hydration is temperature dependant [63, 65, 76, 77]. At low temperatures below *ca.* 10-15 °C, the formation of CAH₁₀ dominates [63, 65]. Above *ca.* 10-15 °C, C₂AH₈ is formed simultaneously with CAH₁₀. The C₂AH₈ forms concurrently with amorphous alumina gel (Al₂O₃·xH₂O), which over time crystallises to form gibbsite. Above about 25-27 °C, CAH₁₀ no longer precipitates and instead, the stable phase C₃AH₆ forms directly. Above *ca.* 50 °C, C₃AH₆ is the only CA-hydrate phase to form. The hydration of CA can generally progress by the following mechanisms (Equations 2.3-2.5) [65];



The mechanisms by which the metastable hydrates can form stable hydrates is known as ‘conversion’, shown in Equations 2.6-2.8 [63, 65, 75, 77]. Conversion is dependent on age, temperature, moisture state and the original w/c [65, 75, 76]. The

metastable CAH_{10} and C_2AH_8 provide the early strength of the system by precipitating into space previously occupied by water. They have a hexagonal structure, low densities and a high proportion of combined water. The conversion of the metastable phases to the thermodynamically stable cubic C_3AH_6 phase is accompanied by a decrease in the solid volume and release of water. This results in an increase in porosity and subsequent loss in strength. Therefore, the long-term strength of CAC is determined by the formation of the stable phases C_3AH_6 and gibbsite [60, 65].



The detrimental effects of conversion can be limited by controlling the initial w/c; by keeping the initial w/c low, water released by conversion is available to react with residual anhydrous CAC particles [65]. To ensure good long-term strength and durability, a w/c < 0.4 is recommended [65]. The use of silica rich SCMs, such as BFS and Silica Fume (SF), has also been shown to limit conversion; by preferential formation of Strätlingite (C_2ASH_8) instead of C_3AH_6 [65, 74, 78-81].

Most of the available literature reports the formation of the crystalline hydrate phases, CAH_{10} , C_2AH_8 , C_3AH_6 and gibbsite, during CAC hydration [65, 75, 82]. However, some of the literature also describes the formation of amorphous phases [72, 83]. These amorphous phases have generally been reported as being amorphous alumina gel phases, though they are not well characterised [61, 63]. Some researchers have suggested that the amorphous materials which form during the early stages of

CAC hydration is a calcium aluminate hydrate (C-A-H) phase [72, 83, 84]. Bushnell-Watson and Sharp suggested based on the chemical balance that amorphous C-A-H must have formed because $\text{Ca}(\text{OH})_2$ or calcium rich aluminate hydrates had not been observed. Edmonds and Majumdar, in a study on the hydration CA at different temperatures [72], discussed the formation of an amorphous calcium aluminate hydrate gel phase, which formed at early stages, and over time crystallised to form CAH_{10} . Majumdar *et al.* [85] also discussed the formation of amorphous calcium aluminate hydrate as the initial hydration product, which may persist for extended periods of time. This amorphous calcium aluminate hydrate was also present in CAC-blended systems which include BFS as SCMs [74, 85].

2.5.4. Setting Retarders

As with PC-based systems, the use of additives with CACs is conventional in order to modify particular properties such as setting time. For example, boric and citric acid are known to act as setting retarders in various cement systems, including CAC-based cementing systems [65, 86-88].

Boric acid undergoes hydrolysis to form BO_2^- ions, which, in the case of CAC systems, react preferentially with Ca^{2+} ions, liberated from CAC particles, to form amorphous $\text{Ca}(\text{BO}_2)_2 \cdot n\text{H}_2\text{O}$ [86]. This calcium borate gel effectively forms a barrier layer surrounding the CAC particles [88], which decreases the dissolution rate of the cement particles and inhibits hydration. Over time, the barrier layer is broken down by Ca^{2+} and Al^{3+} ions, thus allowing normal hydration to proceed [86].

2.5.5. Applications in Radioactive Waste Treatment

Some work has investigated the potential use of CACs for the immobilisation of radioactive waste. Fryda *et al.* [89] studied the use of a mix of CAC and SF to

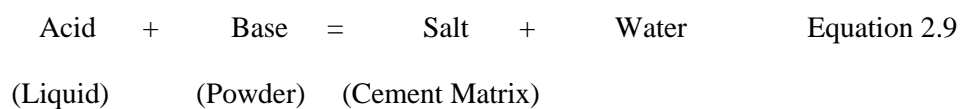
immobilise caesium. The caesium was immobilised by the formation of a caesium bearing zeolitic phase. The phase was found to be thermally stable up to temperatures of *ca.* 750 °C. However, CACs are generally considered unsuitable for radioactive waste immobilisation due to the conversion of metastable phases to stable phases, and the subsequent changes in solid volume, porosity, permeability, and strength [4, 43, 65]. Also, the hydration of CAC, like that of PC, generates significant amounts of heat. Therefore, the use of SCMs would be essential to avoid thermally induced issues when used in large volumes.

The hydration of CAC does not precipitate $\text{Ca}(\text{OH})_2$, and CACs have a low alkali content, which results in cementitious matrices pore solutions with lower pH compared to PC-based cementing systems [4]. This relatively low pore solution pH may be advantageous in immobilisation of certain types of radioactive waste, for instance by limiting the corrosion of reactive metals such as aluminium.

2.6. Chemically Bonded Cements

2.6.1. Acid-Base Cements

Acid-Base Cements (ABCs) are formed at ambient temperature, by reaction of an acidic liquid with a base, usually a cation-leachable powder (Equation 2.9) [90, 91].



The reaction precipitates a salt, which acts as a binding phase between partially- and un-reacted powder particles, resulting in a cementitious matrix [92]. Wilson [90, 93] suggested that the formation of acid-base cement involves the initial rapid acid-base reactions followed by longer-term hydration of the reactions products.

2.6.2. Chemically Bonded Materials - Cements or Ceramics?

The distinction between cements and ceramics can be thought of as being one of production routes [94]; cements are generally produced by mixing a hydraulic powder with water at room temperature, whereas ceramics are produced by the compaction, and subsequent fusion of powders by high temperature heat treatment. The distinction may also consider the bonding mechanisms within the materials, which are responsible for connecting neighbouring particles and result in strength. Cements are generally a mixture of crystalline and amorphous phases bonded by relatively weak van der Waals forces and hydrogen bonding, whereas ceramics are highly crystalline materials formed by strong ionic or covalent bonds [95]. However, several systems developed in the last few decades defy or overlap these distinctions. These systems include [94, 95]:

- Refractory cements;
- Warm-pressed cements;
- FUETAP (Formed Under Elevated Temperature and Pressure) cements;
- Macro-defect-free cements;
- Geopolymers;
- Acid-base cements.

Roy, D. M. [95] discussed some of these systems, which were collectively termed ‘Chemically Bonded Ceramics’ (CBCs), in a review on ‘new strong cement materials’. The bonding which is responsible for the consolidation and strength of these materials was described as a mixture of ionic, covalent, and van der Waals bonding [95]. They exhibit properties somewhere between those of cements and ceramics, despite being formed at low temperatures.

The term CBC was first coined by Roy, R. [96], to describe ‘polycrystalline inorganic bodies or monoliths that are bonded or held together without the use of thermally activated solid-state diffusion’. This definition is more general than that given by Roy, D. M., and encompasses PC and other conventional cements and concretes. Wagh [94] reiterated that CBCs include ‘all inorganic materials that are consolidated into a hard mass by chemical reactions and not by sintering’. The use of the term ‘CBC’ is, in their case, somewhat serendipitous as it negates the semantic issues of whether such materials are ceramics or cements as the ‘C’ can represent either. In practice, this ambiguity is appropriate because these materials incorporate properties of both cements and ceramics.

2.6.3. Chemically Bonded Phosphate Cements

Wagh gives a detailed account of many aspects of Chemically Bonded Phosphate Cements (CBPCs) [54]. CBPCs are a type of acid-base cement [94]; they are phosphate-based CBCs that are formed at ambient temperatures, and have potential for a wide range of applications [96]. CBPCs, specifically zinc phosphate cements, were first developed for dentistry applications in the late 19th century [90, 97]. Subsequently, other phosphate systems, including aluminium, iron, and copper phosphate, were investigated, though found not to be suitable for any particular application.

Kingery [98] reviewed the state of phosphate-bonded materials in 1950; stating that phosphate-bonded materials have been recognised for a long time, and patent literature suggested these materials had become well established although information in general literature was limited. Kingery conducted a systematic study [99] of cold-setting phosphate-bonded materials, synthesised by reaction between

metal oxides and phosphoric acid, and reported the effect of temperature on bond strength and bond structure. The cold-setting phosphate-bonded materials form through the development of mono- and di-basic phosphates. These phosphates were inherently adhesive due to hydrogen bonding, which resulted in a strong structure as well as extended chemical bonding between contiguous crystallites. Kingery also concluded that, for a cold-setting phosphate material to form, a weakly basic or amphoteric cation is required [99]. Strongly basic cations react violently, and acidic and inert cations do not react. The strongest bonding was formed by using a weakly basic cation, with a relatively small ionic radius; resulting in a non-ordered structure.

The development of interest in the CBPCs was somewhat slow; the literature on phosphate-based ‘cements, limes and plasters’ surmounted to only 7 % of the total literature published on phosphate ceramics at 1977 [100], the majority of which was to be found in the patent literature. It is more recently that the interest in CPBCs became significant [97]. The majority of this interest was related to biomedical and dentistry applications, with only 5.6 % relating to structural materials, according to a literature review on phosphate cements and ceramics from 1988-2002 [97].

2.6.4. Magnesium Phosphate Cements

Much of the work associated with CBPCs for non-biomedical and non-dentistry applications has focused on Magnesium Phosphate Cements (MPCs) [56]. Patents show that magnesium-based CBPCs were first developed in the mid-20th century for casting alloys [97]. Magnesium oxide (MgO) was mixed with phosphoric acid to form a cementitious material, magnesium dihydrogen phosphate ($\text{Mg}(\text{H}_2\text{PO}_4) \cdot x\text{H}_2\text{O}$), which set very rapidly [101]. However, the cementitious reaction product was a water-soluble magnesium phosphate, which, together with a rapid setting time,

deemed the system unsuitable for practical applications [97, 101]. Since then, various acid phosphates have been used to produce insoluble magnesium phosphate cements [30, 34, 102-105].

MPCs have found applications as road and runway repair materials, owing to rapid setting and strength development properties. The majority of these systems used ammonium-based phosphate powders as the acidic phosphate-based liquid precursor, which, when mixed with MgO formed struvite ($(\text{NH}_4)\text{MgPO}_4 \cdot 6\text{H}_2\text{O}$). However, release of ammonia during mixing and hardening [106, 107], and from the decomposition of struvite above *ca.* 50 °C [108], was found to be problematic.

Ceramicrete, a particular type of MPC was developed by Wagh *et al.* [97, 109] at Argonne National Laboratory for use in hazardous and radioactive waste management. Wagh *et al.* replaced the ammonium-based phosphate powders with potassium dihydrogen phosphate (KH_2PO_4) as the acid-phosphate powder, thus avoiding the issue of gaseous ammonia generation. When MgO and KH_2PO_4 were mixed in water, magnesium potassium phosphate hexahydrate ($\text{MgKPO}_4 \cdot 6\text{H}_2\text{O}$) was formed as the principle reaction product. $\text{MgKPO}_4 \cdot 6\text{H}_2\text{O}$ is an analogous to struvite, and as such has been designated the name struvite-K [110].

Ceramicrete has been used to immobilise a wide variety of radioactive wastes in the U.S. [55]. Wagh describes a series of case studies where Ceramicrete was used to successfully immobilise several wastes [54] and radionuclides including U, Tc, Cs, Ra, CeO_2 (as a surrogate for U_2O_3 , P_2O_3) [55].

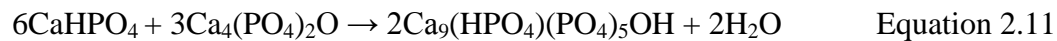
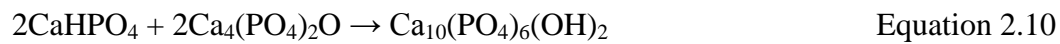
MPCs have been of interest as alternative cementing systems for immobilisation of radioactive waste in the UK [4, 27, 30, 34, 44]. Hayes and Godfrey [44] showed a

potential of MPC as an encapsulation matrix for ILW containing reactive metals. MPC incorporated a high proportion of mix water into the reaction products, which resulted in low pore solution content. This, together with low pH (pH ~ 5-7) of pore solution, resulted in reduced corrosion of encapsulated aluminium over a 40 day period compared to a conventional PC-based cementing system. Covill [34] reported that MPC formulations, developed by AMEC Nuclear UK, fulfilled processing requirements for disposal in a geological disposal facility.

2.6.5. Calcium Phosphate Cements

Calcium Phosphate Cements (CPCs) were developed in the 1980s, initially for applications in dentistry as a synthetic bone replacement material [111-114]. LeGeros first suggested the use of calcium phosphates for the synthesis of a dental repair material [112]. Though, it is Brown and Chow [111] who are credited with the early development of self-hardening CPCs. Equimolar amounts of tetracalcium phosphate (TTCP, $6\text{Ca}_4(\text{PO}_4)_2\text{O}$) and dicalcium phosphate anhydrous (DCPA, CaHPO_4), or dicalcium phosphate dihydrate (DCPD, $\text{CaHPO}_4 \cdot 2\text{H}_2\text{O}$) were mixed with water, resulting in self-hardening cement paste. Hardening occurred within *ca.* 20 mins, at physiological temperature and pH, resulting in the formation of hydroxyapatite (HAp, $\text{Ca}_5(\text{PO}_4)_3(\text{OH})$ or $\text{Ca}_{10}(\text{PO}_4)_6(\text{OH})_2$) [111]. HAp is the main inorganic component of bone, thus CPC is highly biocompatible [111, 114-117]. CPCs bond well to bone and can be sculpted during surgery to fit the contours of wounds. Many similar systems have since been investigated and developed, which are based on soluble calcium phosphates, and in general result in the formation of HAp [118, 119]. HAp exists over a compositional range, with different Ca/P ratios. The stoichiometric HAp synthesised by Brown and Chow [111] had a Ca/P ratio of 1.67 (Equation 2.10

[120]). Later, Brown and Fulmer [120] precipitated calcium deficient HAp with a Ca/P ratio of 1.5 (Equation 2.11 [121, 122]). Natural bone contains carbonate resulting in calcium deficiency. Thus, calcium deficient HAp is compositionally similar to bone, even more so than stoichiometric HAp.



Some have suggested that amorphous calcium phosphate (ACP) is an intermediate phase in the preparation of HAp [123-125]. ACP has a general structure $\text{Ca}_x\text{H}_y(\text{PO}_4)_z \cdot n\text{H}_2\text{O}$, where $n = 3-4.5$ and Ca/P ratio of 1.0-2.2. ACPs have been found to exist in many biological systems as a precursor to HAp-like phase during bone mineral development [123]. ACP is inherently unstable and will crystallise to apatite and other calcium phosphate phases. It has been suggested that there are several amorphous to crystalline conversion mechanisms that may exist depending on the nature of the ACP and conditions under which conversion proceeds [125].

2.7. Phosphate-modified Calcium Aluminate Cements

2.7.1. Introduction

CPCs are attractive for encapsulation of reactive metals, such as aluminium, due to the physiological or near neutral pH they exhibit. Apatites, of which HAp is a type, are been known to possess the ability to substitute many species, including halides, heavy metals and many radionuclides [59, 126-130], thus may be suitable for immobilisation of radionuclides. However, source materials for CPCs are expensive which makes their use on a large scale unviable.

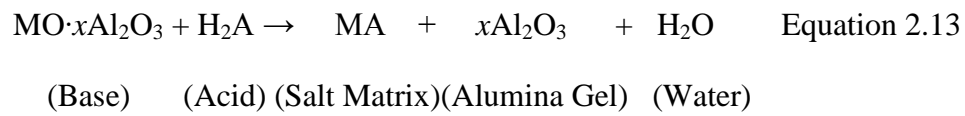
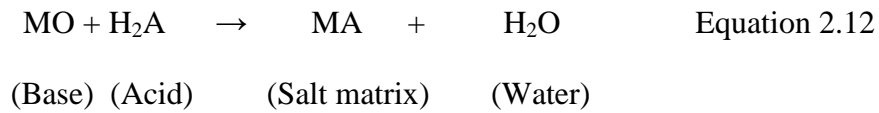
Phosphate-Modified Calcium aluminate cements (PMCs) were developed as an alternative method to synthesise CPCs. Literature on PMCs is limited; the majority

has been published by Sugama *et al.* [86, 87, 131-141]. In a series of studies, they investigated the use of phosphate-modified CACs as carbonation resistant cementing systems for geothermal well applications. These cements were demonstrated to have lower pH (pH \approx 9.7 at time of set [142]) than conventional PC-based cementing systems (pH \approx 12.5 [4]). Therefore, they are of interest as an alternative cementing system to inhibit the corrosion of reactive metals such as aluminium from the UK's radioactive waste inventory [4, 27, 28, 59]. These systems can be hydrothermally treated to form hydroxyapatite, which has the ability to incorporate and retain halides, heavy metals and radionuclides as mentioned in a previous section [59, 126-130].

2.7.2. Development of PMCs

Sugama and Carciello [135] first synthesised PMC as an alternative to MPC. MPC was found to deteriorate due to hydrolysis of unreacted MgO particles. The hydrolysis caused *in situ* transformation of MgO to Mg(OH)₂, which resulted in expansive reaction products and was associated with loss of strength [135].

PMCs were synthesised by a two-stage reaction mechanism [133-138]. Firstly, exothermic acid-base reactions between a cation-leachable powder, as the solid-base reactant, and a phosphate-based solution, as the acidic-liquid, at ambient temperature resulted in rapid-setting cementitious materials. The resulting cementitious materials were then hydrothermally treated in an autoclave at temperatures up to 300 °C, to simulate the conditions of geothermal wells. The cation-leachable basic powder consisted of a metal oxide, as either a single component system, or a binary or ternary system. Examples of such reactions are demonstrated by the generic equations given below in Equation 2.12 and Equation 2.13 [134, 142];



Where M and A represent cations and acid anions, respectively. The consequence of these acid-base reactions was the formation of complex salts, which acted as binding phases, and were responsible for strength development in the cementitious materials at ambient temperature.

Ma and Brown [143] modified CAC with a variety of phosphate-based solutions to assess the potential of inorganic cement-based composites as alternatives to Macro Defect Free (MDF) cements. They also evaluated the rate of hydration for various PMCs by studying the reaction kinetics using isothermal calorimetry [144]. Walter and Odler [107] investigated the setting and mechanical properties of cement resulting from mixing CAC with various sodium polyphosphates, having varying chain lengths. These studies will be discussed in more detail in Section 2.7.3.

2.7.3. Hydration Reactions and Reaction Products

In early studies [134-137], Sugama *et al.* used an ammonium-based fertiliser (Poly-N) as the acidic phosphate-based liquid. Ammonium dihydrogen monobasic orthophosphate (AmDHOP, $\text{NH}_4\text{H}_2\text{PO}_4$) was identified as the major component of Poly-N. In an initial study [135] commercially available CAC (Refcon) was mixed with Poly-N at ambient temperature, and then hydrothermally treated at temperatures up to 300 °C. Based on FTIR results it was suggested that on mixing Poly-N with CAC at ambient temperature, the AmDHOP formed amorphous ammonium calcium pyrophosphate (AmCPP, $(\text{NH}_4)_2\text{Ca}(\text{P}_2\text{O}_7) \cdot x\text{H}_2\text{O}$), based on the rupture of P=O bond in AmDHOP. Subsequent hydrothermal treatment at 200 °C resulted in conversion of

amorphous AmCPP and residual CAC to crystalline HAp and anorthite ($\text{CaAl}_2\text{Si}_2\text{O}_8$, AN), as identified by XRD. The proportion of crystalline phases increased with temperature due to hydrothermally catalysed conversion. After hydrothermal treatment at 300 °C for 20 h, HAp and AN were the only crystalline phases identified by XRD, suggesting the amorphous to crystalline conversion was complete at this temperature.

The characteristics of PMCs synthesised by reacting Poly-N with various calcium aluminate compounds; $\text{CaO}\cdot\text{Al}_2\text{O}_3$ (CA), $3\text{CaO}\cdot\text{Al}_2\text{O}_3$ (C_3A), and $\text{CaO}\cdot 2\text{Al}_2\text{O}_3$ (CA_2) was also investigated [134]. Studies of the reaction kinetics showed that CA had the greatest affinity to Poly-N, with the extent of reactivity between CAC compounds and Poly-N showing the following trend: $\text{CA} > \text{C}_3\text{A} \gg \text{CA}_2$. This suggested that commercially available CAC, which consist of a high proportion of CA, will react favourably with Poly-N. After a careful review of pyrophosphates and orthophosphates as reference materials, the authors proposed that absorption bands detected by FTIR for these systems were due to formation of an orthophosphate; ammonium calcium orthophosphate ($\text{NH}_4\text{CaPO}_4\cdot x\text{H}_2\text{O}$, AmCOP) salt. Also, it was suggested that Poly-N was responsible for catalysing the decomposition of CAC compounds, thus liberating Ca^{2+} ions, which were taken up by AmDHOP, the principle component of Poly-N, to form AmCOP. Furthermore, it was suggested that hydrated aluminium oxide and hydrated aluminium hydroxides formed by the hydration of aluminium oxide liberated from the decalcification of CAC. In these systems, ammonium ions, liberated from Poly-N, react with hydroxide ions to form gaseous ammonia according to Equation (2.14) [134], which makes such systems environmentally questionable [138].



Sodium phosphate-based solutions were subsequently investigated as alternative acidic reactants to mix with CAC [138]. Cement pastes cured at ambient temperature contained amorphous phases described as sodium calcium orthophosphate ($\text{NaCaPO}_4 \cdot x\text{H}_2\text{O}$, SCOP) salt and hydrated alumina gel ($\text{Al}_2\text{O}_3 \cdot x\text{H}_2\text{O}$). Hence, the principle reaction products were analogous to that resulting from the ammonium phosphate-derived systems. Hydrothermal treatment caused conversion of this amorphous phase to crystalline HAp, along with acceleration of reaction between phosphate and unreacted CAC. It was shown that sodium polyphosphate ($(\text{NaPO}_3)_n$) reacted more favourably with CAC than sodium dihydrogen monophosphate (NaH_2PO_4). In subsequent investigations, Sugama *et al.* revised their earlier assertion and proposed that the principle reaction products were calcium hydrogen phosphate hydrate ($\text{Ca}(\text{HPO}_4) \cdot x\text{H}_2\text{O}$) and $\text{Al}_2\text{O}_3 \cdot x\text{H}_2\text{O}$ [132, 145, 146].

Ma and Brown [143] modified CAC with a variety of sodium phosphate-based solutions. Sodium hexametaphosphate $(\text{NaPO}_3)_n^2$, sodium metaphosphate $(\text{NaPO}_3)_n \cdot \text{Na}_2\text{O}$, sodium tripolyphosphate $\text{Na}_5\text{P}_3\text{O}_{10}$, sodium trimetaphosphate $(\text{NaPO}_3)_3$ and dicalcium phosphate $\text{Ca}_2\text{P}_2\text{O}_7$ were mixed with CAC (Secar 71) and deionised water to make up the various phosphate-modified cement pastes. Differences were observed in the mechanical properties of the phosphate-based modified systems compared to pure Secar 71 system, as well as the XRD results.

² The designated names are according to the reference, and contradict the present authors notation which describes $(\text{NaPO}_3)_n$ as sodium polyphosphate and $(\text{NaPO}_3)_6$ as sodium hexametaphosphate, as given by the manufacturers literature.

When considering the pure Secar 71 system, a decrease in the intensity of reflections associated with CA was observed suggesting that CA was consumed. It was suggested that this resulted in precipitation of calcium aluminate hydrate phases in the usual CAC hydration reactions, although no reflections associated with the crystalline phases are apparent following review of their XRD results. In the phosphate-modified systems, reflections for neither the conventional CAC hydration products nor other phases were apparent, despite the reduction in intensity for the CA reflection. It was suggested that CA was consumed, but formed an amorphous reaction product instead of the usual crystalline calcium aluminate hydrate phases. This phase was proposed to be an ‘aluminate-phosphate gel’, though no further characterisation results were provided to support this assertion. Although they suggested that the hydration reaction of CAC was accelerated by phosphate-based modifications, as more CA was consumed, it would be more appropriate to say that the conventional hydration was suppressed and a distinctive reaction took place, resulting in an amorphous phase.

Ma and Brown also investigated the kinetics of various PMCs using isothermal calorimetry [144]. Phosphate-modifications accelerated the onset of the principle exotherm, which occurred immediately after mixing and at a high rate. For pure CAC, the principle exothermic peak is usually associated with the hydration reaction of CAC, occurring *ca.* 20 h after mixing. Despite the initial rapid rate of heat evolution, when the cumulative heat evolution over the first 30 h of hydration was considered, the phosphate-modified systems evolved less total heat than the unmodified system. The EDX of these samples showed that the main reaction products consisted of aluminium, phosphorus, and calcium. The relative proportions of these constituents were very similar in all phosphate-derived systems, existing

within a narrow compositional range. It was proposed that the main reaction product was an amorphous calcium aluminate phosphate hydrate (C-A-P-H) gel, which acted as a binding phase between the anhydrous CAC particles and calcium aluminate hydrates. There was some evidence of the presence of crystalline CA-hydrate phases given by the EDX results, which showed hexagonal calcium aluminate hydrate crystals, suggested to be C_2AH_8 .

Walter and Odler [107] investigated the setting and mechanical properties of cement systems resulting from mixing CAC and various sodium polyphosphates with varied chain lengths. They concluded that phosphate-modified CAC resulted in amorphous reaction products, and setting and mechanical properties could be controlled by the chain length of sodium polyphosphate used.

Table 2.3 summarises the published works related to PMCs, which demonstrates the general lack of consensus regarding PMC hydration reactions, and specifically the principle reaction products.

Table 2.3 Summary of previous investigations related to PMCs at ambient temperatures

Year/ Reference	CAC/ Phase	SCM	Phosphate	Curing conditions	Principle reaction products
1991, [135]	Lumnite	-	Poly-N	1 h, 25°C	$(\text{NH}_4)_2\text{Ca}(\text{P}_2\text{O}_7) \cdot x\text{H}_2\text{O}$
1992, [134]	CA	-	Poly-N	7 d, 25°C	$\text{NH}_4\text{CaPO}_4 \cdot x\text{H}_2\text{O}$, Al_2O_3 hydrate gel
	CA ₂	-	Poly-N	7 d, 25°C	$\text{NH}_4\text{CaPO}_4 \cdot x\text{H}_2\text{O}$, Al_2O_3 hydrate gel
	C ₃ A	-	Poly-N	7 d, 25°C	$\text{NH}_4\text{CaPO}_4 \cdot x\text{H}_2\text{O}$, Al_2O_3 hydrate gel
1992, [143]	Secar 71	-	$(\text{NaPO}_3)_n$	≤ 300 d, RT	Aluminate-phosphate gel
	Secar 71	-	$(\text{NaPO}_3)_n \cdot \text{Na}_2\text{O}$	≤ 300 d, RT	Aluminate-phosphate gel
	Secar 71	-	$(\text{NaPO}_3)_3$	≤ 300 d, RT	Aluminate-phosphate gel
	Secar 71	-	$\text{Na}_5\text{P}_3\text{O}_{10}$	≤ 300 d, RT	Aluminate-phosphate gel
1994, [144]	Secar 71	-	$(\text{NaPO}_3)_n$	-	Calcium-aluminate- phosphate-hydrate gel
	Secar 71	-	$(\text{NaPO}_3)_n \cdot \text{Na}_2\text{O}$	-	Calcium-aluminate- phosphate-hydrate gel
	Secar 71	-	$(\text{NaPO}_3)_3$	-	Calcium-aluminate- phosphate-hydrate gel
	Secar 71	-	$\text{Na}_5\text{P}_3\text{O}_{10}$	-	Calcium-aluminate- phosphate-hydrate gel
1995, [138]	Refcon	-	NaH_2PO_4	24 h, 25°C	$\text{NaCaPO}_4 \cdot x\text{H}_2\text{O}$, $\text{Al}_2\text{O}_3 \cdot x\text{H}_2\text{O}$
	Refcon	-	$(\text{NaPO}_3)_n$	24 h, 25°C	$\text{NaCaPO}_4 \cdot x\text{H}_2\text{O}$, $\text{Al}_2\text{O}_3 \cdot x\text{H}_2\text{O}$
1996, [107]	Secar 51	-	$\text{Na}_{n+2}\text{P}_n\text{O}_{3n+1}$ (where $n = 4,$ 7, 28 and 30)	20±2°C and 50±2°C	‘amorphous material of marginal crystallinity’
	Secar 71	-	$\text{Na}_{n+2}\text{P}_n\text{O}_{3n+1}$ (where $n = 4,$ 7, 28 and 30)	20±2°C and 50±2°C	‘amorphous material of marginal crystallinity’
1999, [145]	Refcon	PFA	$(\text{NaPO}_3)_n$	24 h, RT	$\text{Ca}(\text{HPO}_4) \cdot x\text{H}_2\text{O}$, $\text{Al}_2\text{O}_3 \cdot x\text{H}_2\text{O}$
2002, [146]	Secar 51	PFA	$(\text{NaPO}_3)_n$	24 h, RT	$\text{Ca}_5(\text{PO}_4)_3(\text{OH})$, γ - AlOOH
	Secar 60	PFA	$(\text{NaPO}_3)_n$	24 h, RT	$\text{Ca}_5(\text{PO}_4)_3(\text{OH})$, γ - AlOOH
	Secar 71 Secar 80	PFA PFA	$(\text{NaPO}_3)_n$ $(\text{NaPO}_3)_n$	24 h, RT 24 h, RT	$\text{Ca}(\text{HPO}_4) \cdot x\text{H}_2\text{O}$ $\text{Ca}(\text{HPO}_4) \cdot x\text{H}_2\text{O}$

2.7.4. Physico-mechanical Properties

As stated previously, most of the work by Sugama *et al.* was performed at elevated temperatures. As such, the majority of mechanical properties reported were attained at non-ambient temperatures.

In their initial study on PMCs [135], Sugama and Carciello reported that AmCPP acted as a binding phase between CAC particles on mixing Poly-N with CAC and was responsible for rapid setting and strength development of > 20 MPa after curing for 1 h. Subsequent hydrothermal treatment at 200 °C resulted in maximum compressive strength of 70 MPa, decreasing to 40 MPa after treatment at 300 °C [135]. Based on the FTIR and XRD results, it was thought that high compressive strength was a result of a moderate mix of amorphous and crystalline phases, caused by the interlocking nature of HAp and AN crystals, which acted to connect the amorphous mass and densify the microstructure. Continued crystal growth and the resultant domination of crystallinity after heating to 300 °C resulted in a more porous microstructure, and a regression in compressive strength [136]. This hypothesis was reiterated in by Sugama *et al.* [134].

The compressive strength of PMCs prepared from pure CA-based phases has also been reported [134]. PMCs prepared from CA and C₃A exhibited compressive strengths of 13 MPa and 15 MPa, respectively, after curing in air at 25 °C for 3 h. CA₂-derived PMC exhibited no significant strength development.

Sugama and Carciello reported the compressive strength of (NaPO₃)_n-derived CPCs to be between *ca.* 7-30 MPa after 24 h curing at room temperature (25 °C), depending on the concentration of the phosphate solution [138]. As phosphate

solution concentration increased, the resulting cement exhibited decreased porosity and increased strength.

The flexural strength has been reported at various ages up to 10 months for the CAC modified with sodium phosphates [143]. At all ages, the modifications resulted in higher flexural strength than unmodified CAC. All systems exhibited rapid strength development over the first 3 to 7 days, then strength regression up to 28 days, followed by gradual increase in strength up to 10 months of hydration. All sodium phosphate-based modifications resulted in flexural strengths of between two and three times that of the unmodified CAC system after 10 months of curing. Porosity measurements using Mercury Intrusion Porosimetry (MIP), suggested that the phosphate-based modifications improved mechanical properties by reducing the average pore size and decreasing the total porosity of the cement pastes.

The subsequent investigation by Ma and Brown [144], suggests that the principle reaction product, described earlier as C-A-P-H, was responsible for strength development, and that the strength regression exhibited by the various phosphate-modified cement systems was due to the conversion of hexagonal C_2AH_8 to cubic C_3AH_6 . Furthermore, they also suggested that the formation of C-A-P-H was responsible for partially mitigating this strength regression. However, as their XRD results exhibited no evidence of crystalline CA-hydrate phases, it is questionable to attribute the observed strength regression to the conversion reactions associated with the crystalline CA-hydrates.

2.7.5. Microstructure and Morphology

Sugama and Carciello [135] used SEM to study the microstructure of PMCs, which had been cured at 25 °C for 1 h. They observed a microstructure exhibiting porous

and fragmentary features. After hydrothermal treatment in an autoclave at 200 °C, crystalline reactions products were observed to have filled much of the porous space. As discussed previously, increasing the hydrothermal temperature to 300 °C resulted in domination of crystalline HAp, and subsequent increase in apparent porosity.

Ma and Brown [144] used EDX and Environmental Scanning Electron Microscopy (ESEM) to characterise the morphology of various PMCs, which allowed the microstructural development of the various cement systems to be observed in real time. It was shown that phosphate modifications resulted in hardened cement pastes with distinct microstructures to those of unmodified CAC. The morphologies of the phosphate-modified CAC were phosphate dependant, as suggested by the formation of apparently discrete phases. Microcracks formed in all systems within minutes of mixing, which the authors suggested, was a result of the exothermic setting reactions.

2.8. Summary

The corrosion of aluminium in PC-based cementitious systems is driven by the high pH and availability of free-water. Therefore, it has been suggested that alternative cementing systems, where the pore solution pH and/or free water content is lower than that of conventional PC-based cementing systems, may be advantageous for the encapsulation of reactive metals, such as aluminium, resulting in a more suitable wastefrom for interim-storage and disposal.

CPCs, formed by acid base reactions between CACs and phosphate-based solutions, should result in a cementitious matrix with a pore solution of relatively low pH. Literature on CPCs is limited and there is a lack of consensus regarding the principle reactions products. Various CACs and phosphate-based solutions have been used to produce, but no systematic study has been undertaken to assess the effect of

phosphate type on the cementitious system behaviour and properties. Additionally, there is no information in the open literature relating to the application of CPCs to the encapsulation of reactive metals for radioactive waste management.

Based on review of the relevant literature, the work presented here aims to develop an alternative cementitious system with a lower pH environment, for the encapsulation of aluminium metal. The following key research themes will be addressed in the following results chapter:

- Various candidate materials have been tested to identify the suitable precursor materials;
- The formulation of the cement matrix has been developed to fulfil certain processing and operational properties requirements, as defined by industry;
- The reaction of the developed formulation with aluminium has been studied;
- The long-term phase evolution of the developed system has been investigated to assess the reaction with aluminium and the long-term behaviour of the materials.

3. Experimental

3.1. Introduction

The project has four distinctive research stages, each of which are covered in the subsequent results chapters. The research stages are as follows;

1. Identification of suitable precursor materials (Chapter 4);
2. Development of CAP formulation envelope (Chapter 5);
3. Encapsulation of aluminium in CAP (Chapter 6);
4. Characterisation of CAP (Chapter 7).

The purpose of this chapter is to provide an overview of the raw materials, formulations, mixing procedures and curing conditions, and the various analysis and characterisation techniques, as well as the sample preparation for each technique. Additional information, specific to particular investigations of the research stages, may also be given in the relevant results chapters. The cementitious system studied in this project is referred to as Calcium Aluminate Phosphate cement (CAP). CAP is used throughout as a collective name for all the systems derived from phosphate-modified CAC.

3.2. Materials

3.2.1. Calcium Aluminate Cement

Secar 51, a commercially available CAC supplied by Kerneos Ltd, was used throughout this project. Preliminary investigations using three commercially available CACs (Secar 41, 51 and 71) and sodium monophosphate suggested that Secar 51 exhibited the most desirable behaviour in terms of setting and strength development. It is thought that this may be due to the relatively high content of CA, which is the principle hydration phase in CACs.

The composition of Secar 51, as determined by X-Ray Fluorescence (XRF), is given in Table 3.1. XRD (Figure 3.1) of the CAC powder confirmed that the principle crystalline phase was monocalcium aluminate (CA), with gehlenite (C₂AS) and perovskite (CT) also present as secondary phases. The CAC was stored sealed in plastic containers in dry and cool conditions according to the manufacturer's instructions.

Table 3.1 Composition of Secar 51 as determined by XRF

Element/Oxide	Quantity (wt%)	Error (wt%)
Al ₂ O ₃	51.10	±0.29
CaO	36.84	±0.24
SiO ₂	5.04	±0.09
TiO ₂	2.08	±0.06
Fe ₂ O ₃	1.98	±0.06
MgO	0.48	±0.03
K ₂ O	0.42	±0.03
P ₂ O ₅	0.13	±0.01
Na ₂ O	0.11	±0.01
S [*]	0.018	±0.005
Total	98.20	

(Note: * determined using Leco analysis)

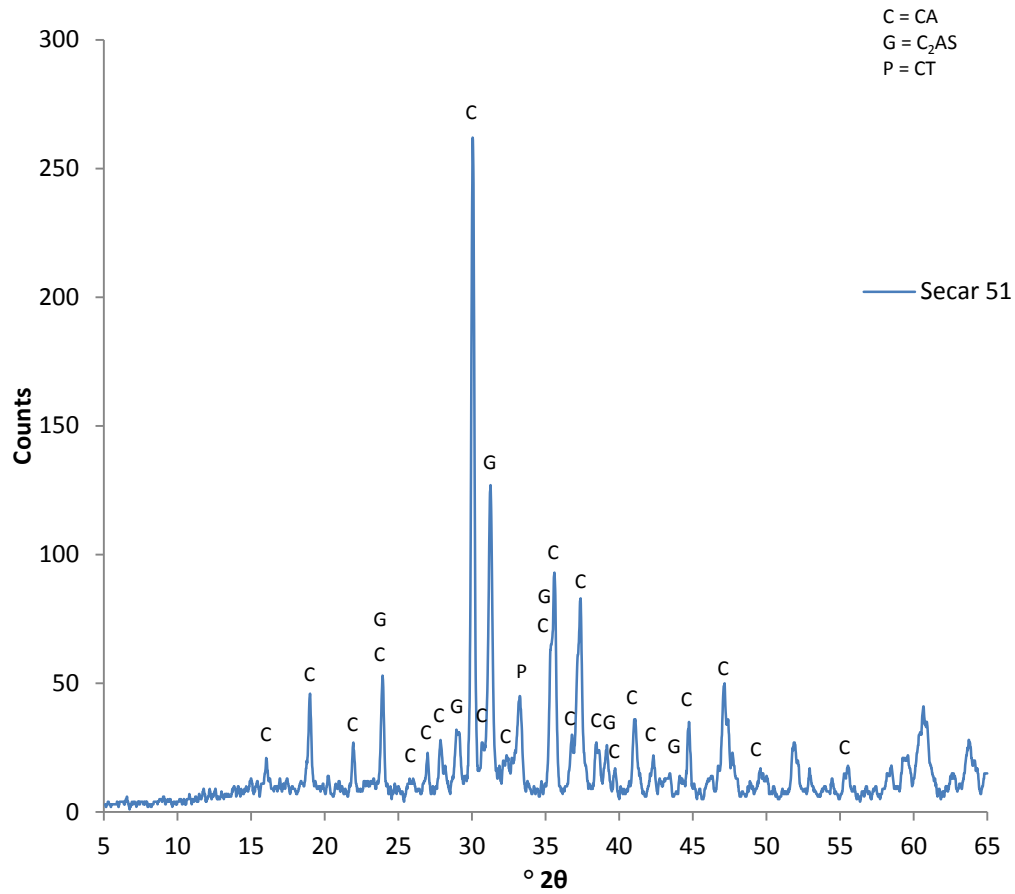


Figure 3.1 XRD pattern of Secar 51

3.2.2. Phosphate-based Powders

Three mono-phosphates, $\text{NaH}_2\text{PO}_4 \cdot 2\text{H}_2\text{O}$ (Alfa Aesar, 99%), KH_2PO_4 (Acros Organics, 99+%), $\text{NH}_4\text{H}_2\text{PO}_4$ (Alfa Aesar, 98%) and two poly-phosphates, $(\text{NaPO}_3)_n$ (Acros Organics, pure) and $(\text{NaPO}_3)_6$ (Fisher Scientific, general purpose grade), were used during this project. All powders were stored in dry and cool conditions.

3.2.3. Pulverised Fuel Ash

PFA in the form of CEMEX 450 S (BS EN 450 - 1 Fineness Category S; LOI Category B), supplied by CEMEX UK Ltd, was used as a SCM. The chemical composition is shown in Table 3.2, as determined by XRF. The results from XRD (Figure 3.2) of the PFA showed reflections related to crystalline quartz, mullite and minor amount of hematite (Fe_2O_3), as well as significant diffuse scattering, which suggested considerable amorphous content. The PFA was stored in dry and cool conditions.

Table 3.2 Composition of PFA as determined by XRF

Element/Oxide	Quantity (wt%)	Error (wt%)
SiO_2	50.18	± 0.28
Al_2O_3	24.68	± 0.20
Fe_2O_3	9.04	± 0.12
C*	3.37	± 0.07
K_2O	2.98	± 0.07
CaO	2.82	± 0.07
MgO	1.71	± 0.05
Na_2O	1.16	± 0.04
TiO_2	1.01	± 0.04
P_2O_5	0.37	± 0.03
S*	0.296	± 0.02
Total	97.62	

(Note: * determined using Leco analysis)

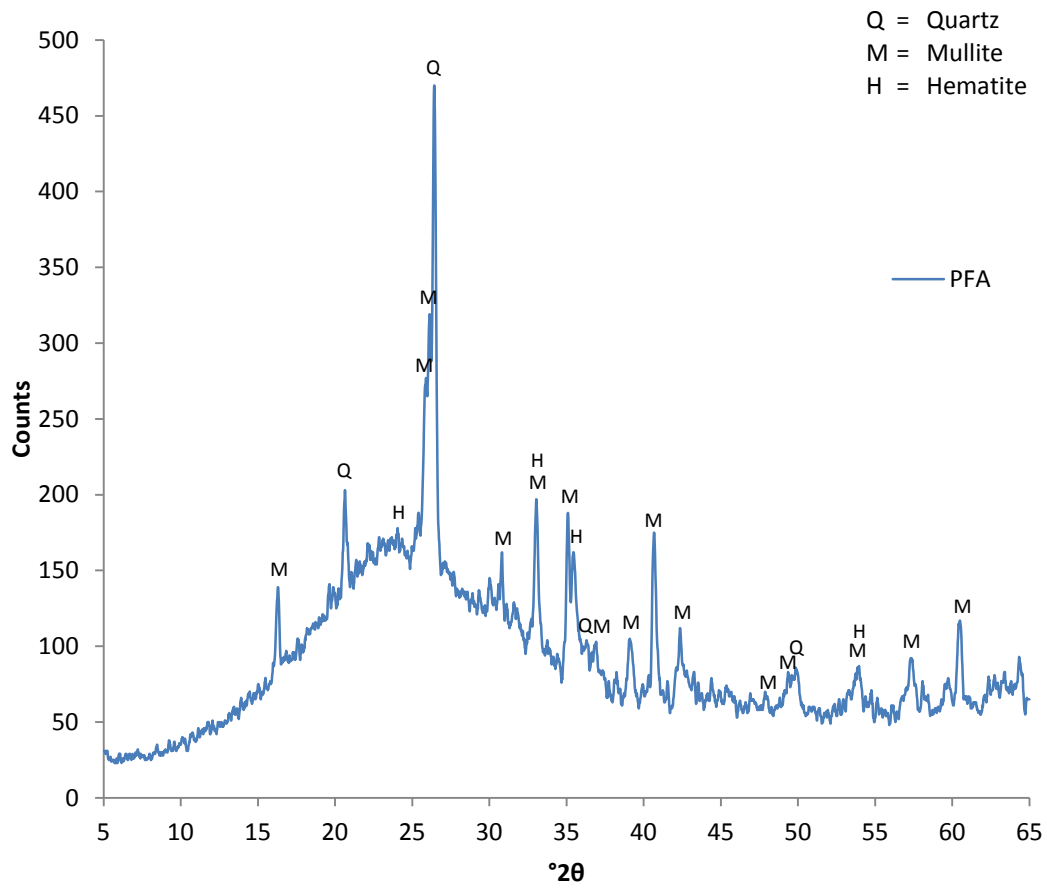


Figure 3.2 XRD pattern of PFA

3.2.4. Boric Acid

Boric acid was used as an additive in order to extend the setting time of the CAP systems studied here. Boric acid is known to act as a setting retarder in various cementitious system including CAC-based cementitious systems and magnesium phosphate cement, by effectively decreasing the dissolution rate of the cement particles and inhibiting hydration [34, 65, 86, 88].

Powdered boric acid (H_3BO_3 , $\geq 99.5\%$) was sourced from Fisher Scientific UK (CAS No. 10043-35-3). The boric acid was stored in dry and cool conditions.

3.2.5. Portland Cement

PC (CEM I) was sourced from Castle Cement Ltd supplied by National Nuclear Laboratory (NNL). The chemical composition is shown in Table 3.3, as determined by XRF. The PC was stored in sealed plastic containers in dry and cool conditions.

Table 3.3 Composition of PC as determined by XRF

Element/Oxide	Quantity (wt%)	Error (wt%)
CaO	62.09	± 0.31
SiO ₂	21.29	± 0.19
Al ₂ O ₃	5.71	± 0.09
Fe ₂ O ₃	2.68	± 0.06
MgO	2.34	± 0.06
S*	0.836	± 0.04
K ₂ O	0.77	± 0.04
P ₂ O ₅	0.32	± 0.02
TiO ₂	0.29	± 0.02
Na ₂ O	0.22	± 0.02
Total	96.55	

(Note: * determined using Leco analysis)

3.2.6. Blast Furnace Slag

The BFS was ground granulated blast furnace slag sourced from Redcar Steel Works and supplied by NNL. The chemical composition is given in Table 3.4, as determined by XRF. Similar to other materials, the BFS was stored in dry and cool conditions.

Table 3.4 Composition of BFS as determined by XRF

Element/Oxide	Quantity (wt%)	Error (wt%)
CaO	39.66	±0.25
SiO ₂	35.19	±0.24
Al ₂ O ₃	13.48	±0.14
MgO	7.44	±0.11
Fe ₂ O ₃	0.97	±0.04
S*	0.786	±0.04
TiO ₂	0.54	±0.03
K ₂ O	0.4	±0.03
Na ₂ O	0.21	±0.02
Mn ₃ O ₄	0.23	±0.02
Total	98.91	

(Note: * determined using Leco analysis)

3.2.7. Aluminium

The aluminium was grade 1050 (> 99.5 % Al) supplied by NNL in 3 mm thick sheet form, which was cut into pieces of *ca.* 3 mm x 3 mm x 20 mm and *ca.* 3 mm x 20 mm x 50 mm.

3.3. Formulations

The various cementitious systems and formulations investigated during the four distinct research stages of this project are defined in this section. It should be noted that more detailed information regarding the formulations are provided within the relevant results chapters. The formulations are defined according to the various constituent ratios, by mass, as follows³:

- Water to cement ratio (w/c);
- Water to solids ratio (w/s);
- Phosphate to cement ratio (p/c);
- Phosphate to solids ratio (p/s);

³ where w = water, c = cement, f = filler (or SCM), s = solid (cement + SCM, i.e. PFA or BFS), p = phosphate, r = retarder (i.e. boric acid).

- Supplementary cementitious material to solids ratio (f/s);
- Retarder to cement ratio (r/c).

In order to identify a suitable phosphate powder for use in producing an appropriate cement matrix for the encapsulation of ILW, various phosphate powders described in Section 3.2.2 were mixed with Secar 51, as the CAC powder, and water.

As identified in Chapter 3, CACs exhibit so-called conversion reactions that result in increased porosity and decreased strength. The detrimental effects of conversion can be limited by controlling the initial water content, and it has been recommended to use a $w/c < 0.4$. Preliminary scoping trials, the results of which are not presented here, suggested that the initial water content should be $w/c > 0.3$, in order to provide a cement paste with sufficient fluidity. Those preliminary scoping trials also suggested that increasing phosphate content decreased the fluidity of the cement paste. Formulations with phosphate content $p/c > 0.4$ had low fluidity and as such were difficult to work. Based on these observations, the w/c and p/c of the formulations investigated during the first stage of the project were 0.37 and 0.2, respectively. Samples of unmodified Secar 51 were hydrated at the same w/c (0.37) to allow direct comparison with the phosphate-modified systems.

Further development of the cement formulation was undertaken in order to define a formulation envelope which satisfies the requirements for industrial application. In addition to the CAC, phosphate (sodium polyphosphate, $(\text{NaPO}_3)_n$) and water, a SCM was introduced to reduce the heat generated during setting by acting as an inert filler material. PFA was selected over other SCMs as it has the additional attribute of increasing the fluidity of cement slurries by the so called ‘ball bearing effect’, due to the spherical nature of the PFA particles [15, 147-149]. Boric acid was selected as a

suitable inorganic setting retarder; it is known to act as a setting retarder in various cement systems, including CAC-based cementing systems and magnesium phosphate cement [34, 65, 86, 88].

Encapsulation of aluminium metal was studied using two representative formulations based on the developed formulation envelop composed of CAC, phosphate and water with PFA and boric acid. This study also used, for comparison, a 3:2 PFA/CAC blend at $w/s = 0.35$ without phosphate or boric acid, in addition to a 3:1 BFS/PC at $w/s = 0.35$. The same four formulations used to study the encapsulation of aluminium were also used to assess the long-term physico-mechanical properties of the systems.

3.4. Sample Mixing and Curing

3.4.1. Small-Scale Mixing

Some of the samples were prepared in small scale (< 500 g) batches. Firstly, the acidic phosphate-based solutions were prepared, and then mixed with CAC powders or CAC and PFA powders. Depending on the formulation, the phosphate powder with or without boric acid was weighed and mixed with the desired amount of distilled water and left on a roller mixer for a minimum of 2 h to allow full dissolution. Then CAC, followed by PFA, was added to the pre-prepared solution over *ca.* 1 min and mixed by hand for *ca.* 2 min. The resulting slurry was then poured into 50 ml centrifuge tubes, which were sealed with a lid and parafilm. The prepared samples were cured in an environmental curing chamber controlled at 20 °C and $\geq 95\%$ Relative Humidity (RH).

3.4.2. Large-Scale Mixing

Some of the samples were prepared in large scale (> 500 g) batches. As with the small scale mixing, the phosphate powder with or without boric acid was first added

to distilled water and left on a roller mixer, typically overnight, to allow full dissolution of the powders. The solution was placed in the mixing bowl of a Kenwood bench-top planetary mixer at speed setting 1 (*ca.* 150 rpm). CAC, followed by PFA, was added to the mixer over a *ca.* 5 min period. The mixer was then stopped and the sides of the bowl were scraped down to incorporate all the powders into the slurry. The mixer was then returned to speed setting 1 for a further 5 min. Then the mixing bowl was transferred to a Silverson high-shear mixer and mixed at 7000 rpm for 10 min. The mixed slurry was either directly used for the subsequent testing of the slurry or poured into stainless steel moulds suitable for the testing of hardened paste. Some samples were prepared in 50 ml centrifuge tubes similar to the smaller scale batching. The samples in the moulds and tubes were cured in an environmental curing chamber controlled at 20°C and $\geq 95\%$ RH.

3.5. Plant Acceptance Tests

3.5.1. Colflow Test

The Colflow test is a standard slurry fluidity test developed by Colcrete Ltd, which is relatively simple and requires minimal equipment meaning it can be used ‘in the field’ to assess the fluidity of cement slurries. The test involves a specific volume of slurry (1.14 L) being released from a tundish into a horizontal channel. Firstly, the channel and tundish were wetted and then stood on end for 1 min to drain. The channel was then placed on a horizontal surface, with the aid of a spirit level, and the tundish attached at the enclosed end with the plug inserted. The required volume of slurry was placed in the tundish and the plug withdrawn. The distance travelled down the channel by the slurry after *ca.* 30 s was recorded to the nearest 10 mm. This value was used as the time = 0 min (t_0) value in the present study. The slurry was, as much as possible, recovered from the channel and tundish, which was then washed down

and rewetted ready for a second test. The test was undertaken in duplicate and the mean value was recorded and referred to as the flow. The slurry was then returned to the mixing bowl and mixed at speed setting 1 (ca. 150 rpm) for a further 150 min, after which another reading, following the same procedure, was taken in duplicate and recorded as the time = 150 min (t_{150}) value.

3.5.2. Vicat Setting Time

An automatic Vicat setting time apparatus was used to investigate initial and final setting times. The principle of the Vicat apparatus is to record how far a weighted free-falling needle penetrates the cement slurry at defined time intervals. Immediately after mixing, the slurry was poured into a well lubricated conical mould with a top surface diameter of 60 mm. The mould was agitated and the top surface scrapped to release any entrapped air to ensure flushness of the slurry with the top of the mould, after which the mould was placed on the rotating platform of the Vicat apparatus. The Vicat test program used 26 penetrations, each 10 mm apart from the last, at intervals of 0.5, 1, 5, 10, 15 or 30 min.

3.5.3. Bleed Water Evaluation

Bleed water is that which is neither incorporated into hydrate phases, nor within the pore structure of the cement paste. It can be thought of as excess formulation water, usually due to high water to cement ratio, which forms as a segregated layer on top of hardened cement pastes. The formation of bleed water was assessed by casting 50 ml of slurry immediately after mixing into a centrifuge tube, which was then cured at 20 °C and 95 % RH for 24 h. The amount of bleed water was then measured by visual examination.

3.6. Physico-mechanical Properties

3.6.1. Compressive Strength

Samples for compressive strength testing were prepared using triplicate 50 mm x 50 mm x 50 mm stainless steel moulds which were lubricated with mould release oil prior to casting. Samples were cast immediately after the mixing period and placed in an environmental curing chamber at 20 °C and 95 % RH for 48 h, apart from 24 h samples, which were demoulded and tested after 24. Samples were demoulded after 48 h, placed in plastic samples bags and returned to the environmental curing chamber. Compressive strength was measured after 1, 7, 28, 90, 180 and 360 days using a Controls Automax automatic compressive strength testing machine.

3.6.2. Dimensional Stability

Samples for dimensional stability measurements were prepared using triplicate 160 mm x 40 mm x 40 mm stainless steel prism moulds which were pre-lubricated with mould release oil. Samples were cast immediately after mixing and placed in an environmental curing chamber at 20 °C and 95 % RH for 48 h. Reference studs were glued to the ends of each prism using hot-melt and moisture resistant adhesives. A digital length comparator, accurate to 0.001 mm, was used to monitor changes in length over time. The length of each specimen was measured, relative to a 160 mm stainless steel reference rod, after 3, 7, 28, 90, 180 and 360 days.

3.6.3. Mercury Intrusion Porosimetry

The porosity of various cement samples was characterised by MIP, which can be used to determine pore volume, pore size, pore size distribution, density of the bulk material etc. Mercury is a non-wetting liquid for most substances meaning that it may be forced under pressure into porous materials including cementitious systems. Only slight pressure will force a non-wetting liquid into the larger (macro-size) pores but

high pressure is required to force fill smaller pores. MIP forces mercury under increasing yet controlled pressure into the pore structure of the material. Washburn [150] described the pressure, P , required to force a non-wetting liquid, such as mercury, into a porous material with cross sectional pore diameter, d , according to Equation 3.1;

$$P = 4\gamma\cos\theta/d \quad \text{Equation 3.1}$$

Where γ is the surface tension and θ is the contact angle of the non-wetting liquid. The volume of intrusion at a given pressure gives information on the pore volume and pore size distribution. MIP measurements were performed using a Micrometrics Poresizer 9320 using samples that had been dried by immersion in acetone followed by drying in a desiccator.

3.7. Phase Analysis

3.7.1. X-ray Diffraction

X-ray Diffraction (XRD) was the principle technique used to identify the crystalline phase composition of the various cementitious systems studied throughout this project.

XRD is a non-destructive technique based on the fact that inorganic crystalline solids have a unique X-ray powder pattern which can be used as a ‘fingerprint’ [151]. This fingerprint can be cross referenced against the International Centre for Diffraction Data’s database known as the Powder Diffraction File (PDF), which holds records for hundreds of thousands crystalline inorganic solids and which is periodically updated.

The structures of crystalline materials are composed of regular arrangements of atoms in three dimensions arranged over large atomic distances [152, 153]. The long-

range ordered structure is composed of smaller repeating units, or unit cells, which are essentially the building blocks of the crystal structure. In the crystalline lattice, atoms can be thought to exist within lattice planes that are stacked to form the three-dimensional structure. Figure 3.3 shows the schematic of XRD in lattice planes. Bragg's Law describes the relationship between the inter-planar distance (d), the wavelength of an incident monochromatic X-ray beam (λ) and the angle of incidence of that X-ray beam (θ). When monochromatic X-rays are scattered by the parallel planes in a crystal, the difference in the path length of X-rays causes either constructive or destructive interference. When the angle of incidence, θ , is such that the path difference (A-C-B, Equations 3.2-3.4) between beams 1-1' and 2-2' is equal to an integer multiple of λ (Equation 3.5) then the diffracted X-ray beams are in phase and will interfere constructively, resulting in an intense signal which can be detected.

$$AC = CB = d\sin\theta \quad \text{Equation 3.2}$$

$$ACB = 2d\sin\theta \quad \text{Equation 3.3}$$

$$ACB = n\lambda \quad \text{Equation 3.4}$$

$$\text{Bragg's Law: } n\lambda = 2d\sin\theta \quad \text{Equation 3.5}$$

A Siemens D500 diffractometer was used throughout this project utilising monochromatic Cu K_α radiation ($\lambda = 1.54178 \text{ \AA}$) operating at a voltage of 40 kV and current of 30 mA. Samples were analysed over the range $5\text{-}65^\circ 2\theta$ with a step size of 0.02° and generally a scanning speed of $2^\circ 2\theta \text{ min}^{-1}$, although in some cases an alternative scan speed of $1^\circ 2\theta \text{ min}^{-1}$ was used.

Sample preparation for XRD involved first arresting the hydration and removing the free-water of the various cement samples. This was performed by crushing the bulk

samples into small pieces either by hand or by using a percussion mortar, and placed in acetone for 3 days followed by being dried in a vacuum desiccator for 7 days. Samples were then further crushed using a percussion mortar and ground using an agate mortar and pestle. The powdered samples were then passed through a 63 μm sieve.

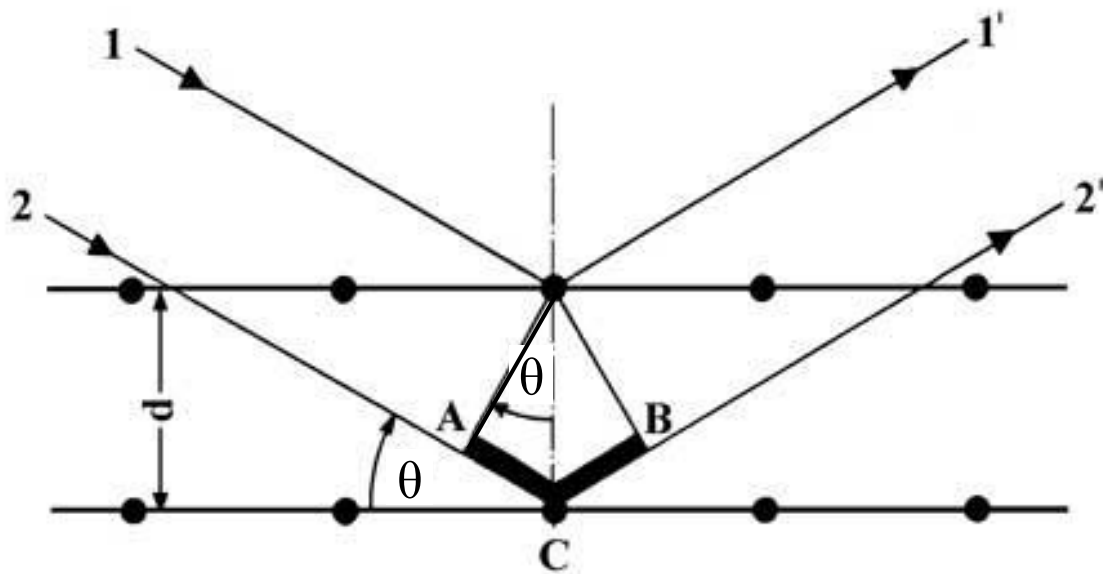


Figure 3.3 Derivation of Bragg's Law [154]

3.7.2. Thermogravimetric Analysis

ThermoGravimetric analysis (TG) was used as an additional phase characterisation technique and in some cases to quantitatively evaluate the amount of free-water. TG is a thermal analysis technique where the mass of a sample is monitored as a function of temperature or time during a specific heating regime under a controlled atmosphere. TG can be used for quantitative phase characterisation of both crystalline and amorphous materials which experience mass change on heating due to dehydration, decomposition or oxidation mechanisms. The derivatives of TG curves, known as Differential ThermoGravimetric (DTG) curves were also calculated. The DTG curves allow the temperature ranges of weight loss events to be determined more accurately. The mass loss experienced can be used to quantify the amount of that particular phase in the sample.

TG was performed using a PerkinElmer Pyris 1 thermogravimetric analyser using a heating rate of $10\text{ }^{\circ}\text{C min}^{-1}$ over a temperature range of 25-1000 $^{\circ}\text{C}$ under a nitrogen atmosphere. Samples for TG were prepared in an identical manner to those for XRD; first arresting the hydration and removing the free-water of the various cement samples followed by crushing, grinding and sieving to form a powder of $\leq 63\text{ }\mu\text{m}$.

3.8. Microstructure Analysis

3.8.1. Scanning Electron Microscopy

Scanning Electron Microscopy (SEM) was used to study the microstructure, morphology and composition of cement samples [155]. SEM is a versatile technique which allows a user to observe a sample over a broad range of scales, from the hundreds of microns down to the nanometre scale. A scanning electron microscope utilises an electron gun to generate electrons which are accelerated through a series

of lenses and apertures in order to condense and focus them into a monochromatic electron beam, typically 5-100 Å in diameter. The electron beam passes through a set of scanning coils which direct the beam in a scanning pattern across the surface of the sample. When high energy electrons bombard a sample, different interactions between electrons and the material occur within the near surface including the emission of secondary electrons, backscattered electrons and the generation of X-rays.

SEM was used in two imaging modes; Secondary Electron Imaging (SEI) or Backscattered Electron Imaging (BEI). In the former, low energy secondary electrons (typically < 50 eV) emitted from the interaction between the incident beam of high energy electrons with the atoms of the sample via inelastic collisions are detected and used to build an image of the surface topography of the sample. Due to the relatively low energies of these secondary electrons, only those from the surface (a very thin layer of tens of nanometres) are able to emerge from the sample. In the case of BEI, the image is derived from scattered or reflected electrons from elastic collisions of the high energy electron beam with nucleus of the atoms at high angles approaching 180°. The yield of backscattered electrons is a function of atomic number. Heavier elements, i.e. those with higher atomic number, reflect a greater proportion of electrons and so appear brighter, and lighter elements with a low atomic number reflect a lower proportion of electrons and appear darker. The contrast indicates the average atomic number of the elements present within the microstructure and is indicative of the varying elemental compositions. In the case of intrinsically porous materials, such as cements, porosity will appear black.

SEM analysis was performed using a JEOL JSM6400 scanning electron microscope. The majority of samples were polished surface samples prepared by first arresting the hydration of small crushed pieces as described previously, which were then mounted in epoxy resin and allowed to set for a minimum of 24 h, ground using silicon carbide grinding paper of increasing fineness (i.e. P120, P240, P400, P800, P1200) and then polished using polishing clothes and diamond paste of 6 μm , 3 μm , 1 μm , $\frac{1}{4}$ μm fineness. To avoid build-up of charge on the samples when analysed, silver dag was used to paint around the circumference of the cylindrical mount and a conductive path between each sample and the circumference. The painted samples were allowed to dry for a minimum of 24 h and were then carbon coated.

3.8.2. Energy Dispersive X-ray Spectroscopy

Energy Dispersive X-ray spectroscopy (EDX) was used to examine the elemental composition of various cement samples. In this technique, a sample is bombarded by electrons of sufficiently high energy, i.e. greater than the critical excitation energy, and the inner shell electrons are ionised and ejected from the atoms of that material. A higher energy electron from an upper shell then makes the transition to fill the vacancy resulting from the ionisation and a characteristic X-ray is liberated corresponding to the energy difference between the respective shells. A detector is used to quantify the number of characteristic X-rays of a given energy.

EDX was used for point spectra analysis and elemental mapping analysis in the present study. In the former analysis, the electron beam is focused onto a fixed point of the sample and an analysis performed for up to 3 min. The typical electron beam interaction volume has a diameter of *ca.* 1-2 μm . The latter allows the distribution of elements within the microstructure of a sample to be determined. A series of scans

are performed over the required area of the sample for a given characteristic X-ray energy which corresponds to a particular element of interest. The resulting data are presented as separate images for each element of interest, or as a composite image in order to ascertain phase distributions. A Link ISIS EDX analyser integrated with the JEOL JSM6400 scanning electron microscope was used throughout the work presented here.

3.9. Hydrogen Generation Measurements

The corrosion of aluminium was assessed by measuring the volume of hydrogen gas generated by aluminium encapsulated in various cementitious systems and formulations. This was achieved by utilising a water displacement experimental setup as illustrated in Figure 3.4.

Either a 100 ml or 250 ml measuring cylinder was filled with distilled water and upturned within a 5 litre glass beaker such that the cylinder was full of water. The level of the water in the beaker was noted in order to allow correction due to evaporation.

50 ml Securitainer poly-pots were filled with the relevant cement, in which aluminium strips of 50 mm x 20 mm x 3 mm were immediately submerged. The poly-pots were then placed in specially made two-piece glass vessels that provided a water-tight seal using silicone grease. The glass vessels possessed a *ca.* 1 mm diameter spout, from which the hydrogen gas could escape. The base of the glass vessels was partially filled with refractory sand in order to avoid issues of buoyancy. The glass vessels were submerged in the water within the 5 litre beaker and the end of the spout placed underneath the upturned measuring cylinder to trap any escaping gas.

Measurements were taken every hour for the initial 6 hours and once a day for the first 9 to 10 days. Thereafter, measurements were recorded every 2 to 3 days for a period of 180 days. The measuring cylinders were replaced when they were nearing capacity. Generally, 100 ml and 250 ml cylinders were used when the rate of gas generation was relatively low and high, respectively.

In addition to the tested systems, a control system using a 25 ml measuring cylinder and 2 litre beaker, but with no sample was also prepared. Because the volume of gas is sensitive to the atmospheric pressure and temperature, these values were also recorded. The volume of the generated hydrogen gas was estimated based on the measured values in comparison with the control system.

3.10. Pore Solution Expression

Samples for pore solution expression were prepared using the procedure described in Section 3.4.2 followed by casting into 320 ml Securitainer poly-pots (62 mm diameter, 113 mm height). The samples were cured at 20 °C and 95% RH for curing periods of 28 days and 90 days.

In order to express the pore solution, the samples were sent to the School of Planning, Architecture and Civil Engineering at Queen's University Belfast. The samples were placed in the chamber of a pore solution extraction instrument (Figure 3.6). The samples were placed in a chamber and a penetration cone with a PTFE seal was placed on top of the sample followed by a piston, which transferred the load from a loading device. The chamber was then placed in the loading device and a cyclic load of up to 300 tonnes was applied to the sample. A drain pipe and vessel were connected to the drain of the chamber that allowed any liquids extracted from the samples to be collected. The resulting pore solutions were analysed by

Inductively Coupled Plasma Optical Emission Spectrometry (ICP-OES) and pH measurements.

3.11. pH measurements

pH measurements of the wet cement pastes and pore solutions were performed using a pH electrode connected to a pH meter. The pH meter was calibrated before each reading was taken using buffer solutions at pH 7.00 and pH 10.00. When measuring the pH of wet cement pastes, the pH electrode was washed thoroughly in distilled water following each reading.

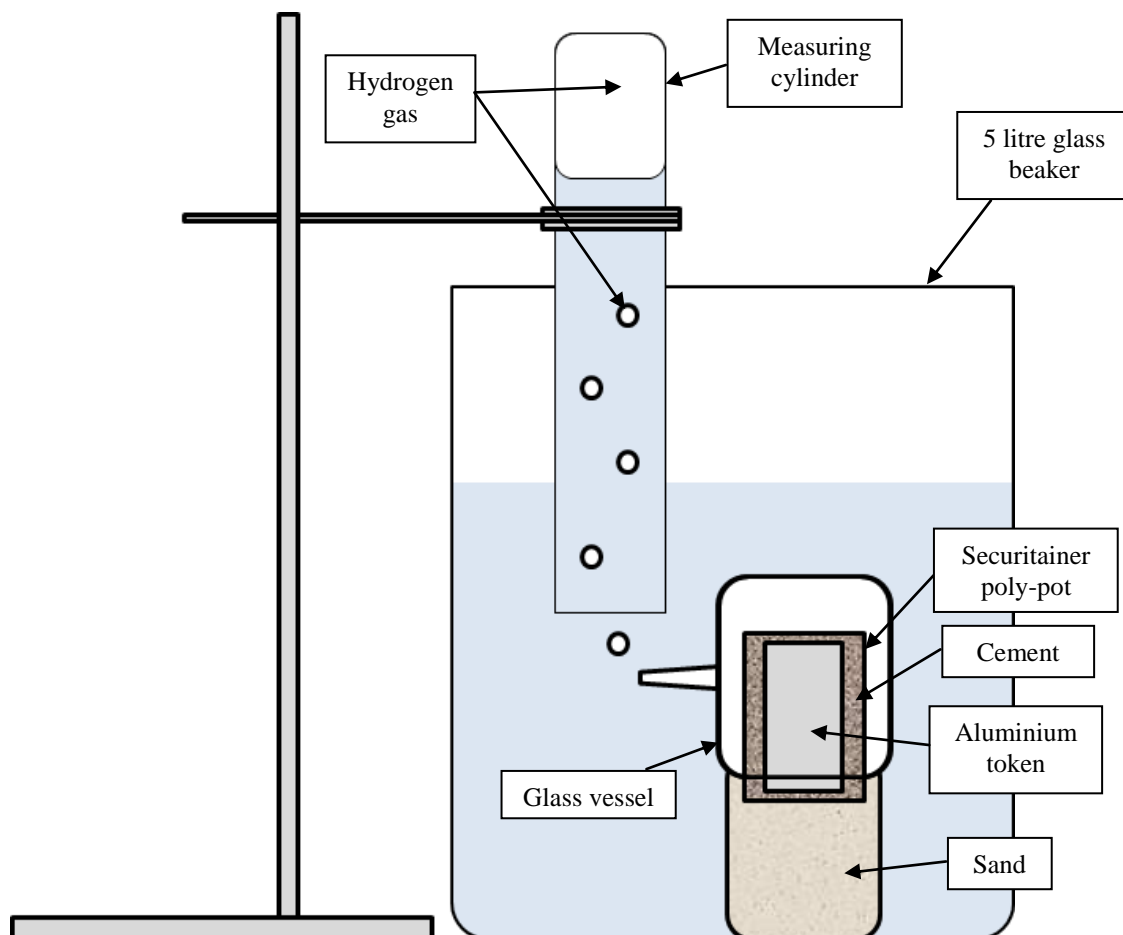


Figure 3.4 Diagrammatic representation of water displacement experimental setup for measuring hydrogen gas generation

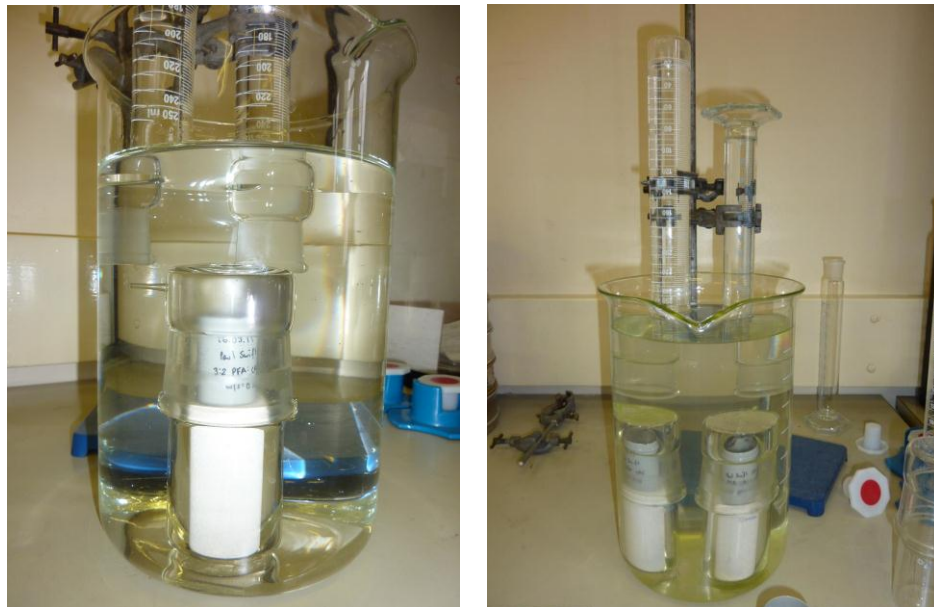


Figure 3.5 Photos of water displacement experimental setup for measuring hydrogen gas generation

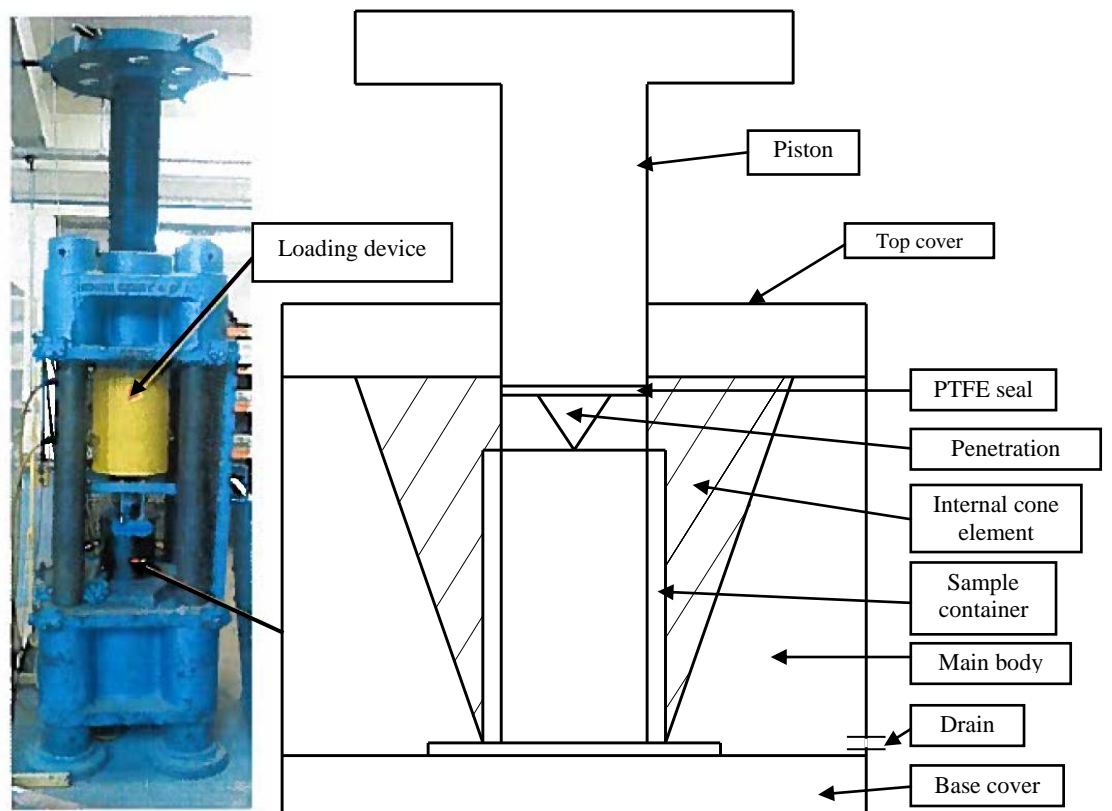


Figure 3.6: Pore solution extraction instrument and chamber

4. Results - Identification of Suitable Precursor Materials

4.1. Introduction

CAC was modified by various monophosphate- and polyphosphate-based solutions in order to identify a suitable phosphate powder for use in producing an appropriate CAP matrix for the encapsulation of ILW. Until now there has been no systematic study to identify a suitable phosphate precursor for the synthesis of a CAP cementing system for radioactive waste encapsulation. As candidate phosphates, some phosphate powders reported in the literature [138, 143, 144] were selected in addition to $\text{NaH}_2\text{PO}_4 \cdot 2\text{H}_2\text{O}$, $\text{NH}_4\text{H}_2\text{PO}_4$ and KH_2PO_4 .

4.2. Formulations

In order to identify a suitable phosphate powder for use in producing an appropriate CAP system for the encapsulation of ILW, various phosphate powders described in the Chapter 3 were mixed with Secar 51, as the CAC powder, and water. The w/c and p/c of the formulations, which were based on preliminary scoping trials, were 0.37 and 0.2, respectively. Samples of unmodified Secar 51 were hydrated at the same w/c (0.37) to allow direct comparison with the phosphate-modified systems. The formulations are shown in Table 4.1.

Table 4.1 Cementitious system formulations

Phosphate Type	Formulation					Total (wt%)
	Formulation ratios		Constituents (wt%)			
	w/c	p/c	CAC	Phosphate	Water	
None	0.37	0	72.99	0	27.01	100
$\text{NaH}_2\text{PO}_4 \cdot 2\text{H}_2\text{O}$	0.37	0.2	63.69	12.74	23.57	100
KH_2PO_4	0.37	0.2	63.69	12.74	23.57	100
$\text{NH}_4\text{H}_2\text{PO}_4$	0.37	0.2	63.69	12.74	23.57	100
$(\text{NaPO}_3)_n$	0.37	0.2	63.69	12.74	23.57	100
$(\text{NaPO}_3)_6$	0.37	0.2	63.69	12.74	23.57	100

4.3. Setting and Physico-mechanical Properties

Table 4.2 shows the results from Vicat setting time measurements for the phosphate-modified CAC systems and unmodified CAC. The unmodified CAC system exhibited initial and final setting times of 330 min and 390 min, respectively. The phosphate modifications resulted in a decrease in the initial setting time of the cement pastes. As shown in Figure 4.1, the setting time appears to be related to the amount of phosphorus introduced to the system. For the final set, although monophosphate-modified systems exhibited an initial setting time ranging from *ca.* 5-180 min, they did not exhibit a final set. In other words, the monophosphate-modified CAC showed some degree of thickening but did not fully harden. As such the compressive strength of these systems was not determined.

The $(\text{NaPO}_3)_n^-$ and $(\text{NaPO}_3)_6^-$ -modified formulations exhibited rapid setting, with initial and final set of *ca.* 5-6 min and *ca.* 11-12 min respectively. On setting, these polyphosphate-modified CAC systems produced a significant exotherm, though no quantitative data was obtained. This exotherm was attributed to the acid-base setting reactions.

These polyphosphate-modified systems attained compressive strengths of *ca.* 75 MPa after 24 h, which is significantly strong compared to *ca.* 40 MPa for conventionally hydrated CAC (Figure 4.2). The strength of $(\text{NaPO}_3)_n^-$ and $(\text{NaPO}_3)_6^-$ -modified systems increased over the first 3 days of curing, then exhibited further strength development to values of *ca.* 95 MPa after 28 days of curing, which was more than four times the compressive strength of the conventionally hydrated CAC system after the same curing period.

The unmodified CAC system exhibited rapid strength gain in the first 24 h of curing, which was followed by a strength regression up to 14 days, after which the strength appeared to plateau. This strength regression up to 14 days is attributable to the thermodynamically-driven metastable to stable phase conversion reactions, which are widely discussed in the literature [63, 65, 75, 84].

Sugama and Carciello studied compressive strength of sodium monophosphate- and sodium polyphosphate-modified CAC after 24 h curing at room temperature, with varying concentration of phosphate solutions [138]. Similarly to the present study, they reported that monophosphate systems did not set and as such compressive strength could not be measured. Their sodium polyphosphate-modified CAC systems attained compressive strengths between *ca.* 6.9-28.4 MPa (data points shown in Figure 4.2) after 24 h curing, which are significantly lower than the strength obtained in the present study. The difference in compressive strength compared to those observed in the present work is likely due to differences in the CAC used and the formulations investigated. In the work by Sugama and Carciello, the effective w/c ratios of the systems derived from 20 wt%, 30 wt%, and 40 wt% solutions were 0.53, 0.47 and 0.4, respectively, compared to w/c = 0.37 for the systems studied here. It is suggested that the higher w/c ratio would result in higher porosity and therefore lower compressive strength.

Table 4.2 Vicat setting time measurements for various phosphate-modified CAC systems

Formulation (phosphate modification)	Initial setting time (min)	Final setting time (min)
Unmodified	330 (± 15)	390 (± 15)
NaH ₂ PO ₄ ·2H ₂ O	30 (± 5)	*
KH ₂ PO ₄	180 (± 7.5)	*
NH ₄ H ₂ PO ₄	6 (± 0.5)	*
(NaPO ₃) _n	6 (± 0.5)	11 (± 0.5)
(NaPO ₃) ₆	5 (± 0.5)	12 (± 0.5)

Note: * = Did not exhibit final set

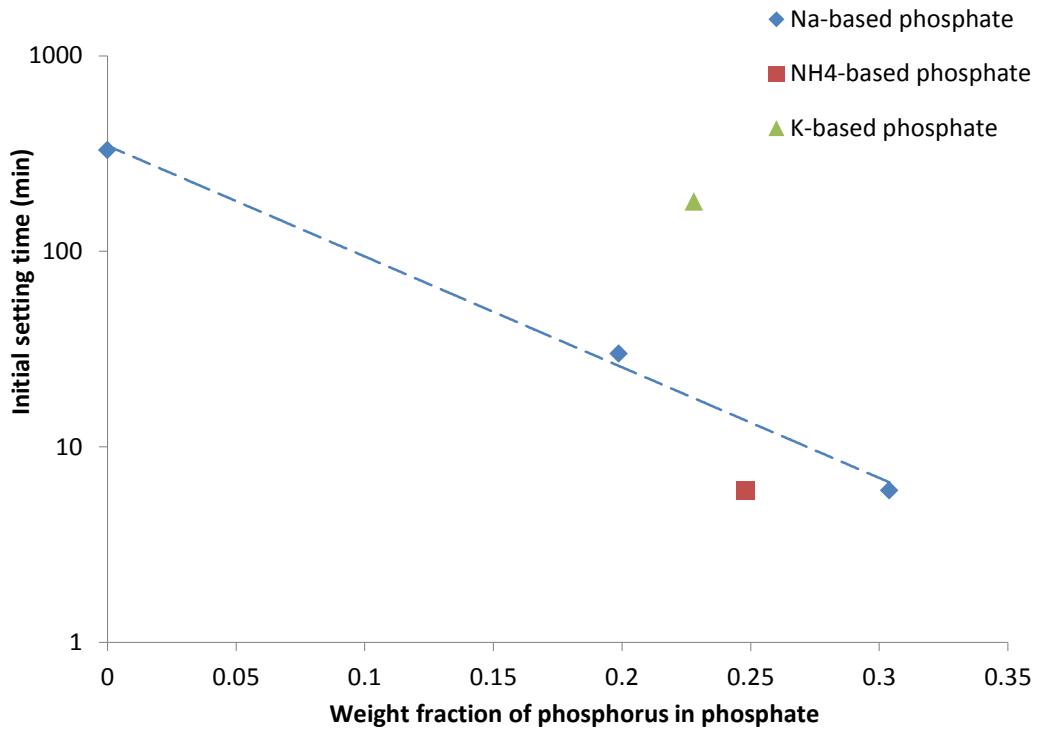


Figure 4.1 Correlation between amount of phosphorus and initial setting time

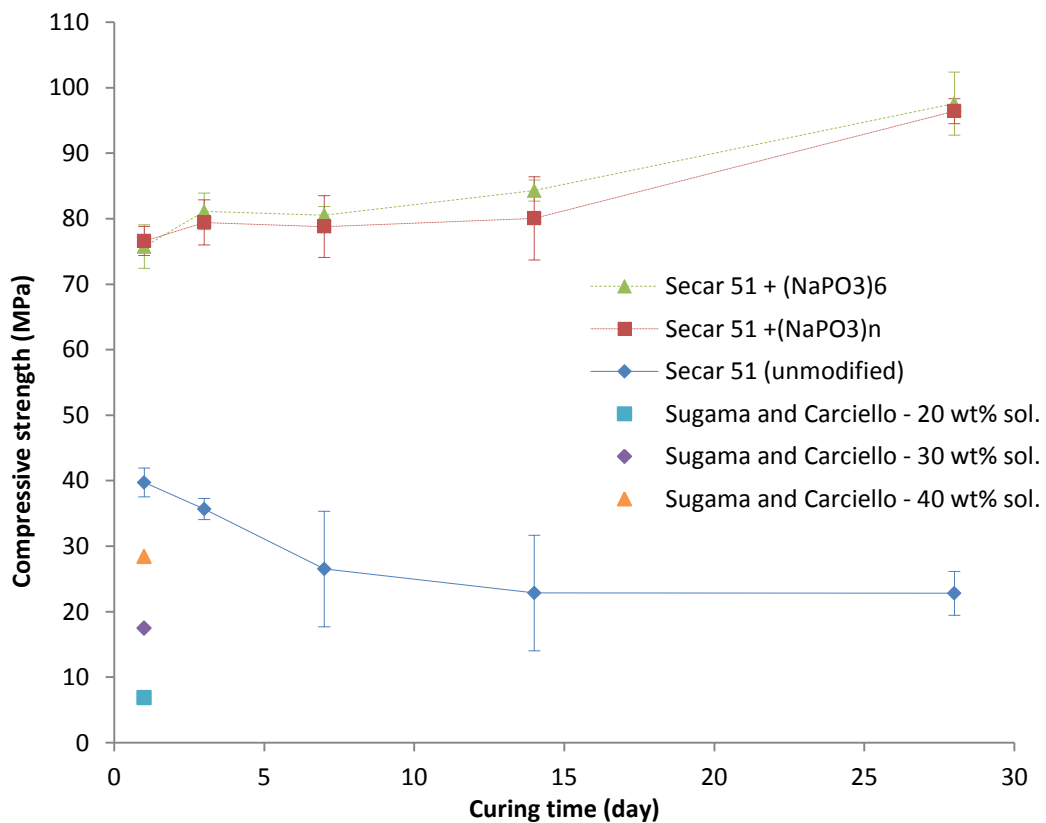


Figure 4.2 Compressive strength of selected formulations up to 28 days

4.4. Phase Analysis

4.4.1. XRD

Figure 4.3 shows the XRD results for the various systems investigated. In anhydrous CAC, CA was the principle crystalline phase present, and C_2AS and CT are present as secondary phases. When hydrated for 7 days, tricalcium aluminate hexahydrate (C_3AH_6) and gibbsite ($\gamma-AH_3$) were identified as hydration products. These phases are known to be stable hydrate phases in conventionally hydrated CAC [65, 75]. The CA-related reflections, the principal of which was observed at *ca.* $30^\circ 2\theta$, decreased in intensity due to CA being consumed in the hydration reactions. The reflections relating to C_2AS and CT also remained present with little or no loss in intensity, suggesting they took little part in the hydration reactions.

The XRD results of the phosphate-modified formulations were very similar to that of anhydrous CAC. The crystalline phases identified were identical to those in the anhydrous CAC powder, with CA present as the principle crystalline phase, and C_2AS and CT present as secondary phases. The $(NaPO_3)_n$ -based system also exhibited very weak reflections associated with the stable crystalline hydrate phase, C_3AH_6 . In some formulations, the intensities of CA-related reflections (*e.g.* the principle reflection at *ca.* $30^\circ 2\theta$) had significantly decreased compared to that of anhydrous CAC powder, suggesting that CA had been consumed in reactions. Polyphosphate modifications caused a larger reduction in the intensity of the CA-related reflections, which was symptomatic of more CA having been consumed in these systems. As discussed previously, all the systems showed at least some degree of thickening and in the case of polyphosphate-modified CAC systems exhibited rapid setting and strength development. However, as no significant crystalline hydrate phases were identified, except the minor formation of C_3AH_6 in $(NaPO_3)_n$ -

based system, it is suggested that the introduction of phosphate must have modified the normal hydration mechanism of CAC. It is therefore suggested that the phase responsible for setting, and in the case of polyphosphate-modified CAC systems high strength development, are of an amorphous nature.

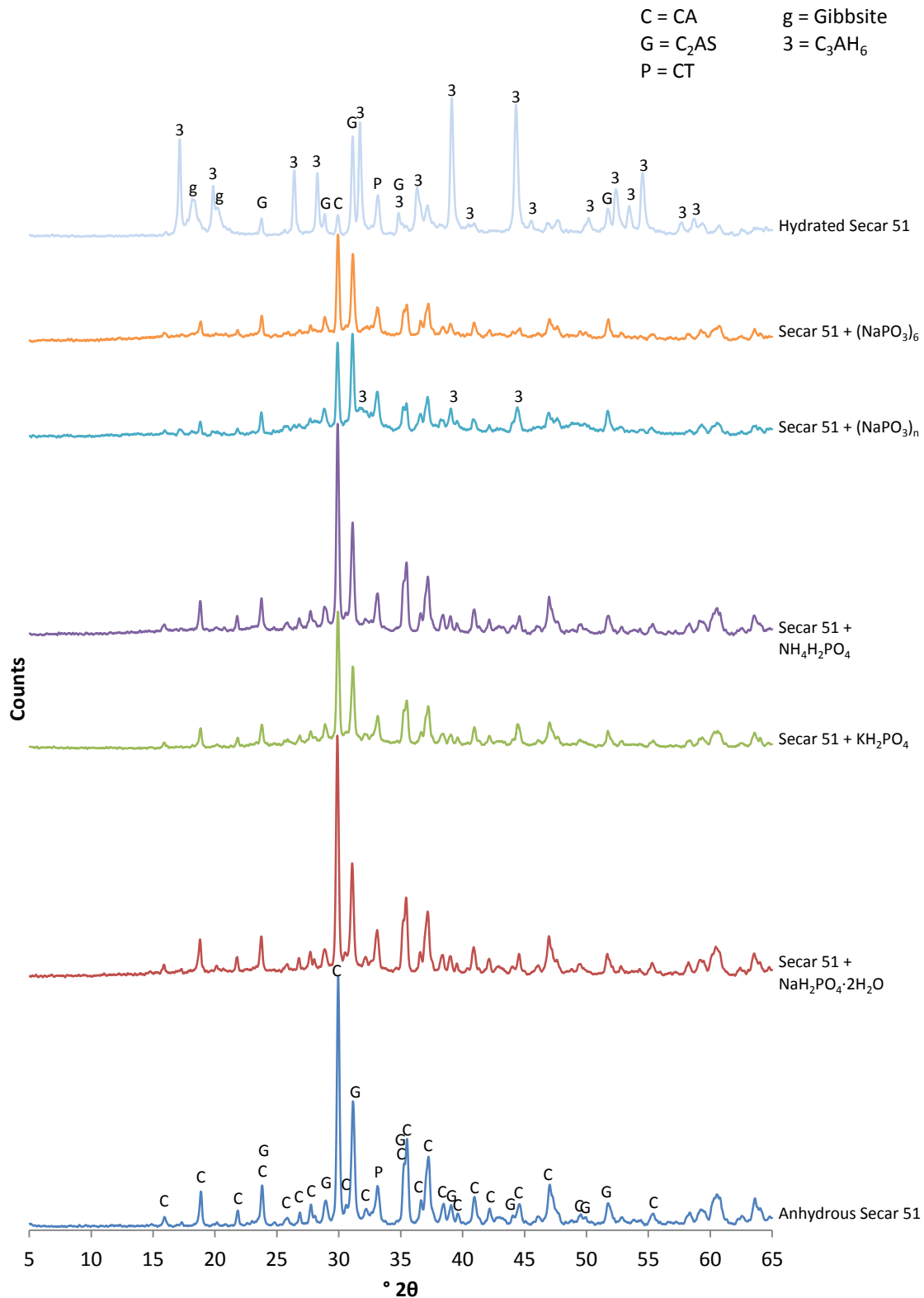


Figure 4.3 XRD results for anhydrous and hydrated CAC, and various phosphate-modified CAC systems after 7 days curing

4.4.2. TG

The TG results are shown in Figure 4.4. The total weight loss of the various systems up to *ca.* 1000 °C varied significantly and can be categorised into three groups; the conventionally hydrated Secar 51 (24.1 wt%), the polyphosphate-modified CAC systems (15.4-16.7 wt%), and the monophosphate-modified CAC systems (7.9-10.1 wt%). These results show that phosphate-modified systems exhibit distinct dehydration behaviour to that of unmodified CAC, assuming most of the weight loss observed in the TG results is due to the dehydration of reaction products.

The DTG curves for monophosphate- and polyphosphate-modified systems up to 500 °C are shown in Figure 4.5 and Figure 4.6, respectively, along with the result from unmodified hydrated CAC. Conventionally hydrated Secar 51 experienced principal overlapping weight losses over the range *ca.* 200-360 °C, which encompasses the temperature range during which γ -AH₃, and C₃AH₆ dehydroxylate and dehydrate, respectively [84]. This supports the XRD results, which asserted that C₃AH₆ was the primary crystalline phase present after 7 days of hydration, with γ -AH₃ also present as a secondary crystalline phase.

Phosphate-modified systems exhibited distinct weight loss behaviours to those of conventionally hydrated Secar 51, with the majority of weight loss occurring over the temperature range *ca.* 50-200 °C and additional minor weight losses at *ca.* 230-280 °C. In addition, the (NaPO₃)_n-modified system exhibited a small weight loss at *ca.* 280-360 °C, which corresponds to the dehydration of C₃AH₆ [84].

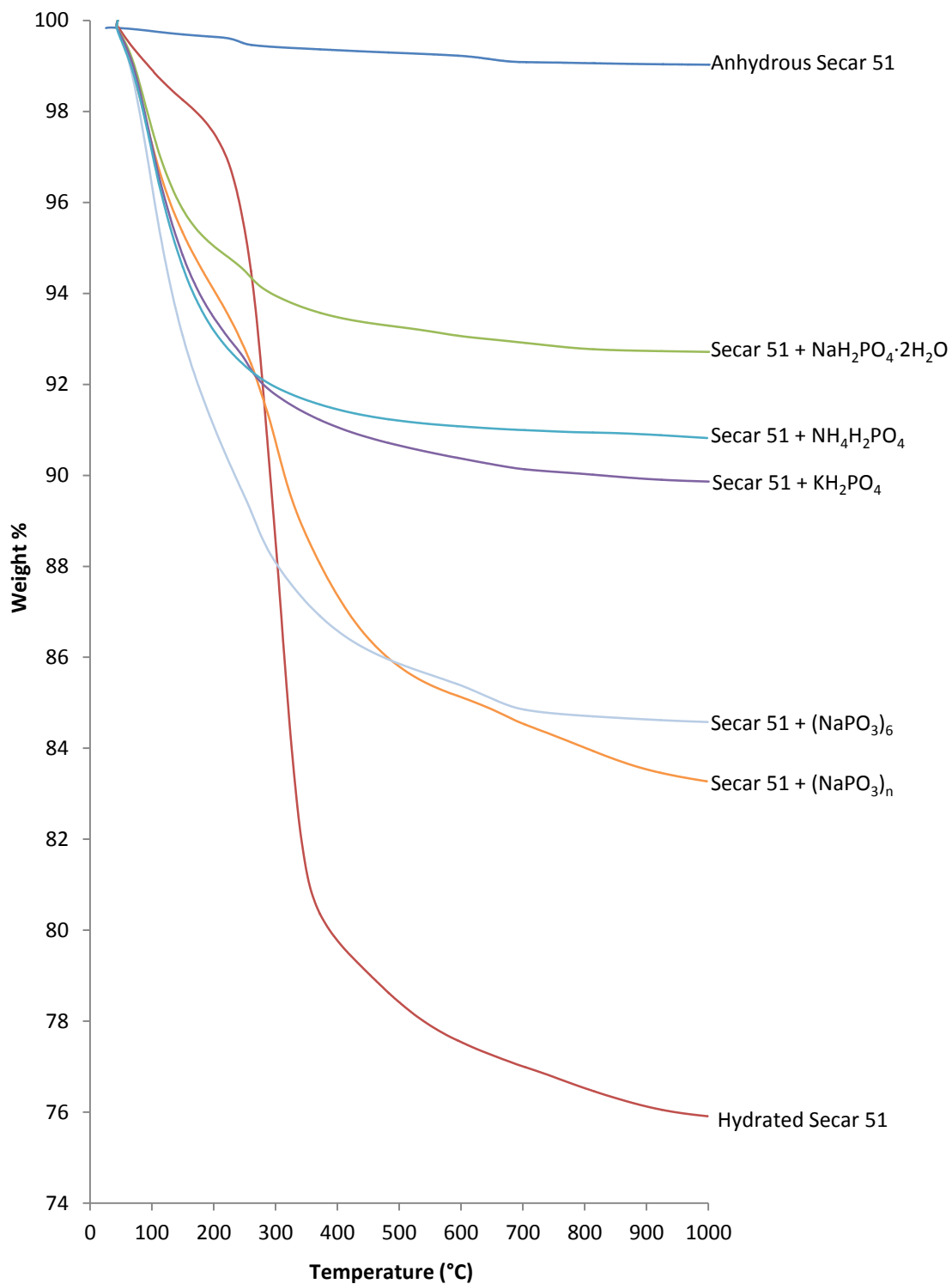


Figure 4.4 TG of an anhydrous and hydrated CAC and various phosphate-modified CAC formulations after 7 days of curing

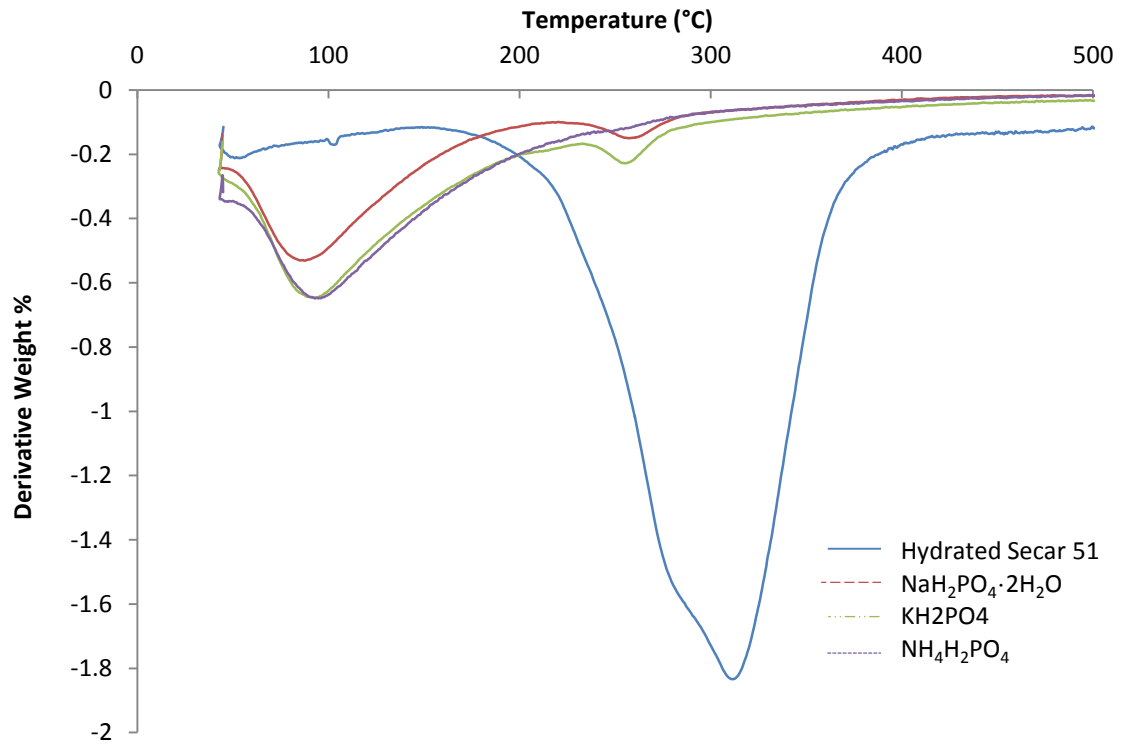


Figure 4.5 DTG of hydrated CAC and monophosphate-modified CAC systems after 7 days curing

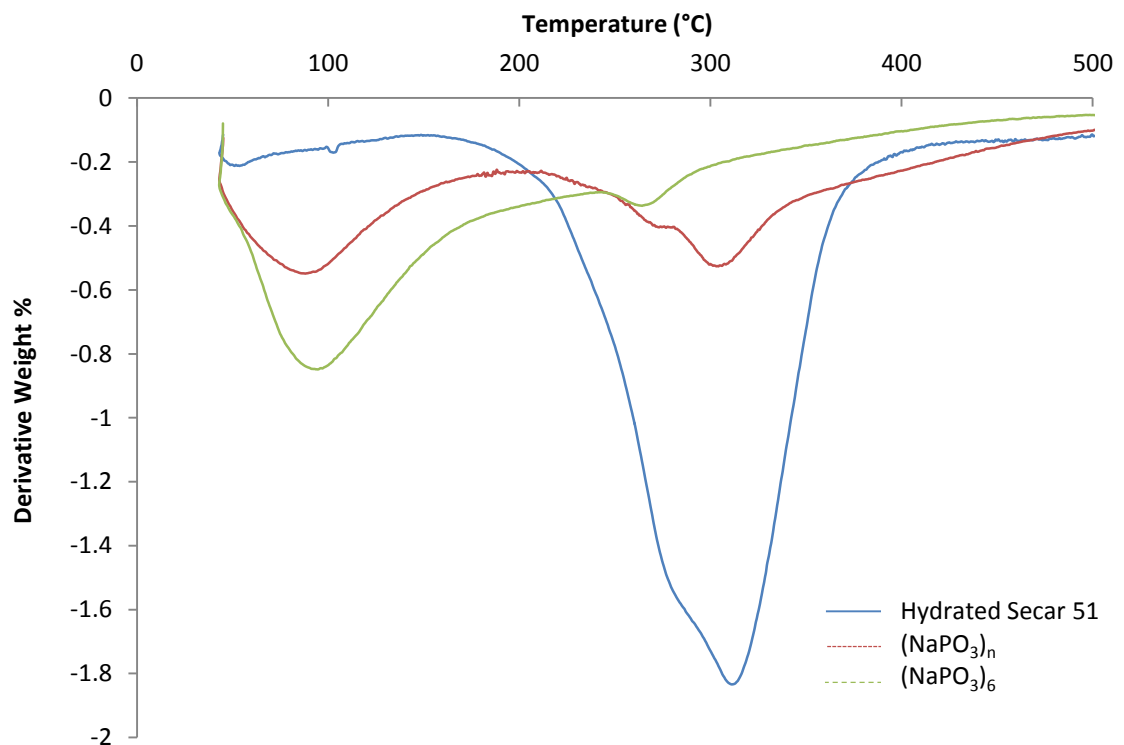


Figure 4.6 DTG of hydrated CAC and polyphosphate-modified CAC systems after 7 days curing

4.5. Microstructure

BEI micrographs obtained from SEM analysis of a $(\text{NaPO}_3)_n$ -modified CAC (Figure 4.7) revealed a microstructure of partially- and un-reacted CAC particles (light grey and medium grey angular particles) surrounded by a dense binding matrix (grey). Micro-cracks and porosity were apparent within the dense matrix as denoted by the dark grey/black cracks and small round features. Micro-cracks may have been the result of thermally induced stresses caused by the exothermic acid-base setting reactions or may have occurred during sample preparation.

EDX elemental mapping (Figure 4.8) showed that the CAC particles consisted of calcium, aluminium, silicon and oxygen. As a matter of fact, the particles appeared to be a binary system or solid-solution consisting of a region rich in calcium, aluminium and oxygen (medium grey) and another rich in calcium, aluminium, silicon and oxygen (light grey). It is likely that the former was CA and the latter C_2AS . The amorphous binding matrix observed in $(\text{NaPO}_3)_n$ -modified CAC consisted of calcium, aluminium, phosphorus and oxygen, with trace amounts of silicon and sodium.

Table 4.3 shows the results from EDX point spectra of the amorphous binding phase, calculated as the average of 12 individual point spectra.

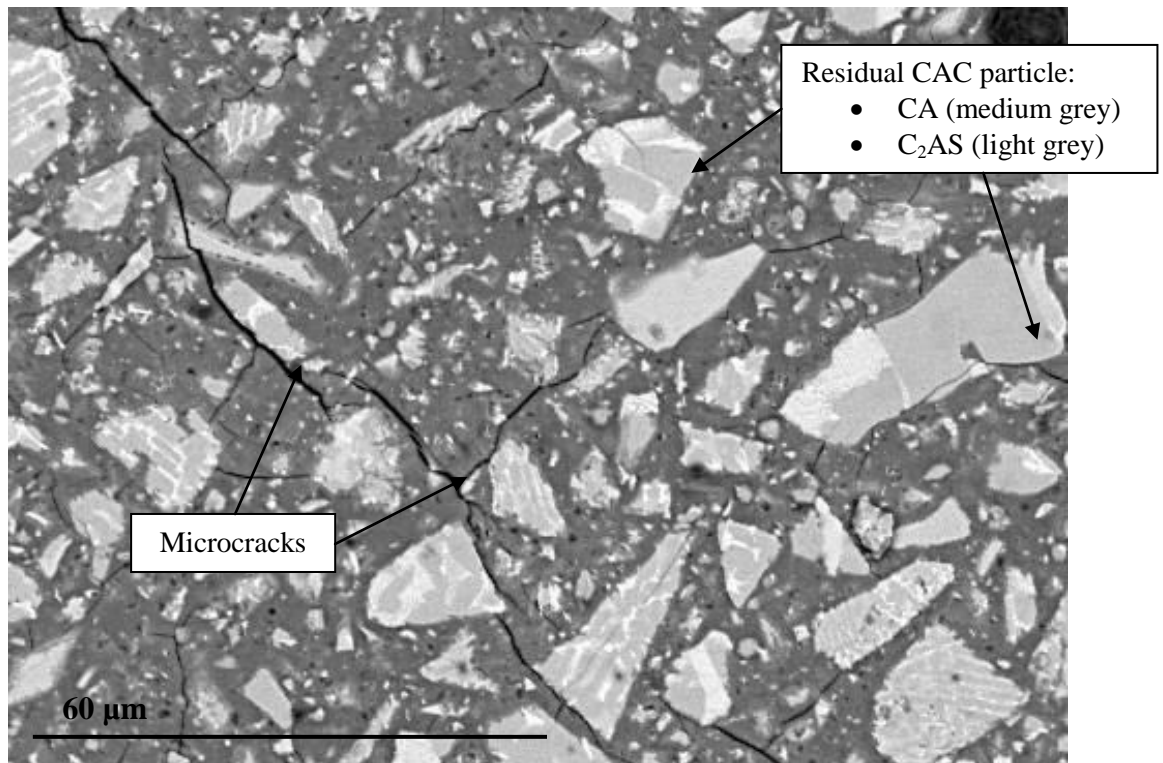


Figure 4.7 SEM-BEI micrograph of polished $(\text{NaPO}_3)_n$ -modified CAC after 7 days

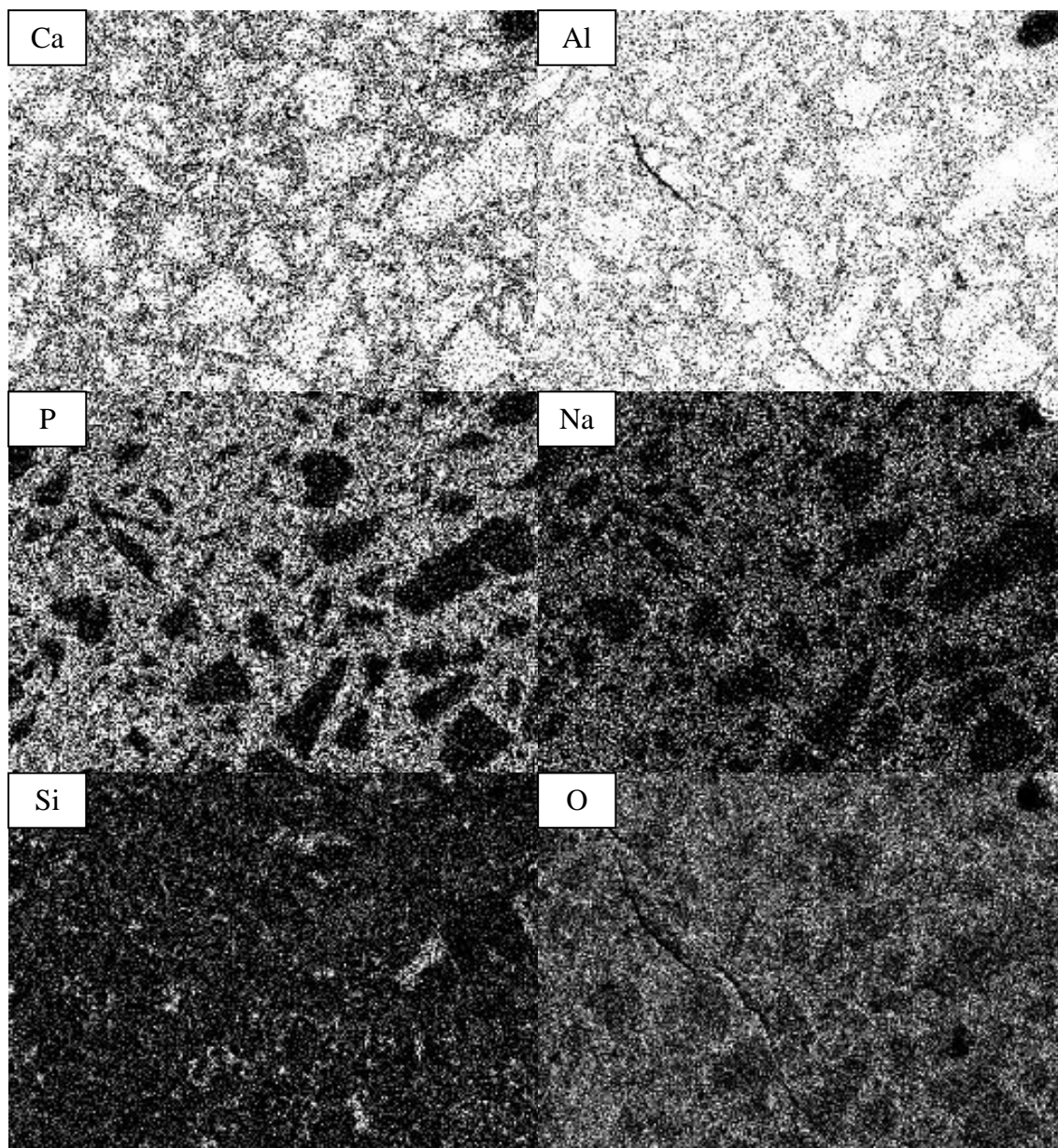


Figure 4.8 EDX elemental maps of polished $(\text{NaPO}_3)_n$ -modified CAC after 7 days

Table 4.3 EDX point spectra data for amorphous binding phase in $(\text{NaPO}_3)_n$ -modified CAC

Element	Atomic %	S.D. (%)
Ca	13.9	2.3
Al	16.9	1.9
P	6.6	1.2
Na	2.4	0.6
Si	1.1	0.3
O	59.1	0.5

4.6. Discussion

Ma and Brown investigated systems derived from Secar 71 and various sodium-based phosphates [143, 144]. Walter and Odler mixed Secar 51 and Secar 71 with sodium polyphosphates of varying chain lengths [107]. Both groups [143, 144] reported similar XRD results as were observed in the present study. They reported that the usual crystalline calcium aluminate hydration products were not developed, despite improved mechanical properties compared to unmodified CAC. As with the result obtained in the present study, this suggests that the phases responsible for setting and strength development in phosphate-modified systems are of an amorphous nature.

The TG results showed that phosphate-modified systems exhibited distinct behaviours compared to conventionally hydrated CAC systems when subjected to a heating regime. In conventionally hydrated CAC, weight losses in the temperature range *ca.* 50-200 °C could be attributable to the dehydration of alumina gel (AH₃-gel) or the calcium aluminate hydrate amorphous phase (C-A-H) described by Bushnell-Watson and Sharp [84], as well as the crystalline CA-hydrate phases, i.e. CAH₁₀ and C₂AH₈. In addition, some of the weight loss below 100 °C may be due to the evaporation of residual free-water and acetone, though this contribution is thought to be minimal. For the phosphate-modified systems investigated here, the initial weight loss events were more likely to be the result of the dehydration of an amorphous phase because, as previously discussed in the XRD results, significant crystalline phases were not observed. This amorphous phase may be AH₃-gel or C-A-H gel, but it may also be a distinct amorphous hydrate phase that incorporates some phosphate, e.g a calcium phosphate-based amorphous phase. The small weight loss *ca.* 230-270 °C may be due to the dehydroxylation of AH₃-gel or aluminium

hydroxide; either gibbsite (γ -AH₃) or bayerite (α -AH₃). In addition, the (NaPO₃)_n-modified system exhibited a small weight loss at *ca.* 280-360 °C, which corresponds to the dehydration of C₃AH₆ [84]. This is supported by the XRD results, which suggested that C₃AH₆ was present as a minor phase

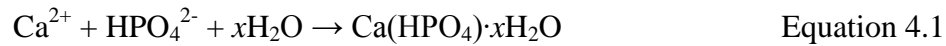
The SEM results discussed previously showed a microstructure of residual CAC particles embedded within a binding matrix. A similar microstructure, observed by Walter and Odler [107], was described as a homogeneous, compact matrix without crystallinity in which residual CAC particles were embedded. They also observed cracks within the cement matrix, attributing them to chemical shrinkage which occurred during hardening. Chemical shrinkage is considered as any change in volume resulting from the hydration and setting reactions [65, 156]. Shrinkage may occur as the result of the formation of new solid phases and is related to the constriction effects, where the water molecules incorporated into the new solid phases have a lower effective molar volume.

The microstructural development of various sodium phosphate-modified CAC systems has also been studied by Ma and Brown [144] using Environmental Scanning Electron Microscopy (ESEM). They also observed the formation of an amorphous phase, which bound the CAC particles, resulting in superior mechanical properties compared to conventionally hydrated CAC. It is suggested that a similar binding mechanism was responsible for the high compressive strength exhibited by the polyphosphate-modified CAC systems in the present study. As previously discussed, monophosphate-based systems did not fully harden or develop significant strength. Therefore, although the TG results suggested the existence of a similar amorphous phase to that in the polyphosphate-derived systems, the nature of the

amorphous phase in the monophosphate-modified system must be different from that in polyphosphate-modified systems.

The exact composition and formation mechanism of the amorphous binding matrix is not well understood in the literature. Ma and Brown [144] used EDX to determine the chemical composition of cement pastes resulting from mixing CAC with various sodium phosphates, observing that the amorphous binding phase consisted of calcium, aluminium, and phosphorus. They inferred that the binding phase was an amorphous calcium aluminate phosphate hydrate (C-A-P-H) gel, the microstructure and composition of which was variable and phosphate dependant. On the other hand, Sugama *et al.* suggested a combination of a calcium phosphate-based amorphous phase and alumina gel. Using X-ray Photoelectron Spectroscopy (XPS), Sugama and Allen [134] reported that on mixing with calcium aluminate compounds with an ammonium phosphate-based fertiliser (Poly-N), the phosphate material reacted preferentially with Ca rather than Al to form ammonium calcium phosphate hydrate ($\text{NH}_4\text{CaPO}_4 \cdot x\text{H}_2\text{O}$) and alumina gel. Sugama and Carciello [138] investigated sodium monophosphate- and sodium polyphosphate-modified CAC cement systems using Fourier Transform Infrared Spectroscopy (FTIR). They suggested that on mixing a $(\text{NaPO}_3)_n$ -based solution with CAC, amorphous sodium calcium orthophosphate hydrate ($\text{NaCaPO}_4 \cdot x\text{H}_2\text{O}$) was formed as the principle reaction product, and was responsible for setting and strength development. In a later study, Sugama *et al.* [145] proposed an alternative composition and formation mechanism of the paste binding phase. Having investigated a $(\text{NaPO}_3)_n$ -modified CAC/PFA system, they suggested that hydrogen phosphate anions (HPO_4^{2-}) produced by the dissolution of sodium polyphosphate reacted favourably with calcium cations released from CAC, to form calcium hydrogen phosphate hydrate ($\text{Ca}(\text{HPO}_4) \cdot x\text{H}_2\text{O}$) according to

Equation 4.1 below. Concurrently, the decalcification of CAC particles liberated reactive alumina, which hydrated to form alumina gel ($\text{Al}_2\text{O}_3 \cdot x\text{H}_2\text{O}$) as shown below in Equation 4.2.



The TG results obtained in the present study support the assertion that alumina gel or at least similar local environment in the amorphous matrix was present as a reaction product, and EDX confirmed the binding matrix contained Ca, P and Al. Therefore, the amorphous binding matrix obtained in a $(\text{NaPO}_3)_n$ -modified CAC appears to be composed of a combination of a calcium phosphate-based phase and alumina gel or two distinct local environments similar to them.

In addition, as the system contains a significant amount of sodium derived from the sodium phosphates used, it should be taken into account. Therefore an alternative composition is proposed for this amorphous binding matrix, albeit via a similar formation mechanism as that suggested by Sugama *et al.* [145]. It is proposed that, on dissolution, $(\text{NaPO}_3)_n$ forms hydrogen phosphate anions which react favourably with calcium cations liberated from CAC, to form amorphous calcium phosphate (ACP, $\text{Ca}_x\text{H}_y(\text{PO}_4)_z \cdot n\text{H}_2\text{O}$) [124, 125]. ACP has variable composition with Ca/P ratio of *ca.* 1.0-2.2, as well as a flexible structure which can incorporate sodium. The results from the EDX point spectra obtained in this study suggested a Ca/P ratio *ca.* 2, which exists within the range for ACP. In addition, a significant amount of sodium may be incorporated into the ACP by substitution for calcium as the ionic radius of Na^+ (0.102 nm) is similar to that of Ca^{2+} (0.100 nm) [157]. As described by Sugama *et al.* [145], hydrated alumina gel would also be formed due to the

decalcification of CAC particles. ACP has been shown to lose adsorbed water up to *ca.* 120 °C, which may account for some of the weight loss exhibited in TG results [158]. ACP has also been reported to gradually lose chemically bound water molecules up to *ca.* 600 °C [158].

4.7. Summary

The results presented in this chapter are consistent with the previous studies and provide additional information on how phosphate modifications significantly affect the setting, mechanical properties and phase composition of CAC-based cementitious systems. The setting and compressive strength development was dependent on the type of phosphate modification; monophosphate-modified formulations did not fully set or develop significant compressive strength, whereas polyphosphate-modified formulations exhibited rapid setting and high strength development.

Although the phosphate-modified systems exhibited similar XRD results, monophosphate-modified systems showed little reduction in the intensity of CA-related reflections, suggesting that very little reaction had occurred and that monophosphate modifications restricted the normal mechanism of CAC hydration. In contrast, the polyphosphate-modified CAC formulations exhibited considerable reduction in the intensity of CA-related reflections, suggesting that significant amounts of CA had been consumed during the acid-base reactions.

Furthermore, these reactions were distinct from the usual hydration mechanism of CAC, as the normal calcium aluminate hydrate phases were not formed. Instead, polyphosphate-modified CAC resulted in the formation of amorphous reaction products, which acted as binding phases between the partially- and un-reacted CAC particles, and were responsible for the high strength development. The results

presented here suggest that hydration was modified rather than accelerated, as described by other researchers [143, 144]. Together with the TG results, it is proposed that the binding matrix consisted of ACP and hydrated alumina gel or similar local environment.

The work presented here has shown that monophosphate-based modifications are not suitable for producing cementitious matrices for radioactive waste encapsulation, based on the lack of setting or significant strength development. On the other hand, sodium polyphosphate-modified CAC set and developed significant strength. As such, these systems have potential as an alternative matrix for the encapsulation of LLW and ILW. However, the rapid setting and significant heat output generated by these systems mean that further development is required before use in industrial applications. Future work will assess the use of additives, such as SCMs and setting retarders to improve these characteristics.

5. Results – Development of CAP Formulation Envelope

5.1. Introduction

In the previous chapter, Secar 51, a commercially available CAC, and sodium polyphosphate were identified as suitable precursor materials, which resulted in a cementitious matrix exhibiting rapid setting (~ 11 minutes), and rapid and high strength development (> 75 MPa after 24 h curing). However, such a rapid setting time and considerable heat generated from the acid-base setting reactions deemed the system unsuitable for industrial application. Cementing systems used as encapsulating matrices for ILW in the UK are required to fulfil processing and property criteria, referred to as ‘plant acceptance tests’ or operational requirements [27, 28], which are defined to demonstrate suitability for industrial application. These plant acceptance tests include;

- Flow > 200 mm after 150 minutes;
- Initial setting time > 4 h;
- Final setting time < 24 h;
- Bleed water < 2 % by volume.

In the work presented in this chapter, two series of investigations were undertaken to further develop the cement system, in order to establish a formulation envelope which satisfies key factors in the plant acceptance tests. Preliminary setting time investigations assessed the effect of PFA and phosphate content whereas further investigations assessed the effects of varying formulation parameters (i.e. boric acid content, PFA content, water content) against the plant acceptance tests and other physico-mechanical properties.

5.2. Formulations

The formulations studied in the preliminary setting time investigations to assess the effect of PFA and phosphate content are presented in Table 5.1 to Table 5.3. These preliminary setting time investigations were based on an iterative approach with the aim being to identify a formulation or formulation envelope that fulfilled the minimum initial setting time requirement of 4 h. PFA was used as a SCM to reduce the heat generated during setting by acting as an inert filler material, as in the conventional PC-based cementing systems [4, 11]. Also, the incorporation of PFA is known to increase both the initial and final setting times [159], as well as improving the flow properties of cementitious systems by the so called ‘ball bearing effect’ [15, 147-149].

Table 5.1 presents the formulations with a fixed phosphate to cement ratio (p/c) to assess the effects of the replacement of CAC with PFA. The formulations were based on that studied in Chapter 4 i.e. $p/c = 0.2$ and water to solid ratio (w/s) = 0.37, to which PFA was added in increasing amounts in replacement for CAC. Two series of formulations were investigated using water to solid ratios⁴ (w/s) of 0.35 and 0.4, in order to also assess the effect of water content on setting time. It should be noted that the w/s ratios were still below that advised in order to avoid the detrimental effect of conversion as discussed in Chapter 2, while still being high enough to produce a cement paste that was workable. In these formulations, because the w/s ratio was constant, CAC and phosphate content decreases as the PFA to solid content ratio (f/s) increased, and the effective water to cement ratio (w/c) also increases.

⁴ where solid content was the total mass of PFA and CAC i.e. $s = c + f$

Table 5.2 presents the formulations investigated in order to assess the effects on setting time of varying phosphate content in terms of the p/c ratio. These formulations had a fixed f/s of 0.7. The f/s was defined based on the results of the formulations defined in Table 5.1, the results of which are discussed in Section 5.3. As with the series of formulation presented in Table 5.1, two series of formulations were investigated with two w/s ratios of 0.35 and 0.4. In the two series of formulations, the w/c was effectively constant.

Table 5.3 shows the formulations investigated in order to assess the effects on setting time of varying PFA content, in terms of f/s, whilst maintaining the phosphate to solid (p/s). Once again, two series of formulations were investigated with different w/s ratios of 0.35 and 0.4, in order to also assess the effects of water content. In each series of formulations, both the p/c and w/c increased with increasing f/s.

It was clear from the preliminary setting time investigations that, although variation of formulation parameters affected the setting time of the CAP system incorporating PFA as a SCM, a setting retarder was required in order to extend the setting time to fulfil the 4 h minimum requirement and satisfy other plant acceptance test criteria. Boric acid was selected as an inorganic setting retarder, as it is known to act efficiently in various cement systems, including CAC-based cementing systems [65, 86, 88].

The formulations studied to further develop the CAP system formulation, incorporating boric acid as well as varying the PFA and water content can be found in Table 5.4. These formulations were based on those investigated in the preliminary setting time studies, the results of which are discussed in Section 5.3, while also incorporating boric acid.

The formulations designated 'Varying H_3BO_3 ' were assessed with the aim of identifying a boric acid content that fulfilled the initial and final setting time requirements of 4 h and 24 h, respectively. The incorporation of boric acid was in terms of boric acid to CAC ratio (r/c), based on the assumption that the retarding effects resulted from the interaction of the boric acid with CAC. These formulations were assessed by the plant acceptance tests as described in Section 3.5 i.e. Vicat setting time measurement, Colflow test, bleed water evaluation.

The formulations designated 'Varying water' were assessed to characterise the effect of decreasing the w/c, principally in order to identify a minimum w/c that fulfilled industrial requirement for flow properties in terms of Colflow measurement. These formulations were assessed by the plant acceptance tests.

Following the iterative approach adopted in the development of the CAP formulation envelope, the results for the formulations presented above were interpreted in order to define those formulations designated 'Varying PFA' in Table 5.4. The relevant results and formulations were also reviewed and endorsed by the project industrial supervisor. The formulations designated 'Varying PFA' were investigated in more detail to assess the effect of varying the f/s ratio. The pH of the wet cement pastes was measured and plant acceptance tests were performed; Colflow test method to determine flow properties; Vicat setting time measurement to determine initial and final setting time; visual inspection to assess the bleeding. The physico-mechanical properties of selected formulations were investigated using compressive strength testing and MIP, and also characterised by phase and microstructure analysis using XRD, TG, and SEM incorporating EDX.

Table 5.1 Formulations to assess the effect of PFA content at p/c = 0.2*

Formulation ratios			Constituents (wt%)				Total (wt%)
f/s	w/s	p/c	CAC	PFA	(NaPO ₃) _n	H ₂ O	
0.4	0.35	0.2	40.82	27.21	8.16	23.81	100
0.5	0.35	0.2	34.48	34.48	6.90	24.14	100
0.6	0.35	0.2	27.97	41.96	5.59	24.48	100
0.7	0.35	0.2	21.28	49.65	4.26	24.82	100
0.8	0.35	0.2	14.39	57.55	2.88	25.18	100
0.9	0.35	0.2	7.30	65.69	1.46	25.55	100
0.4	0.4	0.2	39.47	26.32	7.89	26.32	100
0.5	0.4	0.2	33.33	33.33	6.67	26.67	100
0.6	0.4	0.2	27.03	40.54	5.41	27.03	100
0.7	0.4	0.2	20.55	47.95	4.11	27.40	100
0.8	0.4	0.2	13.89	55.56	2.78	27.78	100
0.9	0.4	0.2	7.04	63.38	1.41	28.17	100

* f/s, w/s and p/c denote fly ash to solid ratio, water to solid ratio and phosphate to cement ratio, respectively.

Table 5.2 Formulations to assess the effect of phosphate content at f/s = 0.7*

Formulation ratios			Constituents (wt%)				Total (wt%)
f/s	w/s	p/s	CAC	PFA	(NaPO ₃) _n	H ₂ O	
0.7	0.35	0	22.22	51.85	0.00	25.93	100
0.7	0.35	0.2	21.28	49.65	4.26	24.82	100
0.7	0.35	0.4	20.41	47.62	8.16	23.81	100
0.7	0.35	0.6	19.61	45.75	11.76	22.88	100
0.7	0.35	0.8	18.87	44.03	15.09	22.01	100
0.7	0.4	0	21.43	50.00	0.00	28.57	100
0.7	0.4	0.2	20.55	47.95	4.11	27.40	100
0.7	0.4	0.4	19.74	46.05	7.89	26.32	100
0.7	0.4	0.6	18.99	44.30	11.39	25.32	100
0.7	0.4	0.8	18.29	42.68	14.63	24.39	100

* f/s, w/s and p/s denote fly ash to solid ratio, water to solid ratio and phosphate to solid ratio, respectively.

Table 5.3 Formulations to assess the effect of PFA content at p/s = 0.2*

Formulation ratios			Constituents (wt%)				Total (wt%)
f/s	w/s	p/s	CAC	PFA	(NaPO ₃) _n	H ₂ O	
0.4	0.35	0.2	38.71	25.81	12.90	22.58	100
0.5	0.35	0.2	32.26	32.26	12.90	22.58	100
0.6	0.35	0.2	25.81	38.71	12.90	22.58	100
0.7	0.35	0.2	19.35	45.16	12.90	22.58	100
0.8	0.35	0.2	12.90	51.61	12.90	22.58	100
0.9	0.35	0.2	6.45	58.06	12.90	22.58	100
0.4	0.4	0.2	37.50	25.00	12.50	25.00	100
0.5	0.4	0.2	31.25	31.25	12.50	25.00	100
0.6	0.4	0.2	25.00	37.50	12.50	25.00	100
0.7	0.4	0.2	18.75	43.75	12.50	25.00	100
0.8	0.4	0.2	12.50	50.00	12.50	25.00	100
0.9	0.4	0.2	6.25	56.25	12.50	25.00	100

* f/s, w/s and p/s denote fly ash to solid ratio, water to solid ratio and phosphate to solid ratio, respectively.

Table 5.4 Formulations to assess the effect of boric acid, water, and phosphate content*

Investigation	Formulation ratios				Constituents (wt%)					Total (wt%)	
	f/s	w/s	p/c	r/c	CAC	PFA	(NaPO ₃) _n	H ₃ BO ₃	H ₂ O		
Varying H ₃ BO ₃	0.7	0.35	0.4	0.01	20.37	47.52	8.15	0.204	23.76	100	
	0.7	0.35	0.4	0.02	20.33	47.43	8.13	0.407	23.71	100	
	**	0.7	0.35	0.4	0.03	20.28	47.33	8.11	0.609	23.66	100
	0.7	0.35	0.4	0.04	20.24	47.23	8.10	0.810	23.62	100	
Varying water	0.7	0.3	0.4	0.03	20.99	48.99	8.40	0.630	20.99	100	
	**	0.7	0.35	0.4	0.03	20.28	47.33	8.11	0.609	23.66	100
Varying PFA	0.5	0.35	0.4	0.03	31.95	31.95	12.78	0.958	22.35	100	
	0.6	0.35	0.4	0.03	26.28	39.42	10.51	0.788	23.00	100	
	**	0.7	0.35	0.4	0.03	20.28	47.33	8.11	0.609	23.66	100
	0.8	0.35	0.4	0.03	13.93	55.71	5.57	0.418	24.37	100	

* f/s, w/s, p/c and r/c denote fly ash to solid ratio, water to solid ratio, phosphate to solid ratio and retarder to cement, respectively.

** The same formulation

5.3. Preliminary Vicat Setting Time Measurements

Figure 5.1 a) and b) shows the effect of PFA content on the initial and final setting of the formulations detailed in Table 5.1. In both $w/s = 0.35$ and $w/s = 0.4$ series, the increase of PFA content resulted in longer setting time, which became prominent at $f/s \geq 0.6$. In these systems, because the w/s ratio is constant, CAC and phosphate content decrease as f/s increases, and the effective water to cement ratio (w/c) also increases. Therefore, it is reasonable to suggest that the increase in setting time was due to the concentration of CAC and phosphate decreasing in the system. Other authors have observed that decreasing cement content results in increasing setting time of cementitious systems [160]. Also, it is known that the use of PFA increases both the initial and final setting times [159]. Only the formulation where $w/s = 0.35$ and $f/s = 0.9$ fulfilled the minimum requirement for initial setting time. However, the resulting hardened cement paste could be crushed by hand, which suggests that the system had failed to develop significant strength.

Figure 5.1 c) and d) show the effect of phosphate content on setting time of formulations detailed in Table 5.2 with fixed $f/s = 0.7$. With no phosphate present, the PFA:CAC systems with $w/s = 0.35$ and $w/s = 0.4$ exhibited relatively quick initial setting times of *ca.* 25 minutes and 35 minutes, respectively. It is known that high alkali content (> 0.5 wt%) may cause undesirable rapid setting of CACs, hence why alkalis content of CACs are controlled to relatively low levels [65]. Therefore, it is suggested that quick setting exhibited here was a result of the relatively high alkali content of the PFA (*ca.* $\text{Na}_2\text{O} + \text{K}_2\text{O} = 3.2$ wt%). When phosphate was incorporated, there was little change in either initial or final setting times in both $w/s = 0.35$ and $w/s = 0.4$ series at $p/c \leq 0.6$. However, when p/c was increased to $p/c = 0.8$, both the

initial and final setting times increased significantly, which suggests that an excess of phosphate has a retarding effect on the setting of the CAP system.

Figure 5.1 e) and f) show the setting time for the systems with fixed $p/s = 0.2$, as shown in Table 5.3. Similarly to $p/c = 0.2$ series, the effect of f/s was not apparent at $f/s \leq 0.5$, but the systems did exhibit increasing setting time with increasing f/s at $f/s \geq 0.6$. It should be noted that both w/s ratio and p/s ratio were constant in this series, meaning that both w/c ratio and p/c ratio increase when f/s ratio increases. Therefore, it is reasonable to have both the effects from the dilution of CAC by the increase in effective water and the retarding effect on setting from the increase in phosphorus content. The systems with $f/s = 0.9$ in both $w/s = 0.35$ and $w/s = 0.4$ series exhibited final setting times of greater than 24 h; as such the data was not recorded and these particular systems were deemed unsuitable based on the setting time criteria for final setting (final setting < 24 h).

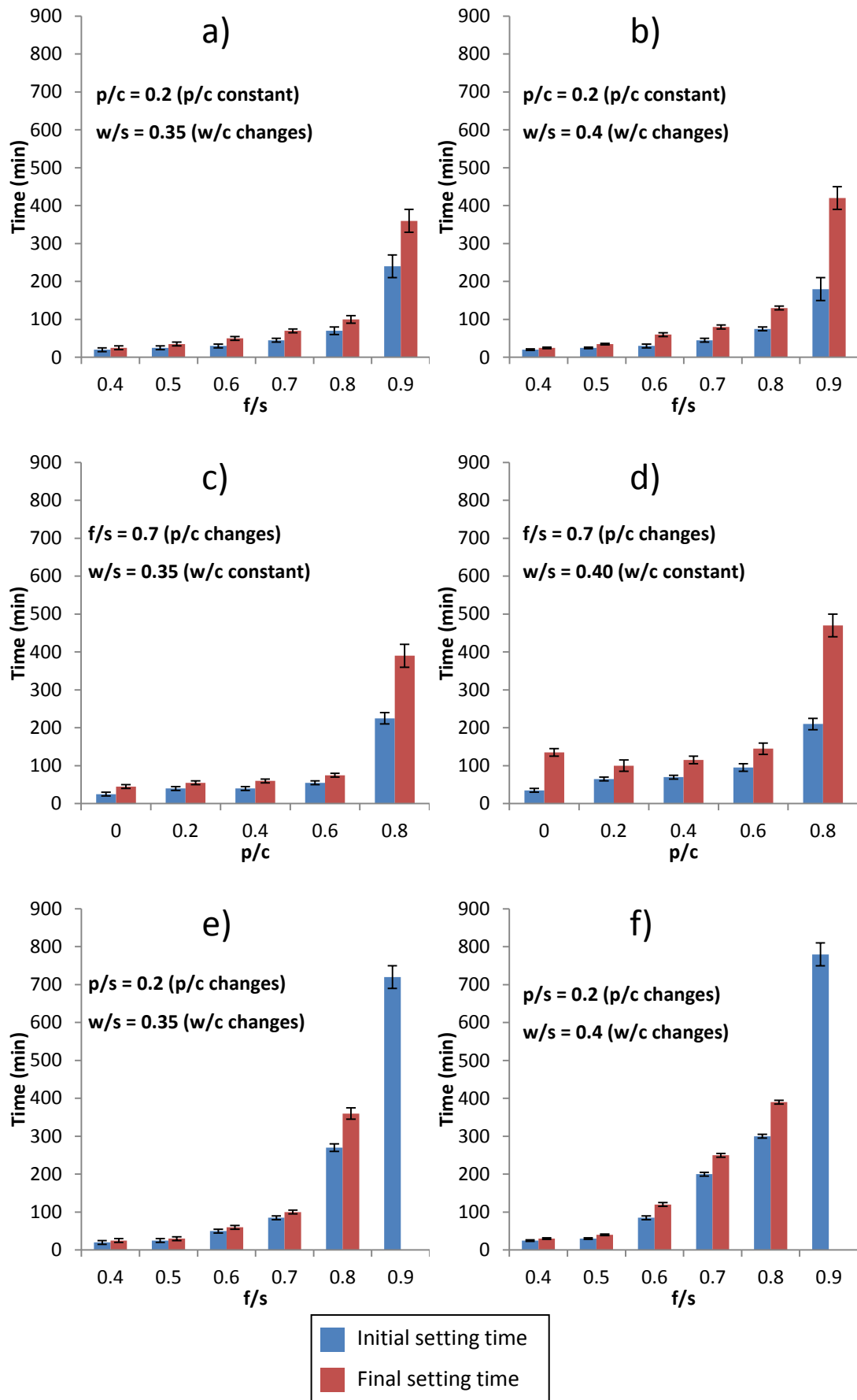


Figure 5.1 Vicat setting time results of CAC-PFA-(NaPO₃)_n system with various formulations

5.4. Effect of Formulation on Plant Acceptance Tests

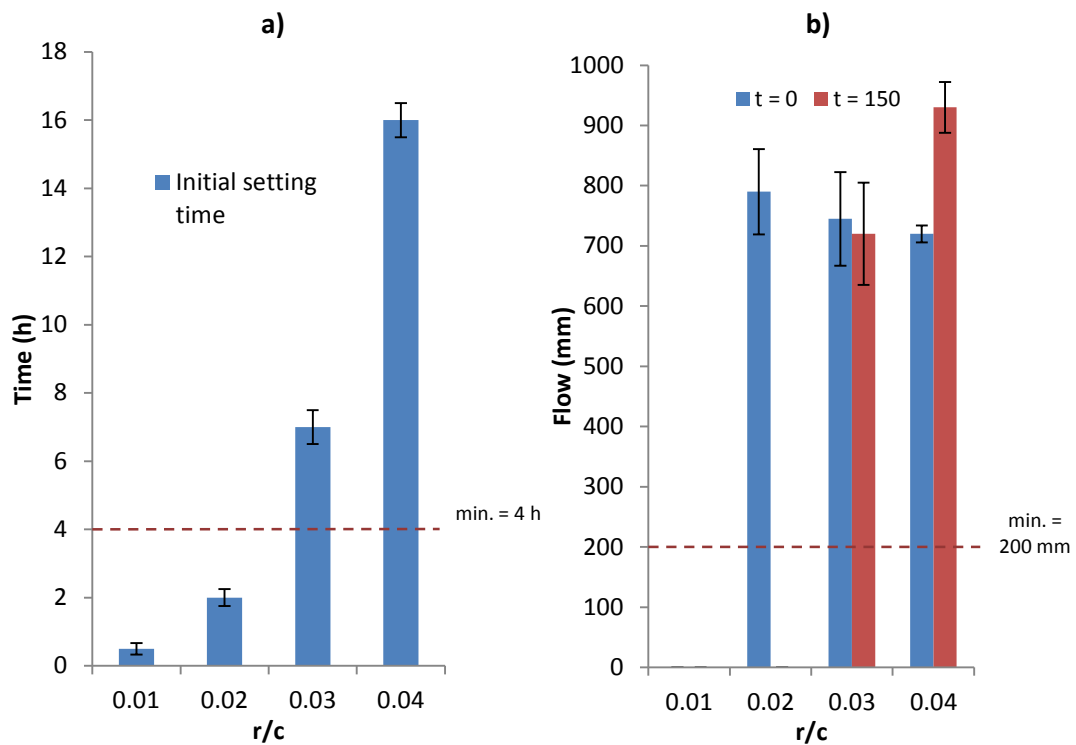
5.4.1. Effect of H₃BO₃ Content

Table 5.5 and Figure 5.2 present the results from plant acceptance tests to assess the effect of boric acid content on the CAP system. The results show that the addition of boric acid had a significant effect on the system properties in terms of the plant acceptance tests. Both initial and final setting times increased with increasing boric acid content (r/c). The results also suggest that the system is very sensitive to boric acid content; a relatively small increase in boric acid content resulted in a large increase in setting times. It was possible to achieve the required initial setting time (Figure 5.2) of > 4 h by introducing boric acid at $r/c \geq 0.03$. The formulation with $r/c = 0.04$ exhibited a final setting time of > 24 h which is outside the acceptance range.

For some formulations, Colflow values could not be measured due to low workability and/or rapid setting. Where Colflow values could be measured, the results showed that the CAP cement slurries exhibited sufficient flow to satisfy the industrial requirement of a minimum of 200 mm after 150 minutes as shown in Figure 5.2. At t_0 , systems with $r/c \geq 0.02$ exhibited similar Colflow values of between *ca.* 720-790 mm. At t_{150} system exhibited steady increase in Colflow value with increasing r/c ratio. It should also be noted that all systems exhibited no bleed water formation after 24 h, which suggested that all water was either incorporated into the cementitious hydrate phases or existed within the pore solution of the cement matrix. These results showed that a boric acid content of *ca.* $r/c = 0.03$ produced a CAP cementing system with suitable properties to fulfil the plant acceptance test criteria.

Table 5.5 Effect of H_3BO_3 on plant acceptance test results for formulations with $f/s = 0.7$, $w/s = 0.35$, $p/c = 0.4$

Formulation (r/c)	Colflow				Vicat setting time (h)		Bleed (%)
	Time (min)	Run		Mean (mm)	Initial	Final	
		1	2				
0.01	0	N/a	N/a	N/a	< 0.5	< 1	0
	150	N/a	N/a	N/a			
0.02	0	740	840	790	2	< 6	0
	150	N/a	N/a	N/a			
0.03	0	690	800	745	7	< 24	0
	150	780	660	720			
0.04	0	730	710	720	16	< 48	0
	150	900	960	930			

**Figure 5.2 Plant acceptance tests for CAC-PFA-(NaPO₃)_n-H₃BO₃-H₂O system with $f/s = 0.7$, $w/s = 0.35$, $p/c = 0.4$; a) Initial setting time, b) Colflow**

5.4.2. Effect of Water Content

Table 5.6 and Figure 5.3 show the plant acceptance test results to examine the effect of water content on the CAP system. The results from the Vicat measurements showed that the $w/s = 0.3$ and $w/s = 0.35$ formulations exhibited initial setting times of *ca.* 6 h and *ca.* 7 h, respectively. Both formulations exhibited final setting time of < 24 h, thus fulfilling the industrial requirement in both cases. The formulations also exhibited no bleed water after 24 h. The results also show that the Colflow value increased with increased water content. The results showed that the industrial requirement of a minimum Colflow value of 200 mm after 2.5 h was satisfied by both systems. Both systems exhibited a slight decrease in Colflow at t_{150} compared to t_0 , but this was minimal in both cases. This is likely to be due to acid-base setting reactions occurring during the period between measurements, which would result in thickening of the cement slurry. The Colflow value of the $w/s = 0.3$ system was less than half that of the $w/s = 0.35$ system both at t_0 and t_{150} , suggesting that the water content of the CAP cementing system in the range $w/s = 0.3-0.35$ has a significant effect on the flow characteristics, but does not significantly affect the setting times of the system.

In general, when considering cementitious systems, reducing the water content will result in lower porosity and permeability, and lower the free-water in the resulting hardened cement paste [25, 65], which may be considered attractive attributes for the purposes of radioactive waste encapsulation. However, the fluidity of the cement slurry must be kept high enough over a certain time period to facilitate operational requirements i.e. facilitate the process and operation of the encapsulation plant and allow full penetration of complex wastes. The results attained here suggested that w/s should have a minimum value of *ca.* $w/s = 0.3$ to fulfil the fluidity requirement after

150 minutes although $w/s = 0.35$ may be more desirable in practicable terms, as the resulting slurry would have more favourable rheological properties.

Table 5.6 Effect of water on plant acceptance test results for formulations with $f/s = 0.7$, $p/c = 0.4$, $r/c = 0.03$

Formulation (w/s)	Colflow			Vicat setting time (h)		Bleed (%)	
	Time (min)	Run		Mean (mm)	Initial		Final
		1	2				
0.3	0	340	360	350	6	< 24	0
	150	300	220	260			
0.35	0	690	800	745	7	< 24	0
	150	780	660	720			

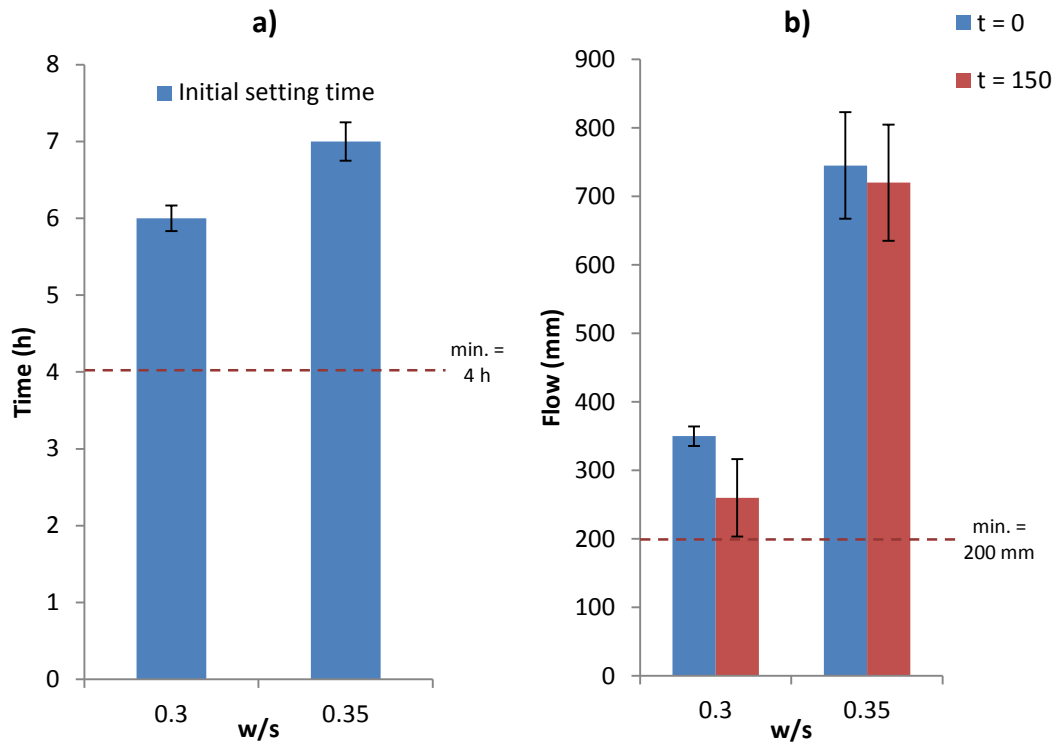


Figure 5.3 Plant acceptance test results for CAC-PFA-(NaPO₃)_n-H₃BO₃-H₂O system with $f/s = 0.7$, $p/c = 0.4$, $r/c = 0.03$; a) Initial setting time, b) Colflow

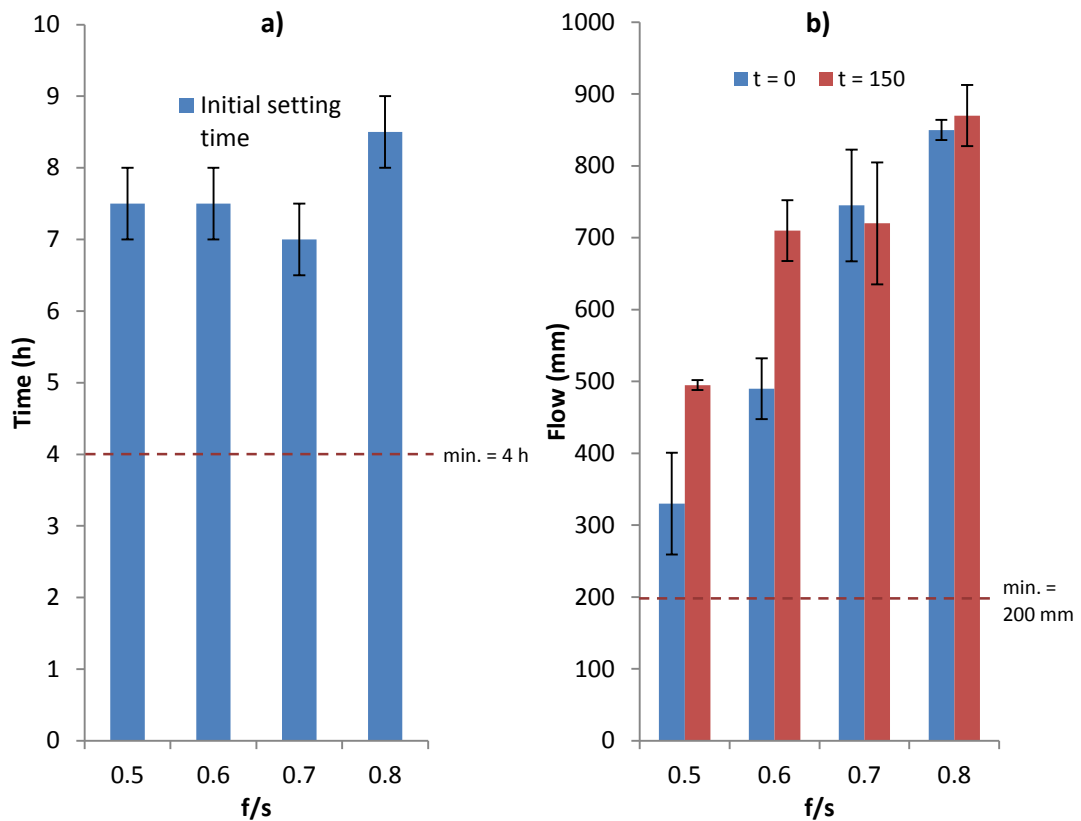
5.4.3. Effect of PFA Content

Table 5.7 and Figure 5.4 show the plant acceptance test result to examine the effect of PFA on the CAP system. The results from Vicat setting times measurements showed that all systems exhibited an initial setting time greater than 4 hours and final set within 24 hours; hence all systems achieved the industrial requirement in terms of setting time. In addition, no bleed water was observed for any of the systems investigated after 24 hours, which suggested that all mix water was either chemically bound within hydration products or existed within the pore structure as pore solution.

The results from Colflow flow measurements showed that all the systems attained a Colflow value greater than the minimum requirement of 200 mm after 150 minutes. Furthermore, the results showed that f/s ratio has a significant effect on the flow properties of the cementing system. The Colflow value increased with increasing f/s , and as such the fluidity of the cement slurries increased with increasing PFA content. The results showed that at t_0 Colflow steadily increased with increasing f/s ; although at t_{150} the increase with increasing f/s was less apparent and showed little change at $f/s > 0.6$.

Table 5.7 Effect of PFA on plant acceptance test results for formulations with $w/s = 0.35$, $p/c = 0.4$, $r/c = 0.03$

Formulation (f/s)	Colflow			Vicat setting time (h)		Bleed (%)	
	Time (min)	Run		Initial	Final		
		1	2				Mean (mm)
0.5	0	280	380	330	7.5	< 24	0
	150	500	480	490			
0.6	0	460	520	490	7.5	< 24	0
	150	740	680	710			
0.7	0	690	800	745	7	< 24	0
	150	780	660	720			
0.8	0	840	860	850	8.5	< 24	0
	150	900	840	870			

**Figure 5.4 Plant acceptance test results for CAC-PFA-(NaPO₃)_n-H₃BO₃-H₂O system with $w/s = 0.35$, $p/c = 0.4$, $r/c = 0.03$; a) Initial setting time, b) Colflow**

5.5. Materials Properties of Selected Formulations

5.5.1. Phase Characterisation

Figure 5.5 shows the XRD results from various CAP formulations with varying f/s examined to assess the effect of PFA content. The results show that all the CAP formulations exhibited similar reflection profiles, suggesting that all the systems consisted of principally the same crystalline phases. The XRD patterns exhibited reflections relating to the anhydrous CAC and PFA phases; CA, C_2AS , CT, quartz and mullite. As expected, with increasing f/s , the intensity of PFA-related reflections (quartz and mullite) increased, while reflections relating to the anhydrous CAC phases (CA, C_2AS , and CT) decreased. The principle reflection for CA (*ca.* $30.0^\circ 2\theta$) appeared to have decreased compared to that associated with C_2AS (*ca.* $31.4^\circ 2\theta$) in the higher f/s formulations. Although not precisely quantitative, this may suggest that a higher proportion of the CA was consumed in the higher f/s formulations. It is suggested that this was due to the w/c effectively increasing with increasing f/s .

No reflections that would indicate the development of new crystalline phases were observed. Hence, the reaction products of these systems, which were responsible for setting and strength development, were amorphous. This is in agreement with the work presented in Chapter 4 on CAP systems without PFA, in which it was proposed that the principle reaction products in a CAP systems were ACP and alumina gel.

All the systems exhibited broad diffuse scattering, which was due to the aforementioned amorphous binding phase as well as the amorphous content of the PFA.

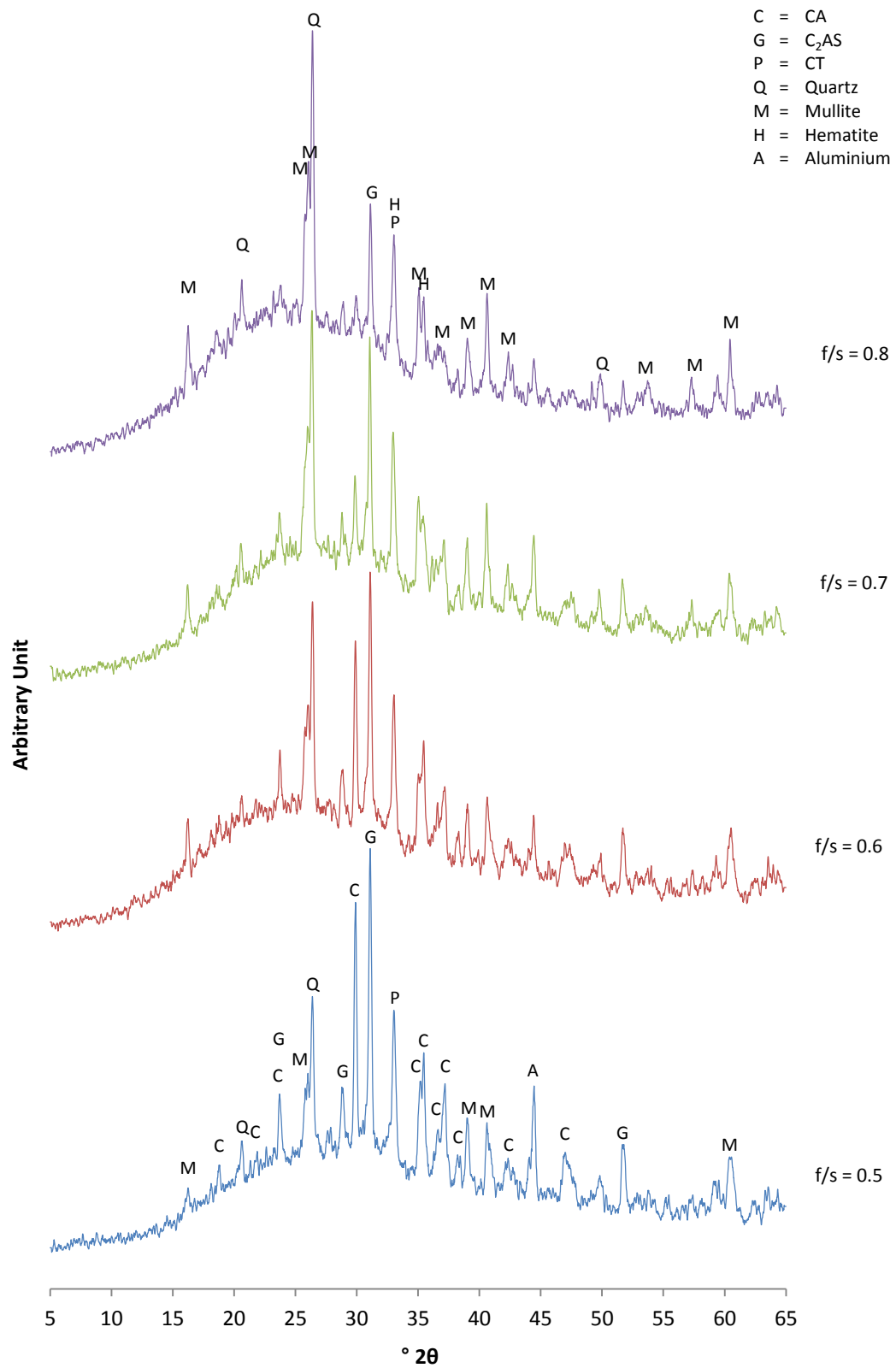


Figure 5.5 XRD pattern of PFA:CAC + (NaPO₃)_n + H₃BO₃ mixed at w/s = 0.35, p/c = 0.4, r/c = 0.03 and varying f/s, after 7 days curing at 20°C

The TG results (Figure 5.6) show that the PFA content had a significant effect on the dehydration and/or thermal decomposition behaviour of the CAP system. The general weight loss mechanism of all systems was similar i.e. the shape of the curve, but the total weight loss up to 1000 °C decreased with increasing PFA content (f/s). The majority of the weight loss for all systems occurred up to *ca.* 350 °C. Between *ca.* 350-1000 °C the systems exhibited similar total weight losses of *ca.* 3 wt% as shown in Table 5.8. The dehydration and/or thermal decomposition of cementitious materials is indicative of the reaction products and hydrate phases present and the quantity of those various phases. The decreasing total weight loss with increasing PFA content (f/s) is a result of the decreasing proportion of CAC and phosphate, the reactions of which are responsible for hydrated reaction products.

The corresponding DTG (Figure 5.7) shows that the principle weight losses occurred below *ca.* 120 °C, with additional minor weight loss events occurring at *ca.* 200-220 °C and over the temperature range *ca.* 550-700 °C. It is suggested that the principle weight loss mechanism was due to the dehydration of the amorphous binding phases ACP and alumina gel [84]. ACP has been shown to lose adsorbed water up to *ca.* 120 °C, which may account for some of the weight loss exhibited in TG results [158]. ACP has also been reported to gradually lose chemically bound water molecules up to *ca.* 600 °C. In addition, some of the weight loss below 100 °C may be due to the evaporation of residual free-water and acetone, though this contribution is thought to be minimal. The minor weight loss event at *ca.* 200-220 °C may have been due to the dehydration of strätlingite (C_2ASH_8), which has been observed to form in CAC-based systems to which silica rich SCMs, such as PFA, were added [65, 79, 161]. The metastable CA-hydrate phases which form during conventional hydration react with silica to form strätlingite. It has also been proposed

that C_2AS may hydrate to form strätlingite, although this usually occurs after extended periods of curing [63, 65]. If present, strätlingite was only present in small amounts of *ca.* 1.5 wt%, as shown in Table 5.8. The minor weight loss over the temperature range *ca.* 550-700 °C is most likely due to the decomposition of calcite, which was present in amounts of *ca.* 3.6 wt%.

Table 5.8 Weight loss over various temperature ranges and estimations of phases present in CAC-PFA-($NaPO_3$)_n- H_3BO_3 - H_2O with w/s = 0.35, p/c = 0.4, r/c = 0.03

Formulation f/s	Weight loss (wt %)			Strätlingite wt%	Calcite wt%
	25-350 °C	350-1000 °C	25-1000 °C		
0.5	12.76	2.86	15.62	1.49	3.32
0.6	11.46	3.00	14.46	1.38	3.57
0.7	9.86	3.42	13.28	1.74	3.76
0.8	7.22	3.10	10.32	1.27	3.64

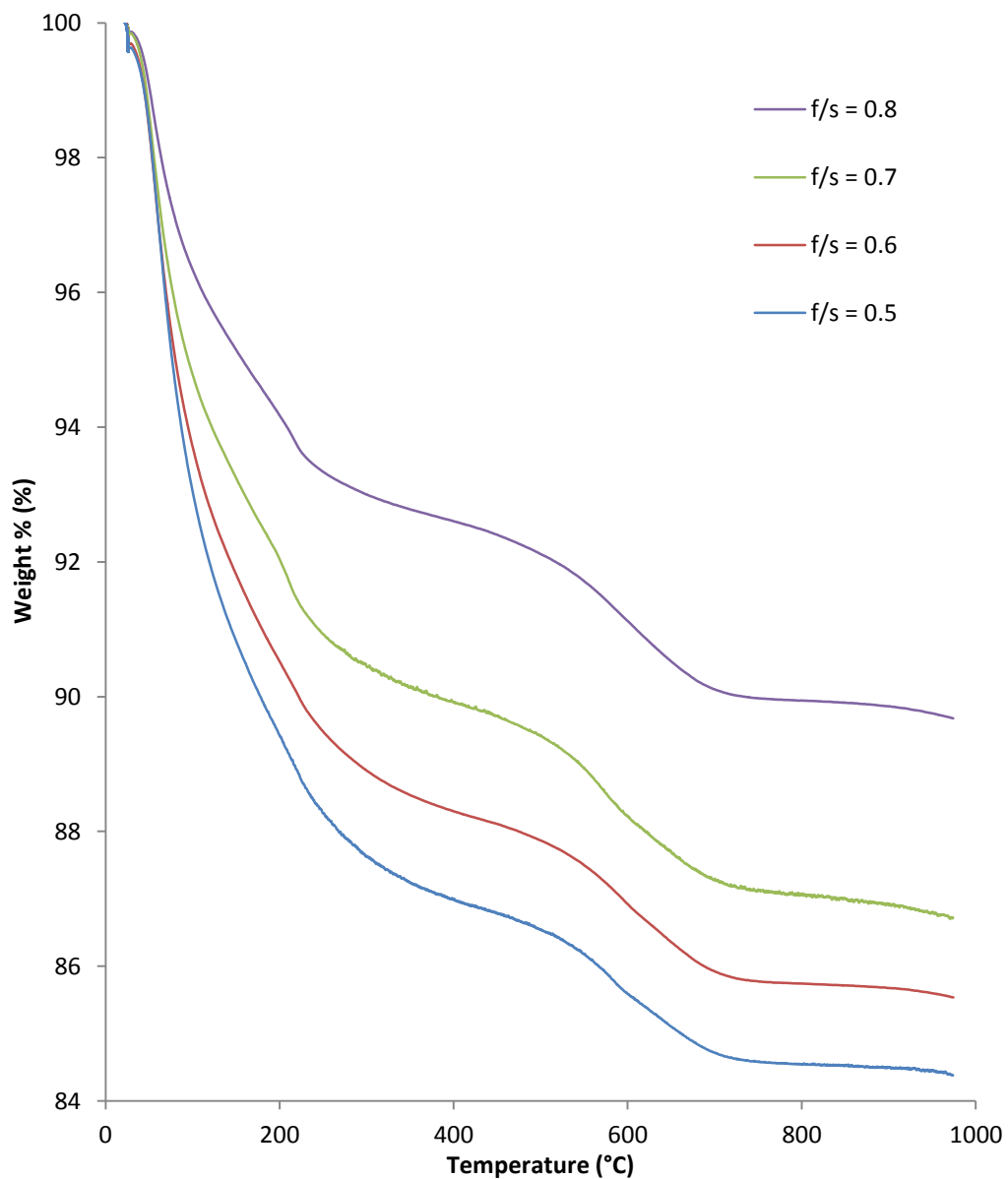


Figure 5.6 TGA of PFA:CAC + $(\text{NaPO}_3)_n + \text{H}_3\text{BO}_3$ mixed at $w/s = 0.35$, $p/c = 0.4$, $r/c = 0.03$ and varying f/s , after 7 days curing at 20°C

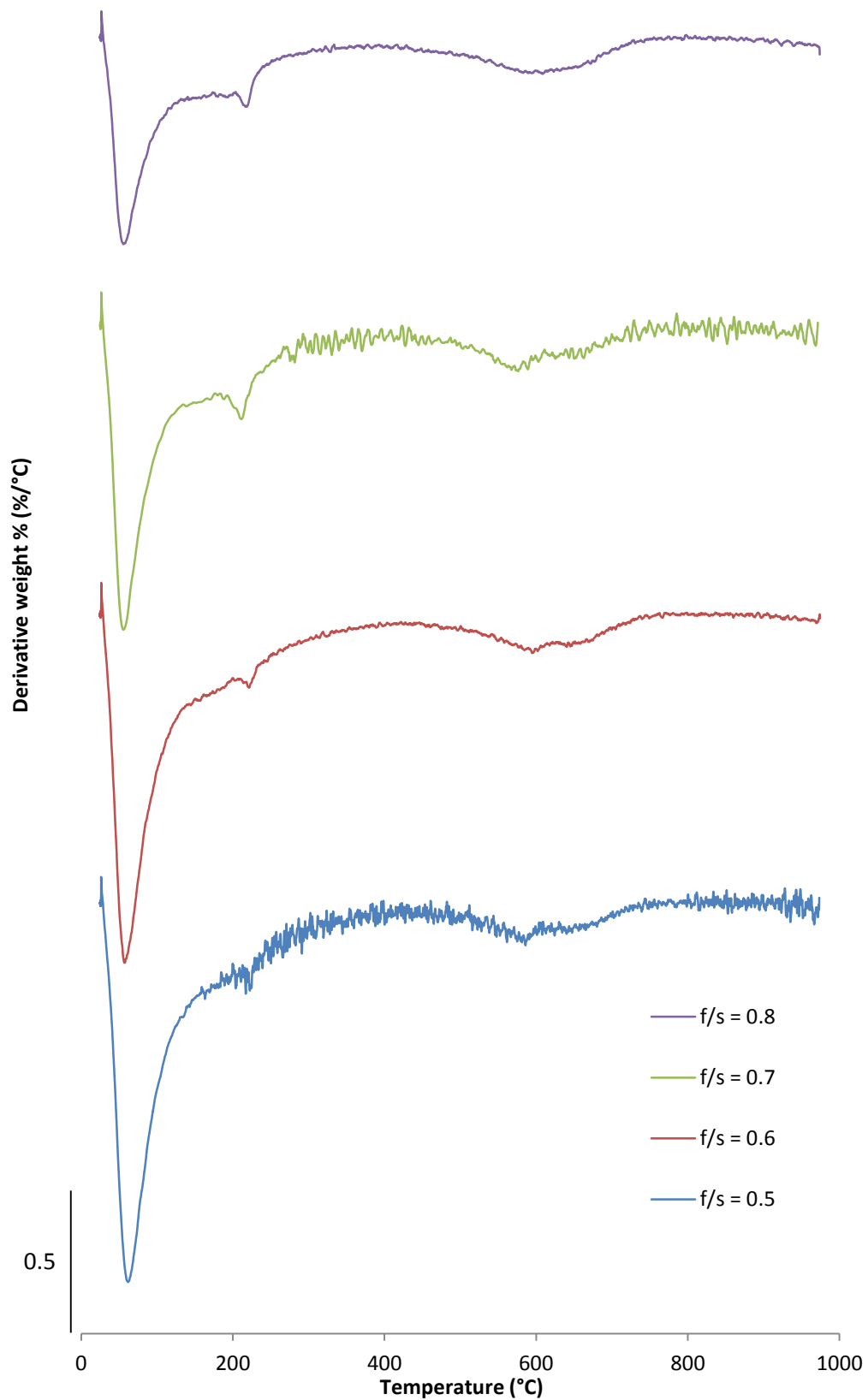


Figure 5.7 DTG of PFA:CAC + (NaPO₃)_n + H₃BO₃ mixed at w/s = 0.35, p/c = 0.4, r/c = 0.03 and varying f/s, after 7 days curing at 20°C

5.5.2. Microstructure

Figure 5.8 to Figure 5.11 show SEM micrographs using Backscattered Electron Imaging (BEI) for two of the CAP formulations with PFA contents of $f/s = 0.5$ and $f/s = 0.8$. Both micrographs exhibit a microstructure consisting of angular particles of unreacted CAC and spherical PFA particles embedded within a matrix, which appeared to act as a binder between those particles. It was apparent that the formulation with $f/s = 0.5$ (Figure 5.8) exhibited a higher proportion of unreacted CAC particles (Labelled **A**) compared to that of the formulation with $f/s = 0.8$. Conversely, the formulation with $f/s = 0.8$ (Figure 5.11) had a higher proportion of PFA particles (Labelled **B**). These results concurred with those from XRD, which suggested that the proportion of unreacted CAC that remained in the hardened cement decreased, and the proportion of PFA increased with increasing f/s . The formulation with $f/s = 0.5$ shown in Figure 5.8 exhibited significant amounts of micro-cracks. The micro-cracks may be the result of thermally induced stresses due the exothermic acid-base setting reactions. However, no micro-cracks were observed in Figure 5.11, suggesting that incorporation of PFA to a larger extent would help to obtain a binding phase with less defects. Alternatively, the larger cracks observed in Figure 5.8 may be due to sample preparation.

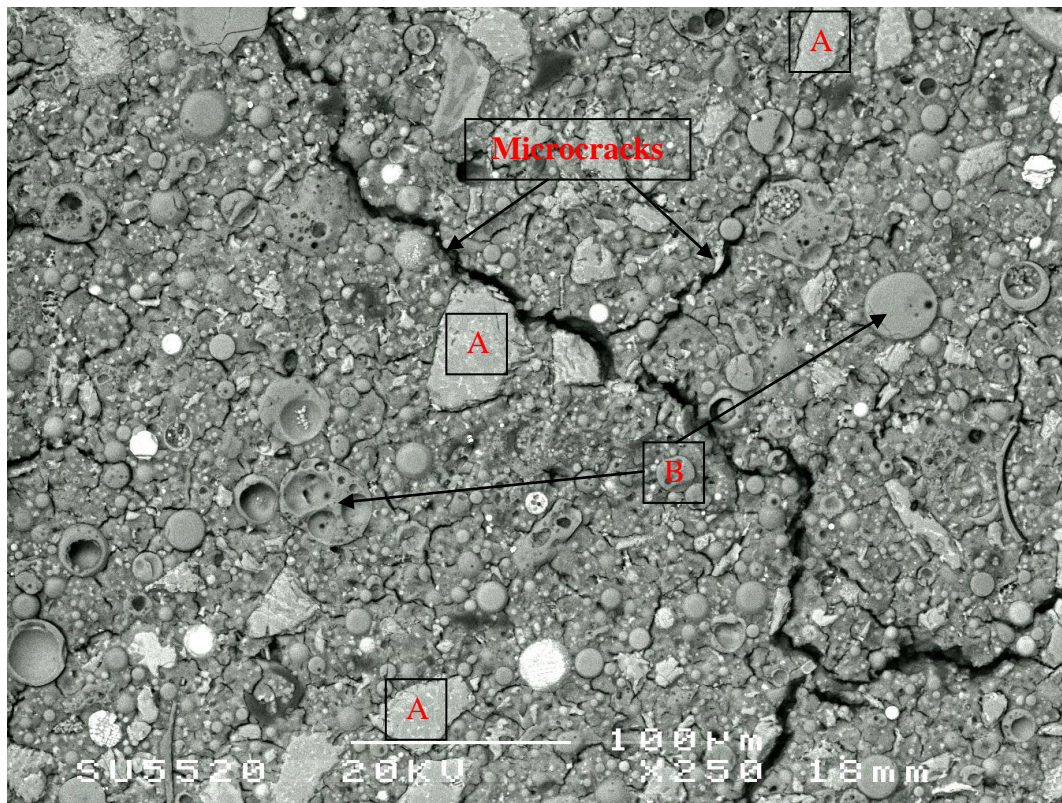


Figure 5.8 SEM-BEI micrograph of PFA:CAC + $(\text{NaPO}_3)_n + \text{H}_3\text{BO}_3$ with $f/s = 0.5$ after 7 days curing (x250)

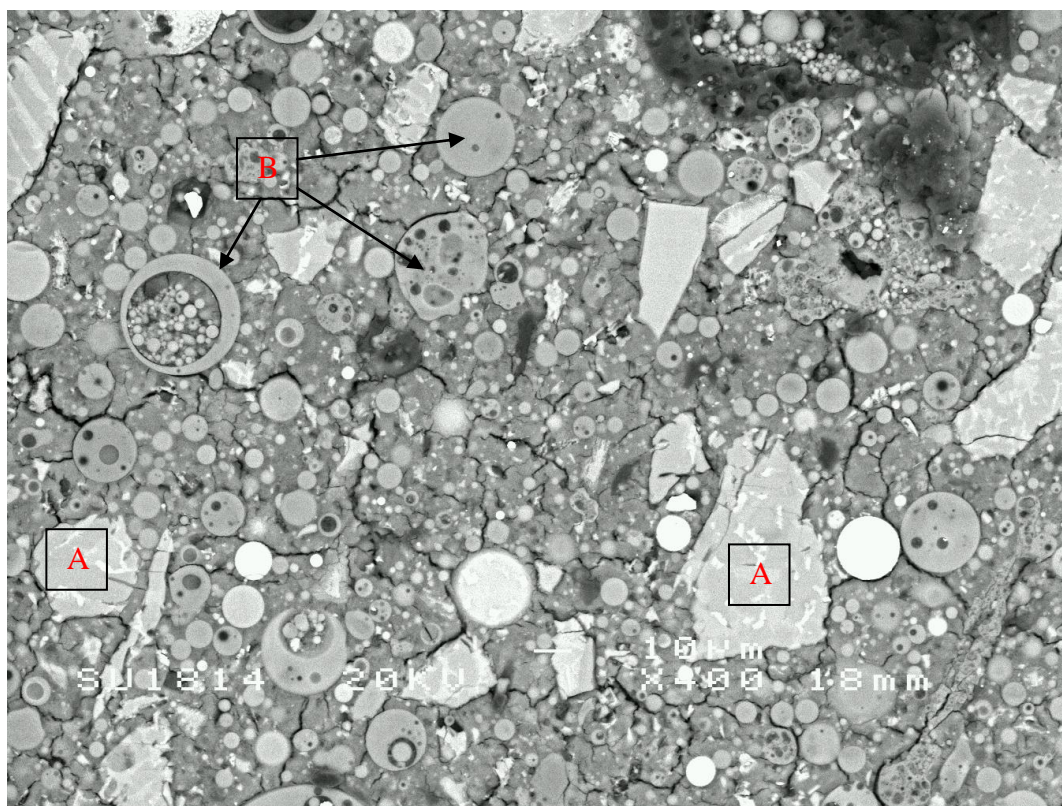


Figure 5.9 SEM-BEI micrograph of PFA:CAC + $(\text{NaPO}_3)_n + \text{H}_3\text{BO}_3$ with $f/s = 0.5$ after 7 days curing (x400)

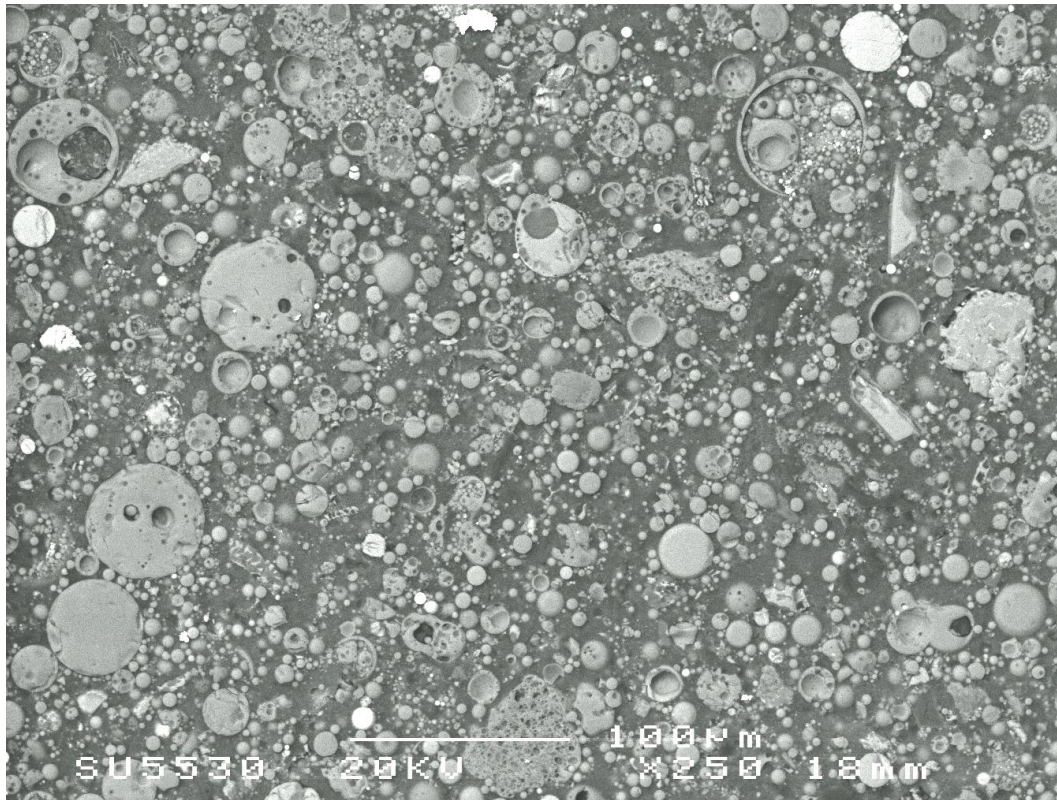


Figure 5.10 SEM-BEI micrograph of PFA:CAC + $(\text{NaPO}_3)_n + \text{H}_3\text{BO}_3$ mixed with $f/s = 0.8$ after 7 days curing (x250)

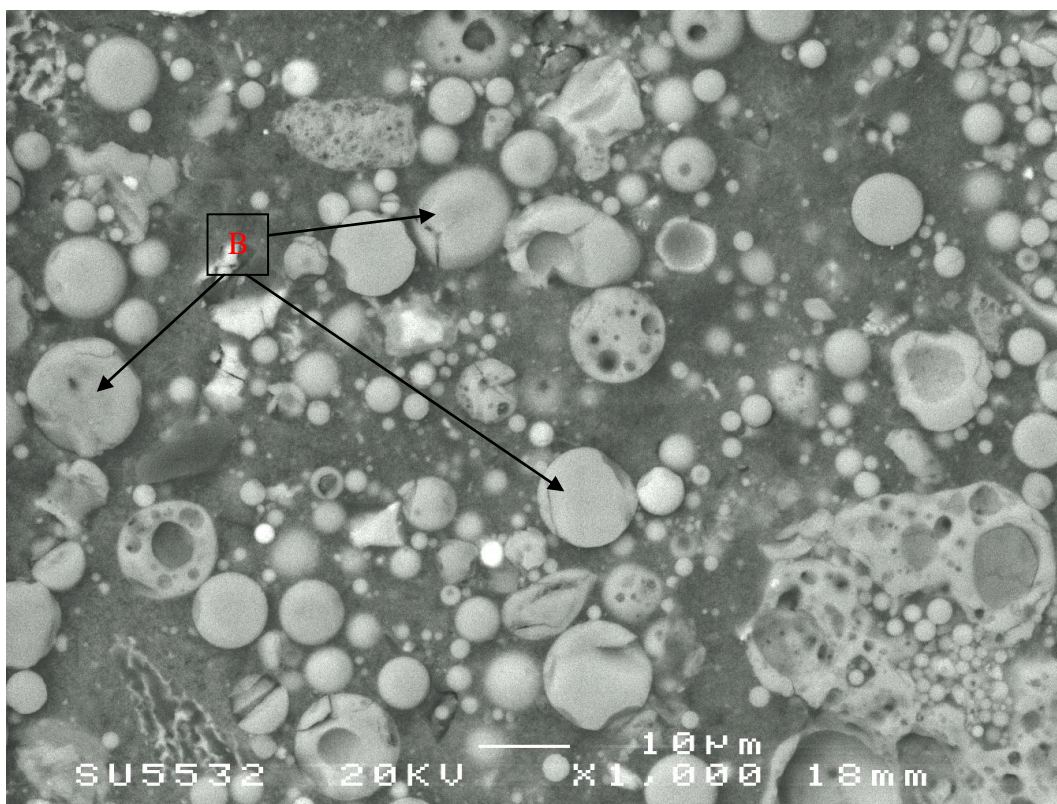


Figure 5.11 SEM-BEI micrograph of PFA:CAC + $(\text{NaPO}_3)_n + \text{H}_3\text{BO}_3$ mixed with $f/s = 0.8$ after 7 days curing (x1000)

Table 5.9 shows the EDX data from analysis of the apparent amorphous binding matrix for the formulations with PFA contents of $f/s = 0.5$ and $f/s = 0.8$. The data presented are averages of 15 individual point spectra of the binding matrix for each system. The results suggested that the binding matrix of both systems consisted of calcium, aluminium, phosphorus, sodium, silicon and oxygen, although the exact compositions did vary. In the work presented previously in Chapter 4, it was proposed that the binding matrix consisted of amorphous calcium phosphate (ACP, $\text{Ca}_x\text{H}_y(\text{PO}_4)_z \cdot n\text{H}_2\text{O}$) and hydrated alumina gel. ACP has a variable composition and a flexible structure, where the Ca/P ratio = 1.0-2.2 and some sodium can be incorporated into the structure by substitution for calcium [124, 125]. Both systems exhibited Ca/P ratios indicative of ACP.

Table 5.9 EDX results for amorphous binding matrix from formulations with $f/s = 0.5$ and 0.8

Element	Formulation			
	$f/s = 0.5$		$f/s = 0.8$	
	Atomic weight (%)	S.D. (%)	Atomic weight (%)	S.D. (%)
Ca	6.4	1.4	8.0	2.0
Al	10.7	1.1	10.9	2.0
P	6.5	1.4	6.8	1.1
Na	3.3	0.7	4.5	0.6
Si	3.0	2.3	4.4	3.7
O	70.7	3.5	65.4	4.7
Ca/P ratio	0.98		1.18	

5.5.3. Physico-mechanical Properties

Figure 5.12 and Figure 5.13 show the compressive strength and porosity results for the CAP systems with $w/s = 0.35$, $p/c = 0.4$, $r/c = 0.03$ and varying f/s . The results from a 3:1 BFS/PC system, a representative of the conventional cementitious system used to encapsulate ILW, are also given as dotted lines for comparison. The results demonstrate that the PFA content significantly affected the mechanical properties of the hardened cement, the reasons for which were two-fold. Firstly, the porosity increased as a result of the effective w/c ratio increasing with f/s ratio. Secondly, the strength decreased as a consequence of the increase in porosity and less binding phase produced because of the lower CAC and phosphate content, the reactions of which form the binding matrix [162].

As stated previously, wastefoms should provide sufficient strength to facilitate handling and transportation of radioactive waste packages. Although there are no specific physical or mechanical properties criteria defined by the relevant regulatory authorities, the industry has recommended that wastefoms meet a minimum requirement for compressive strength of 4 MPa [27, 29]. All the systems studied here developed compressive strength of greater than 4 MPa after 7 days of curing. The systems with $f/s \leq 0.6$ developed higher compressive strength compared to the 3:1 BFS/PC system, which developed *ca.* 28 MPa, after 7 days curing. The CAP systems with $f/s \leq 0.7$ exhibited porosity less than that of the 3:1 BFS/PC system, which exhibited a porosity of *ca.* 30.5 %, after 7 days curing. Porosity is an important property to consider when developing a cementitious matrix for radioactive waste encapsulation. To some extent porosity will control the permeability, which influences the potential for diffusion and mobility of radionuclides [14].

Figure 5.14 shows the pore size distribution in the CAP systems system up to 7 days, based on the results of MIP. The vertical axis is the log differential intrusion volume, obtained using the following equation:

$$\log (\text{differential volume}) = dV/d\log D \quad \text{Equation 5.1}$$

where V and D represent the intrusion volume and the pore diameter, respectively. The derivative with respect to $\log D$ was used instead of that to the intrusion pressure, which gives the incremental intrusion volume, to clarify the pore size distribution. The result shows that majority of pores are in the range of $< 0.2 \mu\text{m}$.

Although the pore diameters obtained from MIP may not directly correspond to the real pore structures of cementitious materials under examination [163], it is still considered reasonable to compare the trend and study the general change of the pore size distribution. The results show that the pore size distribution is dependent on the f/s ratio; the population of pores shifts to smaller pore size with decreasing f/s ratio. A similar trend has been observed by elsewhere for PFA/PC systems [164, 165]. In the CAP systems studied here, the higher proportion of larger pores in system with increasing f/s may result from the effective increase in w/c. The significant quantity of larger pores may be responsible for the lower compressive strength of this system with increasing f/s ratio.

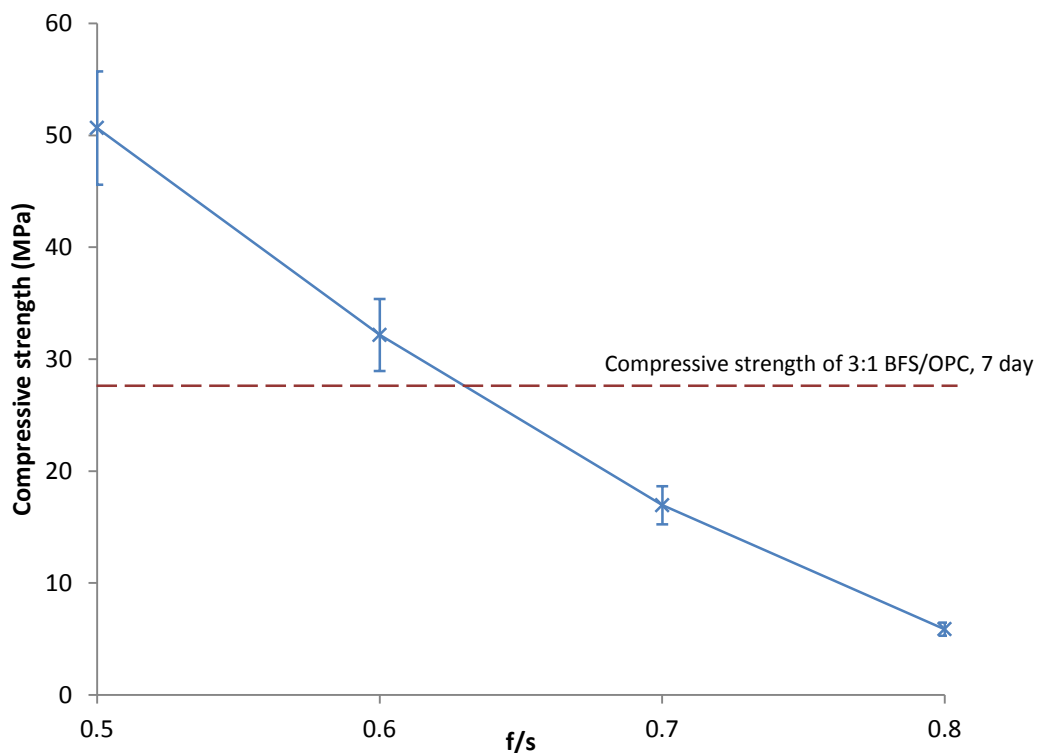


Figure 5.12 Compressive strength of PFA:CAC + $(\text{NaPO}_3)_n$ + H_3BO_3 mixed at $w/s = 0.35$, $p/c = 0.4$, $r/c = 0.03$, after 7 days curing at $20\text{ }^\circ\text{C}$

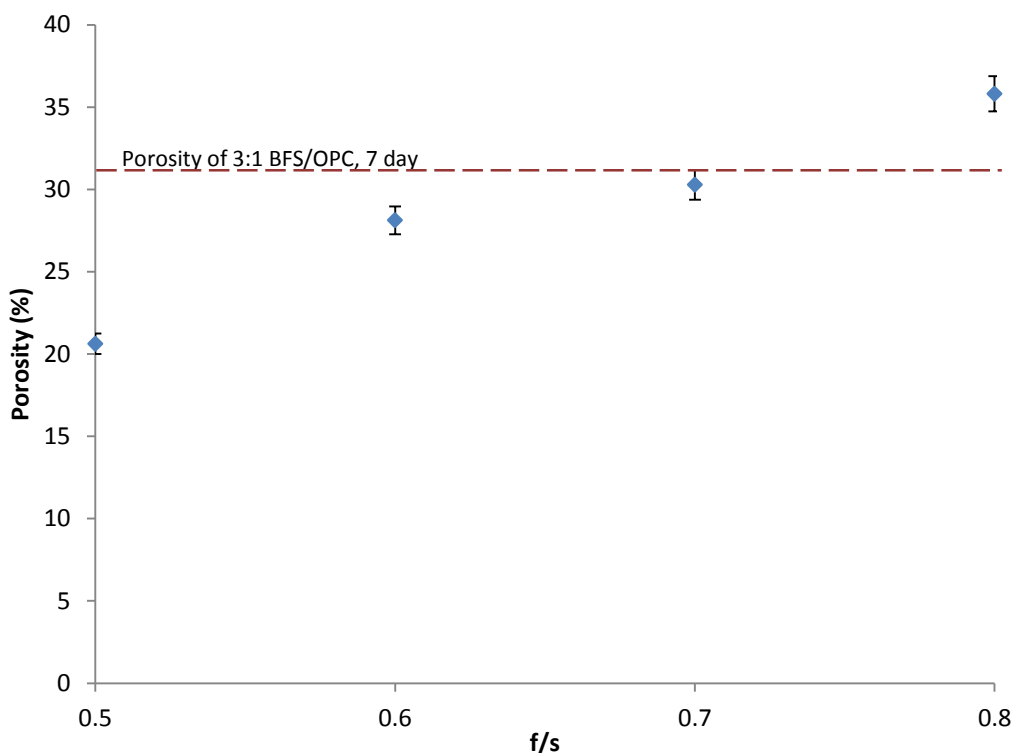


Figure 5.13 Porosity of PFA:CAC + $(\text{NaPO}_3)_n$ + H_3BO_3 mixed at $w/s = 0.35$, $p/c = 0.4$, $r/c = 0.03$, after 7 days curing at $20\text{ }^\circ\text{C}$

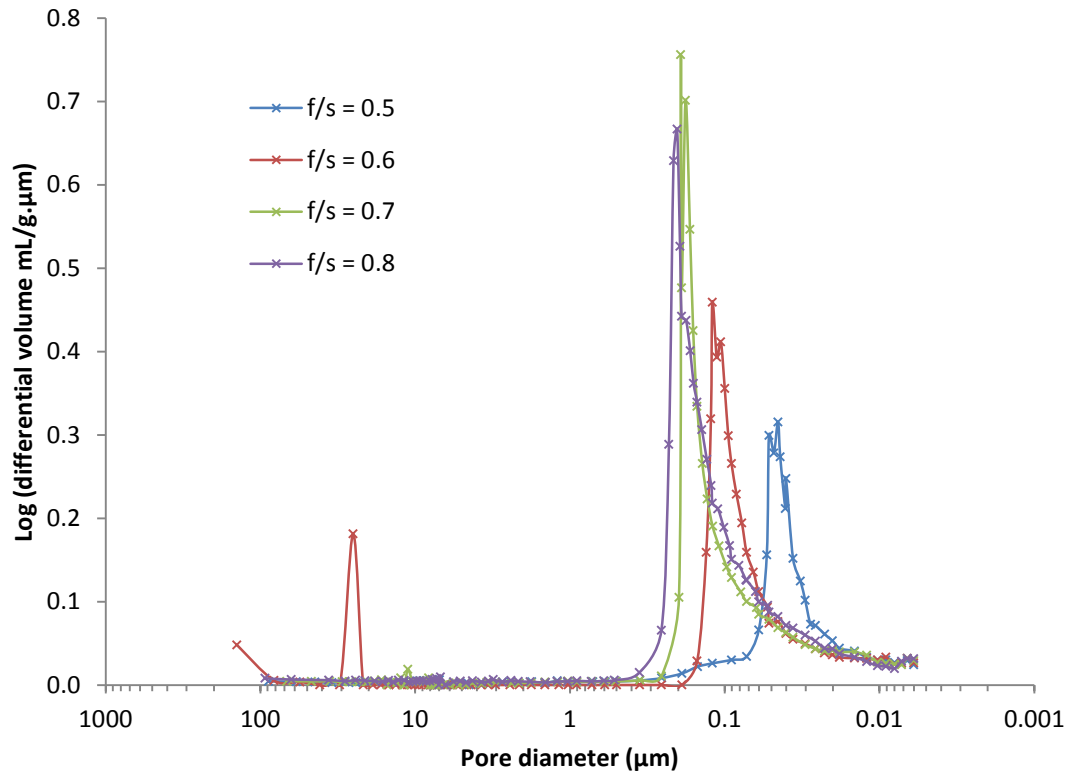


Figure 5.14 Pore size distribution in PFA:CAC + $(\text{NaPO}_3)_n$ + H_3BO_3 mixed at $w/s = 0.35$, $p/c = 0.4$, $r/c = 0.03$, after 7 days curing at 20°C

5.5.4. pH

Figure 7 shows the pH of wet cement slurries measured up to 150 minutes for CAP mixed at $w/s = 0.35$, $p/c = 0.4$, $r/c = 0.03$ with varying f/s . The figure also shows the pH of a typical cementing system currently used to encapsulate LLW and ILW in the UK; 3:1 BFS:PC mixed at $w/s = 0.35$. Although these pH measurements are not representative of the pore solution pH of the hardened cement pastes, they can be indicative of the initial host environment for encapsulated aluminium metal.

The BFS:PC system exhibited pH values between *ca.* pH 12.5-13.0 up to 150 minutes. Such a highly alkaline environment, in conjunction with readily available water, would cause significant corrosion of encapsulated aluminium metal [3, 4, 40, 166]. The various CAP systems exhibited significantly lower pH than the BFS:PC cementing system at all times, with pH values between *ca.* pH 9.0-10.5 up to 150 minutes. The pH of these systems increased with time, from values of *ca.* pH 9.0-10.0 at t_0 up to *ca.* pH 10.0-10.5 at t_{150} . This may have been due to the continued release of alkalis during the dissolution of PFA and CAC particles. Also, as the f/s increased, there was less of the acidic solution forming powders, $(\text{NaPO}_3)_n$ and H_3BO_3 , available to participate in the acid-base setting reactions. Consequently, pH increased with increasing f/s , with the formulation with $f/s = 0.8$ exhibiting the highest pH value at all times.

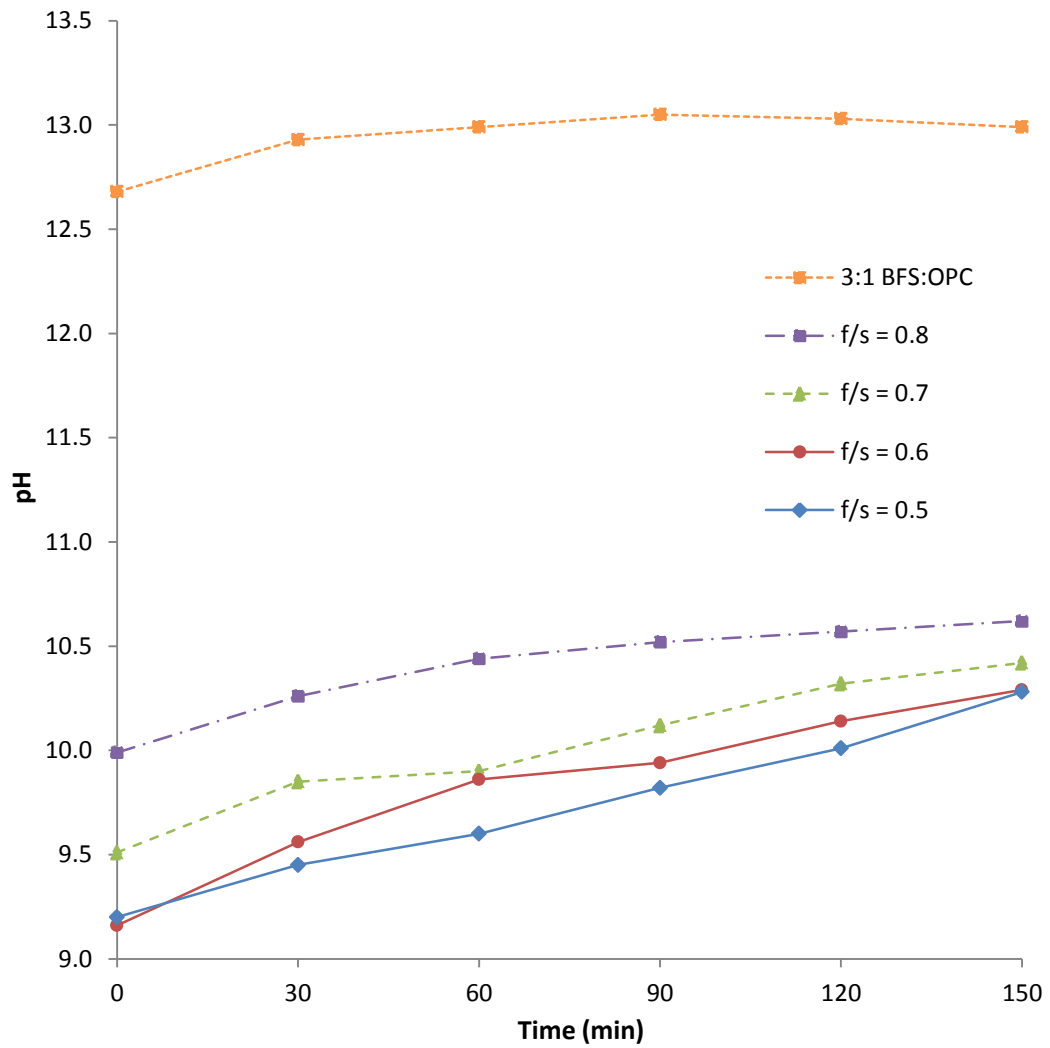


Figure 5.15 pH of cement slurries of PFA:CAC + (NaPO₃)_n + H₃BO₃ series and 3:1 BFS:PC system

5.6. Summary

The results from the preliminary investigations showed that the formulation parameters, such as the PFA and phosphate content, have an effect on the setting time of CAP systems. These results suggest that it is possible to control the setting time of the CAP cementing system by varying the formulation parameters. Water content had a limited retardation effect on setting, and phosphate content also indicated a retardation effect on setting time.

Boric acid significantly affected the setting characteristics of the CAP system leading to a satisfactory setting time which fulfilled the industry-defined requirement. The setting time of CAP was highly sensitive to boric acid content; a small increase in boric acid content resulted in a large increase in the setting time. The results presented here suggested that the boric acid content should be *ca.* $r/c = 0.03$ in order to attain acceptable setting time. The results from the plant acceptance tests demonstrated that the processing properties, i.e. the fluidity and setting times, of cementing system can be controlled by the inclusion of SCMs and additives, and the formulation parameters.

Decreasing the w/s decreased the fluidity of the cement slurry, as demonstrated by decreasing Colflow flow value. The results attained suggested that w/s should have a minimum of *ca.* $w/s = 0.3$ to fulfil the fluidity requirement after 150 minutes, although a $w/s = 0.35$ would be more practicable. It was also shown that the use of PFA, as a SCM, had a significant effect on the fluidity of the CAP system; increasing the PFA content resulted in increased slurry fluidity.

The XRD results suggested that no new crystalline phases formed in the hardened CAP cement pastes. It is proposed that the principle reaction phases responsible for

setting and strength development were ACP and alumina gel. This was in agreement with the results presented in Chapter 4 in which it was proposed that the principle reaction products in CAP systems were amorphous. The TG and DTG results suggested that the principle weight loss occurred below 120 °C, which may have been due to the dehydration of ACP and alumina gel. The SEM-BEI images showed the microstructure of the CAP systems, which exhibited PFA and partially-reacted CAC particles embedded within, what we can assume to be, the amorphous binding matrix. EDX results of the formulations investigated here suggested that the principle binding phase had a Ca/P ratio ≈ 1 , which is indicative of ACP.

The CAP systems developed significant strength after curing for 7 days at varying degrees depending on the replacement-level of SCMs. A typical porosity-strength trend was observed, whereby increased porosity corresponded to decreasing compressive strength. The pH measurements of CAP wet cement slurries up to 150 minutes were significantly lower than those of a conventional BFS:PC cementing system for ILW encapsulation, which suggests that these systems would cause significantly less corrosion of encapsulated aluminium metal.

The results presented here suggested that CAP cementing system may have potential as an alternative encapsulation matrix for problematic aluminium metal from the UK's legacy waste streams.

6. Results – Encapsulation of Aluminium in CAP

6.1. Introduction

The results discussed in the previous chapters demonstrated that the CAP system can satisfy the industry-defined plant acceptance test requirements for operational properties such as Colflow, setting times and bleed water, and a formulation envelope of the CAP system that satisfies these requirements have been identified. The purpose of this chapter is to study the behaviour of aluminium metal encapsulated in the CAP system in comparison to the BFS/PC and PFA/CAC systems.

Two representative CAP systems were used as a cement matrix to encapsulate aluminium metal, and the corrosion of aluminium was assessed by monitoring the volume of hydrogen gas generated and observing both the interface between aluminium and cement matrix and the corrosion surface using SEM and EDX. Aluminium was also encapsulated in PFA/CAC and BFS/PC systems to allow comparison. The initial pH of the wet cement slurries was also measured prior to setting as an indicator of the pH for each system. The corrosion of aluminium was studied up to 360 days.

6.2. Formulations

Two CAP formulations, CAP 1 with w/s = 0.35 and CAP 2 with w/s = 0.32, were used as representative systems to assess the corrosion of encapsulated aluminium. The CAP 1 formulation results from the development work reported in Chapters 4 and 5. CAP 2 was studied in order to assess the effect of reducing the water content of the system on corrosion behaviour of encapsulated aluminium. The results presented in Chapter 5 suggested that the CAP formulation should have a minimum water to solids ratio (w/s) of *ca.* 0.3. CAP 2 represents the lower end of the

formulation envelope in terms of water content, below which the cement would not provide sufficient fluidity to exhibit a suitable Colflow value. The other formulation parameters were defined based on the results presented in Chapter 5 and based on review and input by the project industrial supervisor. It was suggested that it may be desirable to increase the phosphate content, effectively increasing the concentration of the phosphate solution in order to reduce the pH of the system with the aim of limiting the corrosion of encapsulated aluminium metal. Therefore, the p/c ratio was increased to 0.4 compared to p/c ratio of 0.2 compared to the majority of the formulations studied previously in the project.

As shown in Table 6.1, both CAP 1 and CAP 2 formulations had $\text{PFA}/(\text{PFA}+\text{CAC}) = 0.6$ ($f/s = 0.6$), $(\text{NaPO}_3)_n/\text{CAC} = 0.4$ ($p/c = 0.4$) and $\text{H}_3\text{BO}_3/\text{CAC} = 0.03$ ($r/c = 0.03$). Two additional systems, BFS/PC ($f/s=0.75$) with $w/s = 0.35$ and PFA/CAC ($f/s = 0.6$) with $w/s = 0.35$, were also investigated for comparison. The PC-based system is a conventional cementing system which is currently used as an encapsulation matrix for ILW in the UK [11]. The CAC-based system was investigated in order to assess the effects of phosphate modification. Detailed formulations are given in Table 6.2.

Table 6.1 Formulations of cementitious systems

Formulation	Formulation ratios			
	w/s	f/s	p/c	r/c
CAP 1	0.35	0.6	0.4	0.03
CAP 2	0.32	0.6	0.4	0.03
BFS/PC	0.35	0.75*	-	-
PFA/CAC	0.35	0.6	-	-

* f/s for this formulation represent BFS/(BFS+PC) ratio.

Table 6.2 Details of formulation constituents for cementitious systems studied

Formulation	Formulation constituents							Total
	Cement		SCM		(NaPO ₃) _n	H ₃ BO ₃	H ₂ O	
	Type	wt%	Type	wt%	wt%	wt%	wt%	wt%
CAP 1	CAC	26.28	PFA	39.42	10.51	0.79	23.00	100
CAP 2	CAC	26.81	PFA	40.21	10.72	0.80	21.45	100
BFS/PC	PC	18.52	BFS	55.56	-	-	25.93	100
PFA/CAC	CAC	29.63	PFA	44.44	-	-	25.93	100

6.3. Initial Corrosion of Aluminium in Cement Matrices

6.3.1. Hydrogen Gas Generation up to 28 days

Figure 6.1 shows the cumulative gas generation resulting from the corrosion of aluminium metal encapsulated in the cementitious systems – CAP 1, CAP 2, BFS/PC and PFA/CAC – for up to 28 days. Figure 6.2 shows the corresponding rate of gas generation for these systems during this period. These results are indicative of the short term corrosion behaviour of aluminium encapsulated in the cementing systems studied.

During the initial 28 day curing period, by far the most gas generated was from the BFS/PC system with encapsulated aluminium. This sample exhibited significant rapid gas generation that commenced as soon as the aluminium plate was submerged into the cement paste; Figure 6.3 shows the bubbles that were observed being released from the surface of the cement sample. The rate of gas generation was *ca.* 8 litres h⁻¹ m⁻² in the first hour from the aluminium plate being submerged. The rate then reduced during the initial 24 h of monitoring, to *ca.* 5 litres h⁻¹ m⁻², having generated a total of *ca.* 300 ml of gas. After 7 days the sample had generated *ca.* 900 ml of gas, and the gas generation rate had reduced significantly to less than *ca.* 0.1 litres h⁻¹ m⁻². These results show that the BFS/PC systems exhibited a typical behaviour of a high-pH cement matrix for reactive metal such as aluminium encapsulated; there was a period of rapid corrosion and gas generation, referred to as the acute phase or acute corrosion rate, followed by a reduction to a lower long-term corrosion rate, referred to as the chronic phase or chronic corrosion rate [40, 167]. The transition from acute phase to chronic phase is demonstrated by the effective plateauing of the cumulative gas generation from *ca.* 7 days onwards as can be seen in Figure 6.1.

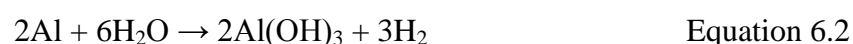
The PFA/CAC system exhibited gas generation within the first few hours after the aluminium plate being submerged in the cement. The rate of gas generation was *ca.* 3 litres h⁻¹ m⁻² after 1 h, having generated 7 ml of gas. The gas generation rate then reduced to a relatively constant rate of between *ca.* 0.1-0.2 litres h⁻¹ m⁻² after the first 24 h, which continued up to 28 days of curing. After 28 days the sample had generated a total of *ca.* 330 ml of gas.

Both the CAP 1 and CAP 2 cementitious systems exhibited effectively no gas generation during the first 24 hour period, and over the first 28 days the systems generated a total of 35 ml and 34 ml of gas, respectively. The average gas generation rates during this period were less than 0.07 litres h⁻¹ m⁻² for both systems. This suggests that very little corrosion occurred during the first 28 days period for both CAP 1 and CAP 2 cementitious systems.

Using these data of H₂ gas volume, the amount of aluminium corroded was estimated. The amount of H₂ gas in moles was firstly estimated using the ideal gas equation:

$$n = PV/RT \quad \text{Equation 6.1}$$

The *n* in Equation 6.1 is the generated H₂ gas in moles, *P* is atmospheric pressure, *V* is the volume of the gas generated, *R* is gas constant and *T* is the temperature, respectively. The amount of aluminium corroded was then estimated based on the reaction given in Equation 6.2. The obtained results are summarised in Table 6.3.



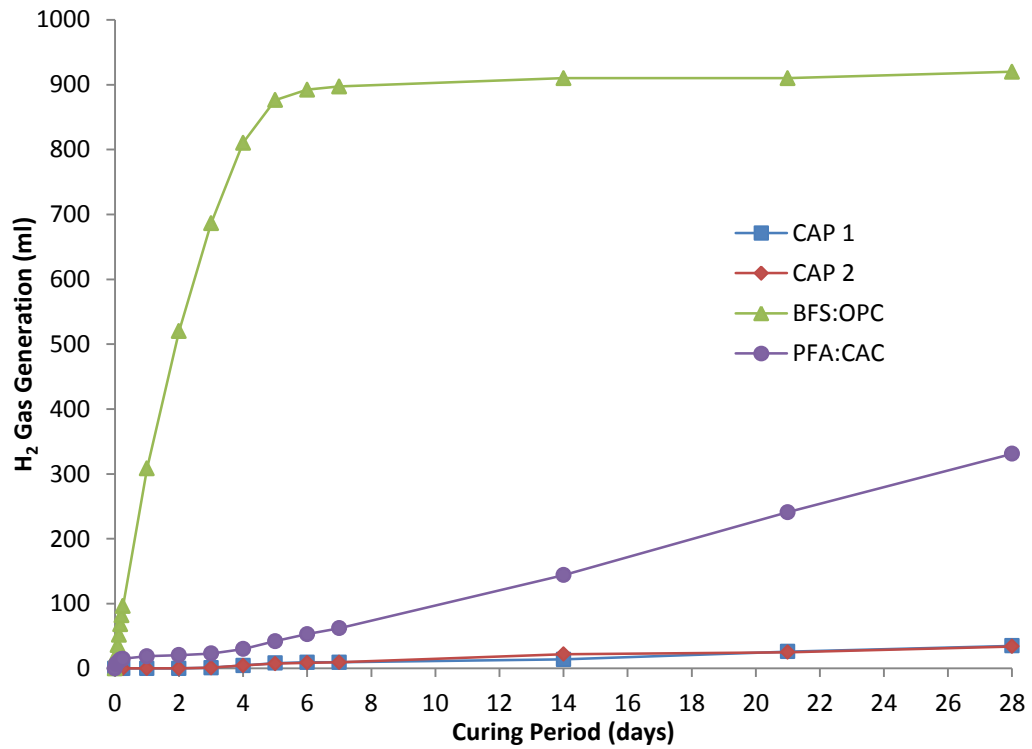


Figure 6.1 Cumulative gas generation from encapsulated aluminium up to 28 days

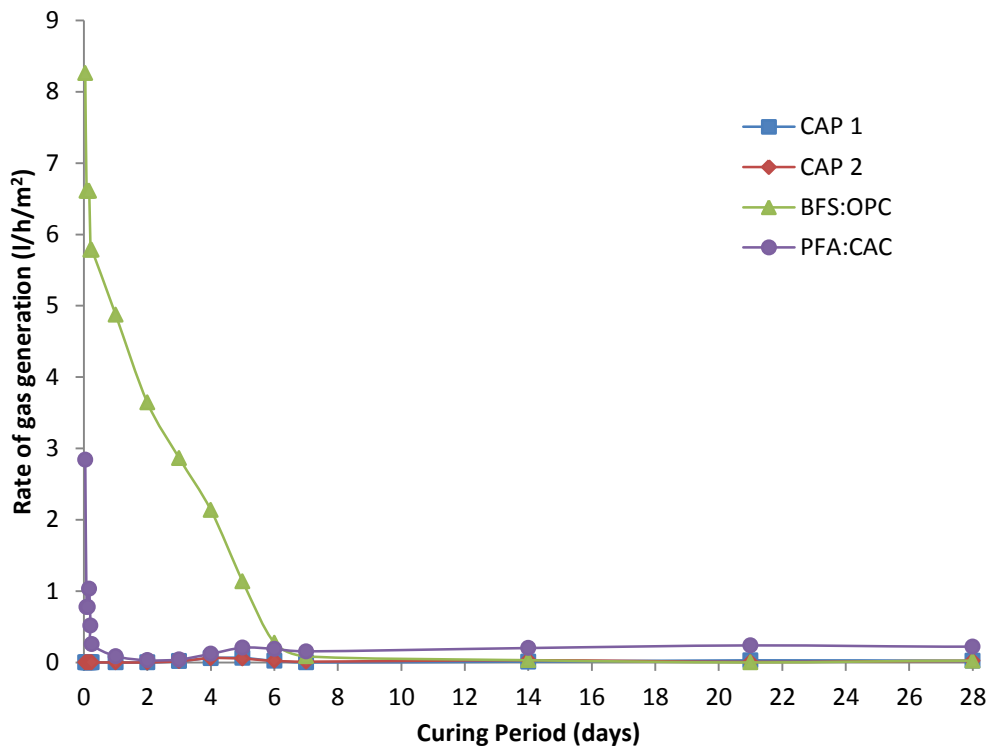


Figure 6.2 Gas generation rate from encapsulated aluminium up to 28 days



Figure 6.3 Gas bubbles formed from aluminium encapsulated in BFS/PC

Table 6.3 Summary of cumulative gas generation and quantity of aluminium corroded from aluminium encapsulated up to 28 days

Formulation	Cumulative Gas Generation (ml)			Aluminium corrosion (g)		
	24 h	7 days	28 days	24 h	7 days	28 days
CAP 1	0	9	35	0.000	0.007	0.026
CAP 2	0	9	34	0.000	0.007	0.025
BFS/PC	308	897	920	0.230	0.671	0.688
PFA/CAC	19	62	331	0.014	0.046	0.248

6.3.2. Initial pH of Cement Pastes

Figure 6.4 shows the pH of the cement systems measured from t_0 , immediately after the initial mixing process without addition of aluminium, up to t_{150} . The pH value for the BFS/PC system was pH 12.7 at t_0 , which then increased with time to a value of *ca.* pH 13.0 at t_0 . This is comparable with the reported values of *ca.* pH 12.9-13.0 in the first 6 h after mixing for a 9:1 BFS/PC system by Collier *et al.* [21]. It has been accepted that such highly alkaline environments are responsible for the rapid and significant corrosion of aluminium when encapsulated [3, 6], which is also demonstrated in the present study by the hydrogen gas generation results presented in Figure 6.1 and Figure 6.2.

The high pH of PC-based systems is due to the release of soluble alkalis, in the form of sulphates of sodium and potassium, during the dissolution of the cementitious phases, and later the formation of $\text{Ca}(\text{OH})_2$ [168].

The pH of the PFA/CAC system was *ca.* pH 11.7 at t_0 . The system exhibited a relatively quick setting time of *ca.* 80 minutes and as such only measurements up to t_{60} were achieved, at which point the PFA/CAC system exhibited *ca.* pH 12.1.

The pH values of both CAP systems are significantly less than those of the BFS/PC system at all times. The results show that the pH of the CAP 1 and CAP 2 systems at t_0 were *ca.* pH 9.1 and pH 8.1, respectively. The pH values of the wet cement slurries gradually increased during the following 150 min period to maximum measured value at t_{150} of *ca.* pH 10.3 and pH 10.0, respectively. The pH of the CAP 1 system was higher than that of the CAP 2 at all times up to t_{150} . This is due to the lower water content of the CAP 2 system effectively resulting in a higher concentration

acidic phosphate solution with lower pH of *ca.* pH 4.6 compared to that for the CAP1 system which was measured to be *ca.* pH 5.2.

The quantity of aluminium corroded in the cementitious systems were plotted against the final pH values of the initial cement pastes in Figure 6.5. The results have a good correlation with the initial aluminium corrosion in the short-term, especially after 28 days as shown in the Figure 6.5, whereby the quantity of aluminium corrosion increases with pH. However, the use of the initial cement paste pH does not correlate well with the longer-term (90 and 175 days) corrosion of aluminium. It should be noted therefore that these pH values are not necessarily representative of the internal pH of the cement pore solution, but do at least give an indication of the initial environment to which the aluminium metal is initially subjected. These results suggests that the pH of the CAP systems in particular may increase with time.

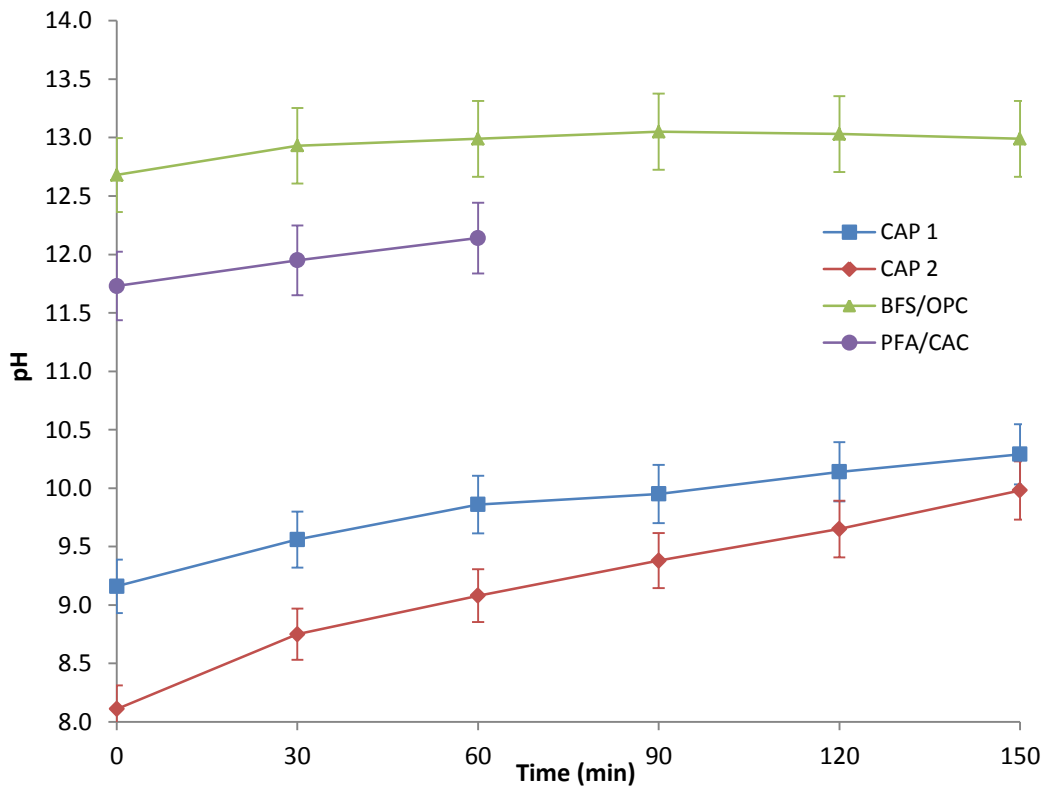


Figure 6.4 pH measurements of cement systems prior to setting

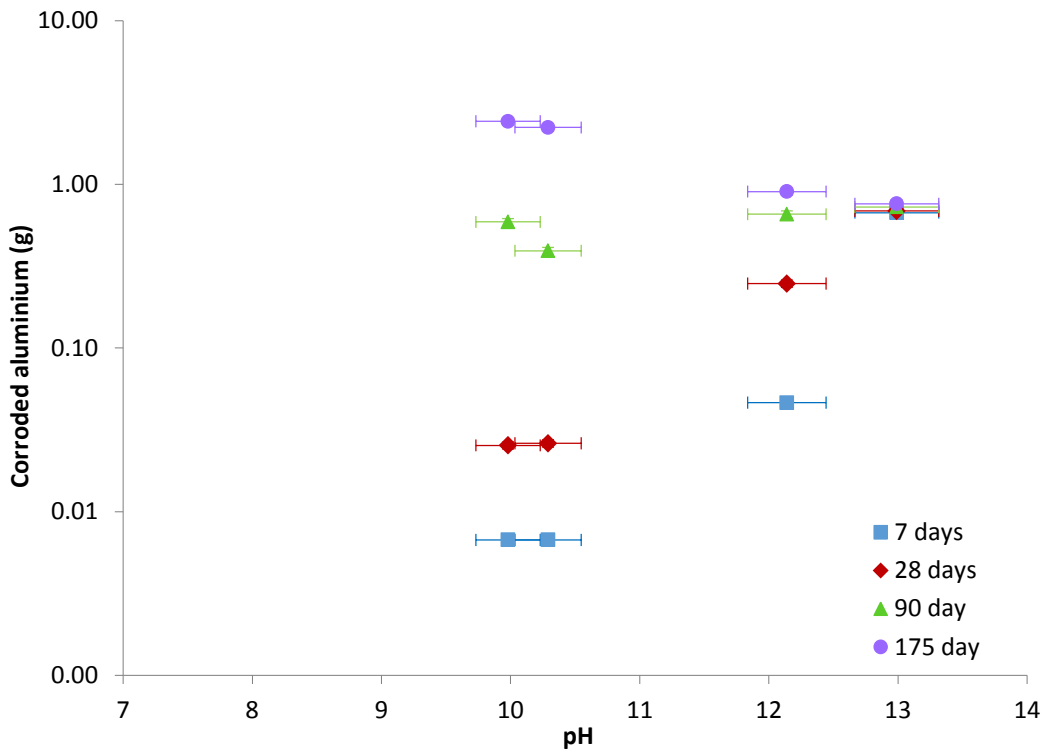


Figure 6.5 Amount of aluminium corroded in the cementitious systems

6.4. Corrosion of Aluminium in the Longer-Term

6.4.1. Hydrogen Gas Generation up to 175 days

Figure 6.6 and Figure 6.7 show the cumulative gas generation and gas generation rates, respectively, from aluminium encapsulated in the cementitious systems for up to 175 days. The BFS/PC system exhibited a very low gas generation rate following the high generation rate of the initial 7 days. The gas generation from the BFS/PC systems from 28 days to 175 days was generally less than $0.02 \text{ litres h}^{-1} \text{ m}^{-2}$, resulting in *ca.* 100 ml of gas generation in the period between 7 days and 175 days, leading to the total gas of *ca.* 1020 ml generated up to 175 days. This is the typical corrosion behaviour for aluminium encapsulated in cementitious systems [167]. In such environment aluminium typically exhibits an initial period of rapid corrosion and hydrogen gas generation, known as the acute corrosion phase. This acute corrosion phase is short-lived and the corrosion rate quickly decreases to a relatively low long-term so called chronic corrosion rate.

The PFA/CAC system exhibited prolonged gas generation which persisted throughout the period studied. The rate of gas generation was generally constant over the first *ca.* 45 days with a value of *ca.* $0.2 \text{ litres h}^{-1} \text{ m}^{-2}$. After *ca.* 45 days the gas generation rate gradually reduced over time; after 175 days the gas generation rate was *ca.* $0.04 \text{ litres h}^{-1} \text{ m}^{-2}$. The PFA/CAC system generated a total of *ca.* 1200 ml of gas during the monitored 175 day period.

The CAP 1 and CAP 2 systems exhibited significant changes in corrosion behaviour during the 175 day curing period, which can be characterised by an apparent dormant period of low corrosion rate followed by a latent corrosion rate. As discussed previously, in the short term, the corrosion rates of these CAP systems were lower compared to the other two systems, in particular the BFS/PC system. However, after

a curing period of *ca.* 55-65 days CAP systems exhibit a significant increase in gas generation rates. The subsequent rate of gas generation for both systems was *ca.* 0.4-0.5 litres h⁻¹ m⁻² for the remaining period of the study up to 175 days. The cumulative gas generation from the CAP1 and CAP 2 systems eventually exceeded that from the BFS/PC and PFA/CAC systems after *ca.* 105 days and resulted in *ca.* 2970 ml and *ca.* 3245 ml of total gas generation after 175 days, respectively.

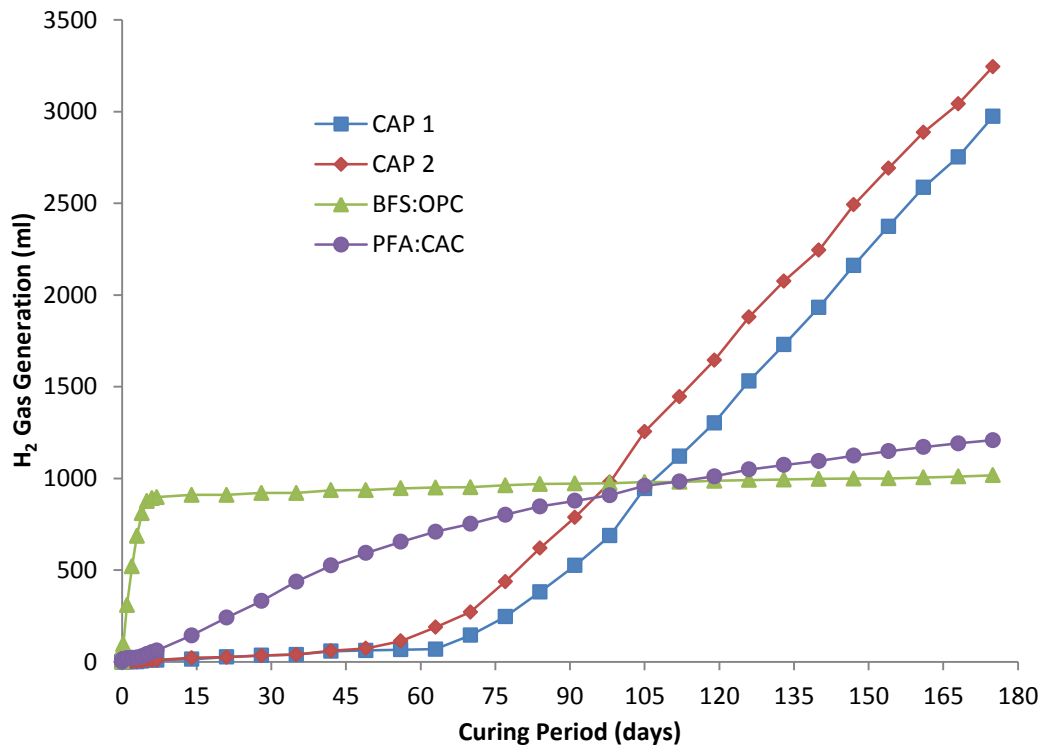


Figure 6.6 Cumulative gas generation from encapsulated aluminium up to 175 days

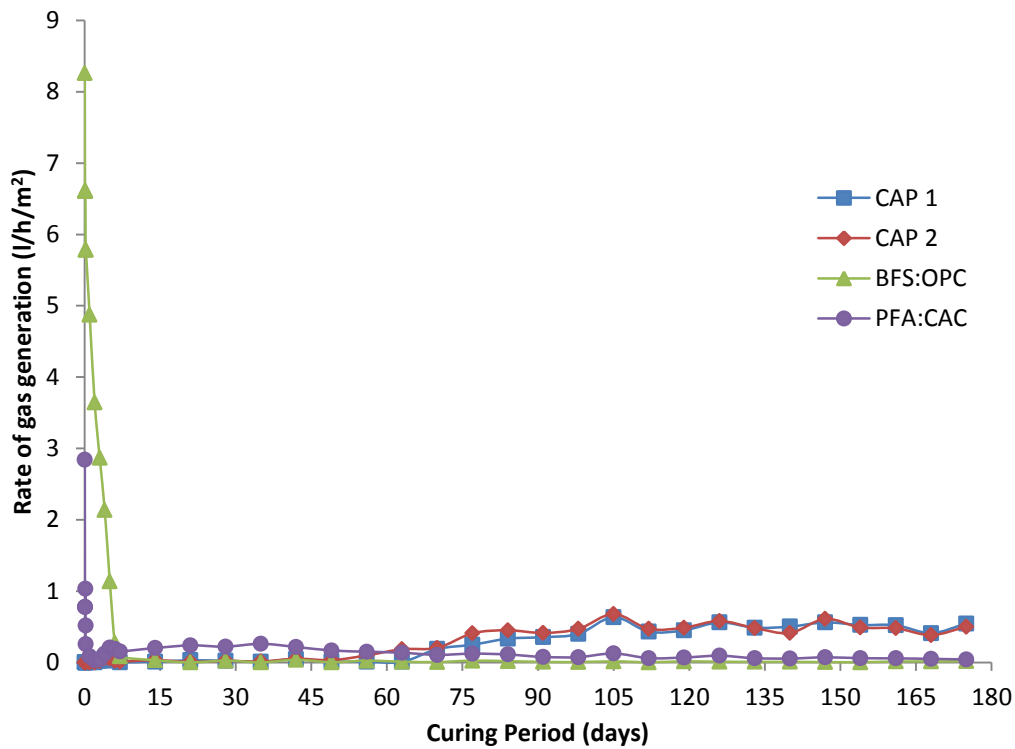


Figure 6.7 Gas generation rate from encapsulated aluminium up to 175 days

6.4.2. Examination of Specimens for BFS/PC System

Figure 6.8 shows the BFS/PC samples with the encapsulated aluminium after 90 days, 180 days and 360 days, respectively. On observation, there was no obvious difference between the samples with increasing encapsulation period, which is consistent with the results of hydrogen gas generation and suggests that significant change in the sample did not occur after 90 days.

The samples were characterised by a grey layer on the top of the sample, with a hole exposing the aluminium specimen within. Setiadi *et al.* observed a similar layer on top of samples of aluminium encapsulated in PC-based systems [3]. The hole was considered to have formed as a gas release pathway due to the significant gas generation during the setting and hardening of the BFS/PC system. They proposed that this layer, consisting of a mixture of strätlingite and gibbsite, was formed by corrosion products being transported to the sample surface by gas generation during the initial acute corrosion phase prior to the cement setting and hardening. The samples did not exhibit any cracking or obvious signs of significant dimensional change up to 360 days.

A white corrosion product that appeared to be a powdery substance adhered to both the aluminium metal and the cement matrix. The adhesion was rather weak as the aluminium specimens were easily removed from the bulk of the cement. The interfacial zone between the aluminium and cement consists of a network of voids, formed by the generation of hydrogen gas during the setting process, into which the white corrosion product precipitated. Beyond the interfacial zone, the bulk cement appears unaffected by the corrosion. It appears that formation of expansive corrosion

products was accommodated by the network of voids and highly porous zone that was formed due to the significant gas generation as discussed previously.

(a) 90 days**(b) 180 days****(c) 360 days****Figure 6.8 Corrosion of aluminium in BFS/PC system: (a) 90 days, (b) 180 days and (c) 360 days**

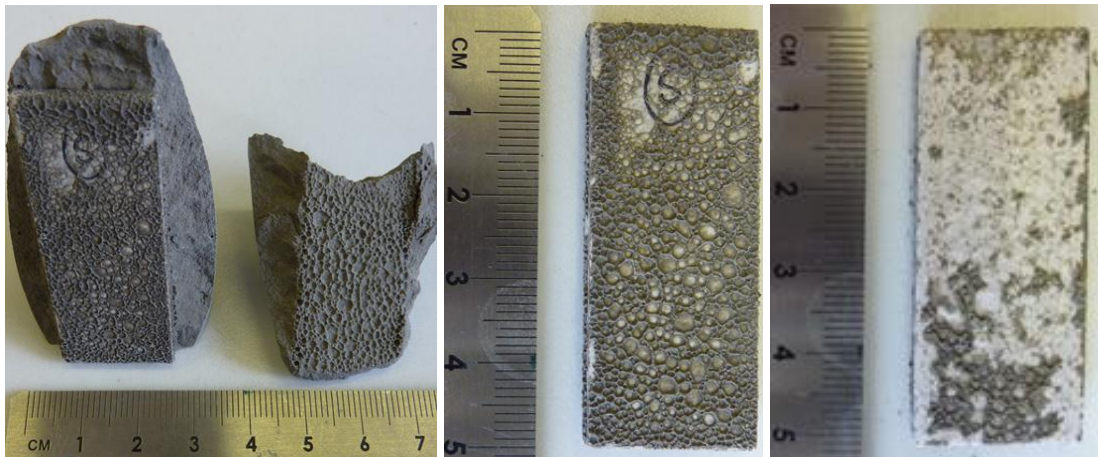
6.4.3. Examination of Specimens for PFA/CAC System

Figure 6.9 shows the PFA/CAC samples with the encapsulated aluminium after 90 days, 180 days and 360 days, respectively. The samples after all curing periods appear to be very similar.

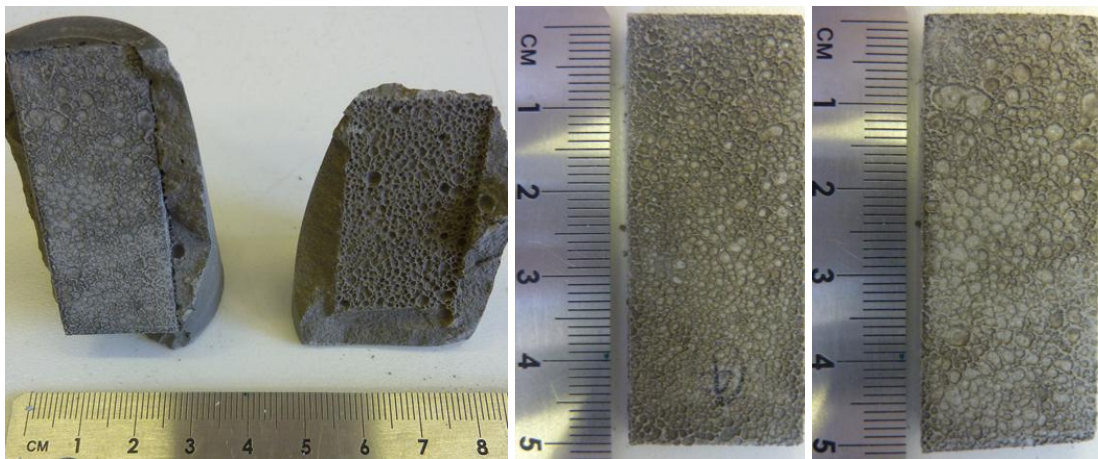
There were no obvious signs of corrosion reaction observed from outside of the samples prior to the samples being broken open, in order to examine the encapsulated aluminium specimens; there was no cracking, significant dimensional changes or bulging. The surface of the cement did not exhibit a hole, thus differing from the BFS/PC system.

On retrieval of the aluminium specimens from the bulk cement, signs of corrosion were observed. There was an interfacial zone between the specimens of aluminium and the bulk cement consisting of a network of voids and porosity. The PFA/CAC systems exhibited a relatively quick initial setting time of *ca.* 80 minutes during which the gas generation rate, as discussed in Section 6.3, was relatively high (*ca.* 1-3 litres h⁻¹ m⁻²). It is therefore suggested that the 'foamed' structure was the result of the generation of hydrogen gas during the setting and hardening of the cement. The surface of the aluminium metal, which was revealed below the foamed interfacial layer, appeared to be covered with white-grey corrosion products. The foamed interfacial zone may have allowed accommodation of expansive corrosion products and therefore avoided significant dimensional changes or cracking of the bulk cement.

(a) 90 days



(b) 180 days



(c) 360 days

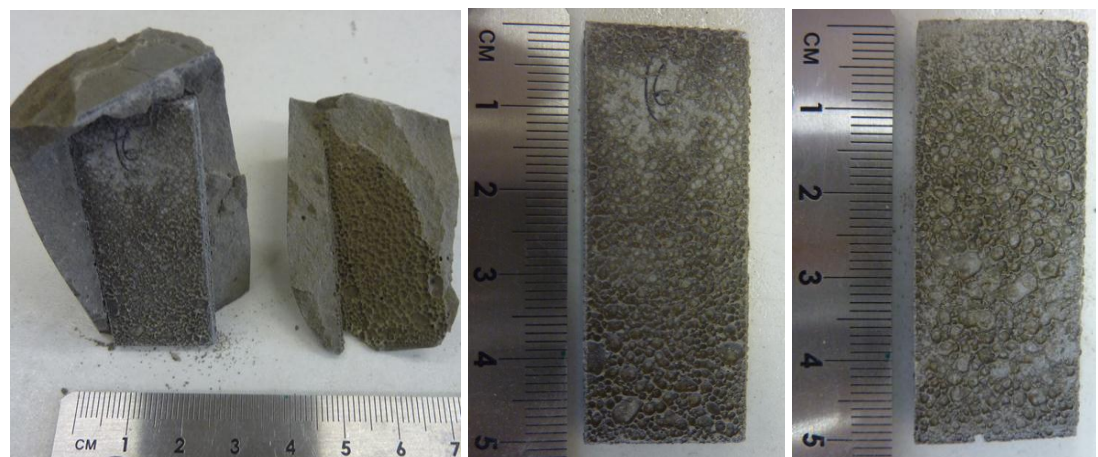


Figure 6.9 Corrosion of aluminium in PFA/CAC system: (a) 90 days, (b) 180 days and (c) 360 days

6.4.4. Examination of Specimens for CAP System

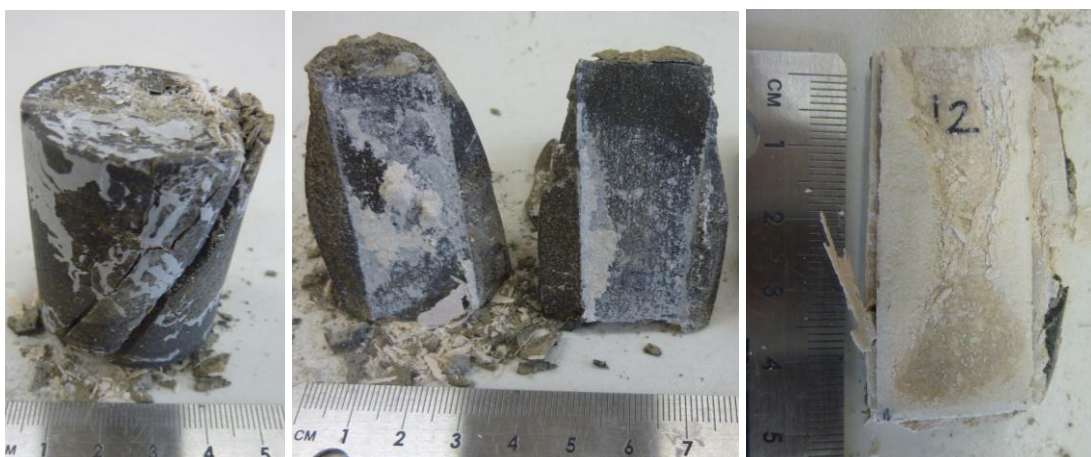
Figure 6.10 shows photographs of CAP 1 samples with aluminium encapsulated for 90 days, 180 days and 360 days. Both CAP1 and CAP 2 samples exhibited very similar behaviour, and as such the results of the CAP 1 system are discussed as a representative of both CAP systems up to 360 days. The corresponding photographs, SEM and BEI micrographs and EDX elemental mapping data for the CAP 2 samples are given in Appendix 3 for reference.

After 90 days, the sample did not show any obvious signs of corrosion or dimensional change e.g. cracks or bulging. Once retrieved from the sample, the aluminium specimen exhibited some degree of corrosion exemplified by a relatively thin layer of white corrosion product that was observed both on the surface of the aluminium and that of the cement.

After a period of 180 days, the sample exhibited signs of corrosion. The cement sample was cracked and had undergone significant dimensional changes; the sample had cracked parallel to the plane in which the aluminium specimen was orientated. The aluminium exhibited a significant white corrosion layer of *ca.* 1-2 mm in thickness on the surface. A significant increase in the corrosion layer during 90 to 180 days is consistent with the increased H₂ gas generation during this period as discussed in the previous sections. The majority of the corrosion layer was adhered to the aluminium specimen, but some was also adhered to the cement surface.

After 360 days, the plastic container had significantly distorted and the cement had cracked severely, exposing the top of the aluminium specimen and associated corrosion product. Once removed from the container, the sample disintegrated and the aluminium specimen was exposed. The white corrosion layer was *ca.* 2 mm in

thickness and was largely adhered to the aluminium. Some of the corrosion product layer was also left adhered to the surface of the cement.

(a) 90 days**(b) 180 days****(c) 360 days****Figure 6.10 Corrosion of aluminium in CAP1 system: (a) 90 days, (b) 180 days and (c) 360 days**

6.5. Aluminium-Cement Interface

6.5.1. BFS/PC system

Figure 6.11 shows BEI of aluminium specimens encapsulated in the BFS/PC system for 28 days, 180 days and 360 days. The samples at all ages exhibit signs of corrosion supporting the results from hydrogen gas generation measurements that suggested the significant corrosion of aluminium encapsulated in this system.

The samples from all curing periods are characterised by a corrosion layer and highly porous interfacial zone between the aluminium and the cement matrix. The corrosion of aluminium appears to be based on the pitting corrosion typically observed for the metals in contact with moisture [40, 169, 170]. The thickness of the corrosion layer did not change significantly during this period suggesting that there was only a slow on-going corrosion subsequent to the initial rapid corrosion that occurred during the first few days, which corresponds to the hydrogen gas generation results. The highly porous zone must have formed as a result of the significant hydrogen gas generation during the setting and hardening of the cement system. The porosity and voids in this area appear to increase over time. This may suggest that the corrosion reaction of aluminium also results in “corrosion” of cement matrix; the hydrate phases such as calcium hydroxide or C-S-H dissolve to provide OH^- ions for the corrosion of aluminium, leaving empty space around aluminium. Further study is required to clarify this aspect.

The EDX elemental mapping results presented in Figure 6.12 and Figure 6.13 appear to show two different types of corrosion products. The corrosion layer adjacent to the aluminium metal consists of high concentrations of aluminium and oxygen, whereas calcium and silicon are also distributed between the corrosion layer and the bulk cement. These must respectively correspond to aluminium hydroxide and strätlingite,

both of which have been reported as a corrosion product of aluminium in cement matrices [3, 40]. Setiadi *et al.* [3] and Setiadi [40] suggested that soluble hydroxyl-aluminate ions ($\text{Al}(\text{OH})_4^-$), formed from the dissolution of aluminium react with C-S-H and possibly calcium hydroxide to form strätlingite. The formation of strätlingite restricts the diffusion of OH^- ions to the aluminium surface, resulting in the decomposition of the hydroxyl-aluminate and precipitation of aluminium hydroxide at the aluminium surface.

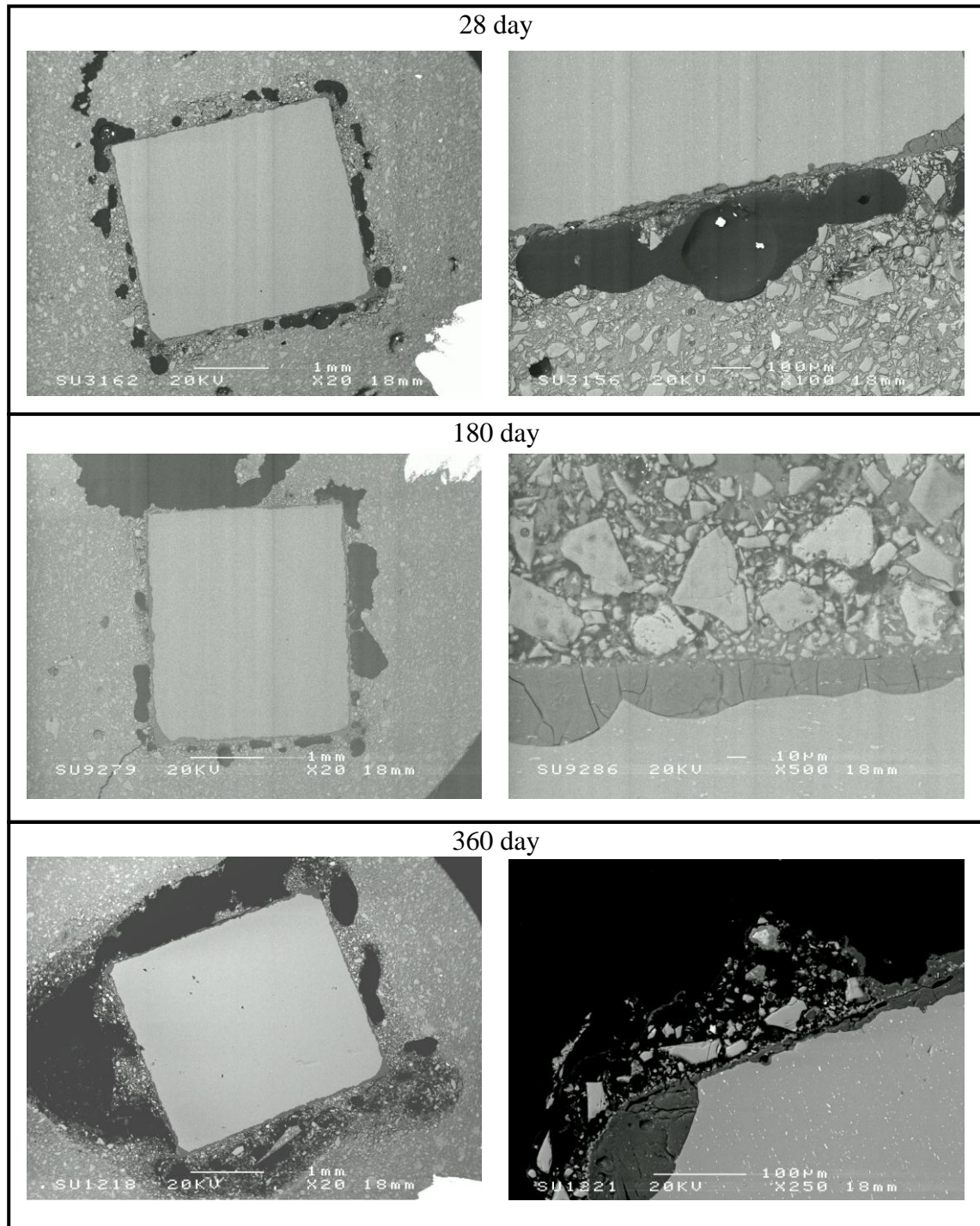


Figure 6.11 BEI of aluminium encapsulated in BFS:PC for 28, 180 and 360 days

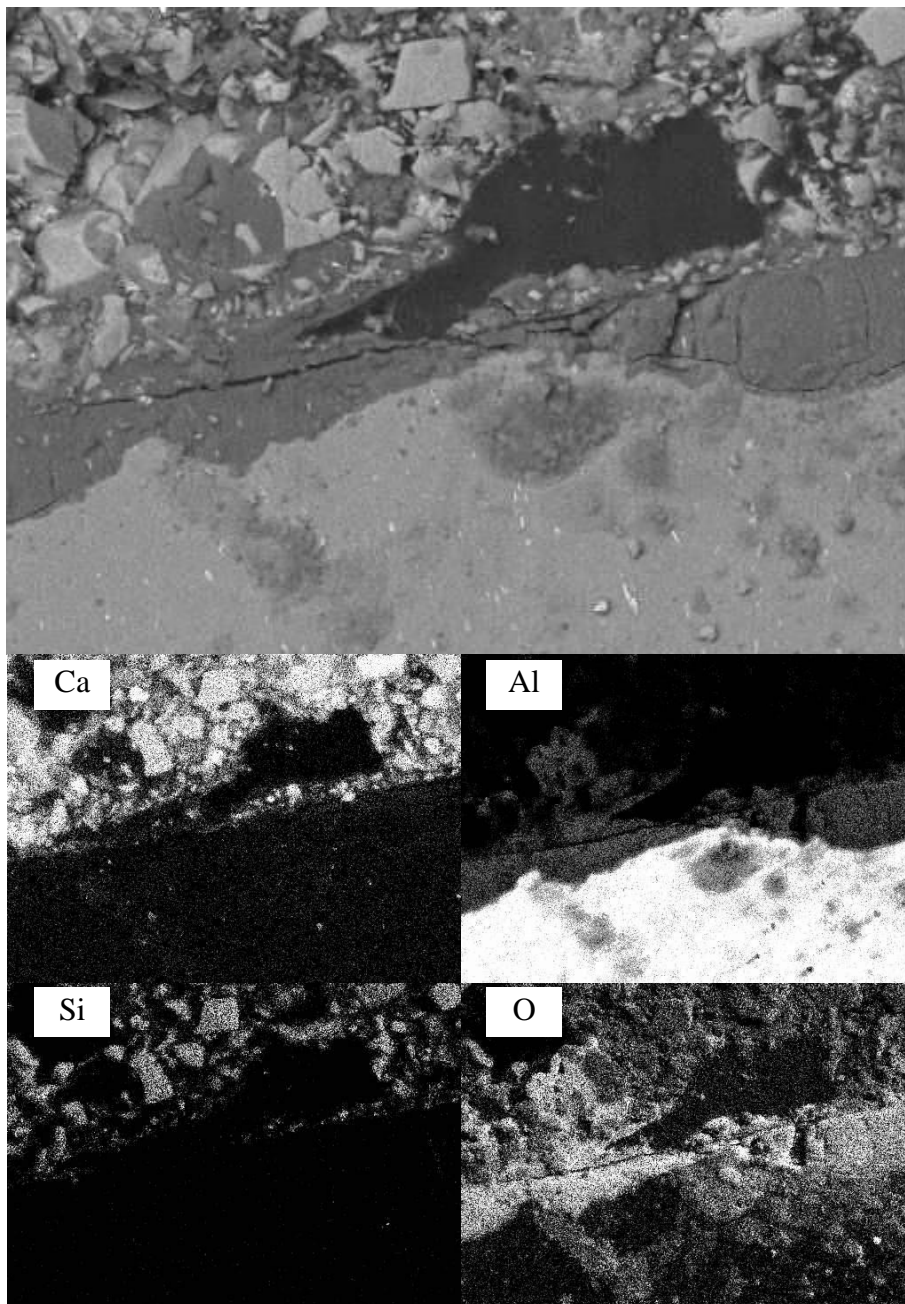


Figure 6.12 BEI and EDX elemental mapping of aluminium-cement interface in BFS/PC after 28 days

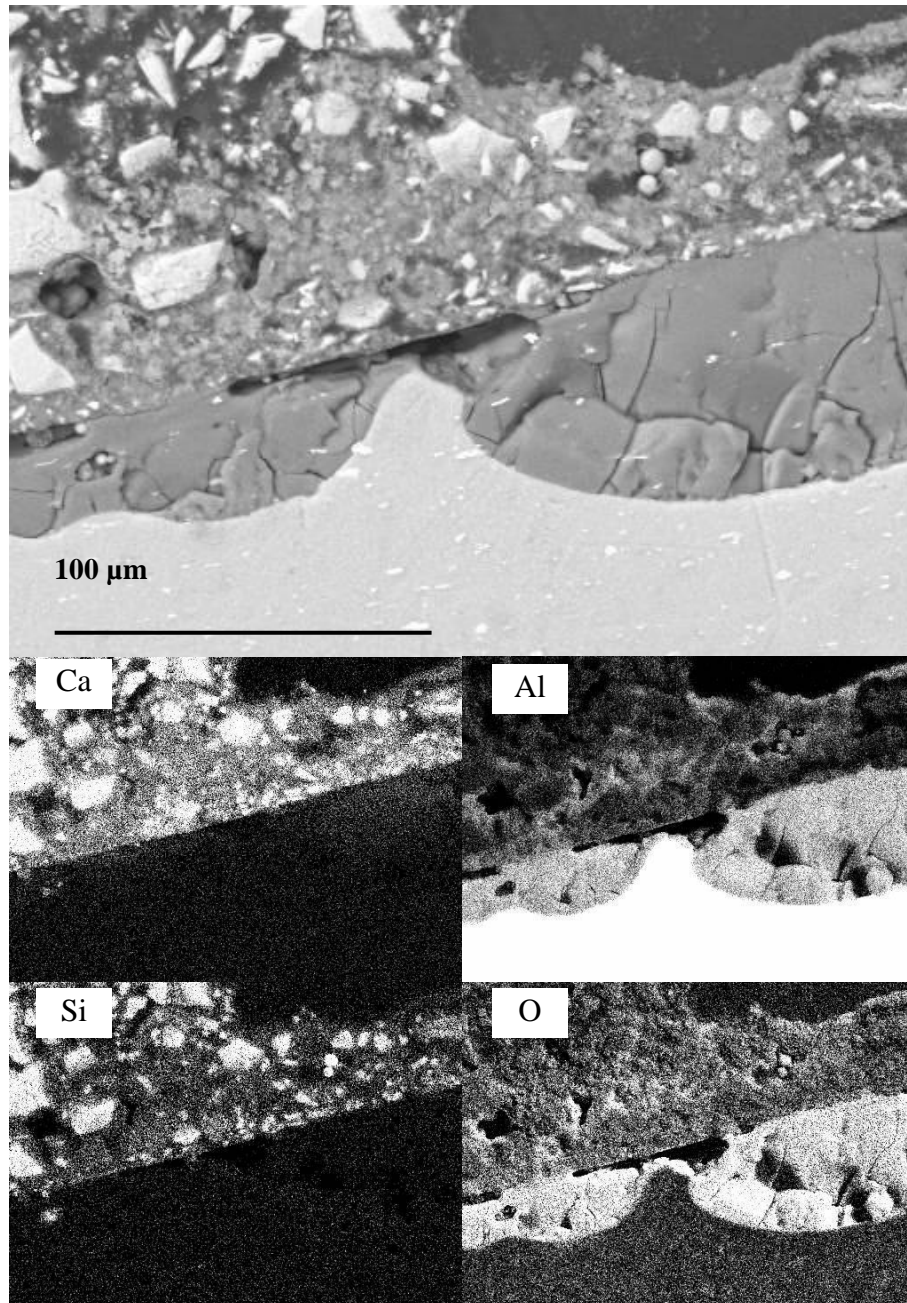


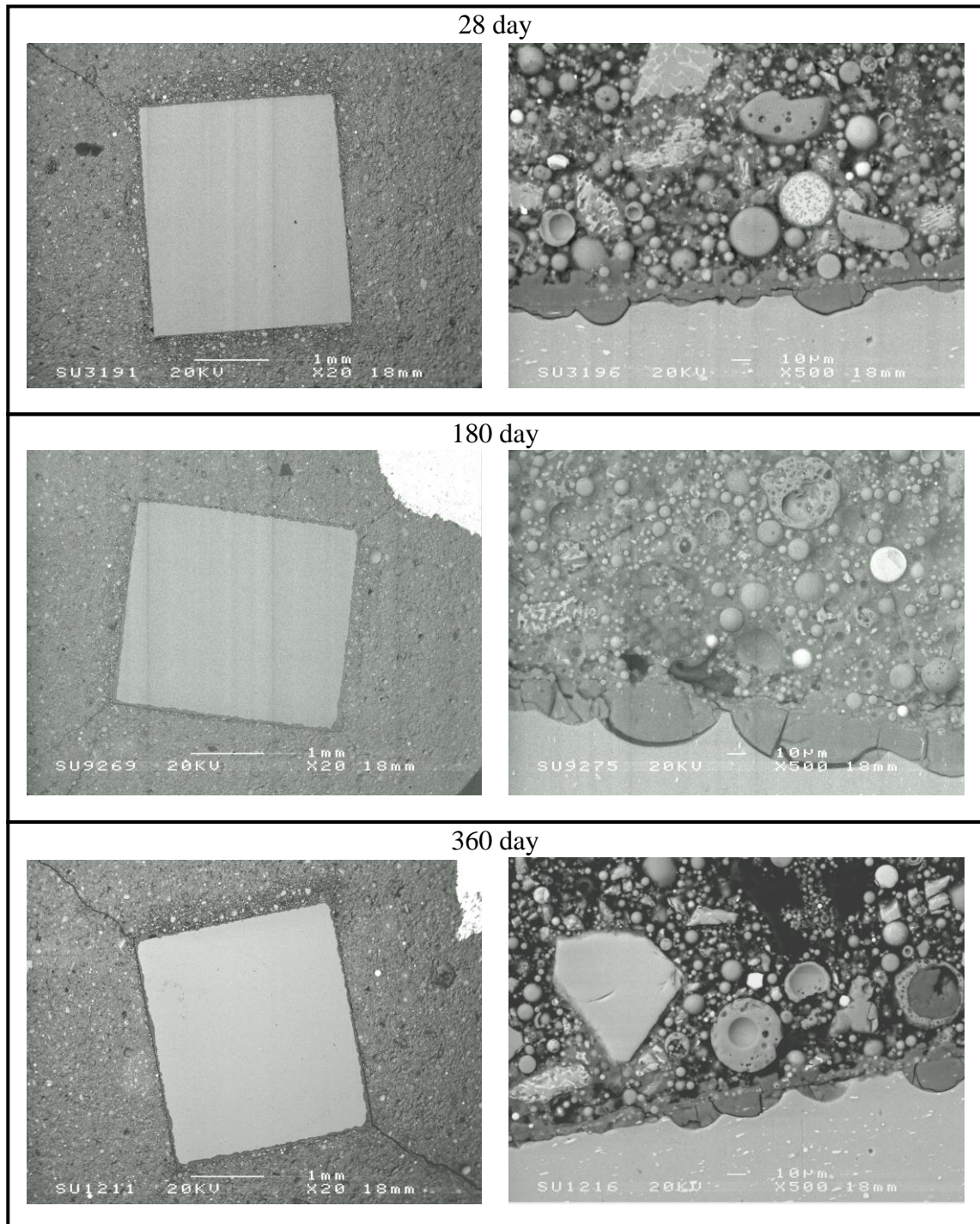
Figure 6.13 BEI and EDX elemental mapping of aluminium-cement interface in BFS/PC after 180 days

6.5.2. PFA/CAC system

Figure 6.14 presents BEI of aluminium specimens encapsulated in the PFA/CAC system for 28 days, 180 days and 360 days.

All the specimens exhibit pitting corrosion and a relatively modest corrosion layer. The thickness of the corrosion layer increased from *ca.* 10-20 μm after 28 days up to *ca.* 50-100 μm after 360 days. These results are consistent with those from the hydrogen gas generation measurements that suggest the aluminium encapsulated in PFA/CAC experiences relatively constant corrosion over time.

The corresponding EDX elemental mapping data (Figure 6.15) suggests that the corrosion layer consists of aluminium and oxygen, and is therefore likely to be aluminium hydroxide, similar to the BFS/PC system based on its rather high initial pH. This system exhibited small cracks that radiated from the corners of the aluminium specimen. These may have occurred due to chemical shrinkage of the cement during setting and the relatively high volume fraction of aluminium in the sample.



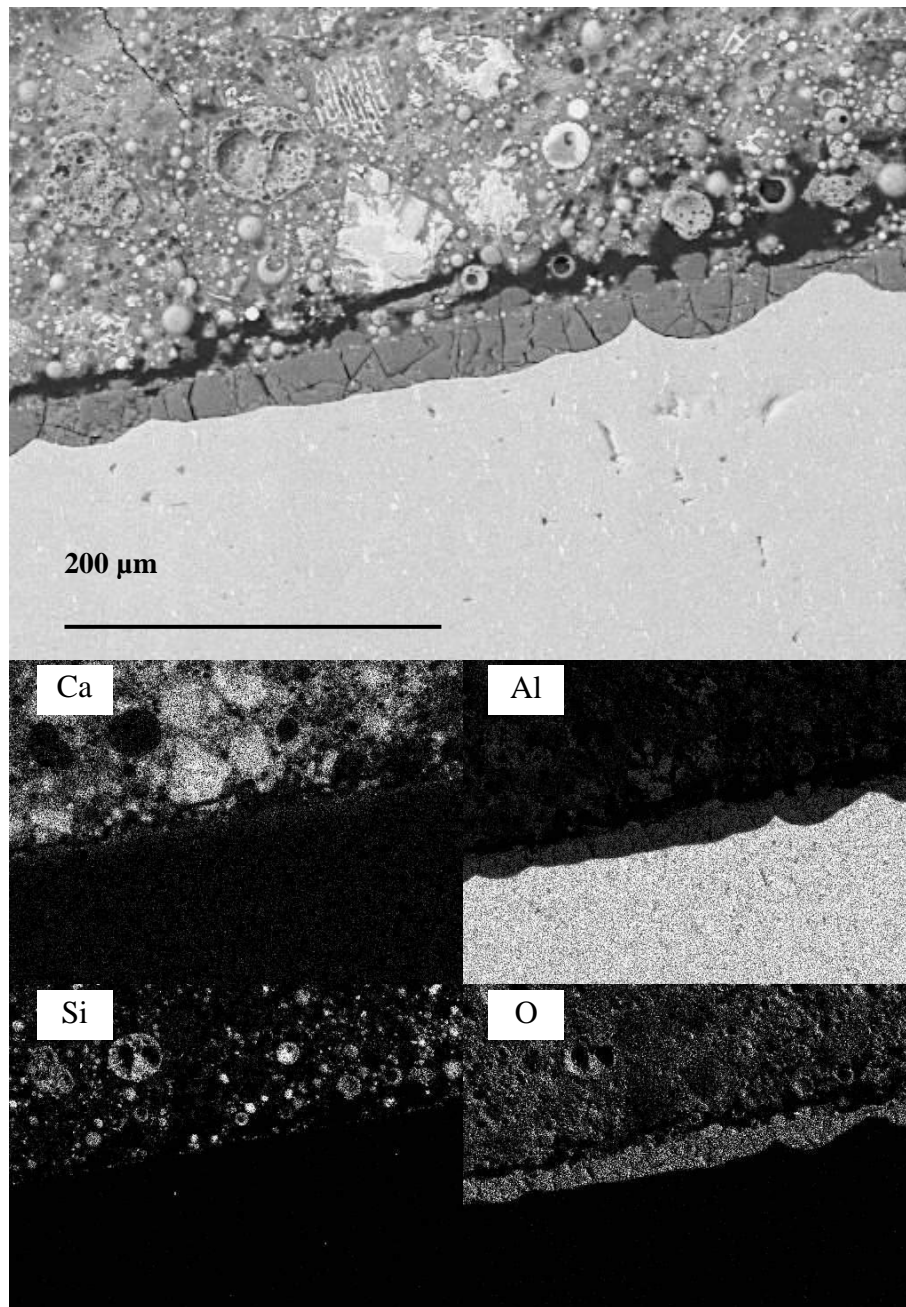


Figure 6.15 BEI and EDX elemental mapping of aluminium-cement interface in PFA/CAC after 360 days

6.5.3. CAP Systems

The SEM BEI presented in Figure 6.16 show specimens of aluminium metal encapsulated in the CAP 1 system for 28, 180 and 360 days. Similar to a previous section, the results of the CAP 1 system are discussed as a representative of both CAP systems up to 360 days as both CAP1 and CAP 2 samples exhibited similar behaviour. The corresponding photographs, SEM and BEI micrographs and EDX elemental mapping data for the CAP 2 samples are given in Appendix 3 for reference.

The sample exhibited some cracking that radiated from the corners of the aluminium specimen after 28 days as shown in Figure 6.16. Because an insignificant amount of aluminium corrosion had taken place at this stage, it is thought that this may be due to the samples having effectively very high volume fraction of aluminium and shrinkage of the CAP cement during the setting process [65, 107, 156, 171]. It was also observed that the cement was not adhered to the aluminium specimen with a gap of *ca.* 20-30 μm between the surface of the aluminium metal and the cement matrix. It is suggested that this may also be the result of chemical shrinkage during setting. The aluminium specimen is estimated to have a thickness of *ca.* 3 mm, which is identical to the original dimensions prior to encapsulation, showing little signs of corrosion.

There appears to be a very thin corrosion layer, less than 10 μm thick, as shown in Figure 6.16, on the surface of the aluminium. The layer consists of aluminium and oxygen, which is likely to be aluminium hydroxide and/or aluminium oxide. It appears that, during the initial 28 days, the CAP system provides an environment in which the initial corrosion layer is stable and acts as a passivation layer to inhibit

further corrosion. It has been known that the passivation layer of aluminium is not stable in a high pH environments [172, 173]. The obtained results imply that the pH environment in the CAP system was low enough to keep the passivation layer stable.

On the other hand, the aluminium specimen exhibited significant corrosion in CAP after 180 and 360 days. The hydrogen gas generation results discussed previously suggested that the significant increase in corrosion began after *ca.* 55-65 days. The thickness of the aluminium specimen encapsulated for 180 days was estimated to be 2.73 mm suggesting that *ca.* 0.14 mm of aluminium metal from the original surface was consumed by the corrosion. The aluminium specimens after encapsulation for 180 days and 360 days were characterised by a corrosion layer with thickness of *ca.* 0.5-1 mm. The geometrical relation of the corrosion layer suggests that the original interface between aluminium and cement matrix has been displaced and the growth of the corrosion layer has been taking place on the aluminium side.

The corrosion layer and interface observed in this system were significantly different from those observed in the BFS/PC and PFA/CAC systems. Although the aluminium metal exhibited pitting, the growth of the pits was not significant, and the corrosion surface was rather smooth. In the BFS/PC and PFA/CAC systems, a significant growth of pitting was observed, and the corrosion layer tended to adhere towards aluminium side rather than the cement side. In the CAP systems, on the other hand, it seems that the adhesion of the corrosion layer to the aluminium is weak maybe related to the rather smooth interface, as seen in Figure 6.8.

The mechanism of the formation of the thick layered structure of the corrosion layer as observed in Figure 6.16 is not clear. A possibility is that, once the latent corrosion is initiated, the porous corrosion layer, as observed in Figure 6.16, allows diffusion of

an alkaline pore solution to the aluminium surface. Figure 6.18 suggests that there may be a concentration of sodium at the aluminium/corrosion layer interface. Figure 6.18 also suggests that the corrosion layer consists of high concentrations of aluminium and oxygen.

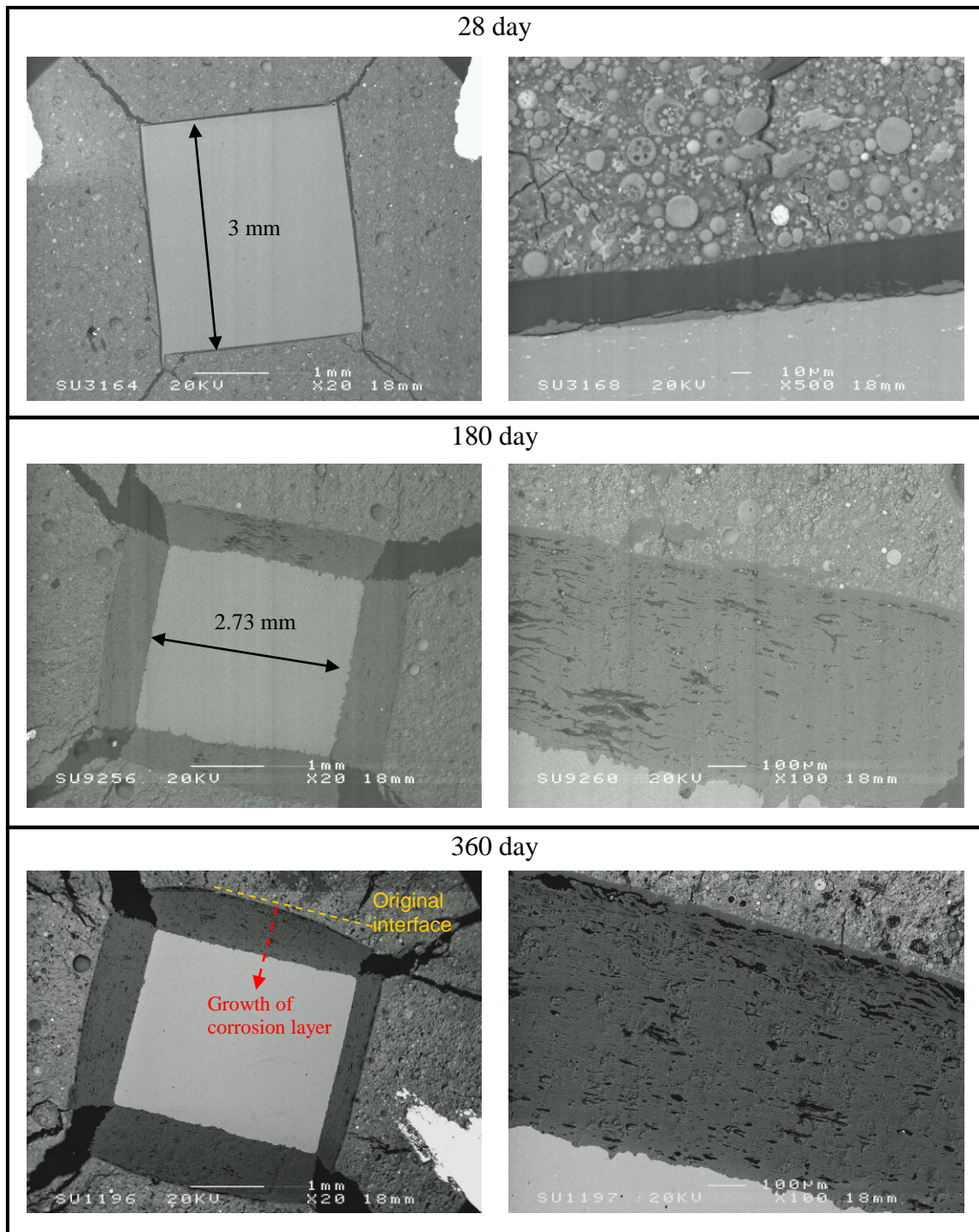


Figure 6.16 BEI micrograph of aluminium encapsulated in CAP 1 for 28, 180 and 360 days

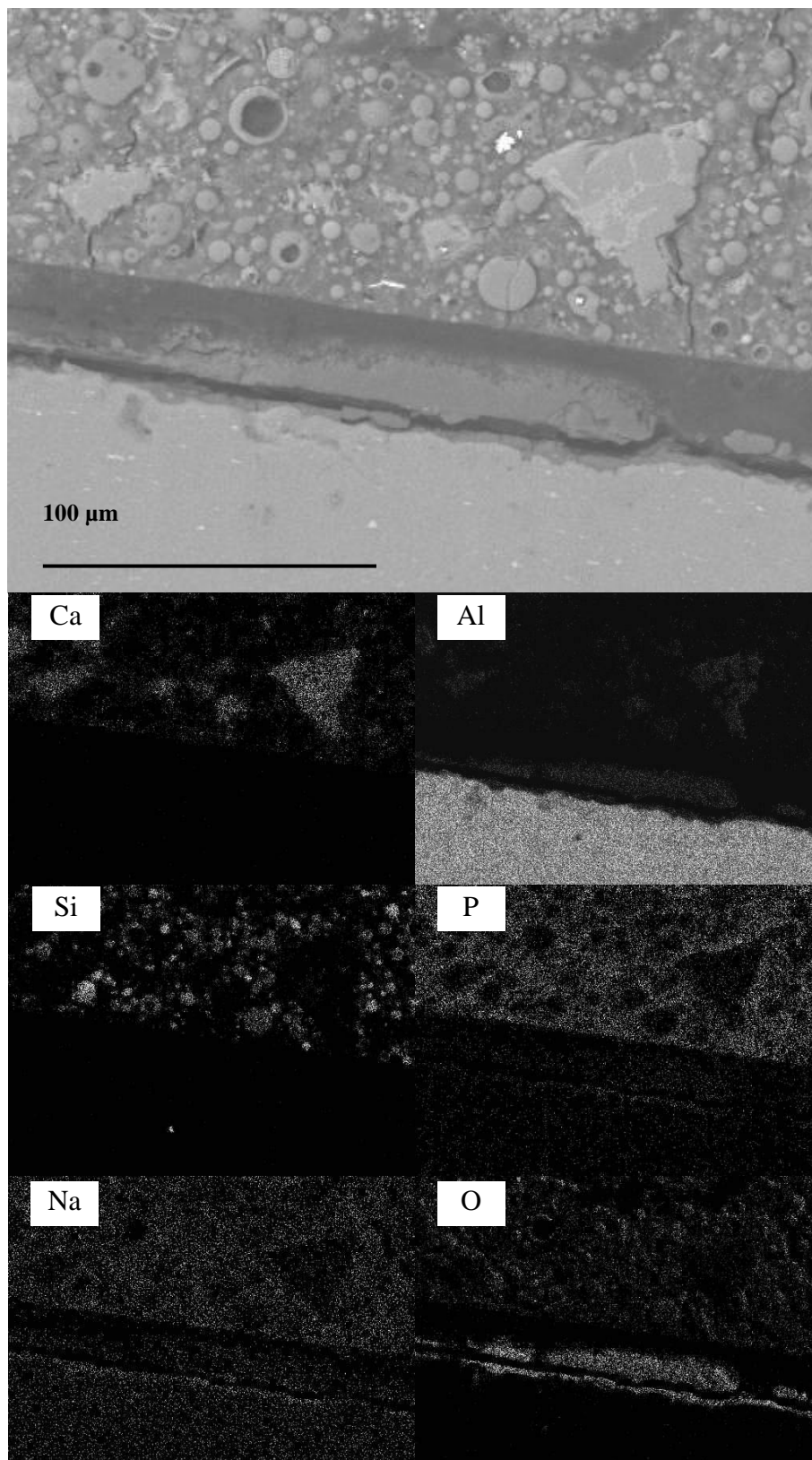


Figure 6.17 SEM BEI and EDX elemental mapping of aluminium-cement interface for aluminium encapsulated in CAP 1 for 28 days

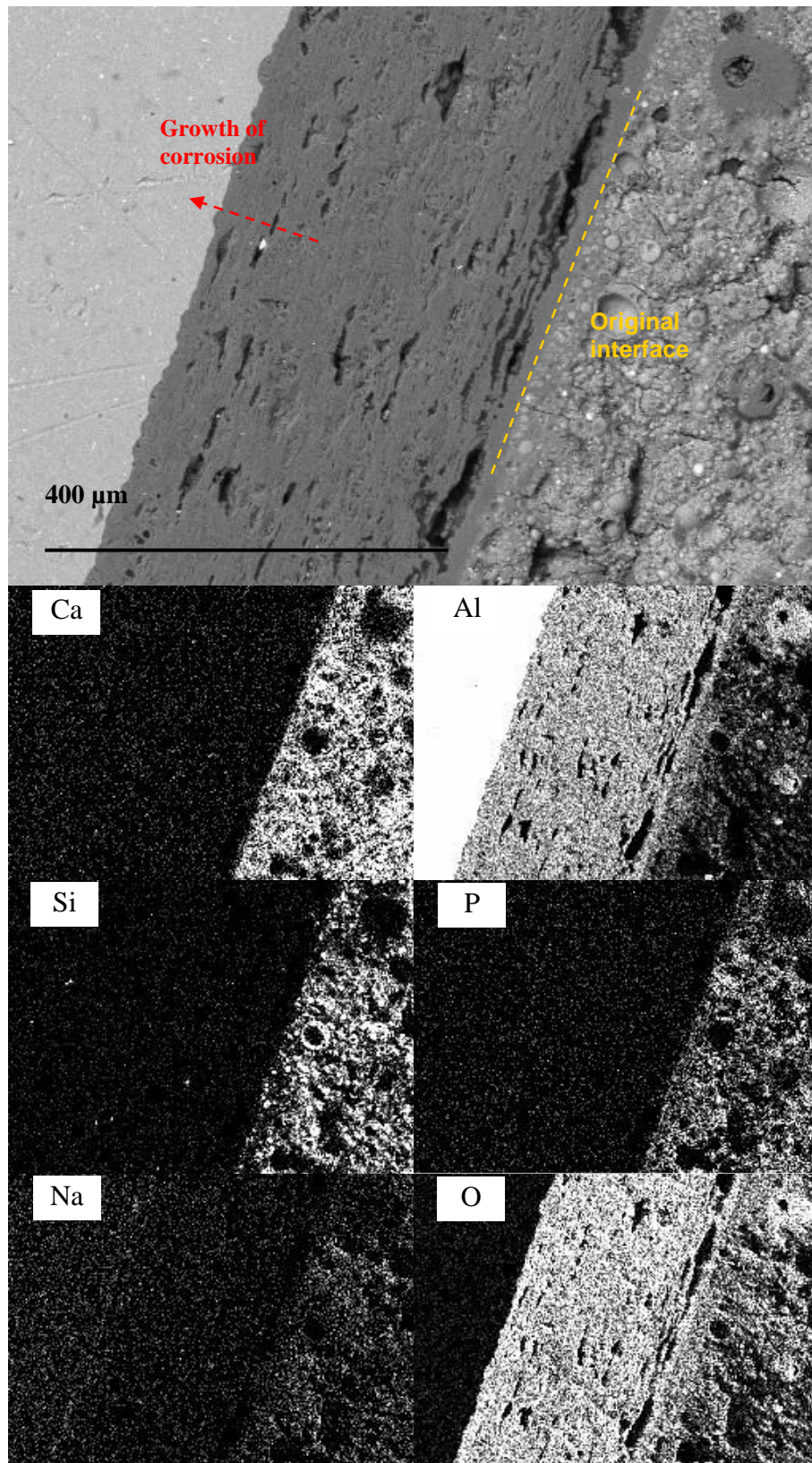


Figure 6.18 BEI and EDX elemental mapping of aluminium-cement interface in CAP 1 after 360 days

6.6. Corrosion Products

6.6.1. Corrosion Product in BFS/PC System

Figure 6.19 shows the aluminium specimens that were encapsulated in BFS/PC for 90 days, 180 days and 360 days. Setiadi *et al.* [3, 40] observed a similar white corrosion layer exhibited on the aluminium encapsulated in PC and BFS/PC cementitious systems. They discussed the layered structure of the aluminium corrosion product. The layered structure is likely to splay off, which would account for some areas of the aluminium surfaces being exposed. They also characterised the corrosion product as aluminium hydroxide in the form of both bayerite and gibbsite, in addition to strätlingite (C_2ASH_8). According to their study, gibbsite was more prevalent at extended curing periods as bayerite is metastable and converts to gibbsite. The EDX results presented here, discussed previously in Section 6.5.3, are consistent with their results.

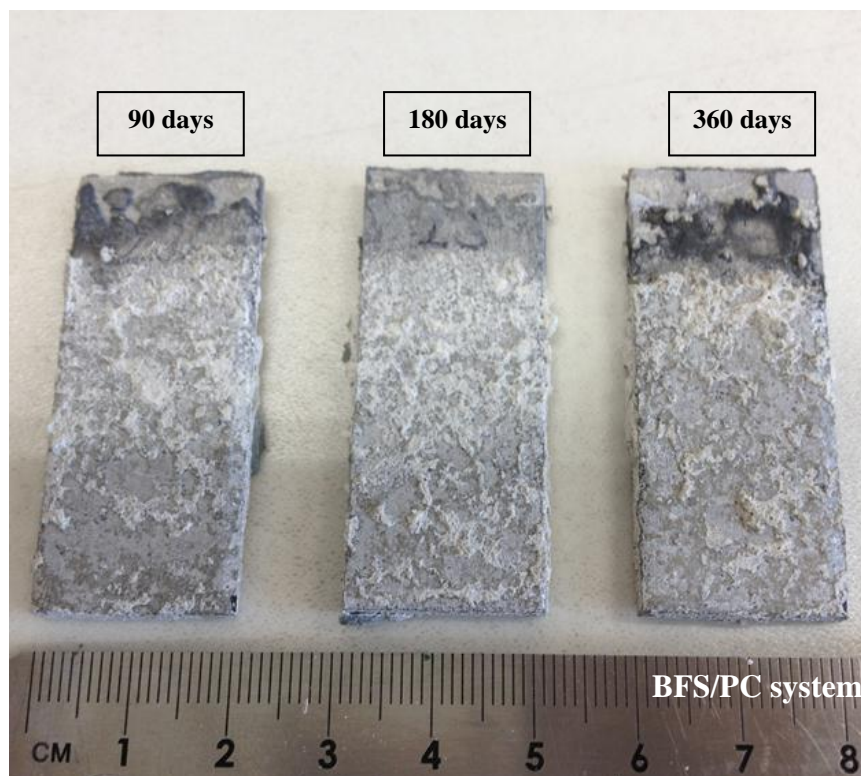


Figure 6.19 Aluminium specimens encapsulated in BFS/PC for 90, 180 and 360 days

6.6.2. Corrosion Product in PFA/CAC System

Figure 6.20 shows the aluminium specimens that were encapsulated in PFA/CAC system for 90, 180 and 360 days. The previously discussed results suggest that the corrosion layer is likely to be aluminium hydroxide based on the clear distribution of aluminium and oxygen in the corrosion layer observed on EDX mapping and the relatively high pH environment of $> \text{pH } 12$ which this system can provide.

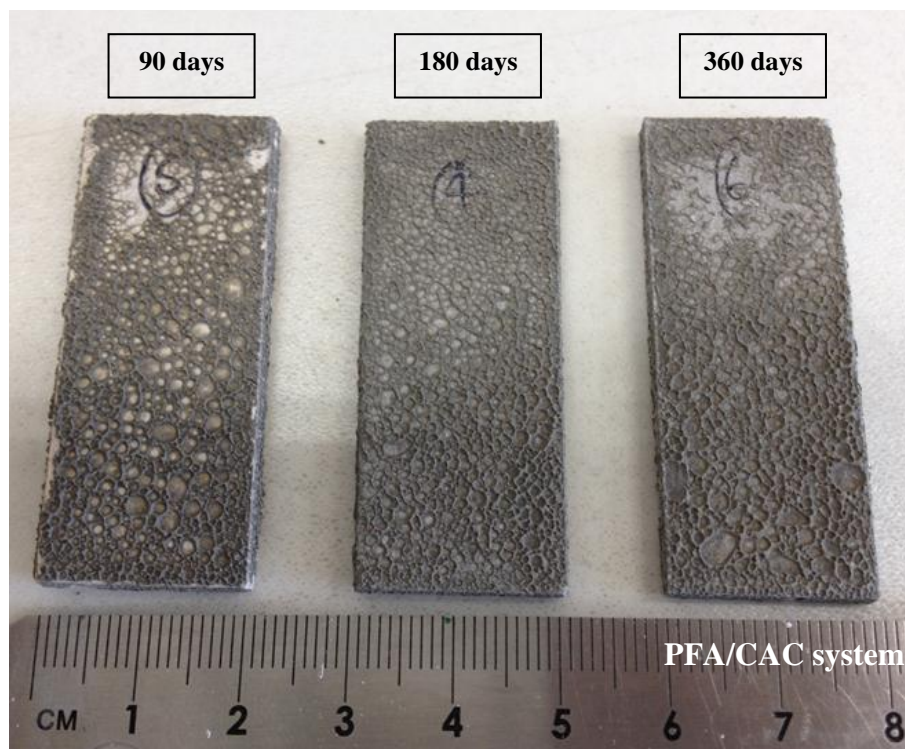


Figure 6.20 Aluminium specimens encapsulated in PFA/CAC for 90, 180 and 360 days

6.6.3. Corrosion Product in CAP Systems

Figure 6.21 shows the aluminium specimens encapsulated in CAP 1 and CAP 2 systems for curing periods of 90, 180 and 360 days. The specimens exhibited increasing corrosion, demonstrated by increasing quantity and thickness of the corrosion layer, with increasing encapsulation period. After 360 days the corrosion layer was *ca.* 2 mm thick. The EDX results of the interface presented and discussed in Section 6.5.3 indicated that the corrosion layer mainly contained aluminium and oxygen. The morphology of the layer was significantly different from those observed in the BFS/PC and PFA/CAC system. To obtain insight into the corrosion products, the surface of this aluminium specimen was further analysed by SEM, BEI, EDX and XRD.

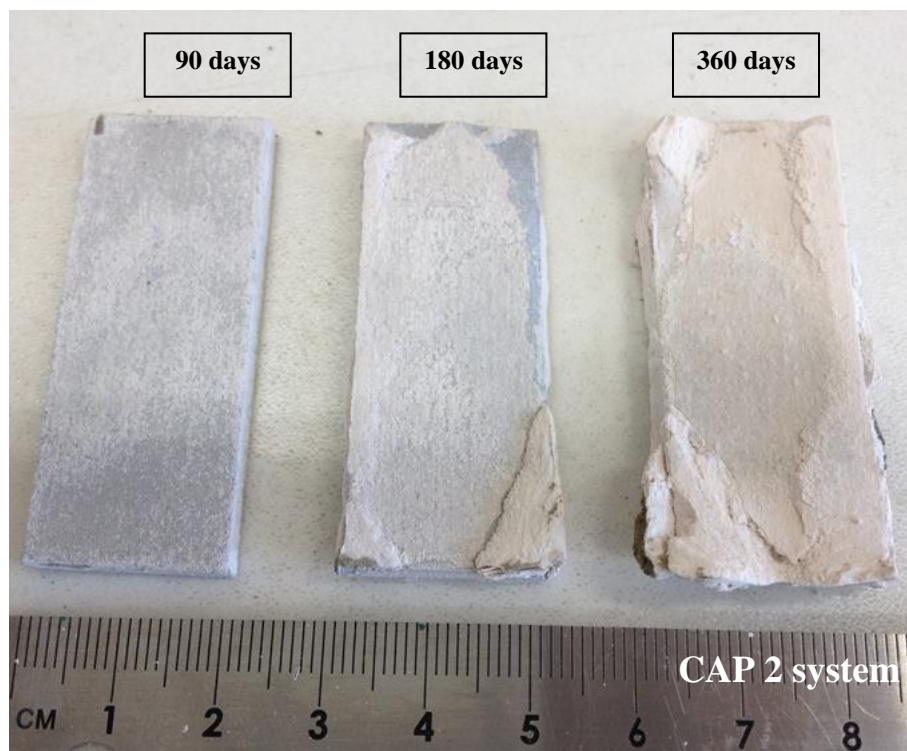
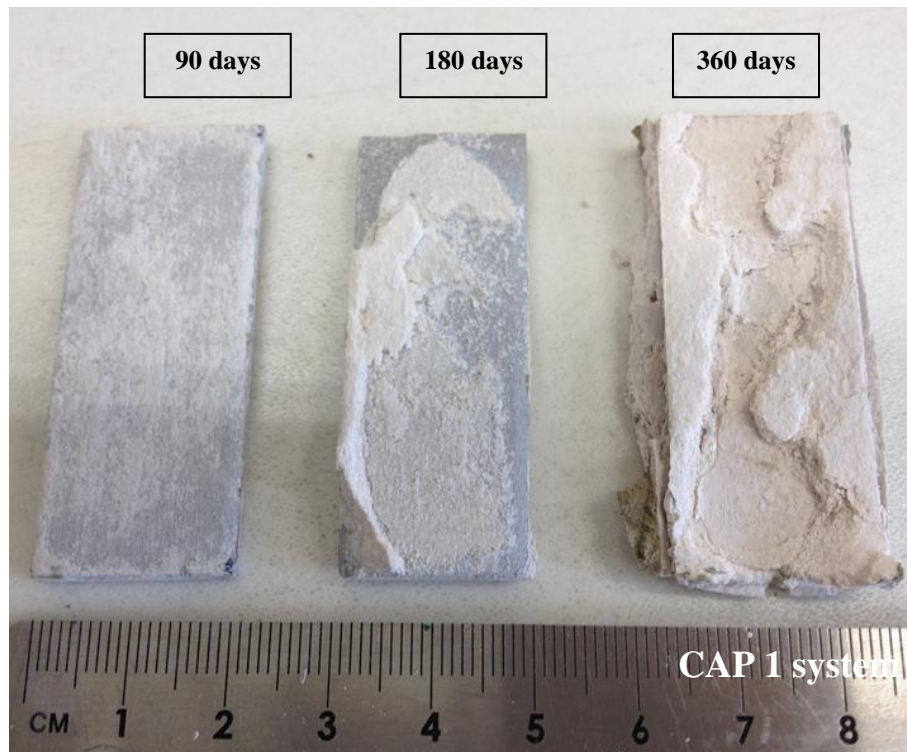


Figure 6.21 Aluminium specimens encapsulated in CAP systems for 90, 180 and 360 days

The corrosion layer exhibited a generally uniform distribution on the surface of the aluminium after 90 days as shown in Figure 6.22. The corrosion layer consists of an intricate network of mainly hexagonal crystallites with prismatic lozenges, faceted plates and blocks of *ca.* 1-5 μm in size. This suggests that the main corrosion product may be gibbsite, as similar morphologies have been observed for gibbsite by Sweegers *et al.* [174]. The EDX point spectra results (Table 6.4) confirms the aluminium:oxygen ratio (Al:O) of *ca.* 1:3, consistent with $\text{Al}(\text{OH})_3$.

The microstructure and morphology of the corrosion layer after 180 days was very similar to that observed for the 90 day sample as shown in Figure 6.23. A relatively uniform microstructure was observed with some cracks and signs of the layered or stratified nature of the corrosion product. The morphology of the corrosion products were again mainly tabular hexagonal crystallites of *ca.* 1-5 μm , but the amount of other products with less defined morphology appeared to have increased, compared with the 90 day sample. The results from EDX point spectra were similar to those of the 90 day sample, confirming that the principle corrosion product was aluminium hydroxide.

The microstructure and morphology of the corrosion product layer after 360 days, shown in Figure 6.24, was similar to those after 90 days and 180 days. The morphology consisted of tabular hexagonal crystallites and faceted plates and blocks were again observable. The EDX point spectra suggested that the corrosion layer was mainly aluminium hydroxide as was the case with other samples after 90 days and 180 days.

Table 6.4 EDX point spectra of the corrosion layer for aluminium encapsulated in CAP after 90 days, 180 days and 360 days curing

Element	Atomic %					
	90 days		180 days		360 days	
	CAP 1	CAP 2	CAP 1	CAP 2	CAP 1	CAP 2
Al	23.64	21.41	22.14	23.23	21.66	23.88
O	75.98	78.46	76.90	75.52	77.66	74.36
Other (e.g. Ca, P, Na)	0.38	0.13	0.96	1.25	0.68	1.76
Al:O	0.31	0.27	0.29	0.31	0.28	0.32

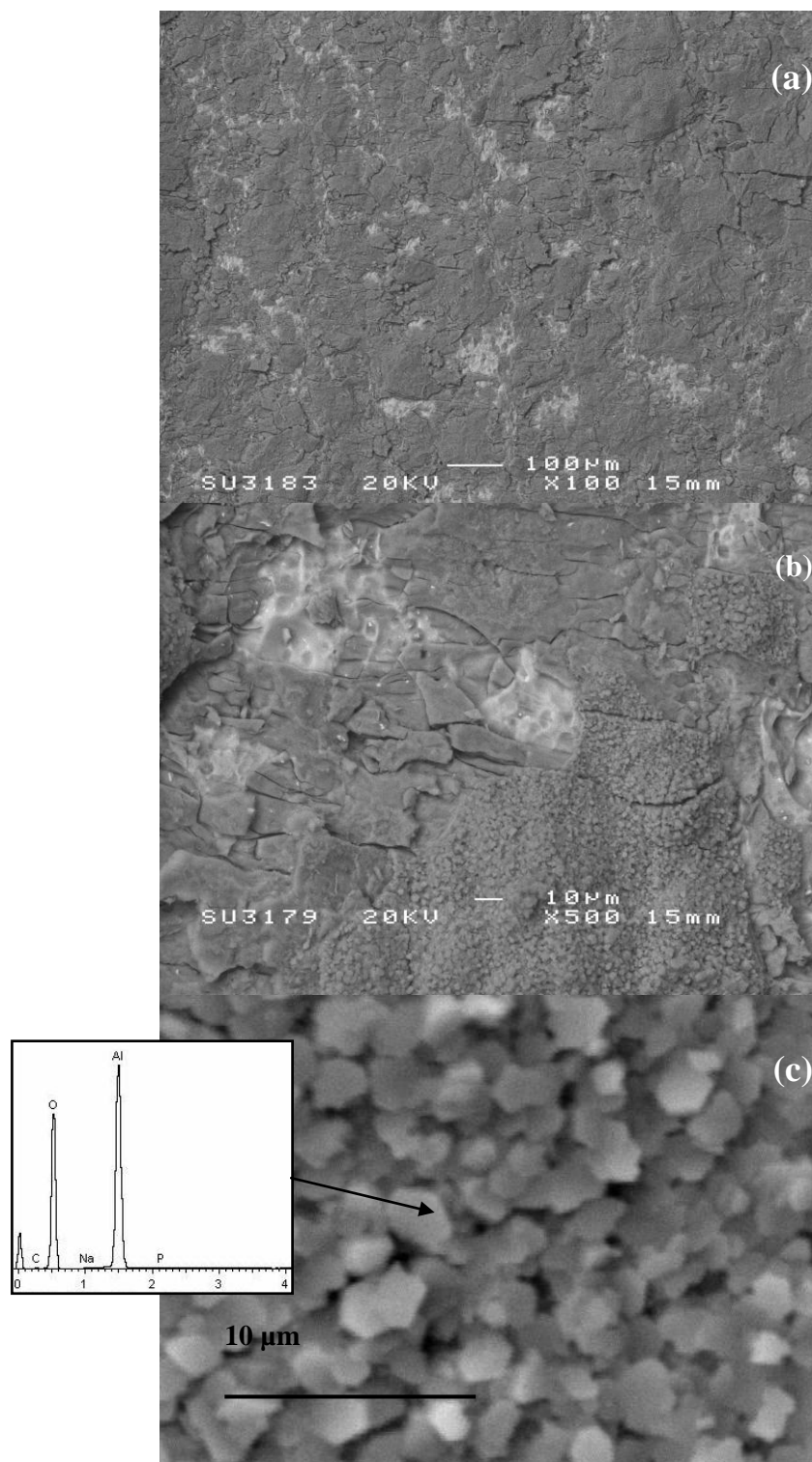


Figure 6.22 BEI and EDX point spectra of the surface of aluminium encapsulated in CAP 1 for 90 days: (a) x 100, (b) 200, (c) x5000

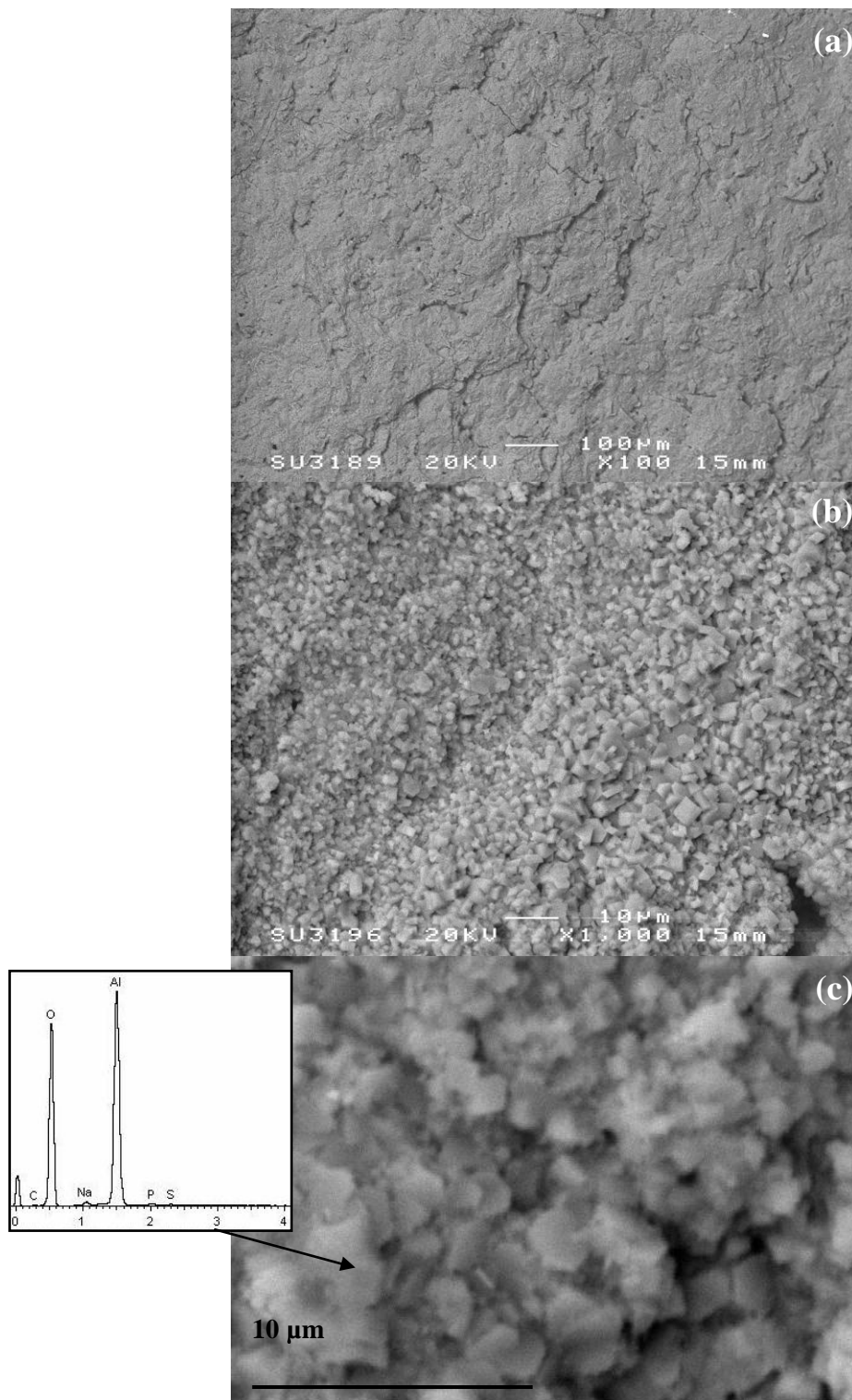


Figure 6.23 BEI and EDX point spectra of the surface of aluminium encapsulated in CAP 1 for 180 days: (a) x100, (b) x1000, (c) x5000.

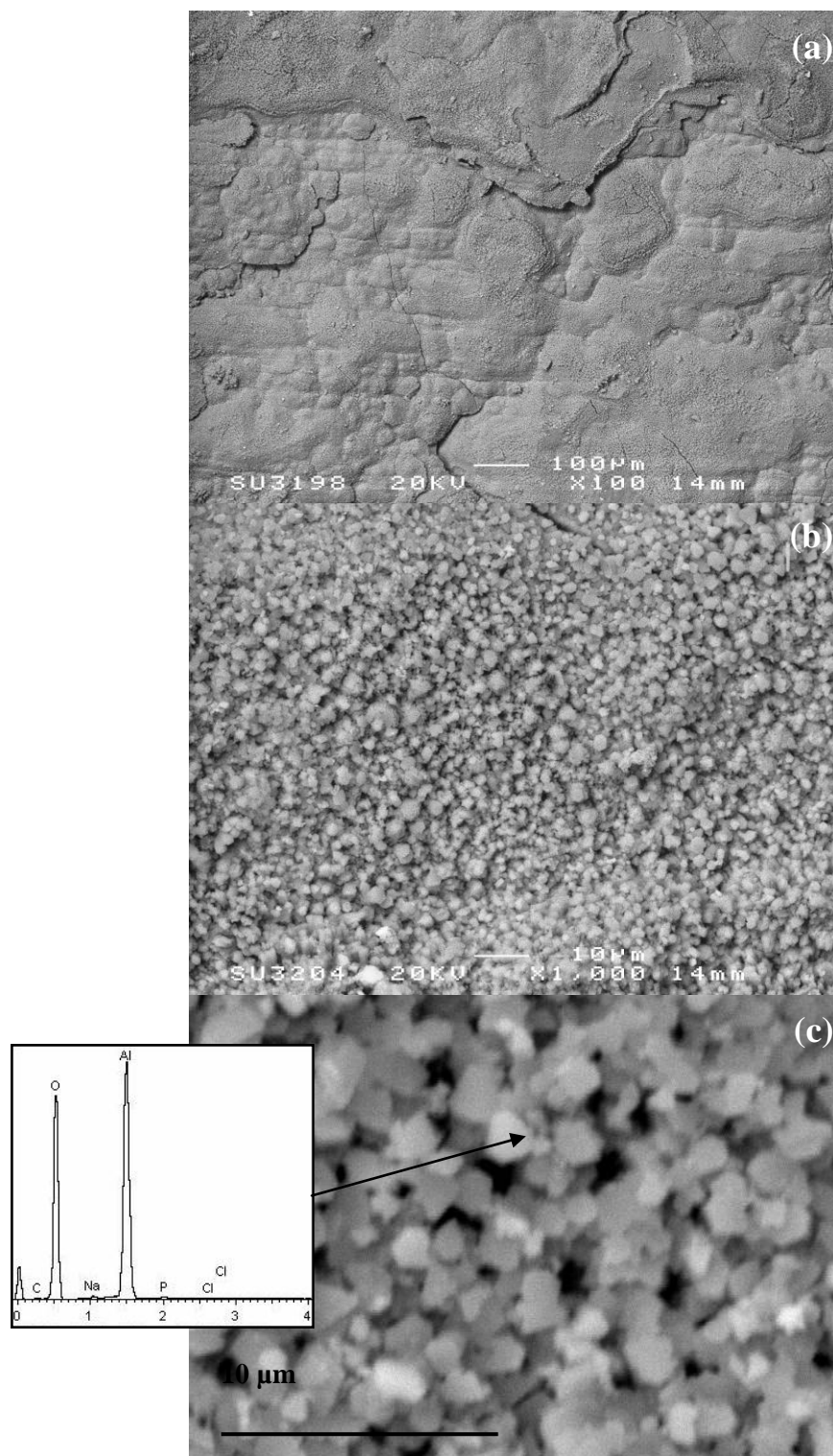


Figure 6.24 BEI and EDX point spectra of the surface of aluminium encapsulated in CAP 1 for 360 days: (a) x100, (b) x1000, (c) x5000

Figure 6.25 shows the XRD patterns of the corrosion products resulting from the encapsulation of aluminium metal in the CAP systems for 360 day. The reflections correspond to gibbsite, the principle of which is observed at *ca.* $18.3^\circ 2\theta$.

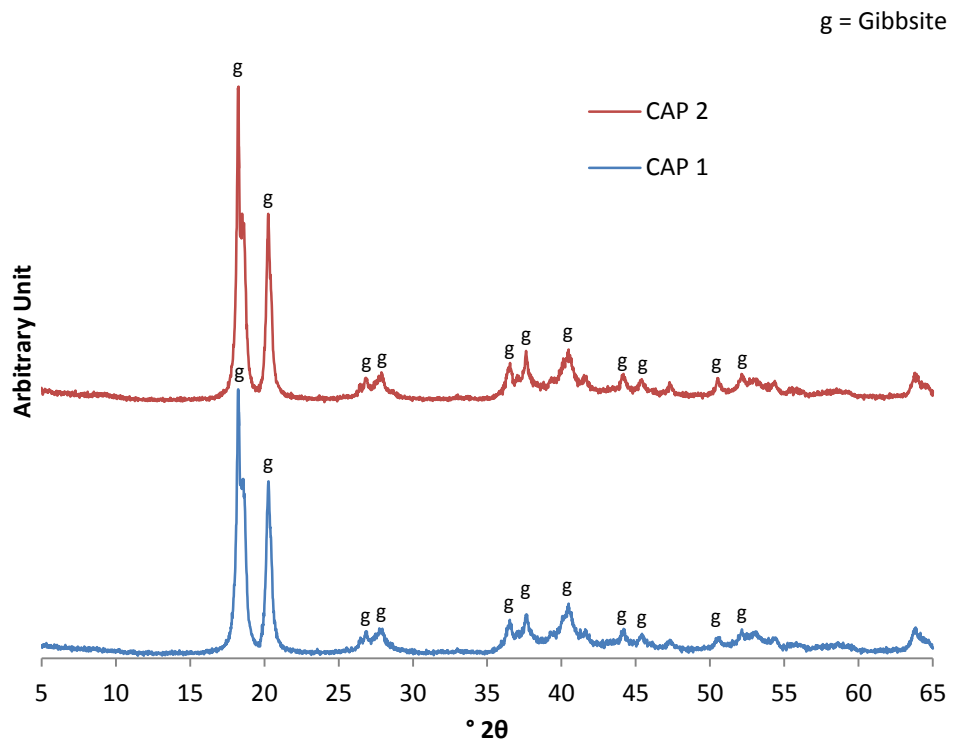


Figure 6.25 XRD of corrosion products from aluminium encapsulated in CAP for 360 days

6.7. Discussion

The results from gas generation measurements concur with those from examination of the aluminium-cement interface and encapsulated aluminium specimens after curing periods of up to 360 days. The corrosion behaviour of aluminium encapsulated in the CAP systems was distinct from that in both the BFS/PC and PFA/CAC systems. The results for the CAP systems suggested that during the first 28 days corrosion rates are very low and that specimens of encapsulated aluminium exhibit no signs of significant corrosion. The results from pH measurements of the cement slurries indicated that pH of the CAP systems (*ca.* pH 8-10) were significantly lower than those exhibited by the BFS/PC (*ca.* pH 12.7-13.0) and PFA/CAC (*ca.* pH 11.7-12.0) systems. It is suggested that the alumina layer, formed by oxidation of aluminium in air, present on the surface of the aluminium specimens is stable in the environment provided by the CAP systems and as such acts as a passivation layer inhibiting corrosion.

After *ca.* 55-65 days of encapsulation, the corrosion rates of aluminium encapsulated in the CAP systems increased. It is suggested that the increase in corrosion rate may be the result of some latent evolution of the cement system in terms of phase assemblage or microstructure, which may modify the internal chemistry of the cement pore solution. This is discussed further in Chapter 7. Furthermore, it is proposed that such changes may result in increased availability of water in order to facilitate the on-going corrosion of the aluminium metal.

The rate of corrosion in the BFS/PC and PFA/CAC systems reduced probably as a result of the physical isolation of aluminium plate from the cement matrix by the porous interface. The corrosion of aluminium appears to be limited under the tested

conditions once this isolation has taken place. However, in an environment where water can intrude the porous interface, the corrosion of aluminium would likely occur.

The CAP system had a quite different interface; both the surface of the cement and aluminium at the aluminium-cement interface was relatively flat with some adhered corrosion product. The corrosion is exemplified by the formation of significant quantities of corrosion products that appeared to form from the surface of the aluminium metal and propagate inward. The formation of corrosion products is expansive i.e. the molar volume of $\text{Al}(\text{OH})_3 > \text{Al}$.

Unlike the interfacial zones exhibited by the samples of aluminium encapsulated in the BFS/PC and PFA/CAC system, the CAP system did not exhibit any voidage or foamed region into which the corrosion products could grow and thus be accommodated. The quantity of corrosion product formed and expansive forces were such that the bulk cement matrices were therefore displaced, resulting in cracking and, after 360 days of encapsulation, loss of structural integrity of the samples. Analysis of the corrosion product confirmed it to be aluminium hydroxide in the form of gibbsite.

6.8. Summary

Aluminium encapsulated in the BFS/PC system exhibited an acute phase of corrosion, exemplified by a very high gas generation rate, which quickly fell to a chronic corrosion rate, demonstrated by a very low long-term gas generation rate. The behaviour of aluminium encapsulated in the BFS/PC was similar to that described elsewhere [3, 4, 21, 40]. Aluminium specimens retrieved following encapsulation for 90 days, 180 days and 360 days were very similar. The samples

were characterised by an interfacial zone of voids and porosity that consisted of a white powdery corrosion product.

The PFA/CAC system exhibited an acute corrosion rate in the first few hours of encapsulation, which then reduced to a relatively low and constant chronic corrosion rate. The chronic corrosion rate persisted for *ca.* 45 days, after which the rate began to decrease with time and may eventually plateau. The samples of encapsulated aluminium after 90 days, 180 days and 360 days were very similar and were characterised by an interfacial zone, between the aluminium specimen and the bulk cement, with an aerated or foamed structure. It was suggested that the foamed structure could accommodate the expansive corrosion products resulting from chronic corrosion.

The corrosion of aluminium encapsulated in the CAP system is characterised by a dormant period during which the corrosion rate is very low. This dormant period is a reason for the smooth interface between aluminium and cement matrix. At *ca.* 55-65 days, the corrosion rate significantly increased, as demonstrated by a relatively high gas generation rate, of *ca.* 0.4-0.5 litres h⁻¹ m⁻², which persisted for the remainder of the monitored encapsulation period. The significant growth of corrosion layer, observed from the original aluminium-cement interface inwards, resulted in cracking and loss of structural integrity of the cement matrix. The obtained results also suggest that the OH⁻ ions can be provided through the corrosion layer, forming mainly aluminium hydroxide. The corrosion behaviour of aluminium encapsulated in the CAP system suggests a corrosion mechanism different from that in the PC based system.

7. Results – Characterisation of the CAP System

7.1. Introduction

The obtained results shown in the Chapter 6 revealed that the response of the CAP system towards the aluminium incorporation was different from the BFS/PC and PFA/CAC systems, resulting in a significant corrosion and associated hydrogen gas generation after *ca.* 55-65 days. These results suggest that significant changes in the chemical and/or physical nature of the CAP systems start taking place around this time period, and the changes may continue.

The purpose of this chapter is to investigate the evolution of the nature and properties of the CAP system in terms of physical and/or chemical properties. Such information would allow better understanding of the corrosion behaviour exhibited by encapsulated aluminium and provide further insight into the CAP to improve this new cementing system. As physico-mechanical properties, the compressive strength, porosity and dimensional stability of the CAP systems have been assessed up to 360 days in comparison with the BFS/PC and PFA/CAC systems. The phase and microstructural evolution of the CAP systems has been further investigated using XRD, TG, SEM and EDX.

As previously discussed, a cementing system applied to encapsulating radioactive waste must fulfil plant acceptance test requirements, in terms of fluidity, setting time, and bleed water, to ensure compatibility with current industrial facilities and practices. As such, the CAP systems were also assessed according to the plant acceptance tests to characterise these properties and to confirm they fulfilled the industry-defined requirements.

7.2. Formulations

The cement systems studied for this chapter are the same as those investigated in Chapter 6, i.e. CAP 1, CAP 2, BFS/PC and PFA/CAC. The detailed formulations of the cement system are shown in Section 6.2 of Chapter 6.

7.3. Physico-mechanical Properties

7.3.1. Compressive Strength

Figure 7.1 compares the compressive strength for the CAP 1 and CAP 2 systems with BFS/PC and PFA/CAC systems up to 360 days. The BFS/PC system exhibited low strength (*ca.* 2 MPa) after 24 h curing followed by a significant strength development to a value of *ca.* 28 MPa after 7 days and further to *ca.* 53 MPa after 28 days. The compressive strength continued to increase throughout the period investigated, up to a maximum value of *ca.* 74 MPa after 360 days curing. This is a typical strength development of PC-based cement system, although data is limited in the literature for BFS/PC systems at curing periods greater than 28 days [13, 21, 32].

The PFA/CAC system demonstrated faster strength development attaining a compressive strength of *ca.* 15 MPa after 24 h. The compressive strength continued to increase significantly up to 28 days at which point it exhibited a compressive strength of *ca.* 25 MPa. The strength development became slower after 28 days, resulting in a value of *ca.* 34 MPa at 360 days. It has been known that high alumina cements exhibit a strength regression due to the conversion of metastable CAH_{10} and C_2AH_8 to stable C_3AH_6 and AH_3 [72, 175]. The obtained results suggest that the introduction of PFA may have contributed to suppress the conversion reaction and avoid the associated strength regression.

Both CAP1 and CAP 2 formulations exhibited rapid strength development, attaining compressive strengths of *ca.* 21 MPa and 31 MPa, respectively, after only 24 h of curing. The compressive strength of both CAP systems continued to increase up to 28 days reaching the maximum values of *ca.* 32 MPa and 45 MPa for CAP 1 and CAP 2, respectively. The system with lower water content, i.e. CAP 2, exhibited higher compressive strengths, which appears to be quite typical for cementitious systems [25, 65].

After 28 days, both CAP systems then exhibited quite dramatic strength regressions up to 180 days, at which point the compressive strengths were *ca.* 8 MPa and 9 MPa for CAP 1 and CAP 2, respectively. These correspond to the regression of approximately 70 % and 80 %, respectively, from the maximum strengths. The compressive strengths after 360 days were *ca.* 17 MPa for both CAP systems, demonstrating a slight strength gain between 180 days and 360 days of curing. Ma and Brown observed a similar strength regression in their samples based on CAC modified with phosphates [143]. In their case, however, the strength regression was completed much faster, within 30 days, and the regression was much less (approximately 30-50 % regression). The difference between their data and present results could be attributed to the difference in the formulation. They used much less water and phosphate, $w/s = 0.182$ ($w/c = 0.17-0.2$) and $p/c = 0.1$ respectively, compared with the present formulation of $w/s = 0.32-0.35$ ($w/c = 0.8-0.875$) and $p/c = 0.4$. It could also be attributed to the amount of aluminium (or calcium) as they used Secar 71 (Al_2O_3 : ~70 wt%, CaO: ~25 wt%) whereas the present systems used Secar 51 (Al_2O_3 : 51 wt%, CaO: 37 wt%).

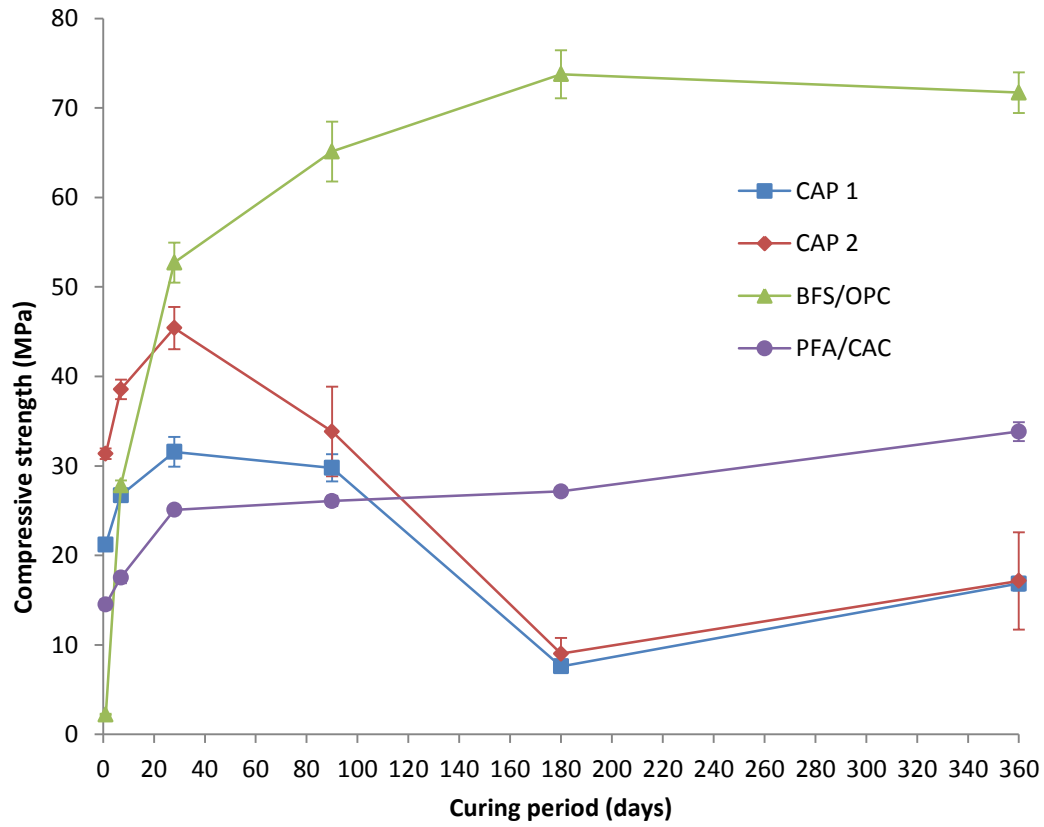


Figure 7.1 Compressive strength of CAP, BFS/PC, PFA/CAC systems up to 360 days

7.3.2. Porosity

Figure 7.2 shows the pore size distribution in the BFS/PC system up to 360 days, based on the results of MIP. The derivative with respect to $\log D$ was used instead of that to the intrusion pressure, which gives the incremental intrusion volume, to clarify the pore size distribution. This technique has previously been used to study the BFS/PC system [19]. The result shows that majority of pores are in the range of $< 0.1 \mu\text{m}$. The pores larger than $0.1 \mu\text{m}$ are often considered as capillary pores whereas those smaller than few tens of nanometers, such as shown in the present work, have been attributed to the C-S-H gel structure [14, 19]. The obtained data show that the pores of $0.1\text{-}0.01 \mu\text{m}$ gradually decrease whereas those of $< 0.01 \mu\text{m}$ increase, as hydration progresses with curing time.

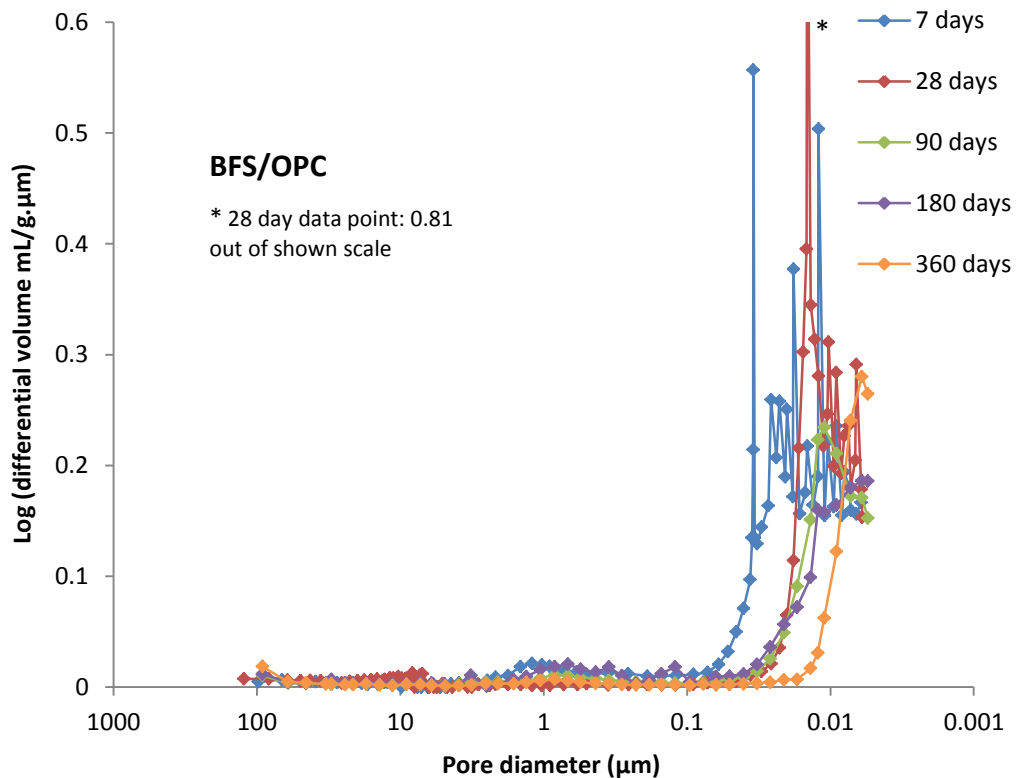


Figure 7.2 Pore size distribution in BFS/PC system up to 360 days

The pore size distribution in the PFA/CAC system, shown in Figure 7.3 was significantly different from that in the BFS/PC system. The pores were widely distributed in the range of $< 1 \mu\text{m}$ and indicated a notable change with curing time. The distribution of pores was largest at *ca.* $0.1 \mu\text{m}$ at 7 days, which later indicated two distinctive populated ranges of at *ca.* $0.5 \mu\text{m}$ and $0.04 \mu\text{m}$. The former seems to decrease with curing time and the latter increases, which it is suggested must be related to the hydration and phase development in this system. Furthermore, it is suggested that the significant quantity of larger pores may be responsible for the lower compressive strength of this system compared to the BFS/PC system.

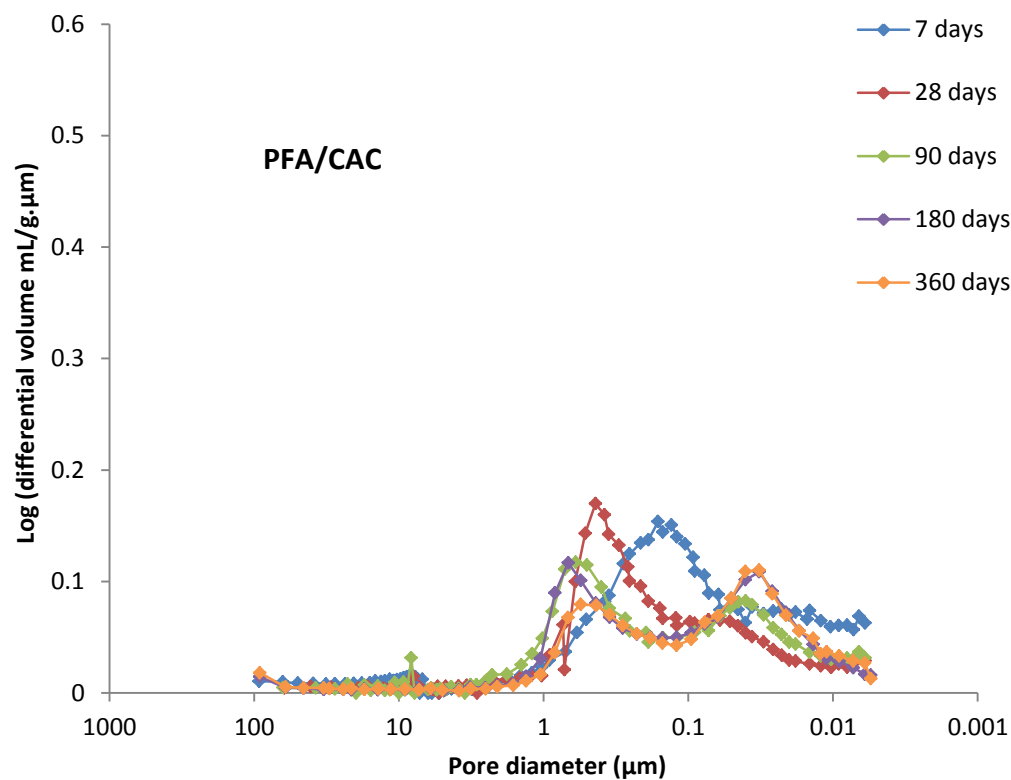


Figure 7.3 Pore size distribution in PFA/CAC system up to 360 days

Figure 7.4 shows the pore size distribution in the CAP systems up to 360 days. The general trends are very similar for both CAP1 and CAP 2 systems, but the CAP 2 indicated less intrusion volume than the CAP 1 system at each stage, showing less porosity resulting from the lower water content of the system.

After 7 days, the pores in the CAP 1 populated mainly around *ca.* 0.12 μm and those in the CAP 2 around *ca.* 0.08 μm . Little change was observed in these distributions after 28 days. After 90 days, however, the population of pores in both systems changed significantly, shifting towards smaller pore size with a wider distribution, and a distinctive peak was observed for the pore size distribution after 180 days at *ca.* 0.05 μm in CAP 1 and *ca.* 0.04 μm in CAP 2. These results suggest that pore structure evolved with time; the original pore structures were lost and new ones emerged. This significant change in pore structure must have contributed to the strength regression observed in Figure 7.1. The gradual shift of the pore size distribution from 180 to 360 days appears to be due to the further hydration of the system.

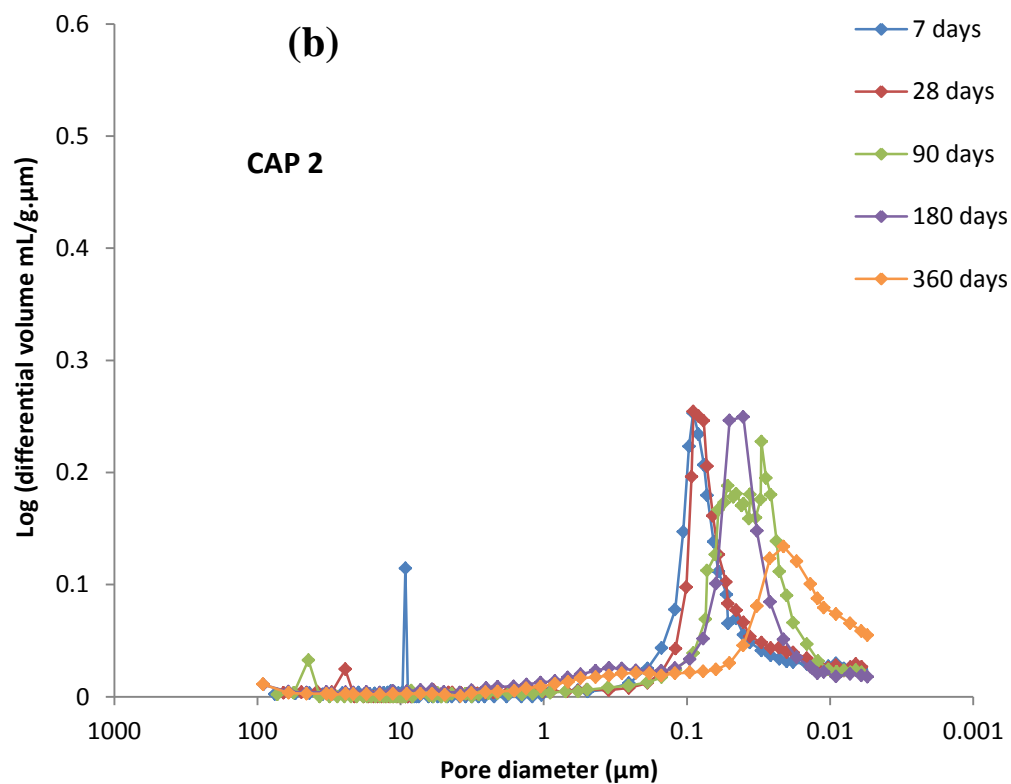
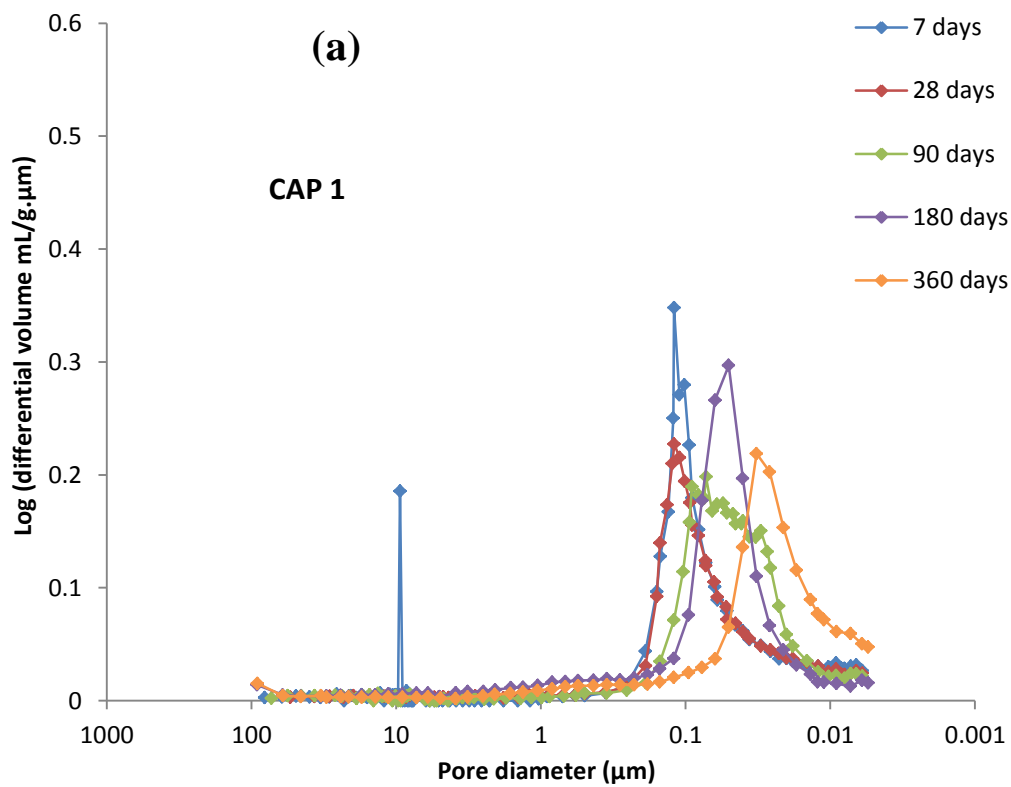


Figure 7.4 Pore size distribution in CAP systems up to 360 days: (a) CAP 1, (b) CAP 2

Figure 7.5 shows the total porosity for the CAP 1, CAP 2, BFS/PC and PFA/CAC systems up to 360 days. The BFS/PC system exhibited continual decrease throughout the period studied, resulting in total porosity of *ca.* 17 % after 360 days. The decreasing porosity is suggestive of continued hydration during this period. The total porosity of the PFA/CAC system was the highest among the tested systems after 7 days, then significantly reduced to *ca.* 27 % by 28 days and remained at the similar level for the remainder of the investigated period.

The CAP 1 and CAP 2 systems initially exhibited significantly lower total porosity than the BFS/PC and PFA/CAC systems. The system with lower water content, i.e. CAP 2, exhibited lower porosity as expected. After 28 days, the porosity of both systems increased up to 180 days curing, at which point the values for CAP 1 and CAP 2 were *ca.* 30 % and 26 %, respectively. As discussed previously, this is suggestive of a significant change in the pore structure having taken place. The porosity values were slightly reduced after this period, resulting in *ca.* 27 % and 22 % for CAP 1 and CAP 2 systems, respectively after 360 days, suggesting further hydration.

Figure 7.6 shows the total porosity plotted against the compressive strength for the tested systems. These results show that, in general the systems exhibited typical behaviour for cementitious systems; that is compressive strength decrease with increasing porosity.

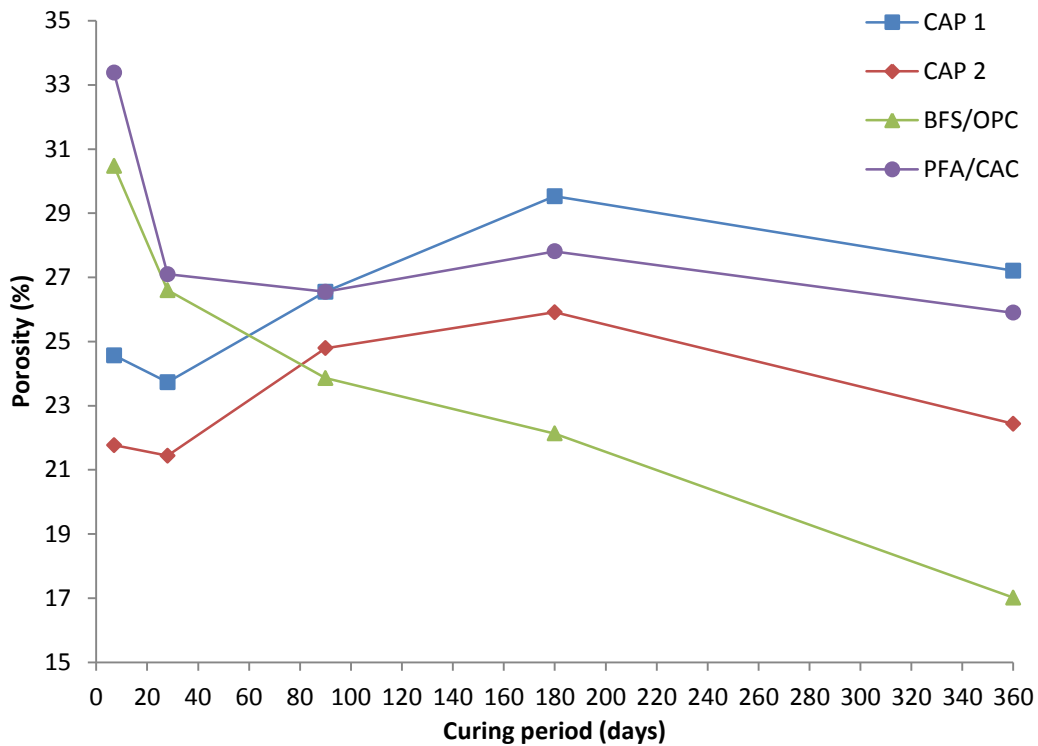


Figure 7.5 Porosity of CAP, BFS/PC, PFA/CAC systems up to 360 days

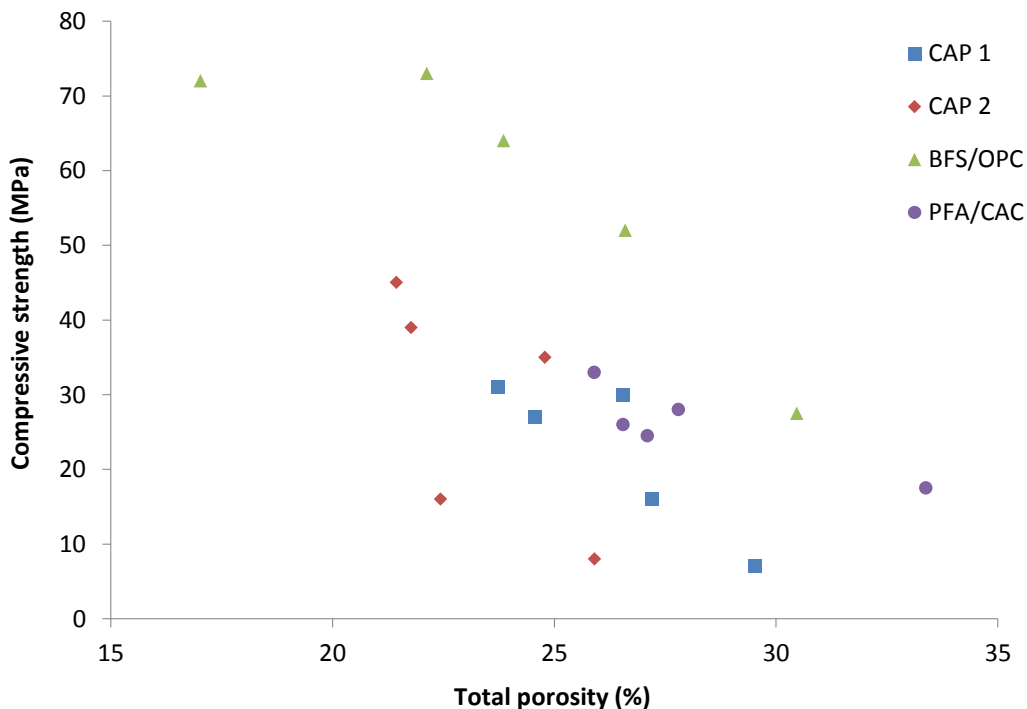


Figure 7.6 Compressive strength of samples plotted against total porosity

7.3.3. Dimensional Stability

The dimensional stability results, shown in Figure 7.7, illustrate that CAP formulations underwent significant dimensional alterations during the 360 days of curing. Both the CAP 1 and CAP 2 cementing systems exhibited relative stability in terms of dimensions up to 28 days, experiencing only minor shrinkages of 0.076 mm (0.047 %) and 0.066 mm (0.042 %), respectively. However, between 28 and 90 days both systems experienced significant shrinkages; 0.71 mm (0.44 %) for CAP 1 and 0.37 mm (0.23 %) for CAP 2.

The rate of shrinkage appeared to have slowed down after 90 days. The CAP 1 cementing system exhibited a constant expansion of 0.64 mm between 90 and 360 days. The CAP 2 cementing system experienced relative dimensional stability between 90 and 180 days curing, exhibiting a negligible shrinkage of 0.01 mm, and then expanded by 0.31 mm between 180 and 360 days. Such a significant change in the trend of the materials behaviour during 28 to 180 days corresponds to the similar change in the porosity and compressive strength, which also coincides with the change in the hydrogen gas generation exhibited by the samples containing aluminium, as discussed in Section 6.4.1 of Chapter 6. After 360 days of curing, the CAP 1 and CAP 2 cementing systems exhibited net shrinkages of 0.07 mm (0.04 %) and 0.08 mm (0.05 %), respectively.

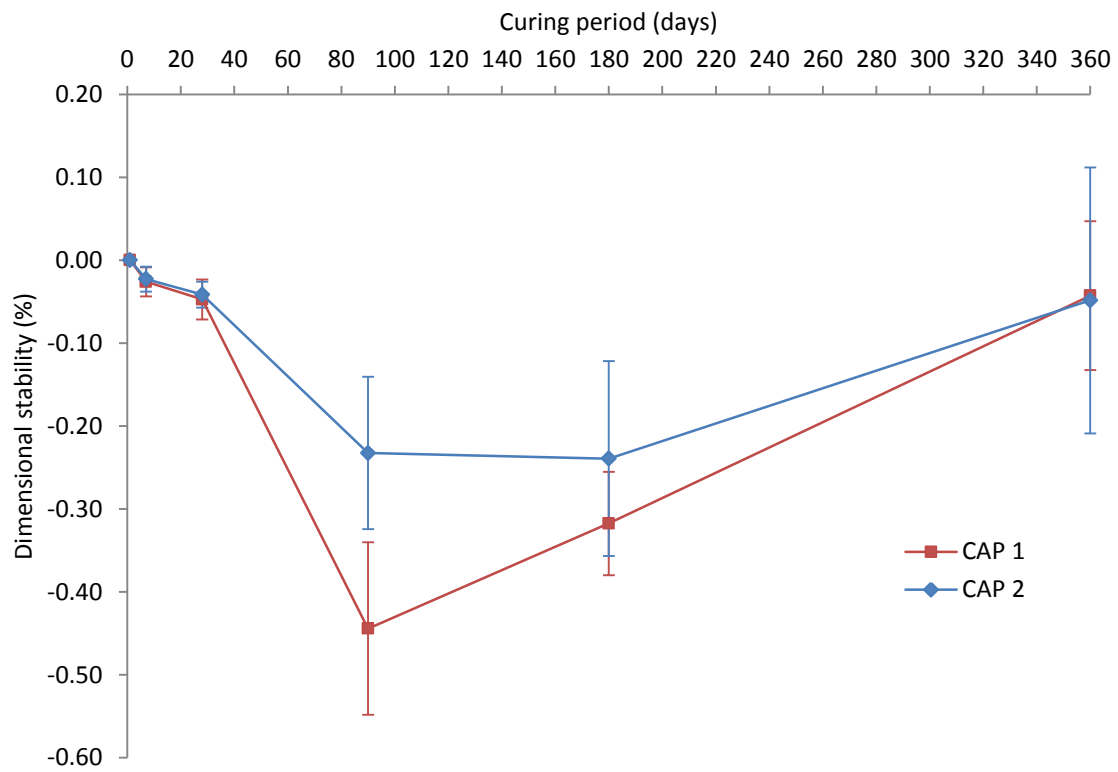


Figure 7.7 Dimensional stability of CAP 1 and CAP 2 systems up to 360 days

7.4. Phase Evolution of CAP Systems

Figure 7.8 shows the XRD results from CAP 1 cementing systems up to 360 days, which clearly indicated that the crystalline phase assemblage is not stable and evolves over time. The XRD pattern for CAP 1 cured for 7 days consisted of the reflections corresponding to the residual constituent phases, specifically CA, C₂AS and CT from the CAC with quartz and mullite from the PFA. No new crystalline phases were identified, but there was a considerable diffuse scattering between *ca.* 15-40° 2θ suggesting that the system contained significant amorphous content.

The diffraction pattern for the 28 day sample was very similar to that of the system after 7 days, with the additional relatively weak reflections associated with the formation of gibbsite, the main reflection of which is at *ca.* 18° 2θ. The intensity of reflections associated with CA, the principle of which exists at *ca.* 30° 2θ, decreased compared to those exhibited at 7 days, suggesting that CA was consumed significantly during this period via on-going hydration reactions.

The reflections corresponding to the residual constituent phases were still observable after 90 days although the reflections associated with CA were very small, suggesting that most of the CA had been consumed during the first 90 days of curing. Reflections associated with gibbsite became significantly more intense than those exhibited after 28 days. Relatively weak and poorly defined reflections associated with the presence of poorly crystalline hydroxyapatite (HAp, Ca₅(PO₄)₃OH), the main reflection of which is at *ca.* 32° 2θ were observed at 90 days, suggesting that a precipitation and/or crystallisation of this phase took place significantly during this period. Similar XRD patterns for low crystallinity HAp have been reported by

Dorozhkin [125]. HAp of low-crystallinity may be formed from the crystallisation of ACP and has been reported to precipitate at pH = 9.5-12 [124, 125, 158, 176].

After 180 days, the reflections associated with CA had all but disappeared, and those for HAp had increased in intensity. There was little change in the intensity of gibbsite reflections. The reflections associated with C₂AS exhibited significantly lower intensity at 180 days compared to those at 90 days, suggesting that C₂AS had been consumed in latent hydration reactions [63, 65]. Furthermore, new relatively weak reflections appeared that can be attributed to the formation of a sodium aluminium silicate hydrate phase that is categorised as the sodium form of the Linde Type A (LTA) zeolite phase ($|\text{Na}^+_{12}(\text{H}_2\text{O})_{27}|_8 [\text{Al}_{12}\text{Si}_{12}\text{O}_{48}]_8\text{-LTA}$ or $|\text{Na}| [\text{Al-Si-O}]\text{-LTA}$) [177, 178].

These trends discussed above continued with time up to 360 days; the intensity of reflections associated with C₂AS decreased, suggesting the further participation of this phase in delayed hydration reactions; reflections associated with newly formed crystalline phases, HAp and the sodium LTA zeolite phase, increased in intensity, demonstrating the continued phase development; reflections associated with gibbsite, quartz, mullite and CT showed no significant change in intensity compared to those at 180 days.

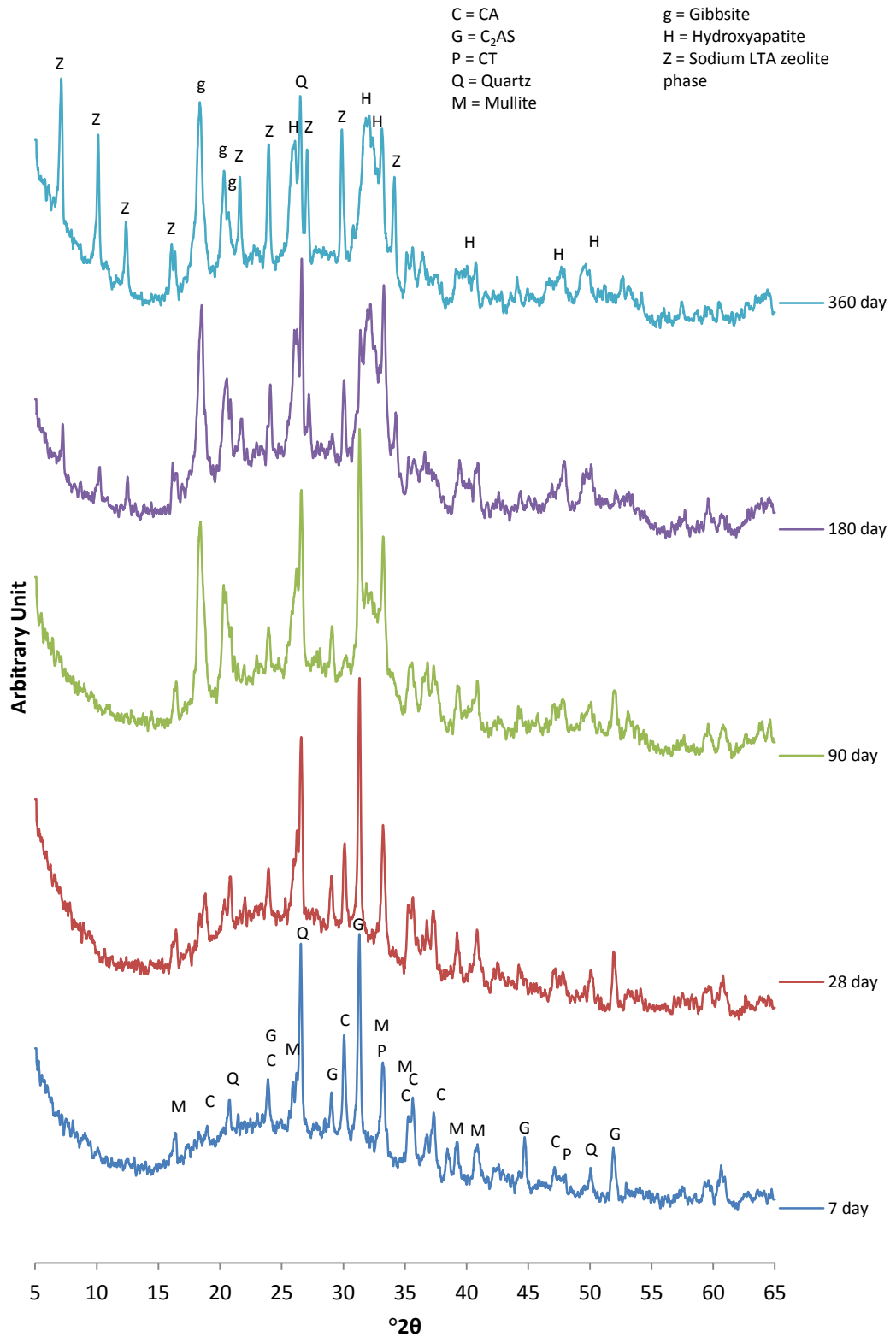


Figure 7.8 XRD pattern of CAP 1 cementing system cured at 20°C up to 360 days

Figure 7.9 shows the XRD results for the CAP 2 cementing system up to 360 days. The results appeared to be very similar to those of CAP 1 system at all ages, suggesting that the crystalline phase assemblages were very similar in these systems during the curing period studies.

It should be noted that both CAP 1 and CAP 2 systems exhibited decreasing intensity of C_2AS reflections, which coincided with the development of reflections associated with a sodium LTA zeolite phase. This suggests that the formation of sodium LTA zeolite phase is related to the consumption of C_2AS . The formation of sodium-type zeolite phase in a phosphate-modified calcium aluminate systems has been reported by Sugama *et al.* [146]. They suggested that the zeolite phase was yielded from the reactions of sodium ions in the system with mullite and C_2AS .

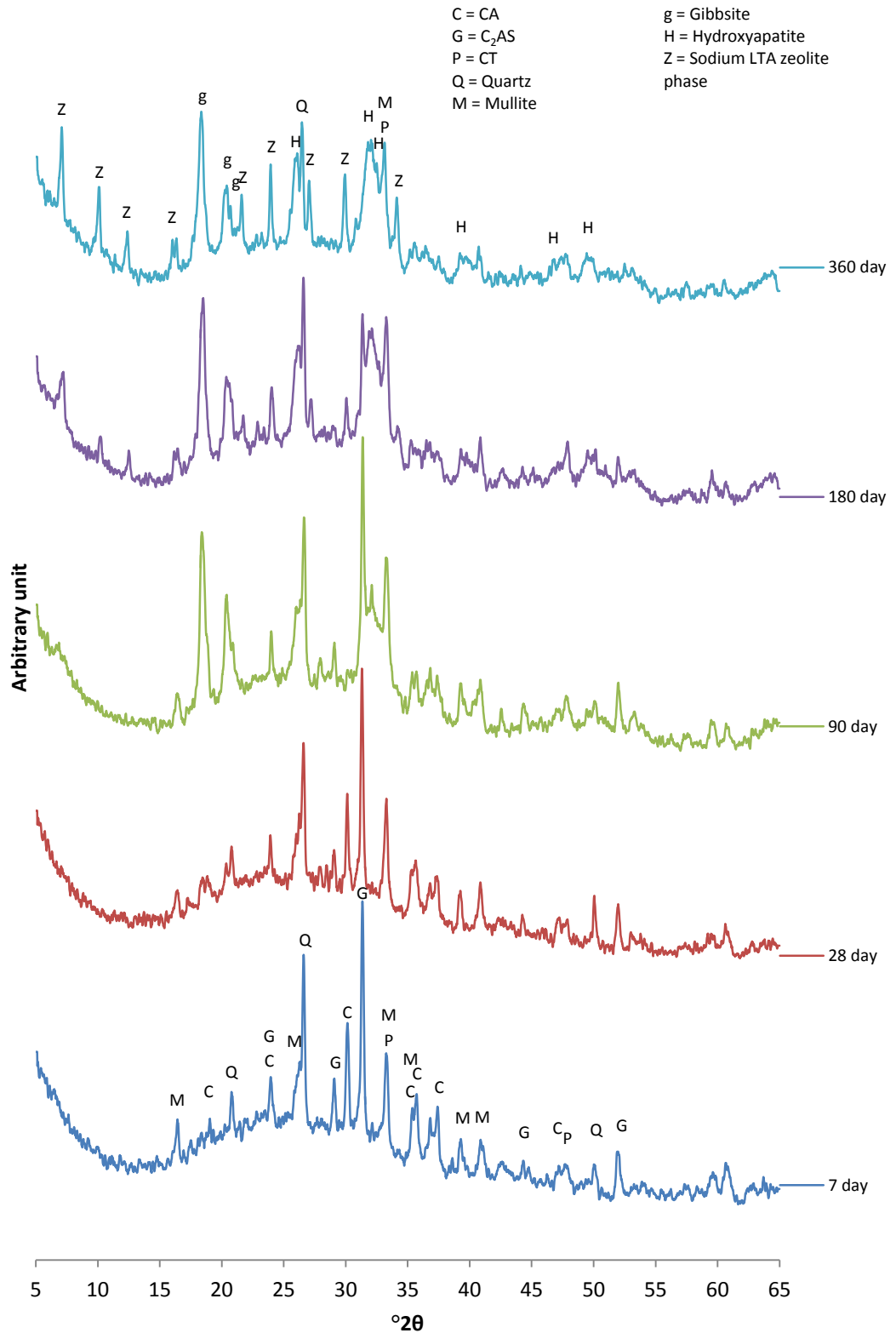


Figure 7.9 XRD pattern of CAP 2 cementing system cured at 20°C up to 360 days

The TG results for CAP 1 up to 360 days (Figure 7.10) showed that the weight loss behaviour up to *ca.* 1000 °C changed with curing age. The weight loss profiles at all ages exhibited gradual weight loss up to 1000 °C, where the total weight losses varied between *ca.* 14.1-18.6 wt%, with the majority of those weight losses occurring below *ca.* 300 °C. The total weight losses for the 7 and 28 day samples were *ca.* 14.1 wt% and 16.5 wt%, respectively. This increase in total weight loss during this period, implies that the proportion of hydrate phases increased from 7 days to 28 days, assuming that the weight loss during the TG measurement was mainly due to the dehydration of hydration products. The total weight loss then decreased to *ca.* 15.2 wt% for the 90 day sample. The 180 day sample exhibited an increase in the total weight loss up to *ca.* 16.0 wt%, with a further increase to *ca.* 18.6 wt% after 360 days of curing.

The DTG curves (Figure 7.11) for the 7 and 28 day samples exhibited similar profiles with the principle weight losses occurring between *ca.* 25-120 °C and an additional minor weight loss at *ca.* 200 °C. These weight losses may be attributed to the dehydration of the amorphous binding phases. ACP has been reported to undergo thermal decomposition by a two-stage dehydration mechanism. Two types of water loss occur; the loss of loosely bound water molecules adsorbed on the surface of ACP which occurs up to at *ca.* 120 °C and the chemically bound water molecules, which can be gradually lost up to *ca.* 600 °C [158]. The crystallisation of ACP to crystalline calcium phosphate phases has been reported to begin at *ca.* 530 °C. Two step dehydration mechanisms in similar temperature ranges have been reported for an amorphous gel phase of the calcium phosphate system [179]. Similar two step dehydration processes have also been reported for phosphate containing minerals; brushite ($\text{CaHPO}_4 \cdot 2\text{H}_2\text{O}$) loses its water initially up to *ca.* 130 °C and then up to *ca.*

200 °C to form monetite CaHPO_4 and an amorphous phase [180]; and taranakite ($\text{H}_6\text{K}_3\text{Al}_5(\text{PO}_4)_8 \cdot 18\text{H}_2\text{O}$) loses water at 80-140 °C and at 140-300 °C to form a non-crystalline phase [181]. Although these are crystalline phases, the amorphous phase under discussion here may have hydroxyl groups in environments similar to those in the crystalline minerals reported elsewhere.

The results at 90, 180 and 360 days indicated less weight losses at *ca.* 25-120 °C and more weight loss at *ca.* 130-240 °C compared to the younger samples, suggesting a significant change in the amorphous binding phase. The obtained data also exhibited broad and overlapping weight loss events, which become more resolved with increased curing age, suggesting that the various hydration products or environments co-existing in the products.

It should be noted that the temperature range between *ca.* 130-240 °C matches the dehydration temperature of C_2AH_8 , strätlingite and gibbsite [84, 182]. The dehydration of gibbsite must also contribute to this weight loss, as its increase is consistent with that of the corresponding XRD patterns. C_2AH_8 and strätlingite (C_2ASH_8) were not detected by XRD, but could be present in small quantities, less than the detection limit of XRD (*ca.* 5 wt%). There is also a broad weight loss at *ca.* 550-750 °C that is likely due to the loss of chemically bound water molecules during the crystallisation of ACP to tricalcium phosphate (β -TCP,) [125, 158]. Alternatively this weight loss may be due to the decomposition of CaCO_3 .

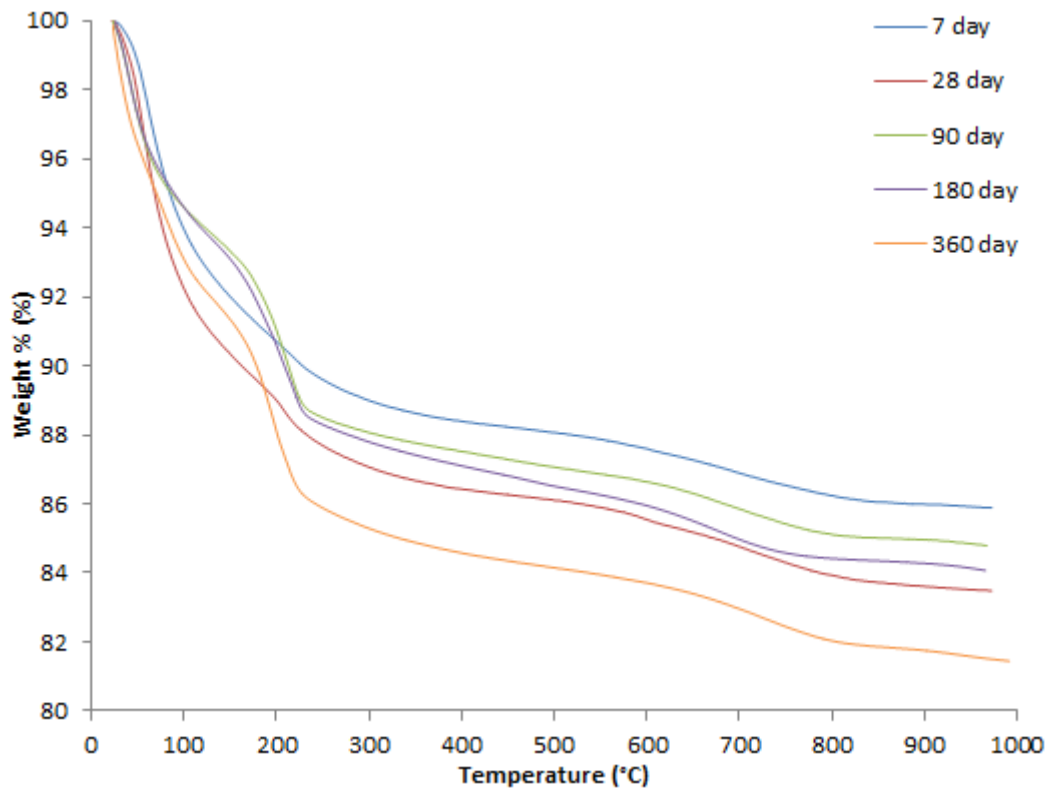


Figure 7.10 TG results for CAP 1 cementing system cured at 20°C up to 360 days

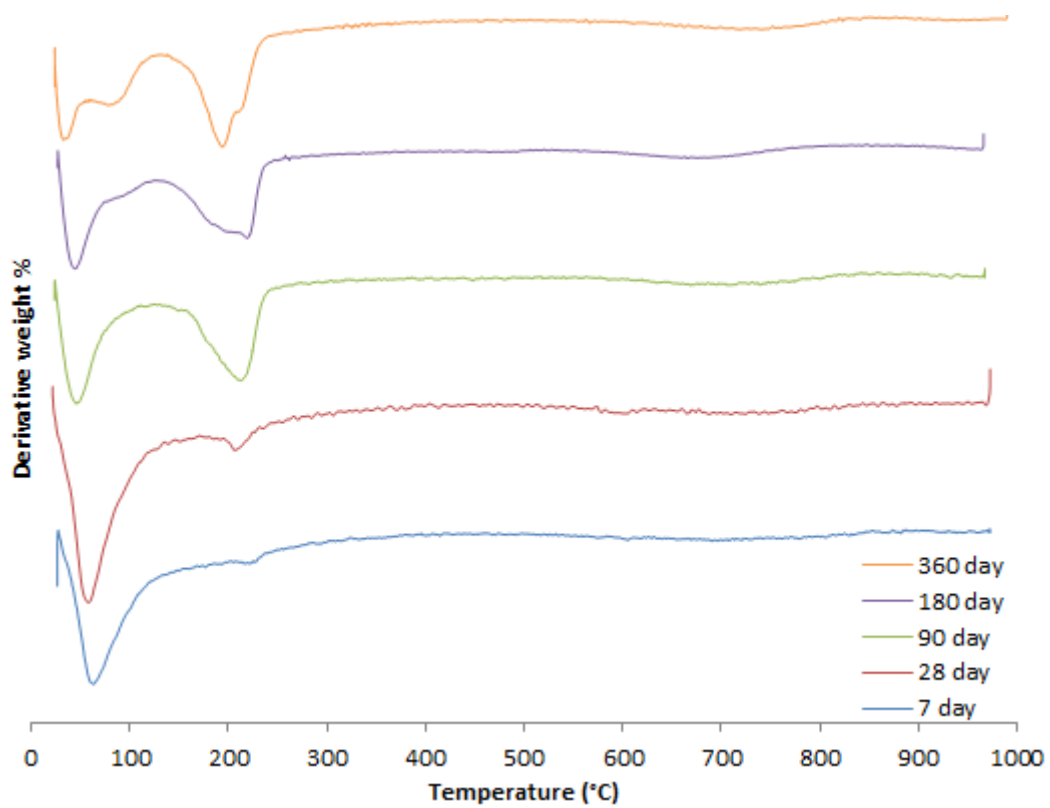


Figure 7.11 DTG results for CAP 1 cementing system cured at 20°C up to 360 days

The TG (Figure 7.12) and DTG (Figure 7.13) curves for CAP 2 up to 360 days exhibited similar weight loss behaviour as the CAP 1 system up to *ca.* 1000 °C, resulting in the total weight losses of between *ca.* 14.5-17.0 wt%. The overall weight losses demonstrated by the TG results for CAP 1 (Figure 7.10) and CAP 2 (Figure 7.12) systems were *ca.* 18.6 wt% and 17 wt%, respectively, which suggested that the higher w/s of CAP 1 resulted in a higher proportion of hydration products.

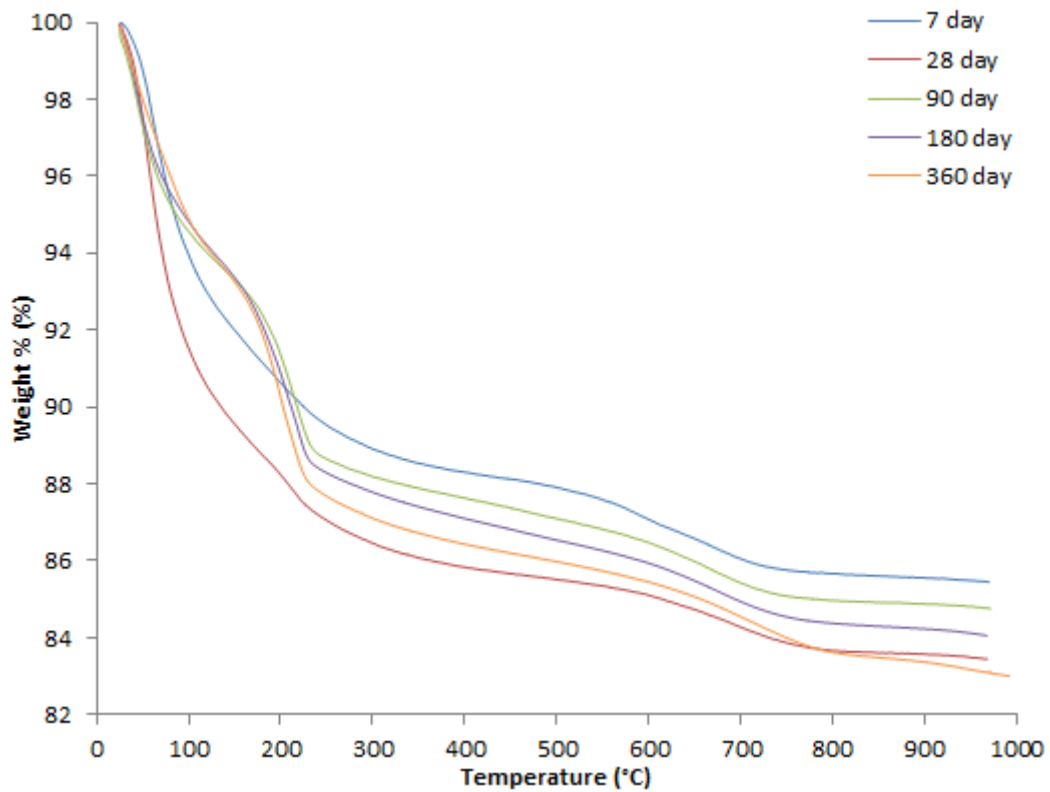


Figure 7.12 TG results for CAP 2 cementing system cured at 20°C up to 360 days

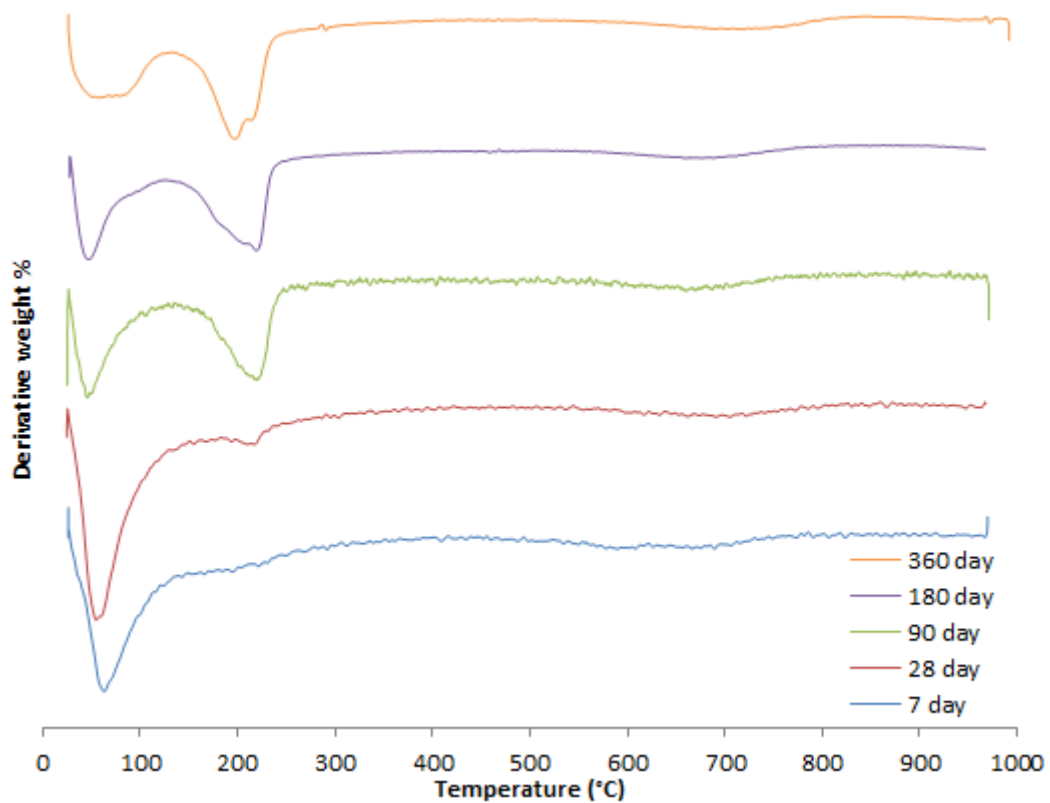


Figure 7.13 DTG results for CAP 2 cementing system cured at 20°C up to 360 days

7.5. Phase Evolution of PFA/CAC System

Figure 7.14 presents XRD patterns of the PFA/CAC system at curing periods up to 360 days. These results allow comparison with the CAP systems in order to assess the effect of phosphate additions. The PFA/CAC systems exhibited a significant strength (*ca.* 17 MPa) after curing for 7 days, suggesting the development of strength-providing hydration products. The principle reflections in the pattern of the 7 day sample corresponded to the anhydrous CAC (CA, C₂AS and CT) and PFA (quartz and mullite). There were also relatively weak reflections relating to CAH₁₀, C₂AH₈, gibbsite and strätlingite. The intensity of the reflections associated with these hydration products are weak such that it is proposed that the phases responsible for early strength development are instead likely to be poorly crystalline or amorphous hydration products. The significant diffuse scattering in the XRD pattern suggests the presence of amorphous content. Some of the diffuse scattering may also be due to the residual amorphous components of the PFA. The reflections at *ca.* 38° 2θ and 45° 2θ correspond to aluminium and are likely to be an artefact resulting from the X-ray beam interacting with the aluminium specimen holder.

The XRD patterns for the periods of between 28 days and 360 days are very similar with the only significant change being that of the relative intensity of reflections. The principle reflection for CA at *ca.* 30° 2θ, decreased in intensity with increasing curing time, suggesting that the CA was consumed in on-going hydration reactions. Similarly, C₂AS appears to have been consumed by hydration reactions, as the intensity of reflections associated with C₂AS also decreased with time. Reflections associated with strätlingite exhibited an increased intensity compared to those exhibited after 7 days curing, showing that formation of strätlingite continued with time.

It should be noted that the reflections associated with CAH_{10} were clearly observable in younger samples and older samples. This metastable phase usually converts, together with C_2AH_8 , to thermodynamically stable C_3AH_6 [65, 72, 175] and is not expected to be present in an older sample such as one aged for 360 days. The reappearance of the reflections associated with CAH_{10} may suggest some latent hydration reaction, resulting in the formation of this particular phase. CAH_{10} could also crystallise from the amorphous C-A-H gel phase, as described by Bushnell-Watson and Sharp [84]. It should be noted that no reflections were observed that would indicate the formation of the thermodynamically stable calcium aluminate hydrate phase, C_3AH_6 .

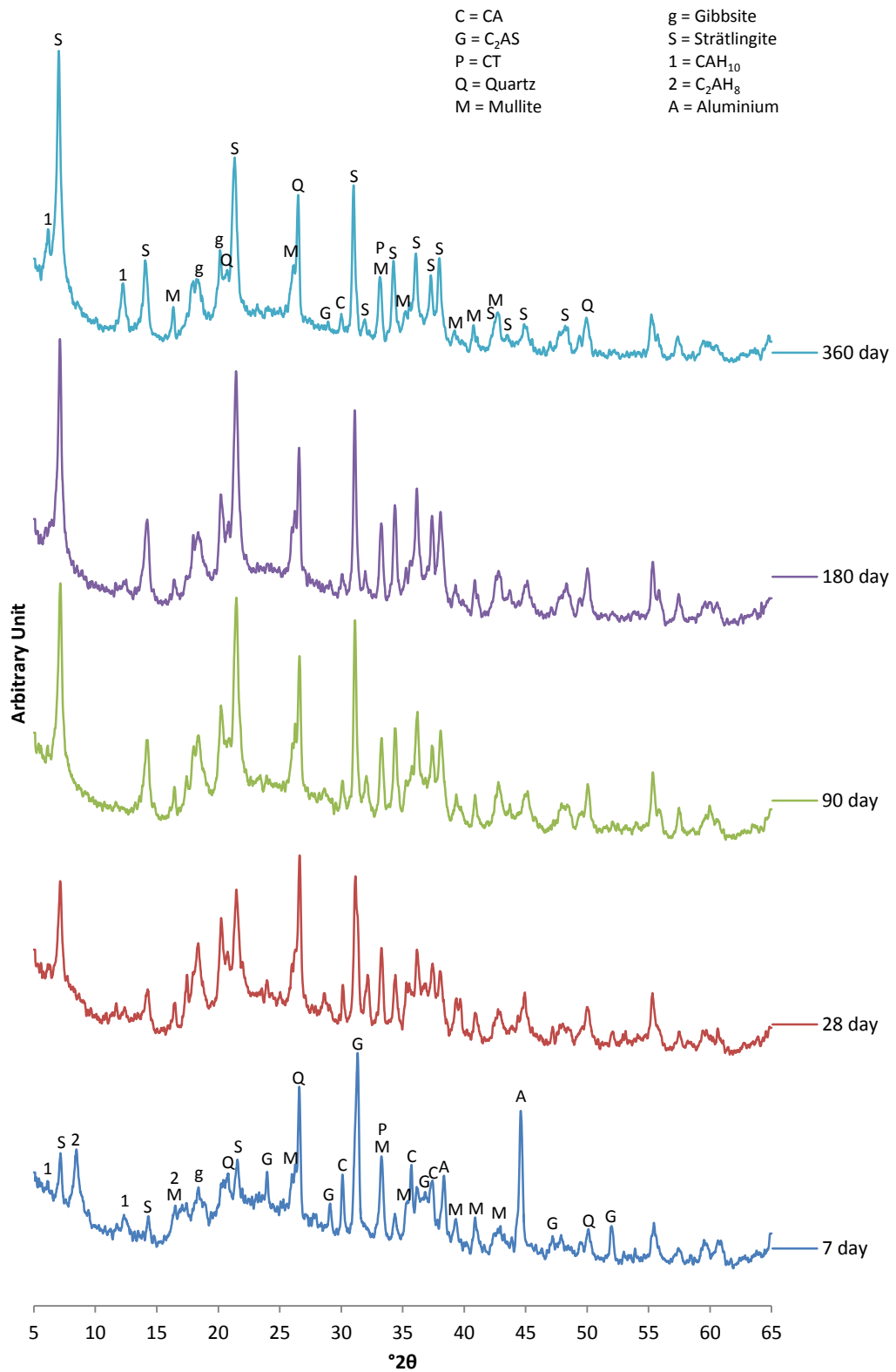


Figure 7.14 XRD pattern of PFA/CAC system cured at 20°C up to 360 days

Figure 7.15 and Figure 7.16 shows the TG and DTG curves, respectively, for the PFA/CAC system up to 360 days. The total weight loss up to 1000 °C gradually increased from *ca.* 16.6 wt % after 7 days to *ca.* 21.2 wt % after 360 days, suggesting continued hydration with time.

The DTG curves were similar at all ages, showing weight losses in the same temperature ranges. There were major weight losses at *ca.* 50-130 °C and from *ca.* 150-230 °C. The weight loss events at *ca.* 50-130 °C are likely to be the result from the dehydration of amorphous binding phases, such as C-A-H phase described by Bushnell-Watson and Sharp [84] and alumina gel. The weight loss at *ca.* 150-230 °C is likely due to the dehydration of strätlingite [182], the presence of which was confirmed by the results of XRD.

The samples also exhibited small weight loss events at *ca.* 130-160 °C and *ca.* 230-300 °C. These may be due to small amounts of CAH_{10} and gibbsite, which in some cases were also detected by XRD. There were also relatively small weight losses that occurred over a broad temperature range of *ca.* 550-800 °C, which are attributed to the decomposition of CaCO_3 .

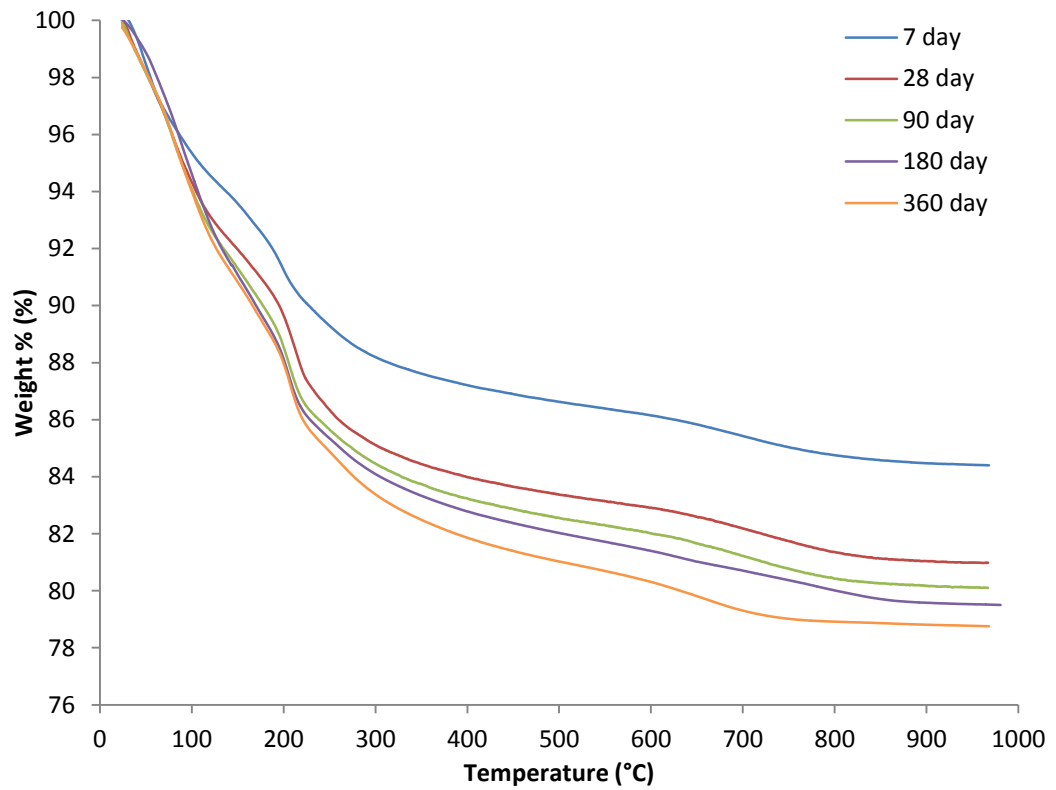


Figure 7.15 TG of PFA/CAC system cured at 20°C up to 360 days

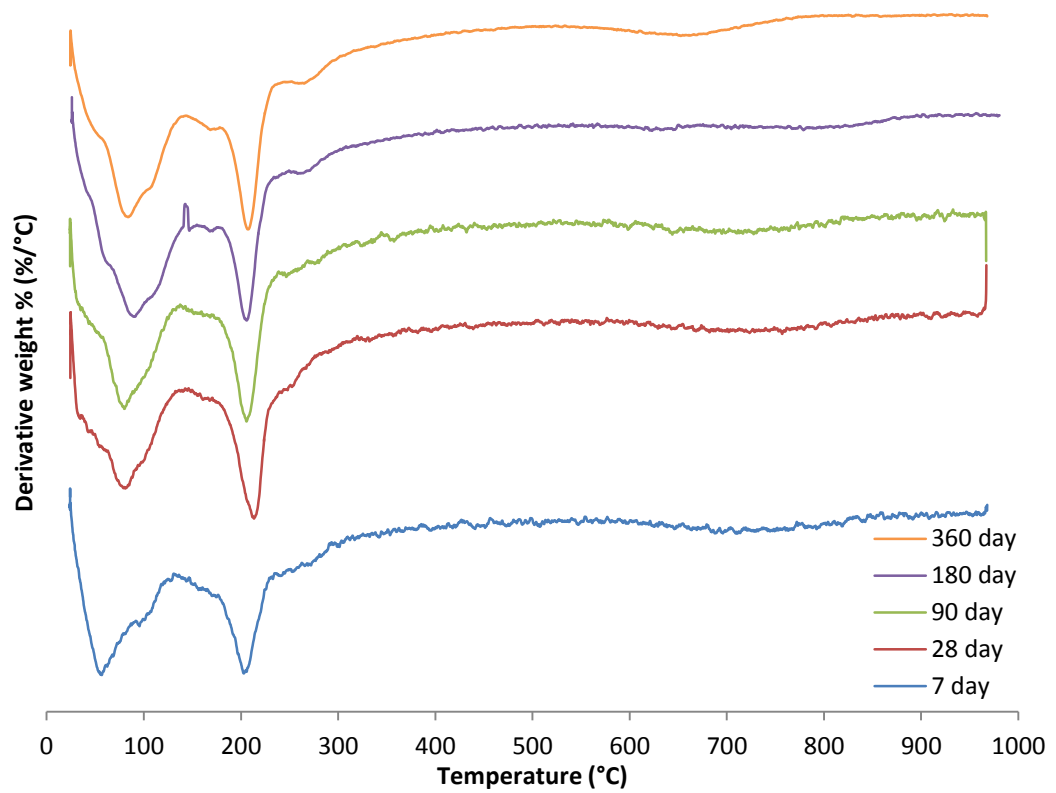


Figure 7.16 DTG of PFA/CAC system cured at 20°C up to 360 days

7.6. Microstructure of CAP Systems

BEI of selected samples for CAP 1 and CAP 2 systems are shown in Figure 7.17, Figure 7.18 and Figure 7.19. The samples after 7, 90 and 360 days of curing were selected as representatives of the short-, intermediate- and long-term cured samples, respectively. Further micrographs for both CAP cementing systems at all ages investigated are available in Appendix 3.

The BEI shown in Figure 7.17 (a) represents the typical feature of CAP 1 after 7 days of curing; a microstructure of spherical PFA particles (labelled **B**) and some residual CAC particles (labelled **A**) embedded with a matrix, which appears to be acting as a binder. The CAC particles consisted of a solid-solution of both CA (medium grey) and C₂AS (light grey), as discussed in Chapter 4. It appears that the surface of the CAC particles were rough or pitted; the light grey area stood proud and the medium grey area was recessed. This can be explained by the fact that the medium grey areas were CA, which was consumed during the acid-base and hydration reactions, whereas the light grey were C₂AS, which does not readily hydrate and so is not consumed. Micrographs at lower magnification (See Appendix 3) demonstrated that the angular particles of CAC were distributed throughout the microstructure of the 7 day cured sample.

The cause of the micro-cracking observed is not clear, but may be due to chemical shrinkage during setting, dimensional instability of the early age hydration products, or an artefact of sample preparation. Thermally induced micro-cracking due to the exothermic acid-base setting reactions may not be a cause as the CAP cementing system did not exhibit a significant exotherm during preparation or setting due to the

acid-base setting reactions. The exotherm during setting was significantly reduced as a result of the incorporation of PFA, effectively diluting the system.

The micrograph shown in Figure 7.17 (b) represents the typical morphology of CAP 2 after 7 days of curing. The microstructure is generally very similar to that exhibited by the CAP 1 system after 7 days curing; the microstructure is dominated by spherical PFA particles, with some residual CAC particles, embedded within a matrix which acts as a binder. There are also micro-cracks visible within the binding matrix.

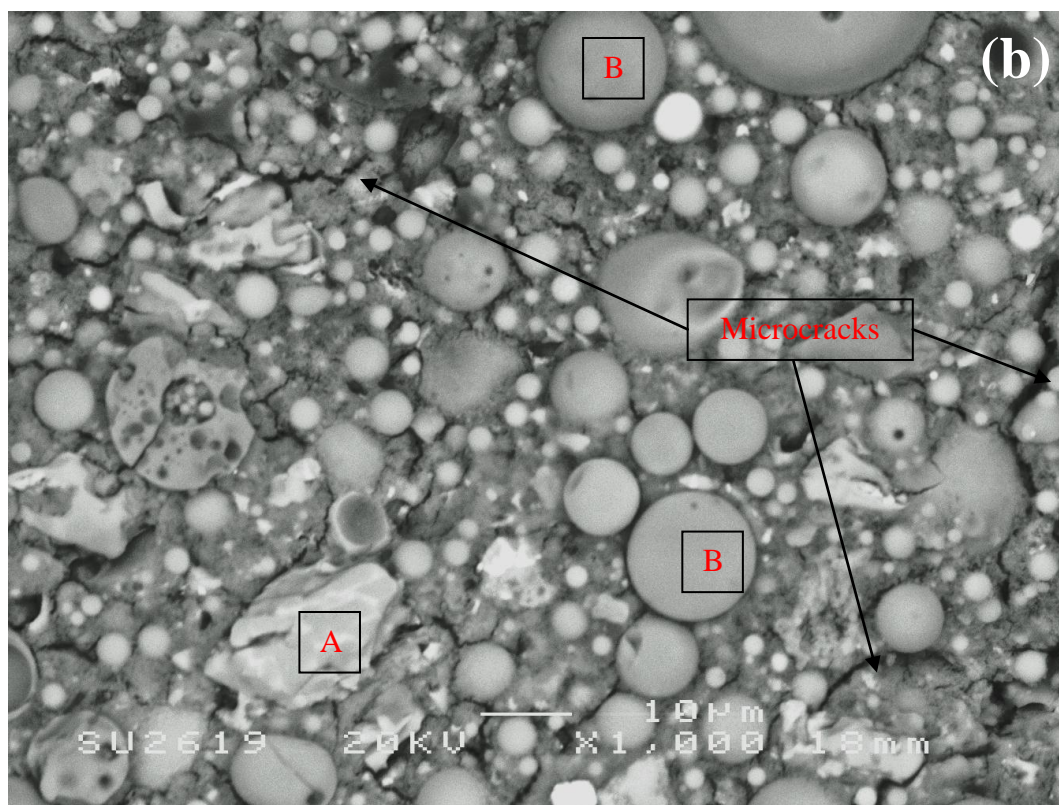
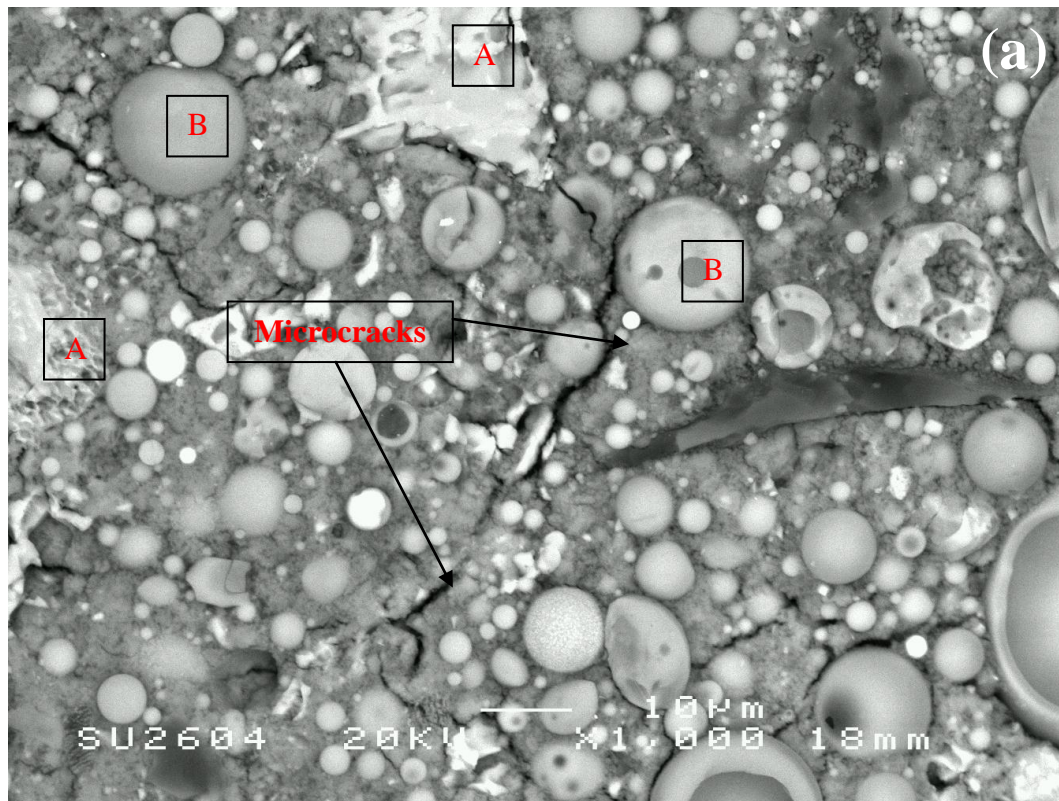


Figure 7.17 BEI of polished CAP sample cured at 20°C for 7 days: (a) CAP 1 (b) CAP 2

The micrograph for the CAP 1 cementing system after 90 days exhibited several differences to the 7 day sample as shown in Figure 7.18 (a). Although some CA particles appear to be embedded within the microstructure of the cement, there were significantly fewer than in the 7 day sample. This was in agreement with the results from XRD, which suggested that the CA particles had mostly been consumed in the acid-base and hydration reactions by this point. The morphology of the cement consisted mainly of the spherical solid particles and cenospheres of PFA embedded within a binding matrix. There did not appear to be significant micro-cracking as was observed in the 7 day sample.

Figure 7.18 (b) shows the microstructure of the CAP 2 system after 90 days curing. Once again, this is similar to that observed for the CAP 1 system after 90 days curing, whereby the microstructure is dominated by spherical particles of PFA embedded within the binding matrix. The angular particles of CAC are not obvious within this particular micrograph and in other micrographs of various magnifications (see Appendix 3). This is consistent with the XRD results, which showed no reflections associated with CA, suggesting that CA had been consumed in on-going hydration reactions after 90 days of curing. The small angular particles remaining are most likely to be residual CAC phases i.e. C_2AS and CT. Some micro-cracking was observed in the microstructure of CAP 2 system after 90 days curing (see Appendix 3).

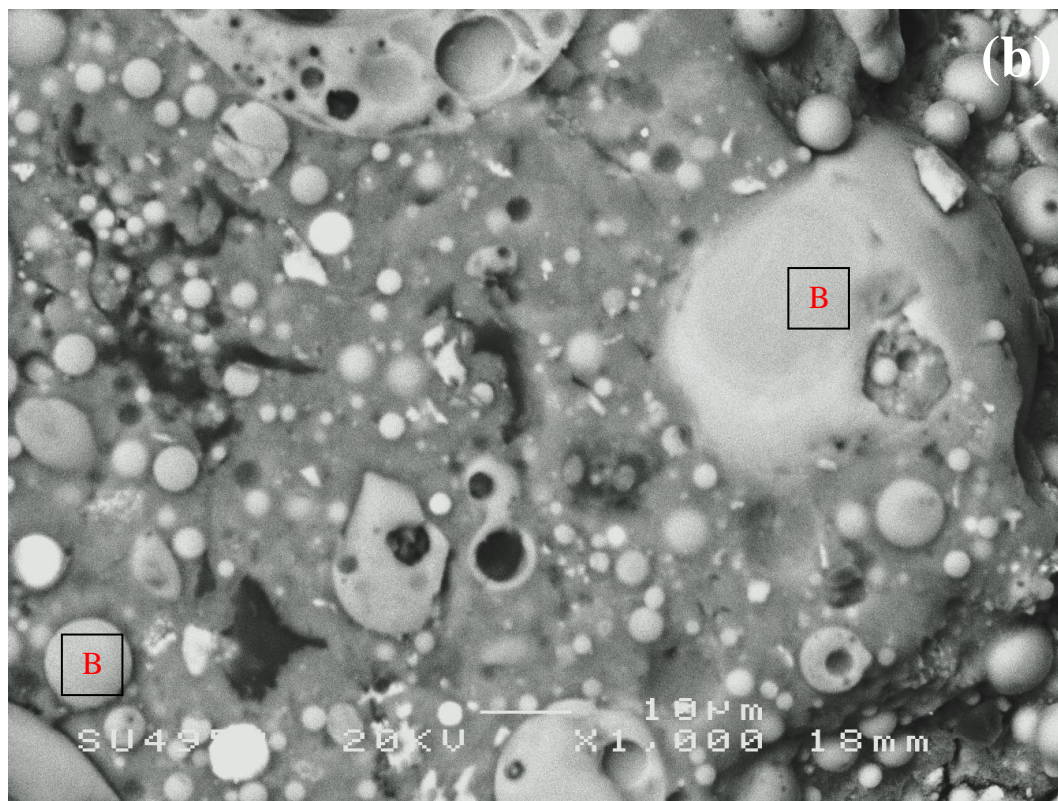
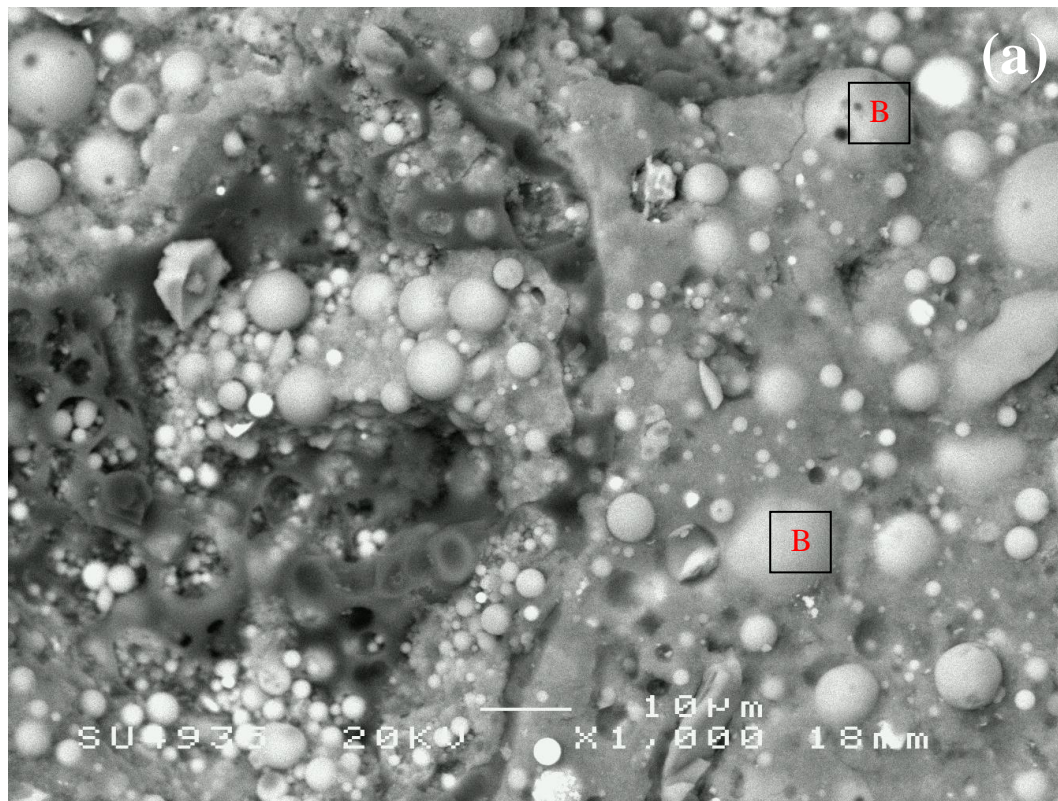


Figure 7.18 BEI of polished CAP sample cured at 20°C for 90 days: (a) CAP 1 (b) CAP 2

Figure 7.19 (a) shows the BEI for the CAP 1 cementing system after 360 days. Generally, the microstructure is similar to that exhibited after 90 days, as shown in Figure 7.18 (a), consisting of spherical particles of PFA embedded within a largely formless matrix, which appears to act as a binder. The micro-cracks observed in the 7 day sample were not observed after 360 days. The microstructure of the CAP 2 shown in Figure 7.19 (b) is similar to that exhibited by the CAP 1 system after 360 days curing. The micrograph exhibits mainly spherical particles of PFA embedded within a binding matrix.

Some of the PFA particles appear to have been removed from the binding matrix, leaving obvious craters as labelled in Figure 7.19 (b). It is suggested that this was a result of the grinding and polishing during sample preparation.

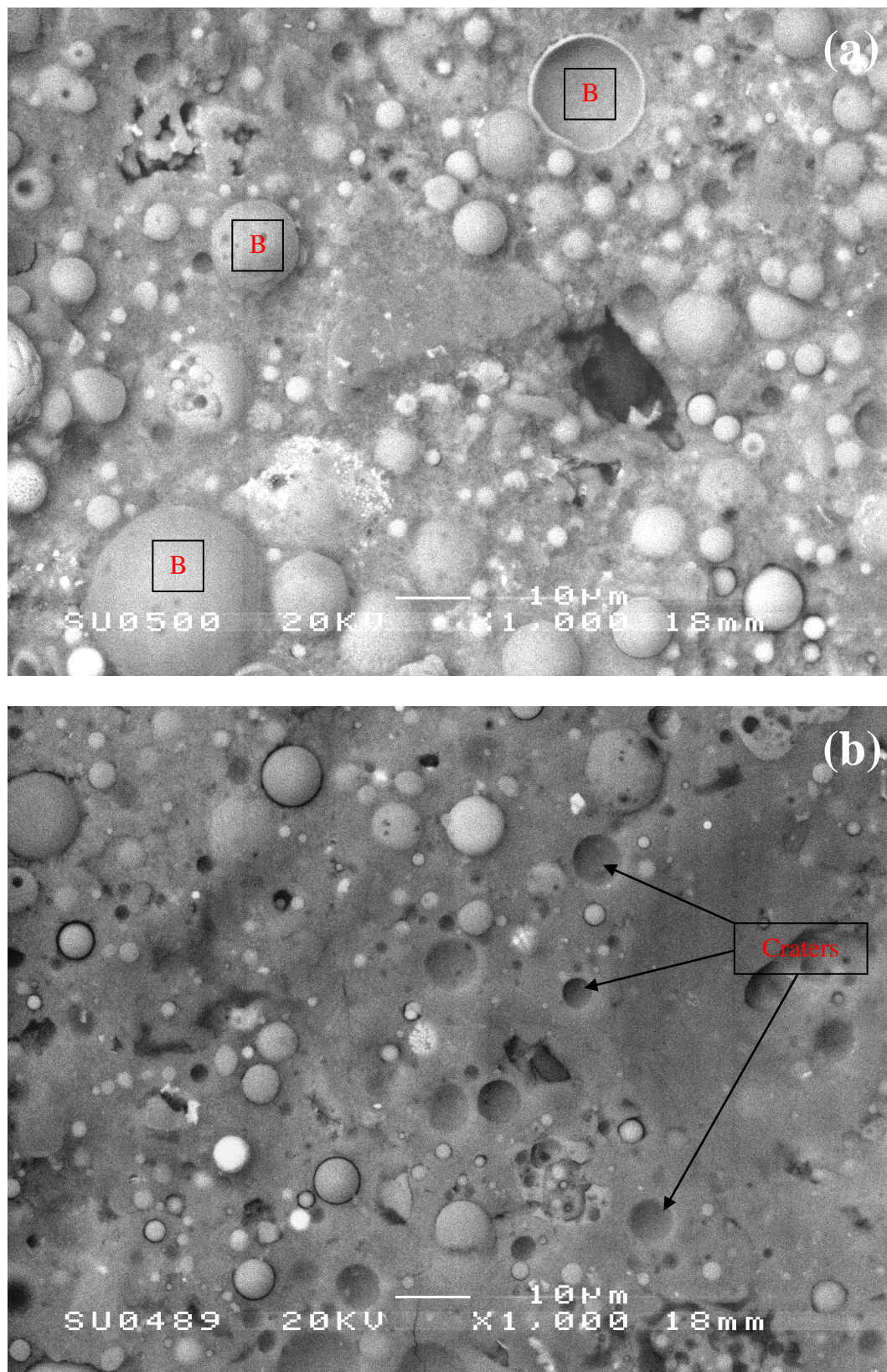


Figure 7.19 BEI of polished CAP sample cured at 20°C for 360 days: (a) CAP 1 (b) CAP 2

7.7. Elemental Composition of CAP Matrix

The elemental composition of the apparent binding matrix in the CAP 1 system, based on the EDX point spectra results, are summarised in Table 7.1. These values have been calculated as the mean of between 6 and 12 individual point spectra. The results showed that the matrix consists of calcium, aluminium, phosphorous, sodium, silicon, and oxygen. Other elements such as iron, potassium and titanium also present as minor constituents.

A similar elemental composition was observed for the $(\text{NaPO}_3)_n$ -modified CAC cementitious system discussed in Chapter 4. Although the exact atomic percentage of elements differed, the same principle elements were present. The difference in elemental composition between these systems is likely due to the differences in formulation, i.e. with/without inclusion of PFA. The PFA principally consists of silicates and aluminosilicates, which may account for the increase of silicon content in the binding matrix. Figure 7.20 illustrates the change in the content of calcium, aluminium, phosphorous, sodium and silicon in the matrix phase with curing time. There are small changes between 7 days and 28 days, but the elemental composition is relatively consistent throughout the curing period studied. Calcium showed the most significant increase of *ca.* 2.4 % between 90 and 180 days. This may be due to the release of calcium ions during the ongoing dissolution and hydration of the CAC particles.

The elemental composition of the apparent binding matrix in the CAP 2 system are summarised in Table 7.2. As expected, the results for CAP 2 were similar to those for CAP 1 system; the binding matrix consists of calcium, aluminium, phosphorous, sodium, silicon, and oxygen, along with other minor constituents such as iron,

titanium and potassium. The changes in elemental composition shown in Figure 7.21 suggest that the elemental composition of the binding matrix is relatively consistent, except a general increase in the amount of calcium in the matrix over the 360 day period; the amount of calcium in the matrix exhibited an increase of *ca.* 2.3 % from 28 days to 90 days, after which it stayed relatively constant.

Table 7.1 EDX data for CAP 1 up to 360 days curing

Element	7 days		28 day		90 day		180 day		360 day	
	Atomic %	S.D.								
Ca	6.21	2.49	6.88	2.14	6.83	1.58	9.18	2.37	7.81	2.65
Al	11.79	1.89	10.42	3.04	10.95	3.07	10.68	3.51	11.78	3.79
P	5.31	1.85	5.65	2.17	5.59	1.52	5.13	1.07	4.44	1.35
Na	2.56	0.85	2.97	0.96	2.47	0.97	2.90	1.03	2.41	1.38
Si	2.63	1.55	2.34	1.36	2.50	1.50	3.49	1.43	2.22	1.95
O	68.60	3.55	70.01	5.13	71.10	3.48	67.25	3.92	70.30	4.24
Other (Fe, K, Ti, etc.)	2.89		1.72		0.56		1.36		1.04	
Total	100		100		100		100		100	
Ca/P	1.17		1.22		1.22		1.79		1.76	

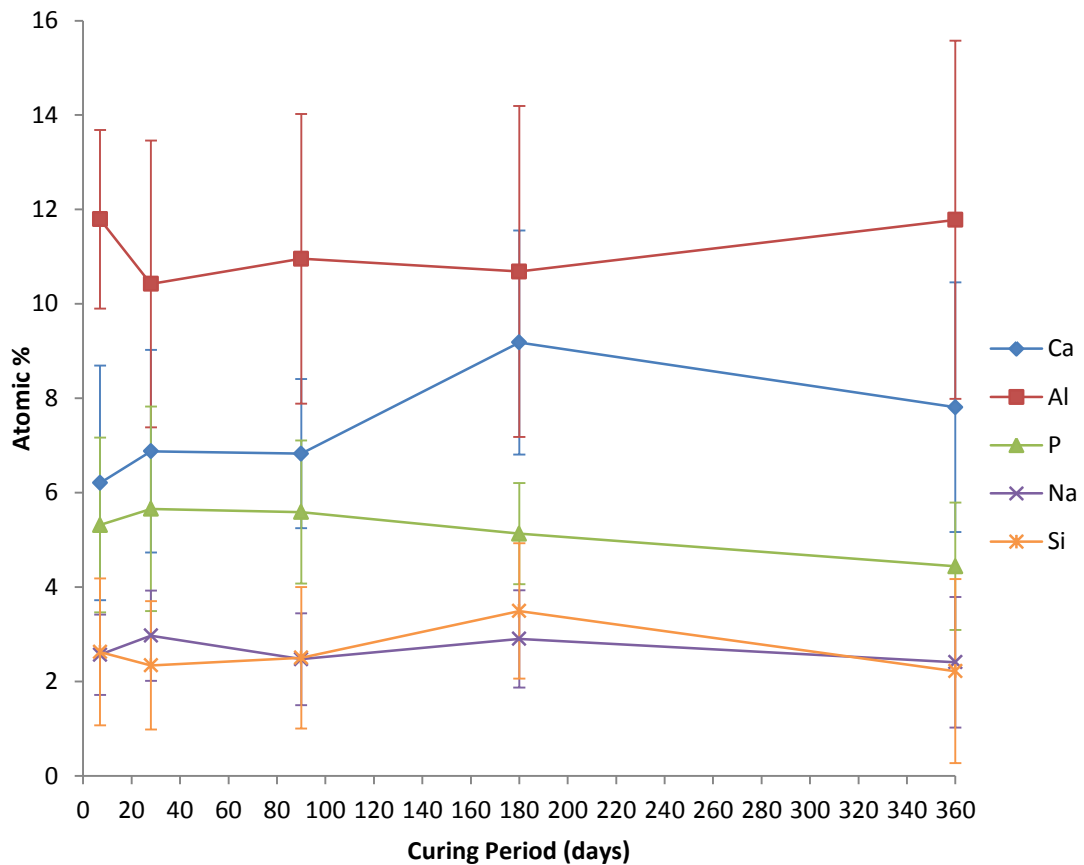


Figure 7.20 CAP 1 binding matrix elemental composition up to 360 days

Table 7.2 EDX data for CAP 2 up to 360 days curing

Element	7 days		28 day		90 day		180 day		360 day	
	Atomic %	S.D.								
Ca	6.04	1.33	5.67	3.51	8.01	1.41	7.53	2.83	7.82	3.19
Al	10.62	0.46	10.93	2.13	10.10	4.12	9.28	3.10	10.36	2.89
P	5.65	1.04	4.87	0.78	5.30	1.32	4.81	1.50	4.23	1.33
Na	2.45	0.71	3.35	0.75	3.63	0.36	3.37	0.67	3.24	1.49
Si	3.14	0.61	2.76	1.69	3.53	0.91	3.34	1.38	2.87	1.53
O	70.86	1.44	71.19	2.65	68.28	5.38	70.39	2.52	70.02	2.72
Other (Fe, K, Ti, etc.)	1.25		1.23		1.14		1.28		1.45	
Total	100		100		100		100		100	
Ca/P	1.07		1.17		1.51		1.57		1.85	

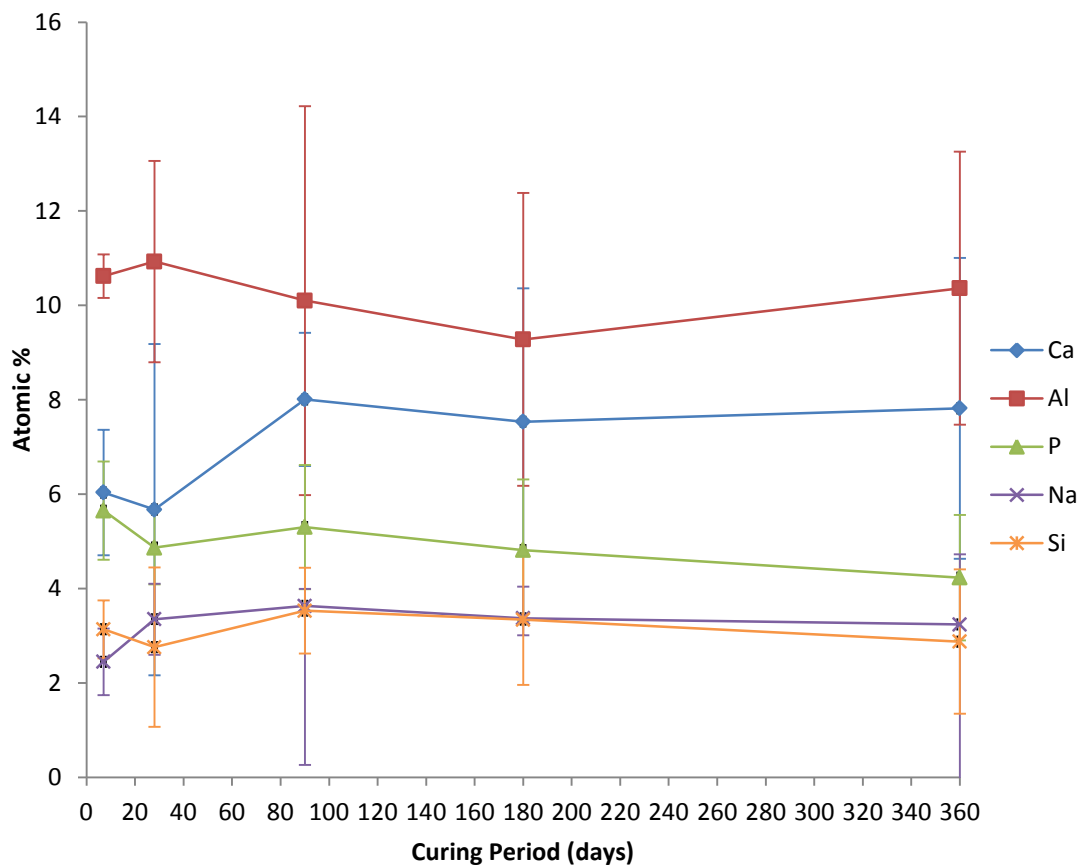
**Figure 7.21 CAP 2 binding matrix elemental composition up to 360 days**

Figure 7.22 shows the calcium to phosphate ratio (Ca/P) of the apparent binding matrix both in CAP 1 and CAP 2 cementitious systems up to 360 days. The results suggested that the Ca/P of both systems increased over the 360 days period studied. As mentioned previously, the continued dissolution of CAC particles, both CA and C₂AS may cause an increase in the amount of calcium present in the system. It is worth noting that the Ca/P ratio of 1.6-1.8 achieved in older samples > 90 days coincides with the Ca/P ratio of 1.67 in HAp (Ca₅(PO₄)₃OH).

The pore solution of CAP samples was prepared using pore solution expression. The resulting solutions were then analysed by ICP-OES; the results are shown in Table 7.3. The results show that the concentrations of various species changed with time. The pore solution exhibited high concentrations of sodium, potassium and aluminium. The high concentration of sodium is expected to be derived from the (NaPO₃)_n and also from the PFA powder. The high concentration of aluminium is likely due to the presence of [Al(OH)₄]⁻ from the dissolution of aluminium hydroxide at high pH. The results also show an increase in the concentration of silicon and calcium. The pH of the pore solutions was measured to be pH 13.5, confirming that the internal pH of the pore solution was significantly higher than that measured for the initial cement pastes (pH < 10.5). The increase in pH is likely responsible for the latent corrosion of encapsulated aluminium discussed in Chapter 6.

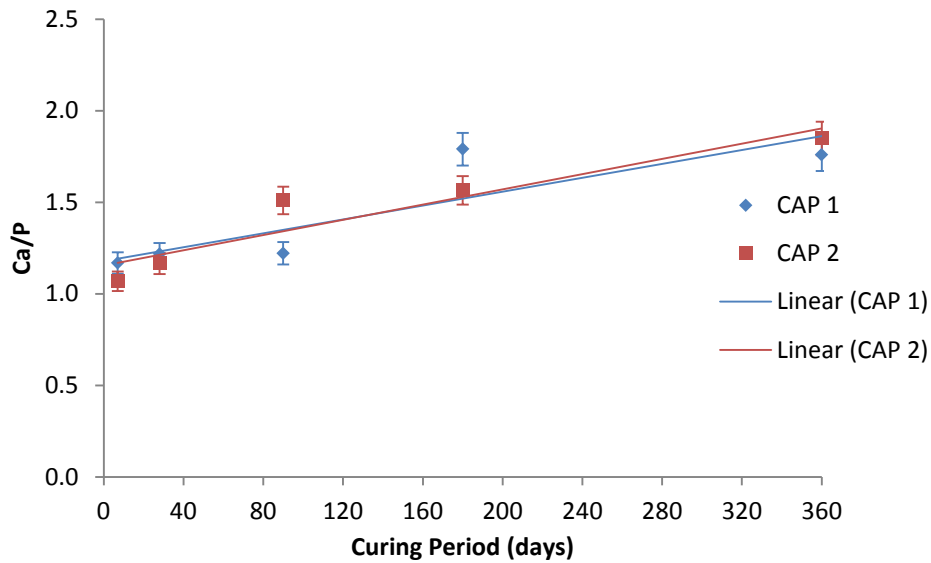


Figure 7.22 Ca/P of CAP 1 and CAP 2 binding matrix up to 360 days

Table 7.3 ICP-OES of CAP pore solution

Formulation	Age (days)	Elemental concentration (mg/L)								pH
		Al	Ca	K	Mg	Na	P	S	Si	
CAP 1	28	14,000	0.2	1,680	<0.1	42,500	3,730	8,850	330	*
	90	10,000	5.4	2,260	0.62	54,000	-	-	4,040	13.5
CAP 2	28	20,200	8.1	2,300	<0.1	45,500	3,440	9,990	433	*
	90	26,000	8.3	3,060	0.68	58,000	-	-	8,100	13.5

* pH not measured

7.8. Plant Acceptance Tests

The results from plant acceptance tests are given in Table 7.4. The flow values of both CAP formulations at t_0 and t_{150} , as assessed by the Colflow fluidity test, exceeded the minimum requirement of 200 mm. The CAP 1 exhibited a higher flow value at both t_0 and t_{150} as expected due to the higher water content. Also, both formulations exhibited higher flow values at t_{150} compared to the t_0 value. This suggests that these cementitious systems may exhibit time-dependent thixotropic properties, whereby the viscosity decreases when shear is applied [183, 184]. It is suggested that the phenomenon may have been caused by the continued use of low-shear mixing after the initial 20 minutes mixing period. The continued application of shear breaks bonds between adjacent cement particles, resulting from the acid-base reactions and hydration reactions, causing structural breakdown and decrease in viscosity.

Both formulations exceeded the minimum requirements of 4 h for initial setting and hardened within the 24 h as required for final setting. There was little difference in terms of setting behaviour between the two systems. Neither formulations exhibited any bleed water, which suggested that all mix water was incorporated into the cement hydrate phases or existed as pore solution within the pore network of the cement microstructure.

Table 7.4 Plant acceptance test results for CAP cementing systems

Formulation	Colflow			Mean	Setting time		Bleed
	Time	Run			Initial	Final	
		1	2				
	(min)	(mm)	(mm)	(mm)	(h)	(h)	(v/v)
CAP 1	0	460	520	490	7.5	< 24	0
	150	740	680	710			
CAP 2	0	220	600	410	8	< 24	0
	150	720	660	690			

7.9. Discussion

The results presented in this chapter clearly showed that the CAP cementitious system exhibited significant changes, both in terms of physical and mechanical properties as a consequence of phase evolution during the 360 day period studied.

After initial acid-base reaction and formation of the amorphous binding phase, the CAP system appeared to be stable up to 28 days. After this 'dormant' period, a notable transition of phase composition occurred, including the development of crystalline gibbsite and HAp. These changes are schematically illustrated in Figure 7.23; the vertical axis is not intended to represent a precise quantity of the phases but rather a demonstration of their existence. The horizontal axis shows the time scale and the arrows represent the change in their quantity. As a decrease of CA and a dehydration of amorphous binding phase are also taking place during this period, the formation of gibbsite and HAp must be related to the consumption of CA and the amorphous phase. Gibbsite is likely to have formed by the crystallisation of amorphous alumina gel, which could form a part of the amorphous matrix as discussed previously. Formation of HAp has been reported by Sugama *et al.* [134, 146] through the hydrothermal conversion of calcium phosphate phases. The results obtained in the present study are suggestive of a similar conversion mechanism that occurred at ambient temperature.

These phase evolutions caused a significant reduction in the volume of the solid hydration products, resulting in the shrinkage, increased porosity and significant loss in compressive strength of the CAP system during this period. These crystallisation reactions may release significant quantities of water molecules which may have facilitated latent hydration reactions of CA and also resulted in an increase in

porosity and decrease in compressive strength. The latent consumption of CA also may have caused the increase in pH of the system. It has been known that HAP forms in an alkaline environments, up to *c.a.* pH 12 [124]. Increase in pH and release of water could be a cause of the aluminium corrosion significantly increasing during this period, as discussed in Chapter 6.

In the later stage, the formation of sodium LTA zeolite phase was observed, which coincides the reduction of C₂AS. It should be noted that the reaction of C₂AS became significant after the exhaustion of CA after 90 days. It has been discussed that the hydration of C₂AS forms strätlingite (C₂ASH₈) after extended curing periods [63, 65], in CAC-based systems with silica-rich SCMs, such as PFA [65, 79, 85, 161]. Ding *et al.* suggested that the formation of strätlingite is promoted in the presence of sodium ions [185]. In the CAP systems studied here, the presence of sodium ions also has an important role in the formation of the sodium LTA zeolite phase. Sugama *et al.* also observed the formation of sodium-type zeolite phase in phosphate modified PFA/CAC systems exposed to hydrothermal conditions [132, 146]. They proposed that the sodium-type zeolite phases were formed by hydrothermal reactions between mullite from the PFA, and Na⁺ from dissociation of the sodium phosphate. The different formation mechanism of the zeolite phase in their case may be due to the hydrothermal treatment applied in their study.

In terms of the applicability of the CAP systems for the encapsulation of radioactive wastes, the systems exhibited a compressive strength greater than 4 MPa throughout the period studied, thus exceeding the minimum value mentioned in the NDA WPSGD [29]. However, the strength development profiles of the CAP systems suggested that significant microstructural changes occurred over the time period

investigated, which were corroborated by the significant evolution in the porosity and dimensional stability during the 360 day period studied. No specific guidelines or criteria exist that advise on or define the acceptable upper and lower limits of dimensional stability. However, industry suggests that if the wasteform remains between the microstrain limits of +1000 expansion and -3000 shrinkage (+0.1 to -0.3%), and had stabilised after prolonged curing and remained intact, then acceptable product quality should be achieved [186]. Although the net dimensional change is within the suitable range in terms of product quality, the shrinkage experienced by CAP 1 cementing system up to 90 days would deem it unsuitable for application as an encapsulation matrix. The expansion of CAP 2 did not exceed the limits in terms of dimensional stability, but the expansion behaviour and dimensional changes exhibited would likely be of concern to nuclear industry regulators.

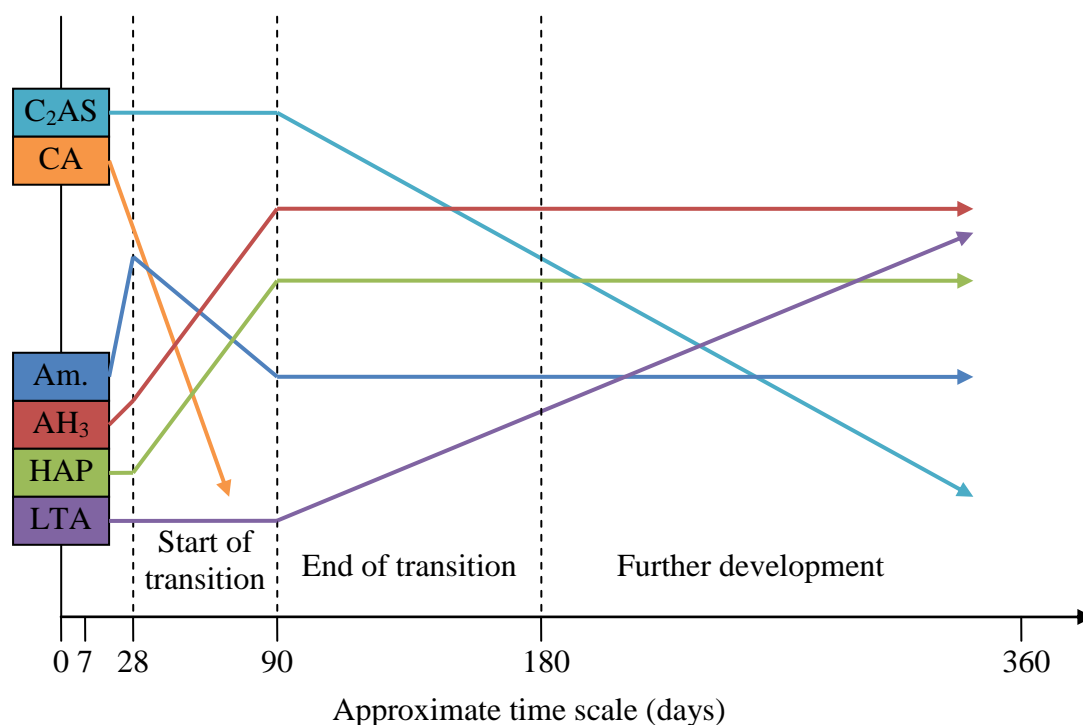


Figure 7.23 Schematic of phase evolution with time

7.10. Summary

The CAP systems exhibited significant evolution during the 360 day period studied, both in terms of physical and chemical characteristics. The compressive strength exhibited a significant strength regression after 28 days, which coincided with an increase in porosity and significant dimensional changes. The XRD and TG results suggested that these effects were the result of the evolution in the phase composition of the CAP systems: delayed crystallisation of the amorphous binding phases to form gibbsite, HAp and a sodium LTA zeolite phase. The phase evolution resulted in the volume change in the amorphous matrix probably due to the release of water. Additionally, the release of water and increase in pore solution pH is responsible for the delayed corrosion of encapsulated aluminium as discussed in Chapter 6.

8. Conclusions

8.1. Overview

A CAP system has been investigated as an alternative cementing system for the encapsulation of aluminium metal for radioactive waste management applications. A CAP system formulation envelope was identified in order to satisfy nuclear industry-defined processing and operational requirements. The interaction of CAP systems with encapsulated aluminium was also assessed. A series of studies on the physical and chemical properties of CAP systems for curing periods of up to 360 days provided further understanding of the longer-term behaviour of the systems and the interaction of the CAP system with aluminium.

8.2. Identification of Suitable Precursor Materials

Various phosphate powders were tested to identify potential materials for use in phosphate-modified CAC-based CAP system. It was confirmed that the setting and strength development was dependent on the type of phosphate used for the modification. Monophosphate-modified systems did not fully set or develop significant strength, whereas polyphosphate-modified systems exhibited rapid setting and high early strength development. It was shown that the phosphate modifications affected the hydration mechanisms, and the calcium aluminate hydrate phases usually formed in CAC systems were not formed. The results suggested that the phases responsible for setting and strength development, which acted as a binding matrix between residual CAC particles, were amorphous. The amorphous binding matrix may consist of ACP and hydrated alumina gel.

It was concluded that monophosphate-based modifications are not suitable for producing cementitious systems for radioactive waste encapsulation, based on their lack of setting or strength development. On the other hand, systems derived from

polyphosphate-based modification of CAC indicated a good potential, developing a significant strength. The rapid setting and exothermic setting reactions would need to be addressed for the polyphosphate-based system in order to make them practicable.

8.3. Development of CAP Formulation Envelope

PFA was incorporated into the CAP system as a SCM in order to reduce the heat output of the system during setting and extend the setting time, as well as to improve the rheological properties of cementitious systems by the ball-bearing effect. Preliminary investigations showed that formulation parameters, such as PFA content and phosphate content, affect the setting characteristics of the CAP system. It was shown that the setting time of the CAP system could be controlled by varying the formulation parameters. Boric acid was also introduced as an additive to allow further control of the setting time of the system to fulfil the industrial requirement relating to setting time.

The results from plant acceptance tests showed that processing and operational properties can be controlled by inclusion of PFA and boric acid. Boric acid significantly affected the setting characteristics of the CAP system resulting in setting times satisfying the requirement stipulated by industry. The CAP system is highly sensitive to boric acid content. The use of PFA as a SCM improved the rheological properties of the CAP system by increasing the fluidity of the CAP slurry. The results identified a CAP formulation envelope that fulfilled the processing properties requirements defined by the nuclear industry.

No new crystalline phases were formed during the setting and hardening reactions of CAP system incorporating PFA and boric acid. The principle reaction products responsible for setting and strength development were amorphous; possibly ACP and

alumina gel based on the TG and DTG results. The microstructure of the hardened cement pastes was characterised by residual CAC particles and spherical particles of PFA embedded within the amorphous binding matrix. EDX results showed that the matrix exhibited a Ca/P ratio ≈ 1 , which is consistent with ACP.

The CAP systems incorporating PFA and boric acid developed significant strength at varying degrees depending on the replacement-level of CAC with PFA and exhibited a typical porosity-strength relationship. Furthermore, it was shown that the initial pH of the CAP slurry was significantly lower than that of BFS/PC that is typically used for encapsulation of ILW in the UK suggesting that CAP may reduce the corrosion of encapsulated aluminium and subsequent hydrogen gas generation compared to conventional cementitious systems.

8.4. Encapsulation of Aluminium in CAP

The reaction of aluminium with the CAP system was characterised by a dormant period with a low corrosion rate less than *ca.* $0.07 \text{ litres h}^{-1} \text{ m}^{-2}$ which lasted for *ca.* 55-65 days. It was suggested that the aluminium oxide layer present on the surface of the aluminium metal must have been passive due to the lower pH environment inferred by the pH of the initial slurry of the CAP system (*ca.* pH 8-10) compared to those of the BFS/PC (*ca.* pH 12.7-13.0) and PFA/CAC (*ca.* pH 11.7-12.0) systems. It was therefore suggested that the low gas generation rates, and consequently implied low corrosion rates, were a result of the relatively low pH environment provided by the CAP systems.

After the dormant period of *ca.* 55-65 days the hydrogen gas generation rate increased from *ca.* $0.07 \text{ litres h}^{-1} \text{ m}^{-2}$ to *ca.* $0.4\text{-}0.5 \text{ litres h}^{-1} \text{ m}^{-2}$, which then persisted

for the remainder of the monitored encapsulation period. The corrosion behaviour of aluminium in the CAP system suggested alternative corrosion mechanisms occurred.

Examination of aluminium-cement interface and encapsulated aluminium specimens demonstrated the formation of significant quantities of corrosion products for samples encapsulated for periods of greater than 90 days. The quantity of corrosion products suggested that corrosion continued to occur throughout the encapsulation period up to 360 days. XRD and EDX of the corrosion product confirmed it to be aluminium hydroxide in the form of gibbsite.

8.5. Characterisation of CAP

The results presented clearly showed that the CAP cementitious system exhibited significant changes, both in terms of physical and mechanical properties as a consequence of phase evolution during the 360 day period studied. The compressive strength exhibited a significant strength regression after 28 days, which coincided with an increase in porosity and significant dimensional changes. The XRD and TG results suggested that these effects were the result of the evolution in the phase composition of the CAP systems. This evolution included the delayed crystallisation of the amorphous binding phases to form gibbsite, HAp and a sodium LTA zeolite phase. The phase evolution resulted in the volume change in the solid matrix, probably due to the release of water, which was responsible for an increase in porosity and decrease in compressive strength. Additionally, the release of water and apparent increase in pore solution pH was responsible for delayed corrosion of encapsulated aluminium.

In terms of the applicability of the CAP systems for the encapsulation of ILW, the systems exhibited a compressive strength greater than 4 MPa throughout the period

studied, therefore exceeding the minimum value mentioned in the NDA WPSGD [29]. However, the evolution of the compressive strength suggested that significant microstructural changes occurred over the time period investigated, which was supported by the significant evolution in the porosity and dimensional stability during the 360 day period studied. Furthermore, the dimensional changes experienced by CAP system would likely be of concern to nuclear regulators and may deem it unsuitable for application as an encapsulation matrix.

8.6. Summary

A CAP system was developed based on mixing calcium aluminate cement and an acidic phosphate solution, with an addition of PFA and boric acid. A CAP system formulation envelope was developed to fulfil industrially defined processing properties requirements. The principle reactions products, which were responsible for setting and early strength development, were possibly amorphous calcium phosphate and alumina gel.

The aluminium encapsulated in the CAP system exhibited low gas generation rate corresponding to the minimal corrosion of the encapsulated aluminium in the short term, but experienced a latent increase in gas generation, which then persisted for the remaining period studied. The aluminium encapsulated in the CAP system exhibited significantly more corrosion and hydrogen gas generation than those encapsulated in the BFS/PC and PFA/CAC system during the 360 period studied.

The latent corrosion was accompanied by significant evolution in physico-mechanical properties. It was suggested that these effects resulted from the evolution of the phase composition of the CAP system; conversion of the amorphous phase (ACP and alumina gel) into crystalline hydroxyapatite and gibbsite in addition to

sodium LTA zeolite phase. The crystallisation may have released water and altered the composition and pH of the pore solution.

The evolution of physico-mechanical properties and phase composition of the CAP system would be of concern to nuclear industry regulators and likely prevent endorsement for application of the CAP system in the current state as an encapsulation matrix for ILW in the UK. It may be possible to further develop the system either to prevent the phase evolution or to make the crystallisation process occur during the initial setting and hardening stage.

9. Recommendations for Further Work

The project presented here contributes to the field of cementitious systems for the encapsulation of reactive metals and radioactive waste. However, it also highlights several areas that require additional investigations in order to further develop and better understand the system the CAP system properties and performance. The following are suggestions for further work:

- The industry-defined plant acceptance test included a requirement relating to the heat of hydration of cementitious encapsulants. It is therefore suggested that the heat of hydration of the CAP system be characterised by Isothermal Conduction Calorimetry.
- Although the flow properties were characterised by the use of the Colflow method, this is considered to be a rather crude evaluation technique designed to be used 'in the field'. It is therefore suggested to perform more comprehensive investigations to characterise the rheological properties of the CAP system.
- PFA was initially deemed to be an appropriate SCM for use in the CAP formulation. However, the results presented here suggest that PFA may participate in the latent reactions. Therefore, it is suggested that other alternative SCMs be evaluated for use in the CAP system.
- Following further development of the CAP system, it is suggested that an optimised CAP formulation envelope be applied to the encapsulation of other reactive metals i.e. Magnox and uranium, exists within the UK radioactive waste inventory.

10. References

1. Ojovan, M. I. and Lee, W. E., *Introduction to Immobilisation*, in *An Introduction to Nuclear Waste Immobilisation*, Elsevier, Oxford, Chapter 1, p. 1-8, 2005
2. *The 2010 UK Radioactive Waste Inventory: Main Report*, Department of Energy and Climate Change and Nuclear Decommissioning Authority, 2010
3. Setiadi, A., Milestone, N. B., Hill, J., and Hayes, M., *Corrosion of aluminium and magnesium in BFS composite cements*, *Advances in Applied Ceramics*, Vol. 105, p. 191-196, 2006
4. Milestone, N. B., *Reactions in cement encapsulated nuclear wastes: need for toolbox of different cement types*, *Advances in Applied Ceramics*, Vol. 105 (1), p. 13-20, 2006
5. *Proposed Research and Development Strategy*, Nuclear Decommissioning Authority Radioactive Waste Management Directorate, 2008
6. Zhou, Q., Milestone, N. B., and Hayes, M., *An alternative to Portland Cement for waste encapsulation - The calcium sulfoaluminate cement system*, *Journal of Hazardous Materials*, Vol. 136 (1), p. 120-129, 2006
7. NDA, *Strategy - Effective from April 2011*, 2011
8. Nirex, *Generic Waste Package Specification Vol. 1 - Specification*, N/104, 2005
9. Nirex, *Generic Waste Package Specification Vol. 2 - Justification*, N/104, 2005
10. *Radioactive Waste Management Glossary*, International Atomic Energy Agency, 2003
11. Glasser, F. P., *Fundamental aspects of cement solidification and stabilisation*, *Journal of Hazardous Materials*, Vol. 52 (2-3), p. 151-170, 1997
12. Glasser, F.P., *Progress in the Immobilization of Radioactive Wastes in Cement*, *Cement and Concrete Research*, Vol. 22, p. 201-216, 1992
13. Wilding, C. R., *The Performance of Cement Based Systems*, *Cement and Concrete Research*, Vol. 22 (2-3), p. 299-310, 1992
14. Atkins, M. and Glasser, F. P., *Application of Portland cement-based materials to radioactive waste immobilization*, *Waste Management*, Vol. 12 (2-3), p. 105-131, 1992
15. Sharp, J. H., Hill, J., Milestone, N. B., and Miller, E. W., *Cementitious systems for encapsulation of intermediate level waste*, in *Proceedings of ICEM '03: The 9th International Conference on Radioactive Waste Management and Environmental Remediation*, Oxford, England, 2003
16. Borges, Paulo H. R., Costa, Juliana O., Milestone, Neil B., Lynsdale, Cyril J., and Streatfield, Roger E., *Carbonation of CH and C-S-H in composite cement pastes containing high amounts of BFS*, *Cement and Concrete Research*, Vol. 40 (2), p. 284-292, 2010
17. Collier, N. C. and Milestone, N. B., *The encapsulation of Mg(OH)₂ sludge in composite cement*, *Cement and Concrete Research*, Vol. 40 (3), p. 452-459, 2010
18. Black, Leon, Purnell, Phil, and Hill, Joanne, *Current themes in cement research*, *Advances in Applied Ceramics*, Vol. 109 (5), p. 253-259, 2010
19. Gorce, Jean-Philippe and Milestone, Neil B., *Probing the microstructure and water phases in composite cement blends*, *Cement and Concrete Research*, Vol. 37 (3), p. 310-318, 2007

20. Palmer, J. D. and Fairhall, G. A., *Properties of cement systems containing intermediate level wastes*, Cement and Concrete Research, Vol. 22, p. 325-330, 1992
21. Collier, N. C., Milestone, N. B., and Swift, P. D., *Immobilisation matrices for intermediate level nuclear wastes using sulphate activated BFS/OPC and PFA/OPC composite cements*, Advances in Applied Ceramics, Vol. 109 (5), p. 269-274, 2010
22. Cau Dit Coumes, C. and Courtois, S., *Cementation of a low-level radioactive waste of complex chemistry: Investigation of the combined action of borate, chloride, sulfate and phosphate on cement hydration using response surface methodology*, Cement and Concrete Research, Vol. 33 (3), p. 305-316, 2003
23. Cau Dit Coumes, Céline, Courtois, Simone, Peysson, Sandrine, Ambroise, Jean, and Pera, Jean, *Calcium sulfoaluminate cement blended with OPC: A potential binder to encapsulate low-level radioactive slurries of complex chemistry*, Cement and Concrete Research, Vol. 39 (9), p. 740-747, 2009
24. Ojovan, M. I. and Lee, W. E., *Immobilisation of Radioactive Waste in Cement*, in *An Introduction to Nuclear Waste Immobilisation*, 1st ed, Elsevier, Oxford, Chapter 15, p. 179-200, 2005
25. Odler, I., *Hydration, Setting and Hardening of Portland Cement*, in *Lea's Chemistry of Cement and Concrete*, 4th ed, ed. Hewlett, P. C., Butterworth-Heinemann, Oxford, Chapter 6, p. 241-297, 2006
26. Taylor, H. F. W., *Hydration of Portland cement*, in *Cement Chemistry*, 2nd ed, Thomas Telford Publishing, London, Chapter 7, p. 199-241, 1997
27. Hayes, M., *Personal communication*, National Nuclear Laboratory, 2010
28. Collier, N. C., *Personal communication*, National Nuclear Laboratory, 2010
29. NDA, *Waste Package Specification and Guidance Documentation WPS/700: 500 litre Drum Waste Package Specification: Explanatory Materials and Design Guidelines*, 8766510, 2008
30. Covill, A. P., *Novel Encapsulants for Intermediate Level Waste in the UK Nuclear Industry*, The University of Sheffield, The Department of Materials Science and Engineering, 2010
31. Bye, G. C., *Portland Cement: Composition, Production and Properties*, in *Portland Cement: Composition, Production and Properties*, 2nd edition, Tomas Telford, London, Chapter 1, 1983
32. Moranville-Regourd, M., *Cements made from Blastfurnace Slag*, in *Lea's Chemistry of Cement and Concrete*, 4th edition, ed. Hewlett, P. C., Butterworth-Heinemann, Oxford, Chapter 11, p. 637-678, 2006
33. Taylor, H. F. W., *Composite cements*, in *Cement chemistry*, 1st edition, Thomas Telford Publishing, London, Chapter 9, p. 276-314, 1992
34. Covill, A., Hyatt, N. C., Hill, J., and Collier, N. C., *Development of magnesium phosphate cements for encapsulation of radioactive waste*, Advances in Applied Ceramics, Vol. 110, p. 151-156, 2011
35. Fairhall, G. A. and Palmer, J. D., *The encapsulation of Magnox Swarf in cement in the United Kingdom*, Cement and Concrete Research, Vol. 22 (2-3), p. 293-298, 1992
36. Collier, N. C., *Personal communication*, 2012
37. Altenpohl, D. G., *Corrosion resistance and protection*, in *ALuminium: Technology, applications, and environment - A profile of a modern metal*, 6th edition, The Aluminium Association Washington, Chapter 12, p., 1998

38. Hollingsworth, E. H. and Hunsicker, H. Y., *Corrosion of aluminium and aluminium alloys*, in *Metals Handbook*, Vol. 13, 9th edition, ASM International, 1987
39. White, J. K. and Jefferies, S. A., *Generic Studies on the Encapsulation of Aluminium in Cement*, Product Evaluation Task Force, PETF(87)P61, 1987
40. Setiadi, A., *Corrosion of metals in composite cement*, The University of Sheffield, Department of Engineering Materials, 2006
41. Varlet, P. C., *Corrosion resistance*, in *The technology of aluminium and its alloys*, 1st edition, Butterworth and Co. Ltd, London, Chapter 11, p., 1970
42. Berger, S. and Fryda, H. *Calcium aluminate cements for nuclear wastes conditioning: literature review and new approaches*, in NUWCEM 2011 - 1st International Symposium on Cement-based Materials for Nuclear Wastes, Avignon, France, 2011
43. Hidalgo, A., Petit, S., García, J. L., Alonso, C., Andrade, C., and Ruren Xu, Zi Gao Jiesheng Chen and Wenfu Yan, *Microstructure of the system calcium aluminate cement-silica fume: application in waste immobilization*, in *Studies in Surface Science and Catalysis*, Vol. 170, Elsevier, 1617-1628, 2007
44. Hayes, M. and Godfrey, I.H. *Development of the Use of Alternative Cements for the Treatment of Intermediate Level Waste*, in Waste Management Symposium 2007 - Global Accomplishments in Environmental and Radioactive Waste Management: Education and Opportunity for the Next Generation of Waste Management Professionals, Tuscon, AZ, (United States), 2007
45. McCague, C., Bai, Y, Zhou, Q., and Basheer, P. A. M. *Early age corrosion of aluminium in calcium sulfoaluminate cement based composites*, in NUWCEM 2011 - 1st International Symposium on Cement-based Materials for Nuclear Wastes, Avignon, France, 2011
46. Bai, Y., McCague, C., Zhou, Q., and Basheer, P. A. M., *Early Age Corrosion of Aluminium in Calcium Sulfoaluminate Cement Based Composites*, Proceedings of the 1st International Symposium on Cement-based Materials for Nuclear Waste, Avignon, France, p. 427-436, 2011
47. Palomo, A. and López dela Fuente, J. I., *Alkali-activated cementitious materials: Alternative matrices for the immobilisation of hazardous wastes: Part I. Stabilisation of boron*, Cement and Concrete Research, Vol. 33 (2), p. 281-288, 2003
48. Roy, D. M. and Silsbee, M. R., *Alkali Activated Cementitious Materials: An Overview*, MRS Online Proceedings Library, Vol. 245, 1991
49. Shao-Dong, W., Xin-Cheng, P., Scrivener, K. L., and Pratt, P. L., *Alkali-activated slag cement and concrete: a review of properties and problems*, Advances in Cement Research, Vol. 7 (27), p. 93-102, 1995
50. Rashad, A. M., Bai, Y., Basheer, P. A. M., Collier, N. C., and Milestone, N. B., *Chemical and mechanical stability of sodium sulfate activated slag after exposure to elevated temperature*, Cement and Concrete Research, Vol. 42 (2), p. 333-343, 2012
51. Rashad, A. M., Bai, Y., Basheer, P. A. M., Milestone, N. B., and Collier, N. C., *Hydration and properties of sodium sulfate activated slag*, Cement and Concrete Composites, Vol. 37 (0), p. 20-29, 2013
52. Bai, Y., Collier, N. C., Milestone, N. B., and Yang, C. H., *The potential for using slags activated with near neutral salts as immobilisation matrices for*

- nuclear wastes containing reactive metals*, Journal of Nuclear Materials, Vol. 413 (3), p. 183-192, 2011
53. Zhang, Tingting, Cheeseman, C. R., and Vandeperre, L. J., *Development of low pH cement systems forming magnesium silicate hydrate (M-S-H)*, Cement and Concrete Research, Vol. 41 (4), p. 439-442, 2011
 54. Wagh, A. S., *Chemically Bonded Phosphate Ceramics: 21st Century Materials with Diverse Applications*, 1st edition, Oxford, Elsevier Ltd, 2004
 55. Wagh, A. S., *Radioactive Wastes Stabilization*, in *Chemically Bonded Phosphate Ceramics*, Elsevier, Oxford, Chapter 17, p. 217-243, 2004
 56. Wagh, A. S., *Magnesium Phosphate Ceramics*, in *Chemically Bonded Phosphate Ceramics: 21st Century Materials with Diverse Applications*, Elsevier, Oxford, Chapter 9, p. 97-111, 2004
 57. Bai, Y., McCague, C., and Basheer, P. A. M., *Magnesium phosphate cement: A new material for waste encapsulation*, SCI Construction Materials Young Researchers' Forum, London, U.K., p. 54-57, 2012
 58. McCague, C., Wang, L., and Bai, Y., *Magnesium Phosphate Cement as a Potential Alternative for Encapsulation of Nuclear Wastes Containing Aluminium*, Novel Developments and Innovation in Cementitious Materials, 31st Cement and Concrete Science Conference, London, U.K., 2011
 59. Milestone, N. B., *Personal communication*, 2008
 60. Juenger, M. C. G., Winnefeld, F., Provis, J. L., and Ideker, J. H., *Advances in alternative cementitious binders*, Cement and Concrete Research, Vol. 41 (12), p. 1232-1243, 2011
 61. Robson, T. D., *High-Alumina Cements and Concretes*, London, F. J. Parsons Ltd., 1962
 62. Robson, T. D., *Aluminous Cement and Refractory Castables*, in *The Chemistry of Cements*, Vol. 2, ed. Taylor, H. F. W., Academic Press, London, Chapter 12, 1964
 63. Bensted, J., *Calcium aluminate cements*, in *Structure and Performance of Cements*, Bensted, J. and Barnes, P., Spon Press, London, Chapter 4, 2002
 64. Taylor, H. F. W., *Calcium aluminate, expansive and other cements*, in *Cement Chemistry*, 2nd edition, Academic press, London, Chapter 10, 1992
 65. Scrivener, K. L. and Campas, A., *Calcium Aluminate Cements*, in *Lea's Chemistry of Cement and Concrete*, 4th edition, Butterworth-Heinemann, Oxford, Chapter 13, p. 711-782, 2006
 66. Deville, Saint-Claire, *Mémoire sur la production des températures très-élevées*. Annales de chimie et de physique, Vol. 46 (3), 1856
 67. Ebelman, M., *Mémoire sur une nouvelle méthode pour obtenir des combinaisons cristallisées par la voie sèche, et sur ses applications à la reproduction des espèces minérales*, Annales de chimie et de physique, Vol. 22 (3), 1848
 68. Bensted, J., *The Development and Usage of High Alumina Cement*, The Institute of Concrete Technology, 2003
 69. Bied, J., *French Patent 320290 and 391454*, France, 1908
 70. Bied, J., *British Patent 8193*, United Kingdom, 1909
 71. *Secar Range*, Editor,
http://www.secar.net/IMG/pdf/SecarRange_05032010_BD.pdf
 72. Edmonds, R. N. and Majumdar, A. J., *The hydration of monocalcium aluminate at different temperatures*, Cement and Concrete Research, Vol. 18 (2), p. 311-320, 1988

73. Rodger, S. A. and Double, D. D., *The chemistry of hydration of high alumina cement in the presence of accelerating and retarding admixtures*, Cement and Concrete Research, Vol. 14 (1), p. 73-82, 1984
74. Edmonds, R. N. and Majumdar, A. J., *The hydration of mixtures of monocalcium aluminate and blastfurnace slag*, Cement and Concrete Research, Vol. 19 (5), p. 779-782, 1989
75. Bradbury, C., Callaway, P. M., and Double, D. D., *The conversion of high alumina cement/concrete*, Materials Science and Engineering, Vol. 23 (1), p. 43-53, 1976
76. Scrivener, Karen L., Cabiron, Jean-Louis, and Letourneux, Roger, *High-performance concretes from calcium aluminate cements*, Cement and Concrete Research, Vol. 29 (8), p. 1215-1223, 1999
77. Ramachandran, V. S. and Feldman, R. F., *Hydration characteristics of monocalcium aluminate at a low water/solid ratio*, Cement and Concrete Research, Vol. 3 (6), p. 729-750, 1973
78. Majumdar, A. J., Singh, B., and Edmonds, R. N., *Hydration of mixtures of 'Ciment Fondu' aluminous cement and granulated blast furnace slag*, Cement and Concrete Research, Vol. 20 (2), p. 197-208, 1990
79. Majumdar, A. J., Edmonds, R. N., and Singh, B., *Hydration of Secar 71 aluminous cement in presence of granulated blast furnace slag*, Cement and Concrete Research, Vol. 20 (1), p. 7-14, 1990
80. Majumdar, A. J. and Singh, B., *Properties of some blended high-alumina cements*, Cement and Concrete Research, Vol. 22 (6), p. 1101-1114, 1992
81. Ramachandran, V. S., Paroli, Ralph M., Beaudoin, James J., and Delgado, Ana H., *Introduction to Non-Portland Cement Binders and Concrete*, in *Handbook of Thermal Analysis of Construction Materials*, William Andrew Publishing, Norwich, NY, Chapter 9, p. 355-402, 2002
82. Chotard, T. J., Smith, A., Rotureau, D., Fargeot, D., and Gault, C., *Acoustic emission characterisation of calcium aluminate cement hydration at an early stage*, Journal of the European Ceramic Society, Vol. 23 (3), p. 387-398, 2003
83. Rettel, A., Seydel, R., Gessner, W., Bayoux, J. P., and Capmas, A., *Investigations on the influence of alumina on the hydration of monocalcium aluminate at different temperatures*, Cement and Concrete Research, Vol. 23 (5), p. 1056-1064, 1993
84. Bushnell-Watson, S. M. and Sharp, J. H., *The application of thermal analysis to the hydration and conversion reactions of calcium aluminate cements*, Materiales de Construcción, Vol. 42 (228), p. 13-32, 1992
85. Majumdar, A. J., Edmonds, R. N., and Singh, B., *Hydration of calcium aluminates in presence of granulated blastfurnace slag*, in *Calcium Aluminate Cements*, Mangabhai, R. J., Chapman and Hall, London, 259-271, 1990
86. Sugama, T., Carciello, N. R., and Gray, G., *Alkali carbonation of calcium aluminate cements: influence of set-retarding admixtures under hydrothermal conditions*, Journal of Materials Science, Vol. 27 (18), p. 4909-4916, 1992
87. Sugama, T., *Citric acid as a set retarder for calcium aluminate phosphate cements*, Advances in Cement Research, Vol. 18 (2), p. 47-57, 2006
88. Csetenyi, L. J. and Glasser, F. P., *Borate retardation of cement set and phase relations in the system $\text{Na}_2\text{O}-\text{CaO}-\text{B}_2\text{O}_3-\text{H}_2\text{O}$* , Advances in Cement Research, Vol. 7 (25), p. 13-19, 1995

89. Fryda, H., Vetter, G., Ollitrault-Fichet, R., Boch, P., and Capmas, A., *Formation of chabazite and silica in mixes of calcium aluminate cement and silica fume used for caesium immobilization*, *Advances in Cement Research*, Vol. 8 (29), p. 29-39, 1996
90. Wilson, A. D., *The Chemistry of Dental Cements*, *Chemical Society Reviews*, Vol. 7 (2), p. 265-296, 1978
91. Wilson, A. D. and Nicholson, J. W., *Introduction*, in *Acid-base cements: their biomedical and industrial applications*, Press Syndicate of the University of Cambridge, Cambridge, Chapter 1, p. 1-4, 1993
92. Wilson, Alan D., Paddon, John M., and Crisp, Stephen, *The Hydration of Dental Cements*, *Journal of Dental Research*, Vol. 58 (3), p. 1065-1071, 1979
93. Wilson, A. D. and Nicholson, J. W., *Theory of acid-base cements*, in *Acid-base cements: their biomedical and industrial applications*, Press Syndicate of the University of Cambridge, Cambridge, Chapter 2, p. 5-29, 1993
94. Wagh, A. S., *Introduction to Chemically Bonded Ceramics*, in *Chemically Bonded Phosphate Ceramics: 21st Century Materials with Diverse Applications*, Elsevier Ltd, Oxford, Chapter 1, p. 1-13, 2004
95. Roy, Della M., *New Strong Cement Materials: Chemically Bonded Ceramics*, *Science*, Vol. 235 (4789), p. 651-658, 1987
96. Simonton, Thomas C., Roy, Rustum, Komarneni, Sridhar, and Breval, Else, *Microstructure and mechanical properties of synthetic opal: A chemically bonded ceramic*, *Journal of Materials Research*, Vol. 1 (05), p. 667-674, 1986
97. Wagh, A. S., *Chemically Bonded Phosphate Ceramics*, in *Chemically Bonded Phosphate Ceramics: 21st Century Materials with Diverse Applications*, 1st edition, Elsevier Ltd, Oxford, Chapter 2, p. 15-27, 2004
98. Kingery, W. D., *Fundamental Study of Phosphate Bonding in Refractories: I, Literature Review*, *Journal of the American Ceramic Society*, Vol. 33 (8), p. 239-241, 1950
99. Kingery, W. D., *Fundamental Study of Phosphate Bonding in Refractories: II, Cold-Setting Properties*, *Journal of the American Ceramic Society*, Vol. 33 (8), p. 242-246, 1950
100. Westman, A. E. R., *Phosphate Ceramics*, in *Topics in Phosphorus Chemistry*, Vol. 9, 1977
101. Hench, L. L., Splinter, R. J., Allen, W. C., and Greenlee, T. K., *Bonding mechanisms at the interface of ceramic prosthetic materials*, *Journal of Biomedical Materials Research*, Vol. 5 (6), p. 117-141, 1971
102. Zurz, I. and Odler, I. *Investigations on Phosphate Cements Hardening at Room Temperature*, in *Specialty Cements with Advanced Properties*, Pittsburgh, 1990
103. Sugama, T. and Kukacka, L. E., *Characteristics of magnesium polyphosphate cements derived from ammonium polyphosphate solutions*, *Cement and Concrete Research*, Vol. 13 (4), p. 499-506, 1983
104. Sugama, T. and Kukacka, L. E., *Magnesium monophosphate cements derived from diammonium phosphate solutions*, *Cement and Concrete Research*, Vol. 13 (3), p. 407-416, 1983
105. Abdelrazig, B. E. I., Sharp, J. H., and El-Jazairi, B., *The chemical composition of mortars made from magnesia-phosphate cement*, *Cement and Concrete Research*, Vol. 18 (3), p. 415-425, 1988
106. Xing, F., Ding, Z., and Li, Z. J., *Study of potassium-based magnesium phosphate cement*, *Advances in Cement Research*, Vol. 23 (2), p. 81-87, 2011

107. Walter, D. and Odler, I., *Investigation of MgO and CaO/Al₂O₃ polyphosphate cements*, Advances in Cement Research, Vol. 8 (29), p. 41-46, 1996
108. Whitaker, A., *The decomposition of struvite*, Mineralogical Magazine, Vol. 36 p. 820-824, 1967
109. Wagh, A. S. and Jeong, S. Y., *Chemically Bonded Phosphate Ceramics: I, A Dissolution Model of Formation*, Journal of the American Ceramic Society, Vol. 86 (11), p. 1838-1844, 2003
110. Zhang, S., Shi, H., Huang, S., and Zhang, P., *Dehydration characteristics of struvite-K pertaining to magnesium potassium phosphate cement system in non-isothermal condition*, Journal of Thermal Analysis and Calorimetry, Vol. 111, p. 35-40, 2013
111. Brown, W. E. and Chow, L. C., *A New Calcium Phosphate, Water-setting Cement*, in *Cements Research Progress*, Brown, P. W., The American Ceramics Society, Westerville, p. 351-379, 1986
112. LeGeros, R. Z., Chohayeb, A., and Shulman, A., *Apatitic calcium phosphates: Possible restorative materials*, Journal of Dental Research (Special Issue), Vol. 61 1982
113. LeGeros, R. Z., *Calcium Phosphate Materials in Restorative Dentistry: A Review*, Advances in Dental Research, Vol. 2 (1), p. 164-180, 1988
114. Chow, L. C. and Takagi, S., *Calcium Phosphate Cements*, in *Cement Research Progress 1994*, Strubble, L. J., The American Ceramics Society, Westerville, Chapter 8, p. 189-201, 1996
115. Fukase, Y., Eanes, E. D., Takagi, S., Chow, L. C., and Brown, W. E., *Setting Reactions and Compressive Strengths of Calcium Phosphate Cements*, Journal of Dental Research, Vol. 69 (12), p. 1852-1856, 1990
116. Chow, L. C., *Development of Self-Setting Calcium Phosphate Cements*, Journal of the Ceramics Society of Japan, Vol. 99 (10), 1991
117. Liu, C., Shen, W., and Chen, J., *Solution property of calcium phosphate cement hardening body*, Materials Chemistry and Physics, Vol. 58 (1), p. 78-82, 1999
118. Chow, L. C., *Calcium Phosphate Cements: Chemistry, Properties, and Applications*, Materials Research Society Symposium Proceedings, Vol. 599 p. 11, 2000
119. Ginebra, M.P., Fernández, E., De Maeyer, E.A.P., Verbeeck, R.M.H., Boltong, M.G., Ginebra, J., Driessens, F.C.M., and Planell, J.A., *Setting Reaction and Hardening of an Apatitic Calcium Phosphate Cement*. Journal of Dental Research, Vol. 76 (4), p. 905-912, 1997
120. Brown, P. W. and Fulmer, M., *Kinetics of Hydroxyapatite Formation at Low Temperature*, Journal of the American Ceramic Society, Vol. 74 (5), p. 934-940, 1991
121. Fulmer, M.T. and Brown, P.W., *Effects of temperature on the formation of hydroxyapatite*, Journal of Materials Research, Vol. 8 (07), p. 1687-1696, 1993
122. Martin, R. I. and Brown, P. W., *Mechanical properties of hydroxyapatite formed at physiological temperature*, Journal of Materials Science: Materials in Medicine, Vol. 6 (3), p. 138-143, 1995
123. Combes, C. and Rey, C., *Amorphous calcium phosphates: synthesis, properties and uses in biomaterials*, Acta Biomaterialia, Vol. 6 (9), p. 3362-3378, 2010

124. Dorozhkin, Sergey, *Calcium Orthophosphates in Nature, Biology and Medicine*, Materials, Vol. 2 (2), p. 399-498, 2009
125. Dorozhkin, S. V., *Amorphous calcium (ortho)phosphates*, Acta Biomaterialia, Vol. 6 (12), p. 4457-4475, 2010
126. Rakovan, J., Reeder, R. J., Elzinga, E. J., Cherniak, D. J., Tait, C. D., and Morris, D. E., *Structural Characterization of U(VI) in Apatite by X-ray Absorption Spectroscopy*, Environmental Science & Technology, Vol. 36 (14), p. 3114-3117, 2002
127. Elliot, J. C., *Preface*, in *Structure and Chemistry of the Apatites and Other Calcium Orthophosphates*, Elsevier Science B.V., Amsterdam, 1994
128. Elliot, J. C., *Hydroxyapatite and Nonstoichiometric Apatites*, in *Structure and Chemistry of the Apatites and Other Calcium Orthophosphates*, Elsevier Science B.V., Amsterdam, Chapter 3, p. 111-189, 1994
129. Domínguez, M. I., Carpena, J., Borschnek, D., Centeno, M. A., Odriozola, J. A., and Rose, J., *Apatite and Portland/apatite composite cements obtained using a hydrothermal method for retaining heavy metals*, Journal of Hazardous Materials, Vol. 150 (1), p. 99-108, 2008
130. Sugiyama, S., Tanimoto, S., Fukuda, K., Kawashiro, K., Tomida, T., and Hayashi, H., *Immobilization of aqueous tetravalent cations of titanium and zirconium with calcium hydroxyapatite*, Colloids and Surfaces A: Physicochemical and Engineering Aspects, Vol. 252 (2-3), p. 187-192, 2005
131. Sugama, T., *Hot Alkali Carbonation of Sodium Metaphosphate Modified Fly Ash/Calcium Aluminate Blend Hydrothermal Cements*, Cement and Concrete Research, Vol. 26 (11), p. 1661-1672, 1996
132. Sugama, T., Brothers, L. E., and Kaspereit, D., *Sodium Polyphosphate-Modified Class C/Class F Fly Ash Blend Cements for Geothermal Wells*, Brookhaven National Laboratory, BNL-75530-2006-IR, 2006
133. Sugama, T., Weber, L., and Brothers, L. E., *Sodium-polyphosphate-modified fly ash/calcium aluminate blend cement: durability in wet, harsh geothermal environments*, Materials Letters, Vol. 44 (1), p. 45-53, 2000
134. Sugama, T., Allan, M., and Hill, J. M., *Calcium Phosphate Cements Prepared by Acid-Base Reaction*, Journal of the American Ceramic Society, Vol. 75 (8), p. 2076-2087, 1992
135. Sugama, T. and Carciello, N. R., *Strength Development in Phosphate-Bonded Calcium Aluminate Cements*, Journal of the American Ceramic Society, Vol. 74 (5), p. 1023-1030, 1991
136. Sugama, T. and Carciello, N. R., *Carbonation of Hydrothermally Treated Phosphate-Bonded Calcium Aluminate Cements*, Cement and Concrete Research, Vol. 22 (5), p. 783-792, 1992
137. Sugama, T. and Carciello, N. R., *Carbonation of Calcium Phosphate Cements After Long-term Exposure to Na₂CO₃-laden Water at 250°C*, Cement and Concrete Research, Vol. 23 (6), p. 1409-1417, 1993
138. Sugama, T. and Carciello, N. R., *Sodium phosphate-derived calcium phosphate cements*, Cement and Concrete Research, Vol. 25 (1), p. 91-101, 1995
139. Sugama, T., Carciello, N. R., Nayberg, T. M., Unocal, and Brothers, L. E., *Mullite microsphere-filled lightweight calcium phosphate cement slurries for geothermal wells: Setting and properties*, Cement and Concrete Research, Vol. 25 (6), p. 1305-1310, 1995

140. Sugama, T. and Wetzel, E., *Microsphere-filled lightweight calcium phosphate cements*, Journal of Materials Science, Vol. 29 (19), p. 5165-5176, 1994
141. Sugama, T., Brothers, L. E., and de Putte, T. R. Van, *Air-foamed calcium aluminate phosphate cement for geothermal wells*, Cement and Concrete Composites, Vol. 27 (7–8), p. 758-768, 2005
142. Sugama, T. and Taylor, M., *Interfacial and mechanical behavior of fiber-reinforced calcium phosphate cement composites*, Cement and Concrete Composites, Vol. 16 (2), p. 93-106, 1994
143. Ma, W. and Brown, P. W., *Mechanical behavior and microstructural development in phosphate modified high alumina cement*, Cement and Concrete Research, Vol. 22 (6), p. 1192-1200, 1992
144. Ma, W. and Brown, P. W., *Hydration of sodium phosphate-modified high alumina cement*, Journal of Materials Research, Vol. 9 (5), 1994
145. Sugama, T., Weber, L., and Brothers, L. E., *Resistance of sodium polyphosphate-modified fly ash/calcium aluminate blend cements to hot H₂SO₄ solution*, Cement and Concrete Research, Vol. 29 (12), p. 1969-1976, 1999
146. Sugama, T., Brothers, L. E., and Weber, L., *Calcium aluminate cements in fly ash/calcium aluminate blend phosphate cement systems: Their role in inhibiting carbonation and acid corrosion at a low hydrothermal temperature of 90°C* Journal of Materials Science, Vol. 37 (15), p. 3163-3173, 2002
147. Blezard, R. G., *The History of Calcareous Cements*, in *Lea's Chemistry of Cement and Concrete*, 4th edition, ed. Hewlett, P. C., Butterworth-Heinemann, Oxford, Chapter 1, p. 1-23, 2006
148. Lee, S. H., Kim, H. J., Sakai, E., and Daimon, M., *Effect of particle size distribution of fly ash-cement system on the fluidity of cement pastes*. Cement and Concrete Research, Vol. 33 (5), p. 763-768, 2003
149. Megat Johari, M. A., Brooks, J. J., Kabir, Shahid, and Rivard, Patrice, *Influence of supplementary cementitious materials on engineering properties of high strength concrete*, Construction and Building Materials, Vol. 25 (5), p. 2639-2648, 2011
150. Washburn, E. W., *The Dynamics of Capillary Flow*, The Physical Review, Vol. 17 (3), p. 11, 1921
151. West, A. R., *Crystallography and Diffraction Techniques*, in *Basic Solid State Chemistry*, 2nd edition, John Wiley & Sons Ltd, Chichester, Chapter 3, 2006
152. West, A. R., *Crystal Structures*, in *Basic Solid State Chemistry*, 2nd edition, John Wiley & Sons, Chichester, Chapter 1, 2006
153. Callister, W. D., *The structure of Crystalline Solids*, in *Materials Science and Engineering An Introduction*, 6th edition, John Wiley & Sons Inc, Hoboken, Chapter 3, 2003
154. *X-ray reflection in accordance with Bragg's Law*, 09/02/2013, Available from: http://serc.carleton.edu/research_education/geochemsheets/BraggsLaw.html, 2013
155. Richardson, I. G., *Electron microscopy of cement*, in *Structure and Performance of Cements*, Bensted, J. and Barnes, P., Spon Press, London, Chapter 22 , p. 500-556, 2002
156. Provis, J. L., *Email communication*, 2013

157. Shannon, R., *Revised effective ionic radii and systematic studies of interatomic distances in halides and chalcogenides*, Acta Crystallographica Section A, Vol. 32 (5), p. 751-767, 1976
158. Kojima, Y., Sakama, K., Toyama, T., Yasue, T., and Arai, Y., *Dehydration of Water Molecule in Amorphous Calcium Phosphate*, Phosphorous Research Bulletin, Vol. 4, p. 47-52, 1994
159. Massazza, F., *Pozzolana and Pozzolanic Cements*, in *Lea's Chemistry of Cement and Concrete*, ed. Hewlett, P. C., Butterworth-Heinemann, Oxford, Chapter 10, p. 471-635, 2006
160. Marar, K. and Eren, O., *Effect of cement content and water/cement ratio on fresh concrete properties without admixtures*, International Journal of the Physical Sciences, Vol. 6 (24), p. 5752-5765, 2011
161. Chatterjee, A. K., *Special cements*, in *Structures and Performance of Cements*, ed. Bensted, J. and P, B., Spon Press, London, Chapter 6, 2002
162. Swift, P., Kinoshita, H., Collier, N. C., and Utton, C. A., *Phosphate-modified calcium aluminate cement for radioactive waste encapsulation*, Advances in Applied Ceramics, Vol. 112 (1), p. 1-8, 2013
163. Diamond, S., *Mercury porosimetry: An inappropriate method for the measurement of pore size distributions in cement-based materials*, Cement and Concrete Research, Vol. 30 (10), p. 1517-1525, 2000
164. Jiang, L. and Guan, Y., *Pore structure and its effect on strength of high-volume fly ash paste*, Cement and Concrete Research, Vol. 29 (4), p. 631-633, 1999
165. Zeng, Q., Li, K., Fen-chong, T., and Dangla, P., *Pore structure characterization of cement pastes blended with high-volume fly-ash*. Cement and Concrete Research, Vol. 42 (1), p. 194-204, 2012
166. Kinoshita, H., Swift, P., Utton, C. A., Carro-Mateo, B., Marchand, G., Collier, N. C., and Milestone, N. B., *Corrosion of aluminium metal in OPC- and CAC-based cement matrices*, Cement and Concrete Research, Vol. 50, p. 11-18, 2013
167. Hoch, A. R., Smart, N. R., Wilson, J. D., and Reddy, B., *A Survey of Reactive Metal Corrosion Data for Use in the SMOGG Gas Generation Model*, Serco, SA/ENV-0895, 2010
168. Collier, N. C., *The Encapsulation of Iron Hydroxide FLoc in Composite Cement*, The University of Sheffield, Department of Engineering Materials, 2006
169. Vargel, C., *The Corrosion of Aluminium*, in *Corrosion of Aluminium*, Elsevier, Oxford, Chapter B.1, 2004
170. Vargel, C., *Types of Corrosion on Aluminium*, in *Corrosion of Aluminium*, Elsevier, Oxford, Chapter B.2, 2004
171. Wilson, A. D. and Nicholson, J. W., *Water and acid-base cements*, in *Acid-base cements: their biomedical and industrial applications*, Press Syndicate of the University of Cambridge, Cambridge, Chapter 3, p. 30-55, 1993
172. Armstrong, R. D. and Braham, V. J., *The mechanism of aluminium corrosion in alkaline solutions*. Corrosion Science, Vol. 38 (9), p. 1463-1471, 1996
173. Moon, S. M. and Pyun, S. I., *The corrosion of pure aluminium during cathodic polarization in aqueous solutions*, Corrosion Science, Vol. 39 (2), p. 399-408, 1997
174. Sweegers, C., de Coninck, H. C., Meekes, H., van Enkevort, W. J. P., Hiralal, I. D. K., and Rijkeboer, A., *Morphology, evolution and other*

- characteristics of gibbsite crystals grown from pure and impure aqueous sodium aluminate solutions*, Journal of Crystal Growth, Vol. 233 (3), p. 567-582, 2001
175. Edmonds, R. N. and Majumdar, A. J., *The hydration of Secar 71 aluminous cement at different temperatures*, Cement and Concrete Research, Vol. 19 (2), p. 289-294, 1989
176. Boskey, A. L. and Posner, A. S., *Conversion of amorphous calcium phosphate to microcrystalline hydroxyapatite, A pH-dependent, solution-mediated, solid-solid conversion*. The Journal of Physical Chemistry, Vol. 77 (19), p. 2313-2317, 1973
177. Baerlocher, C., McCusker, L. B., and Olson, D. H., *Atlas of Zeolite Framework Types*, 6th edition, Oxford, Elsevier, 2007
178. Treacy, M. M. J. and Higgins, J. B., *Collection of Simulated XRD Powder Patterns for Zeolites*, Oxford, Elsevier, 2001
179. Sinyayev, V. A., Shustikova, E. S., Levchenko, L. V., and Sedunov, A. A., *Synthesis and Dehydration of Amorphous Calcium Phosphate*, Inorganic Materials, Vol. 37 (6), p. 619-622, 2001
180. Dosen, Anja and Giese, Rossmann F., *Thermal decomposition of brushite, CaHPO₄·2H₂O to monetite CaHPO₄ and the formation of an amorphous phase*, American Mineralogist, Vol. 96 (2-3), p. 368-373, 2011
181. Fiore, S. and Laviano, R., *Brushite, hydroxylapatite, and taranakite from Apulian caves (southern Italy): New mineralogical data*, American Mineralogist, Vol. 76, p. 1722-1727, 1991
182. Bakolas, A., Aggelakopoulou, E., Moropoulou, A., and Anagnostopoulou, S., *Evaluation of pozzolanic activity and physico-mechanical characteristics in metakaolin-lime pastes*, Journal of Thermal Analysis and Calorimetry, Vol. 84 (1), p. 157-163, 2006
183. Wallevik, Jon Elvar, *Rheological properties of cement paste: Thixotropic behavior and structural breakdown*, Cement and Concrete Research, Vol. 39 (1), p. 14-29, 2009
184. Wallevik, J. E., *The Particle Interaction Theory - Thixotropic Behaviour and Structural Breakdown*, in 36th Conference on Our World in Concrete & Structures, Singapore, 2011
185. Ding, J., Fu, Yan, and Beaudoin, J. J., *Strätlingite formation in high alumina cement - silica fume systems: Significance of sodium ions*, Cement and Concrete Research, Vol. 25 (6), p. 1311-1319, 1995
186. Collier, N. C., *Personal Communication*, 2011

Appendix 1 – XRD Data

Phase	Chemical Formula	ICDD* Card No.
CA	CaAl_2O_4	23-1036
C_2AS	$\text{Ca}_2\text{Al}_2\text{O}_7$	35-755
CT	CaTiO_3	22-153
Quartz	SiO_2	46-1045
Mullite	$\text{Al}_6\text{Si}_2\text{O}_{13}$	15-776
Hematite	Fe_2O_3	33-664
CAH_{10}	$\text{CaAl}_2\text{O}_4 \cdot 10\text{H}_2\text{O}$	12-408
C_2AH_8	$\text{Ca}_2\text{Al}_2\text{O}_5 \cdot 8\text{H}_2\text{O}$	45-564
C_3AH_6	$\text{Ca}_3\text{Al}_2\text{O}_6 \cdot 6\text{H}_2\text{O}$	76-557
AH_3	$\text{Al}(\text{OH})_3$	70-2038
C_2ASH_8	$\text{Ca}_2\text{Al}_2\text{SiO}_7 \cdot 8\text{H}_2\text{O}$	29-285
Hydroxyapatite	$\text{Ca}_5(\text{PO}_4)_3(\text{OH})$	84-1998, [1]
[Na] [Al-Si-O]-LTA	$\text{Na}_{12}\text{Al}_{12}\text{Si}_{12}\text{O}_{48} \cdot 27\text{H}_2\text{O}$	39-222, [2]

*International Centre for Diffraction Data

Appendix 1 References

1. Dorozhkin, S. V. , *Amorphous calcium (ortho)phosphates*. Acta Biomaterialia, Vol. 6 (12), p. 4457-4475, 2010
2. Treacy, M. M. J. and Higgins, J. B., *Collection of Simulated XRD Powder Patterns for Zeolites*, Oxford, Elsevier, 2001

Appendix 2 – TG Data

Phase	Weight loss mechanism	Temperature (°C)	Reference
Acetone	Evaporation	56	[1]
Water	Evaporation	100	[1]
C-A-H gel	Dehydration (loss of water)	60-130	[2]
CAH ₁₀	Dehydration (loss of water)	100-160	[2]
C ₂ AH ₈	Dehydration (loss of water)	140-200	[2]
		200	[3]
C ₂ ASH ₈	Dehydration (loss of water)	180-200	[4]
		230	[3]
AH ₃	Dehydration (loss of water)	260-330	[2]
C ₃ AH ₆	Dehydration (loss of water)	290-350	[2]
CaCO ₃	Decomposition (loss of CO ₂)	600-800	[5]

Appendix 2 References

1. *CRC Handbook of Chemistry and Physics*, 81st ed, 2000
2. Bushnell-Watson, S. M. and Sharp, J. H., *The application of thermal analysis to the hydration and conversion reactions of calcium aluminate cements*. *Materiales de Construcción*, Vol. 42 (228), p. 13-32, 1992
3. Nithya, R., *et al.*, *A Thermal Analysis Study on Blended Ternary Cement Paste*. *International Journal of Chemistry*, Vol. 2 (1), 2010
4. Bakolas, A., *et al.*, *Evaluation of pozzolanic activity and physicommechanical characteristics in metakaolin-lime pastes*. *Journal of Thermal Analysis and Calorimetry*, Vol. 84 (1), p. 157-163, 2006
5. Taylor, H. F. W., *Cement Chemistry*, Second Edition, London, Thomas Telford, 1997

Appendix 3 – Supporting SEM and EDX

SEM BEI of aluminium-cement interfaces

CAP 1

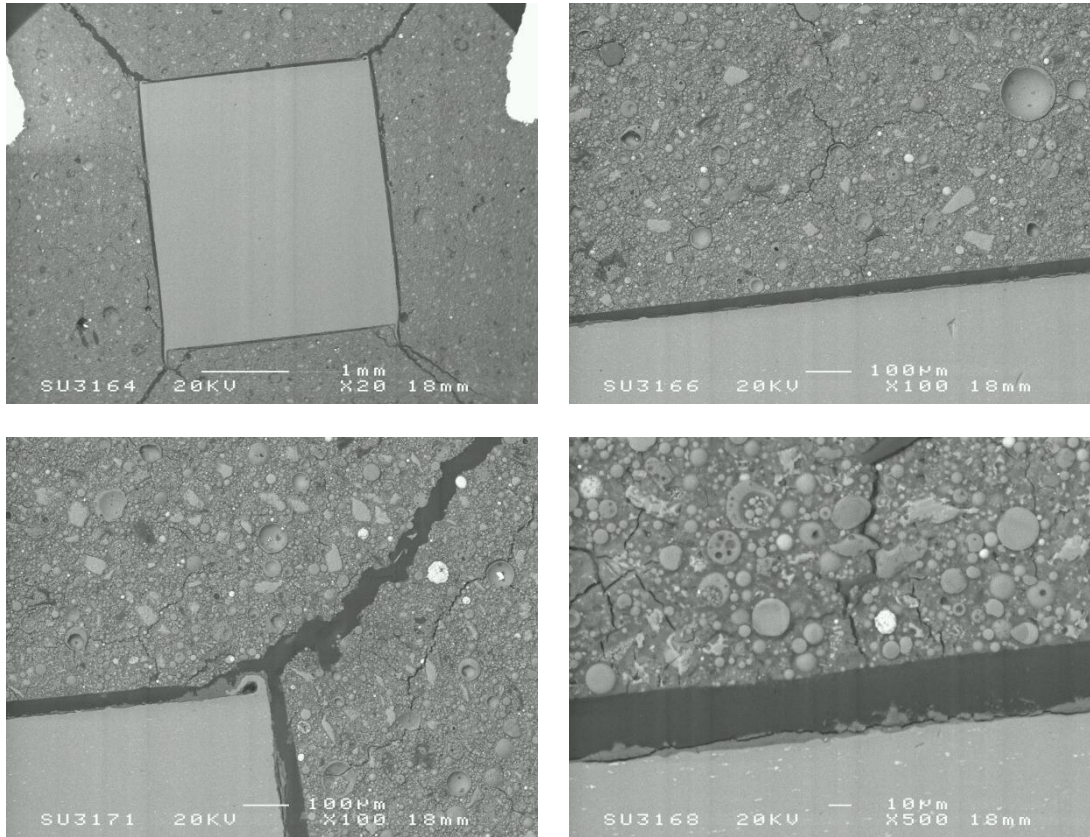


Figure A. 1 SEM BEI micrograph of aluminium encapsulated in CAP 1 for 28 days



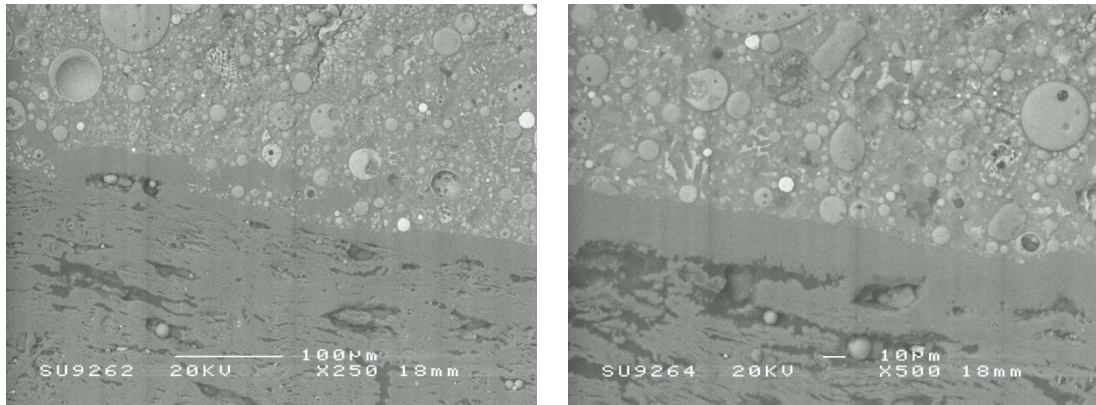


Figure A. 2 SEM BEI micrograph of aluminium encapsulated in CAP 1 for 180 days

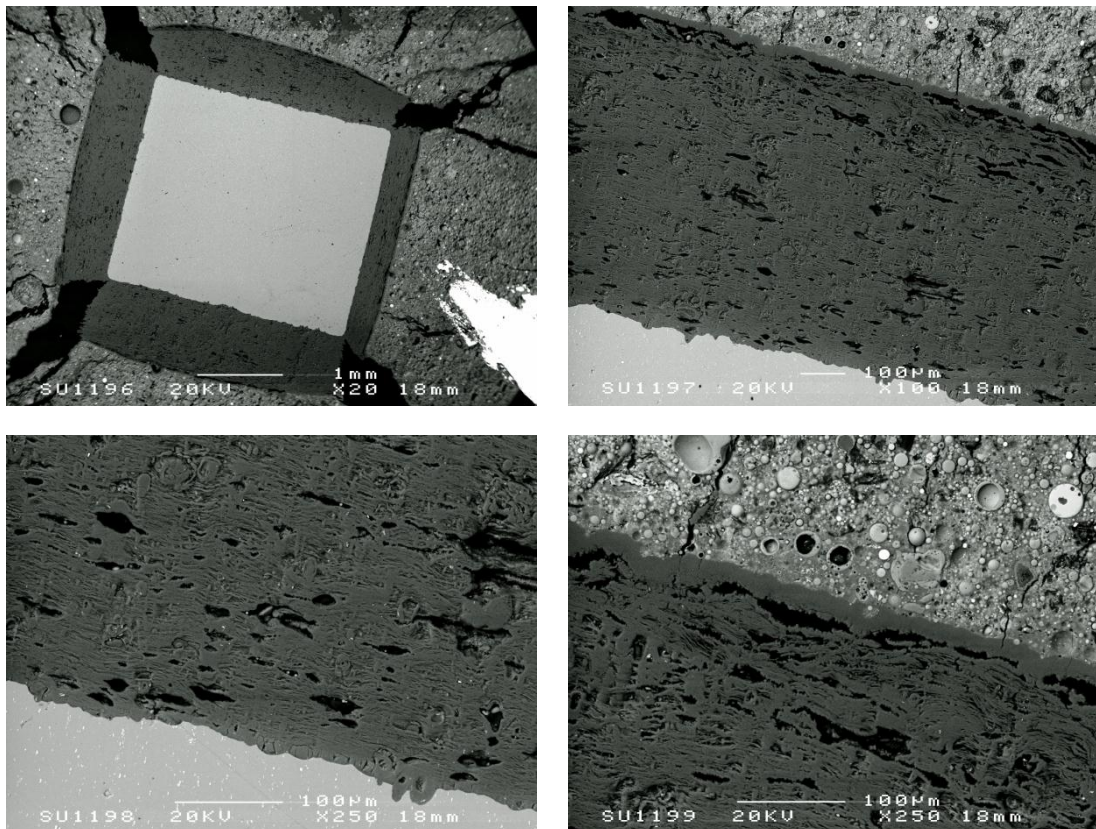


Figure A. 3 SEM BEI micrograph of aluminium encapsulated in CAP 1 for 360 days

CAP 2

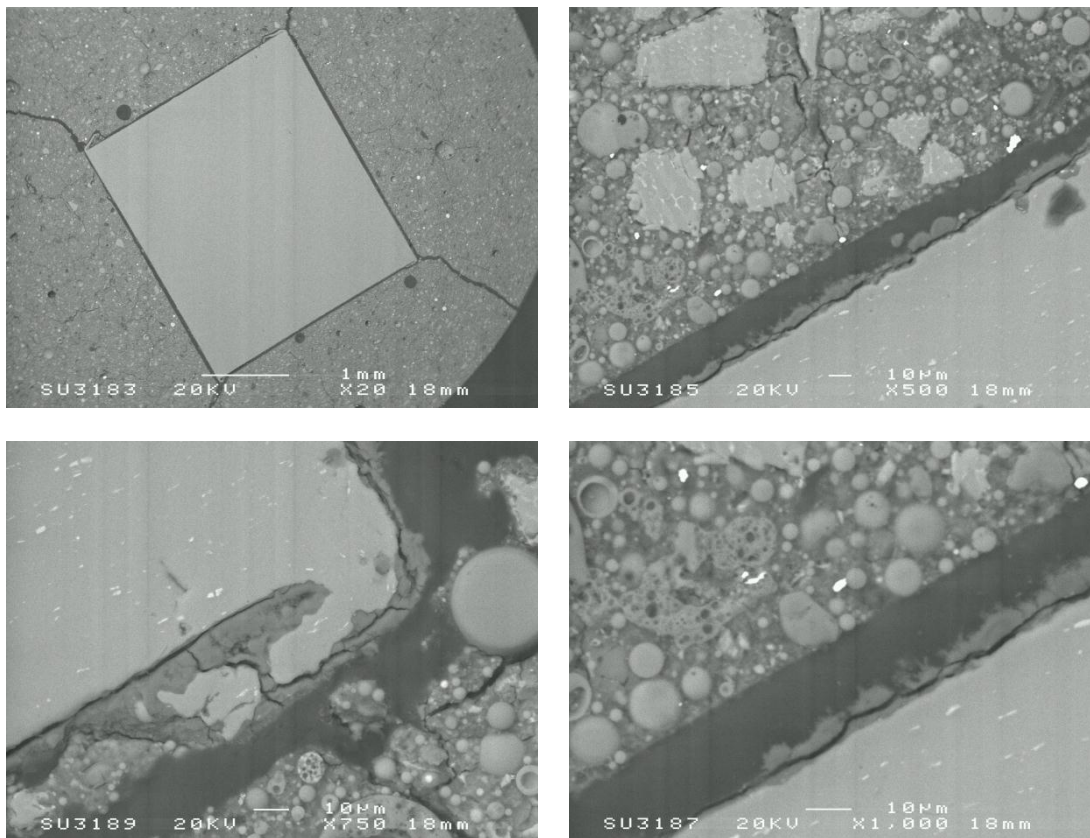


Figure A. 4 SEM BEI micrograph of aluminium encapsulated in CAP 2 for 28 days

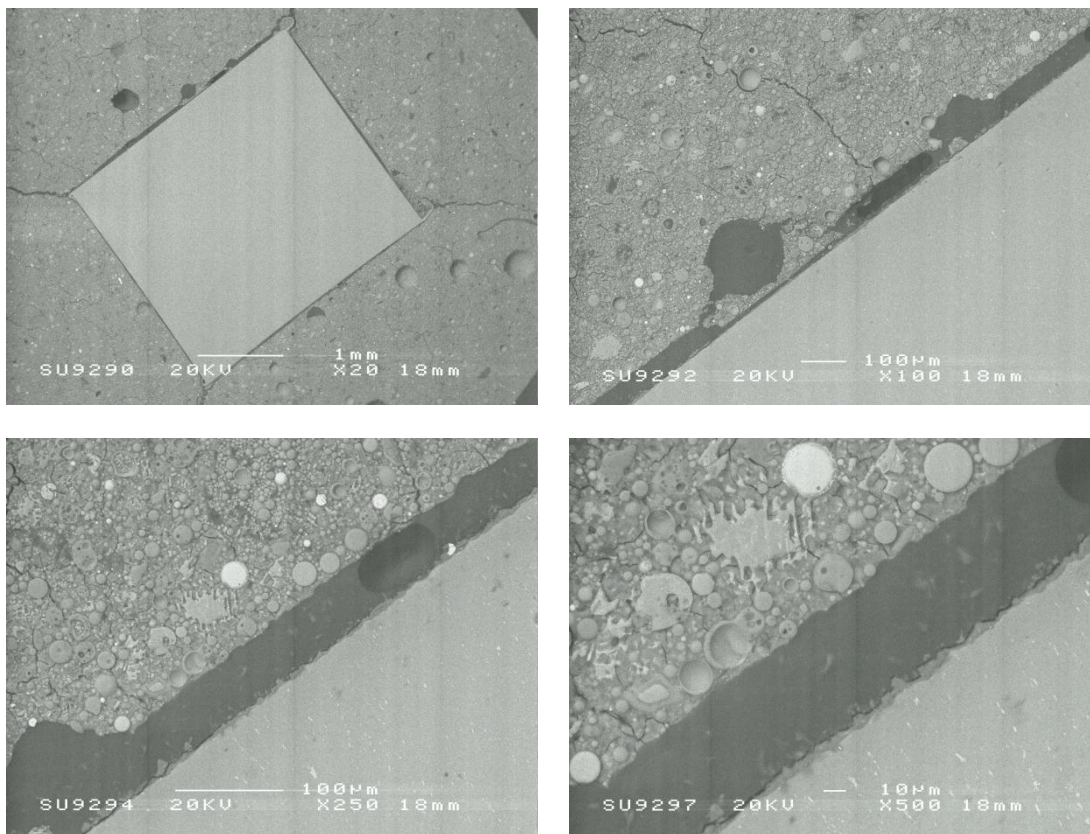


Figure A. 5 SEM BEI micrograph of aluminium encapsulated in CAP 2 for 180 days

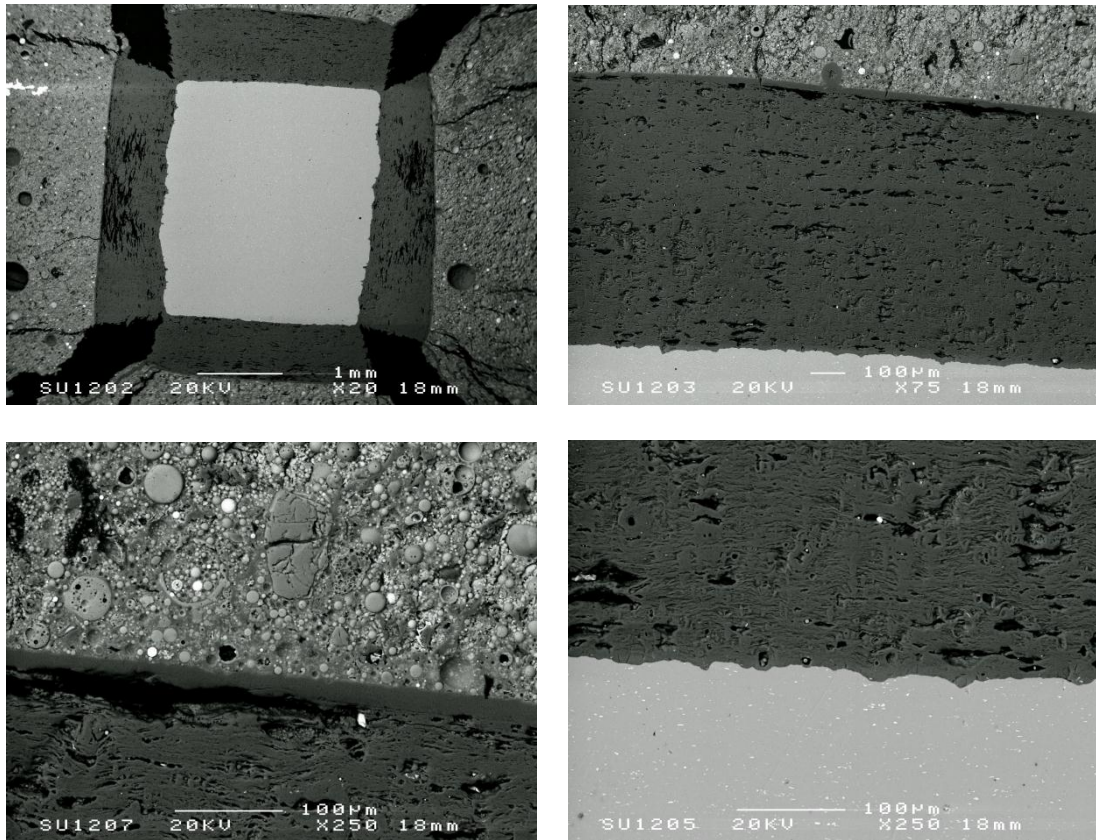


Figure A. 6 SEM BEI micrograph of aluminium encapsulated in CAP 2 for 360 days

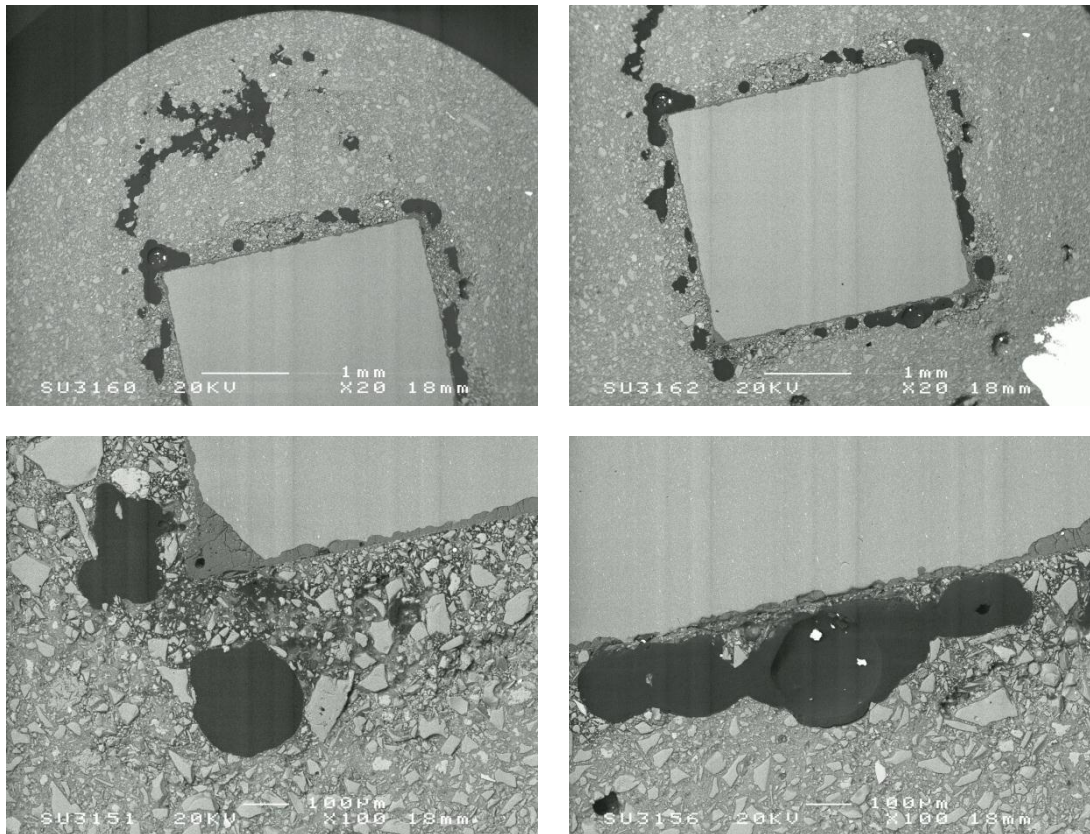
BFS/PC

Figure A. 7 SEM BEI micrograph of aluminium encapsulated in BFS:PC for 28 days

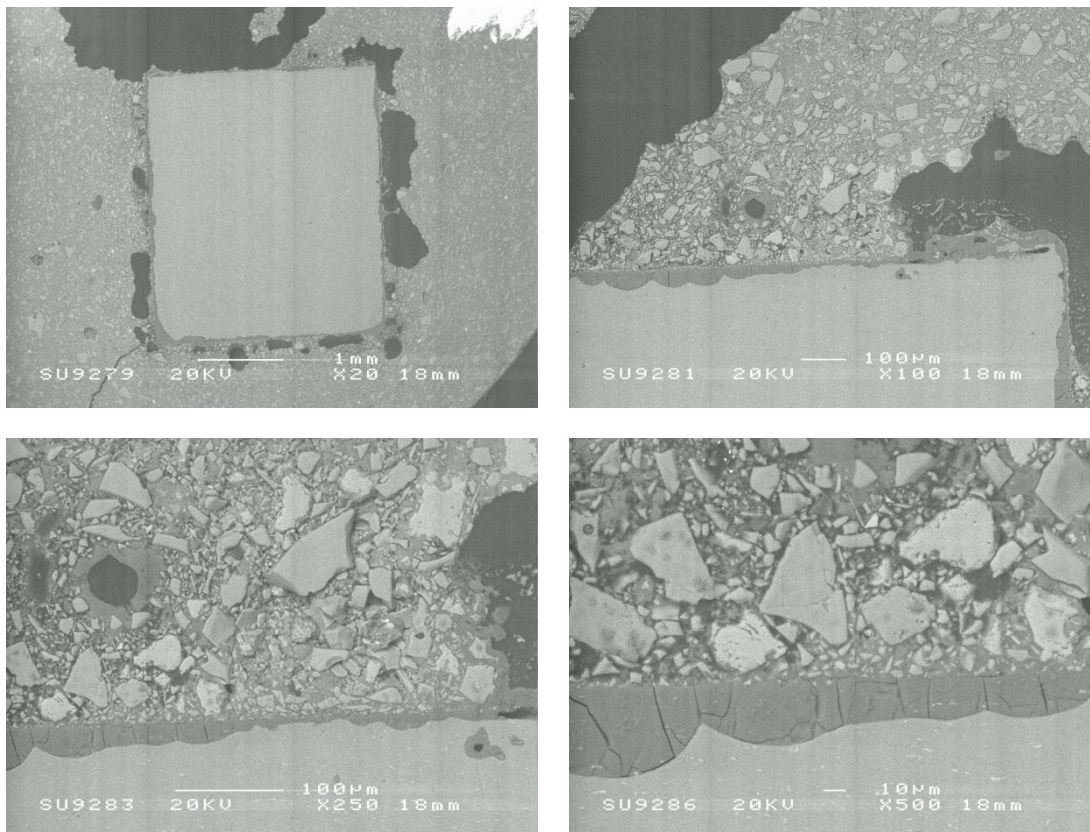


Figure A. 8 SEM BEI micrograph of aluminium encapsulated in BFS:PC for 180 days

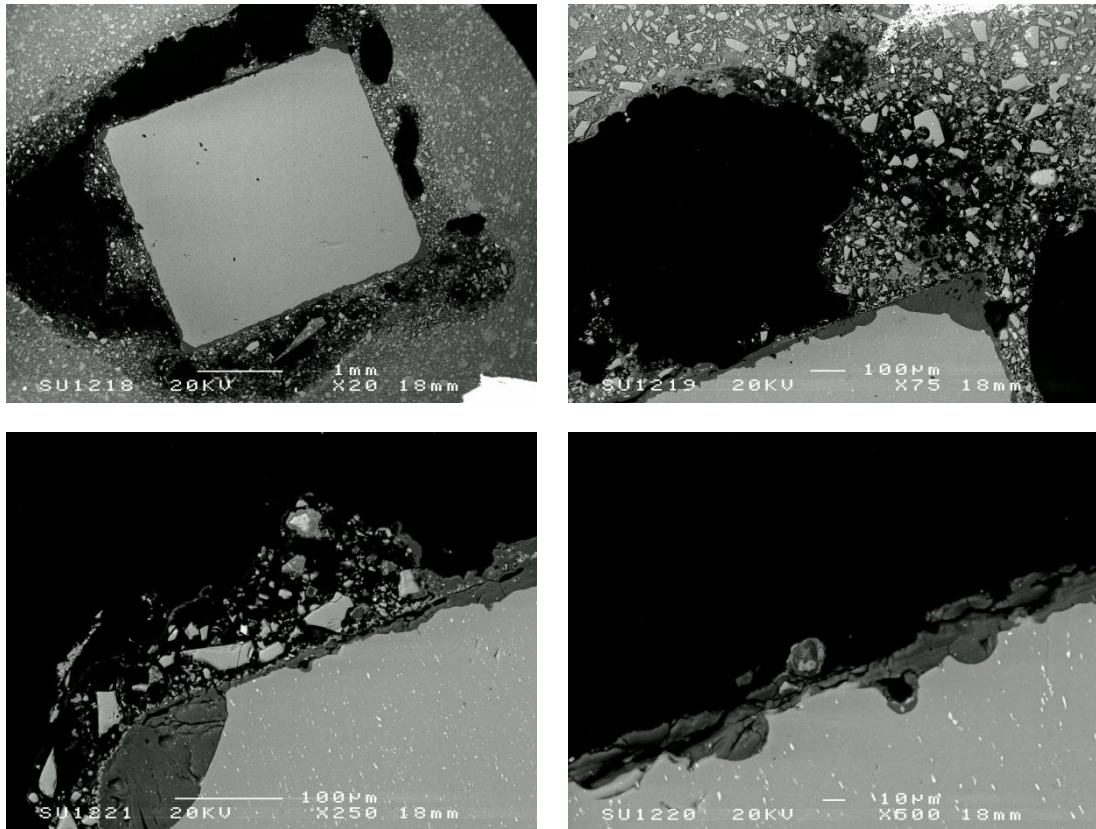


Figure A. 9 SEM BEI micrograph of aluminium encapsulated in BFS:PC for 360 days

PFA/CAC

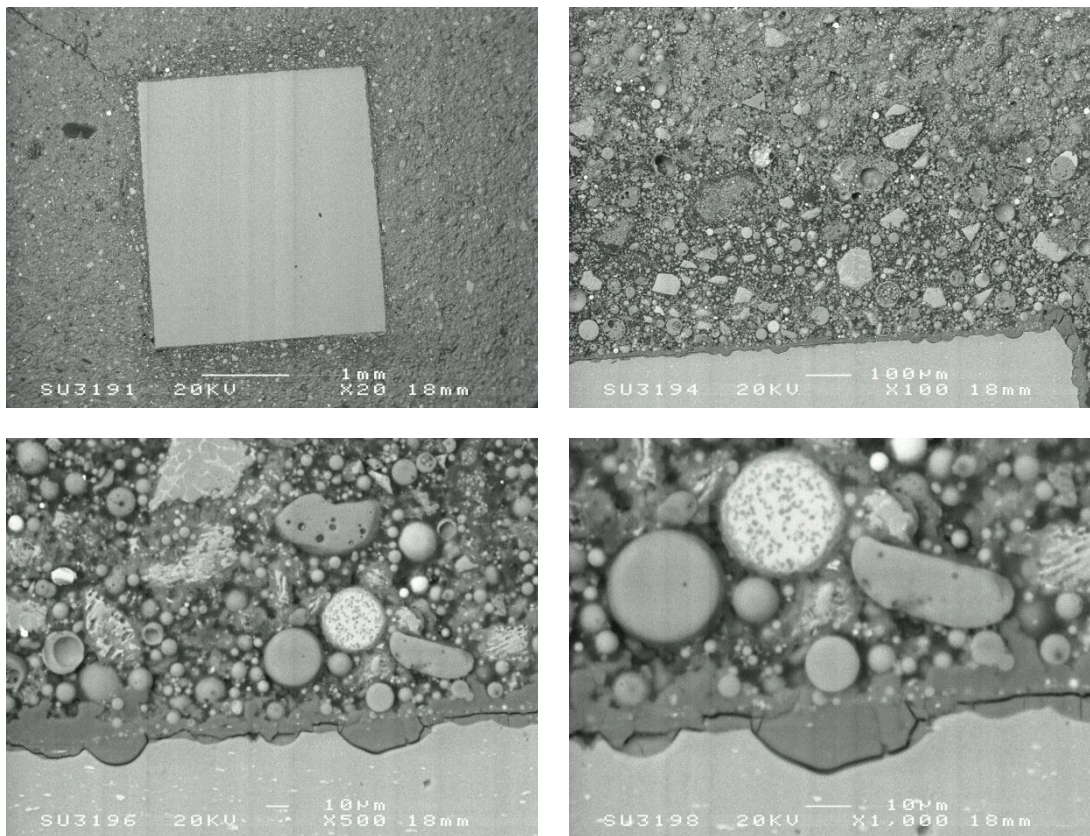


Figure A. 10 SEM BEI micrograph of aluminium encapsulated in PFA:CAC for 28 days

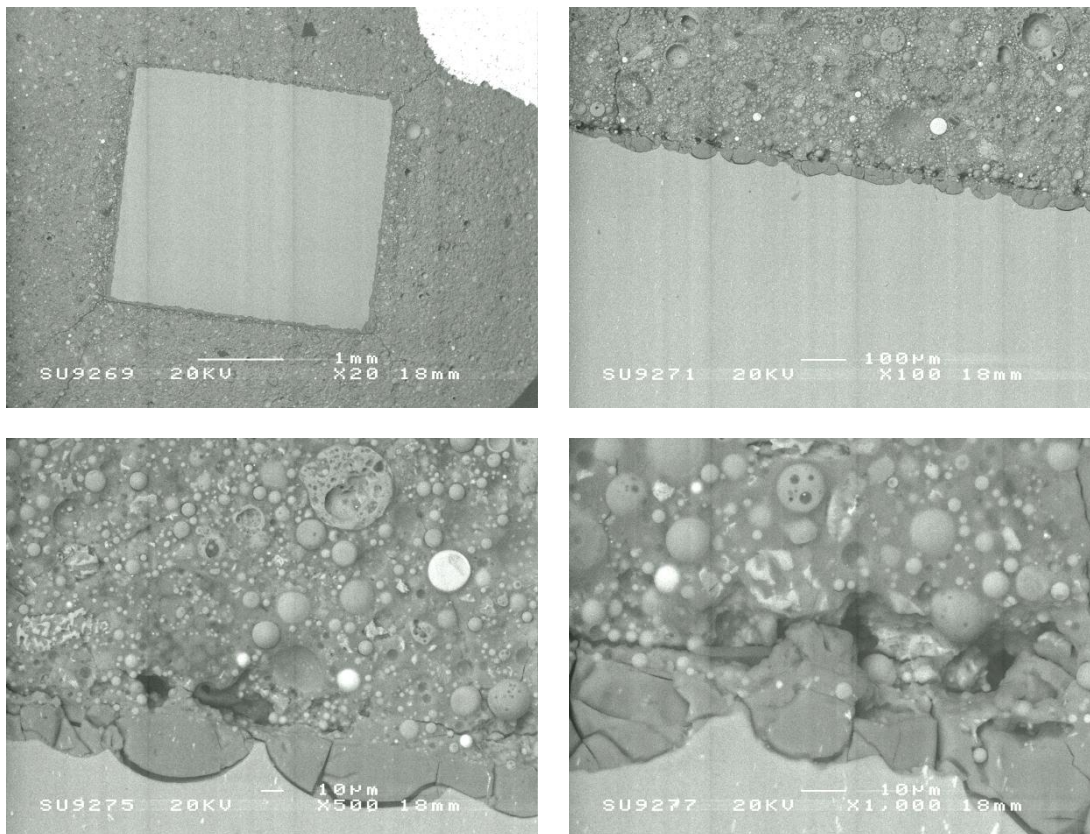


Figure A. 11 SEM BEI micrograph of aluminium encapsulated in PFA:CAC for 180 days

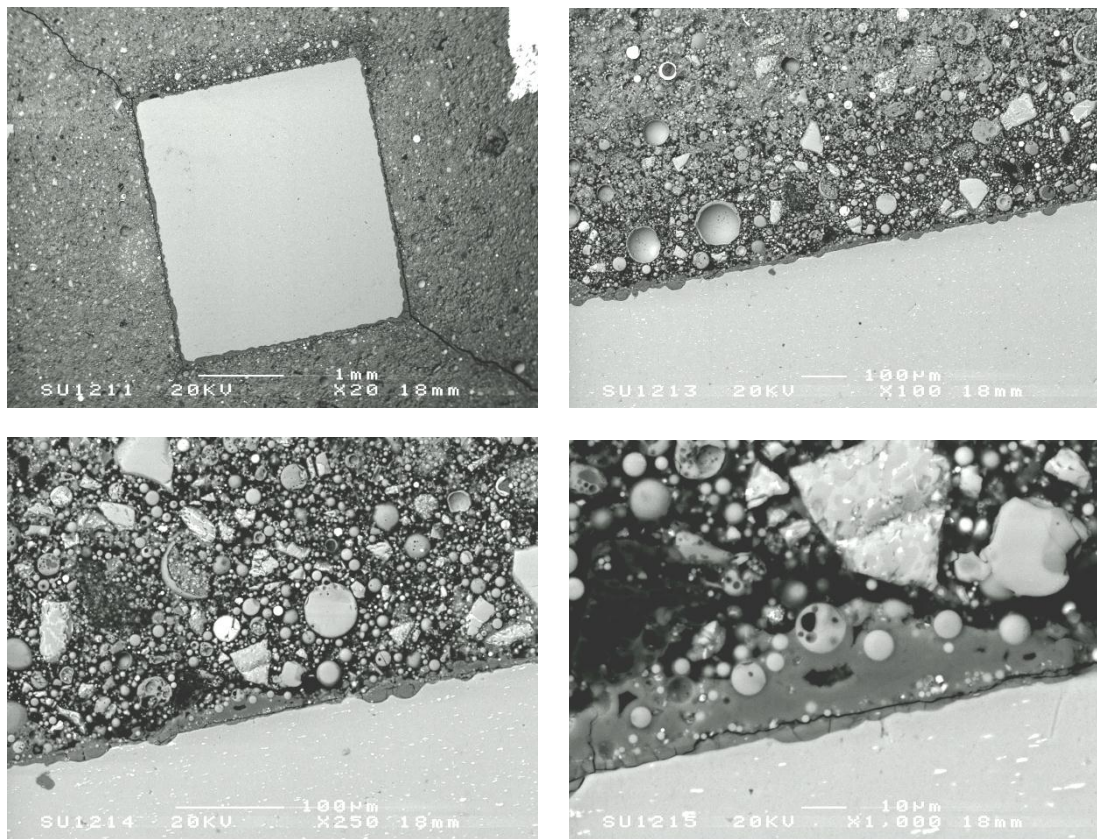


Figure A. 12 SEM BEI micrograph of aluminium encapsulated in PFA:CAC for 360 days

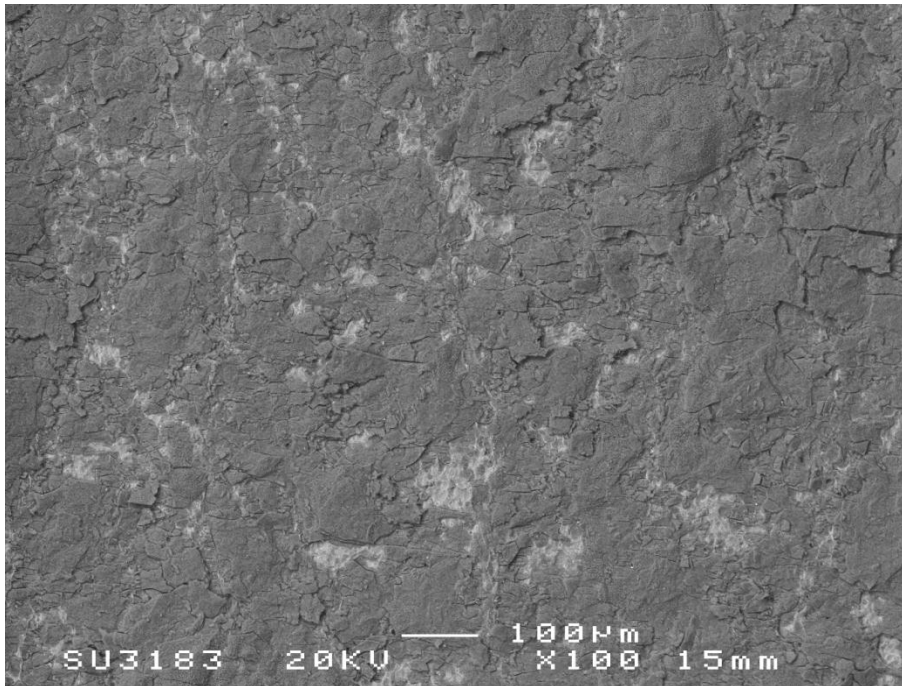
SEM BEI of aluminium corrosion layer

Figure A. 13 SEM BEI of the surface of aluminium encapsulated in CAP 1 for 90 days (x100)

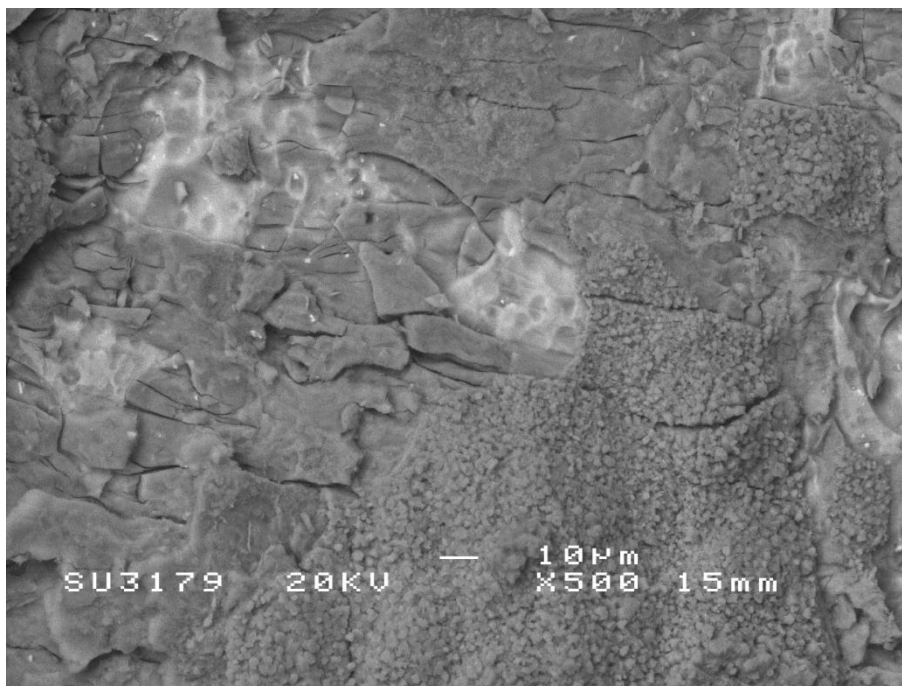


Figure A. 14 SEM BEI of the surface of aluminium encapsulated in CAP 1 for 90 days (x500)

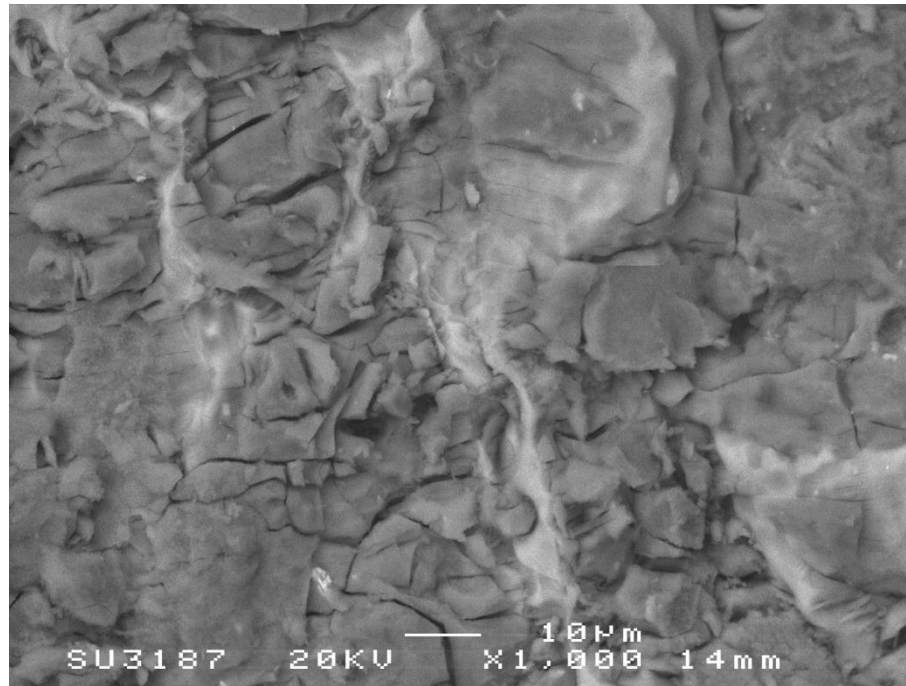


Figure A. 15 SEM BEI of the surface of aluminium encapsulated in CAP 1 for 90 days (x1000)

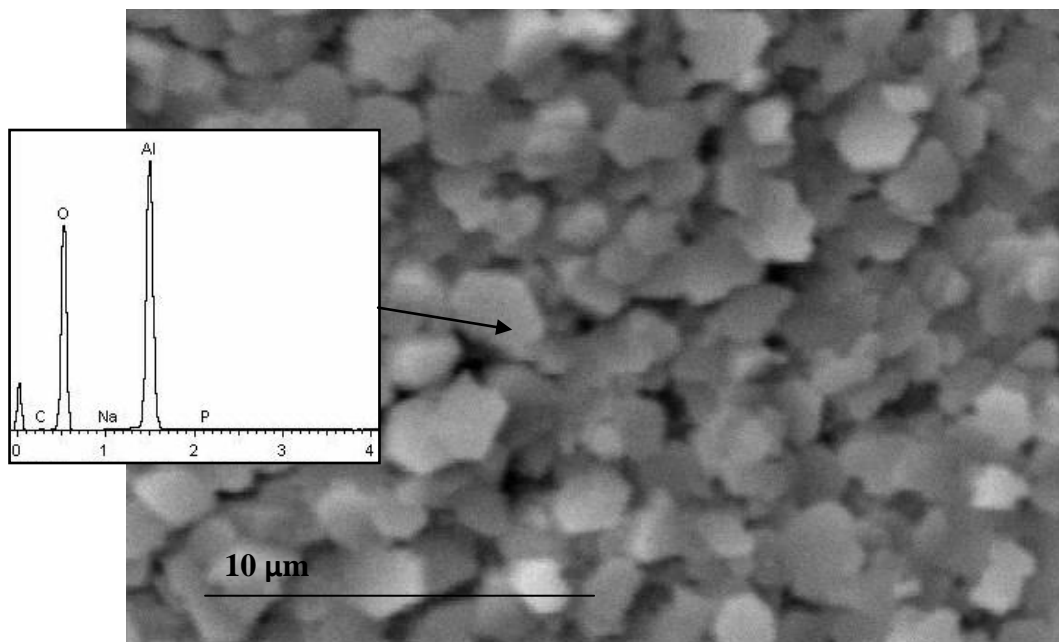


Figure A. 16 SEM BEI and EDX point spectra of the surface of aluminium encapsulated in CAP 1 for 90 days (x5000)

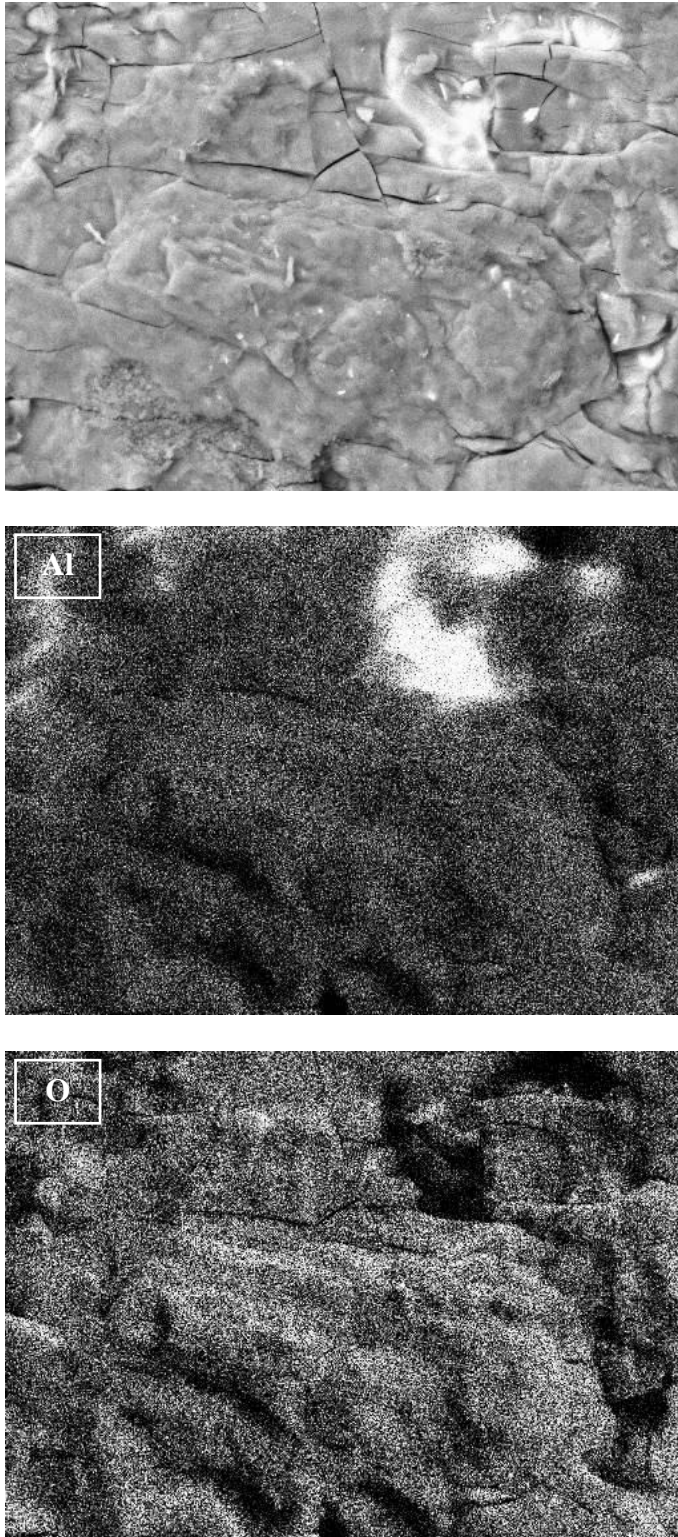


Figure A. 17 EDX elemental mapping of surface of aluminium encapsulated in CAP 1 for 90 days (x1000)

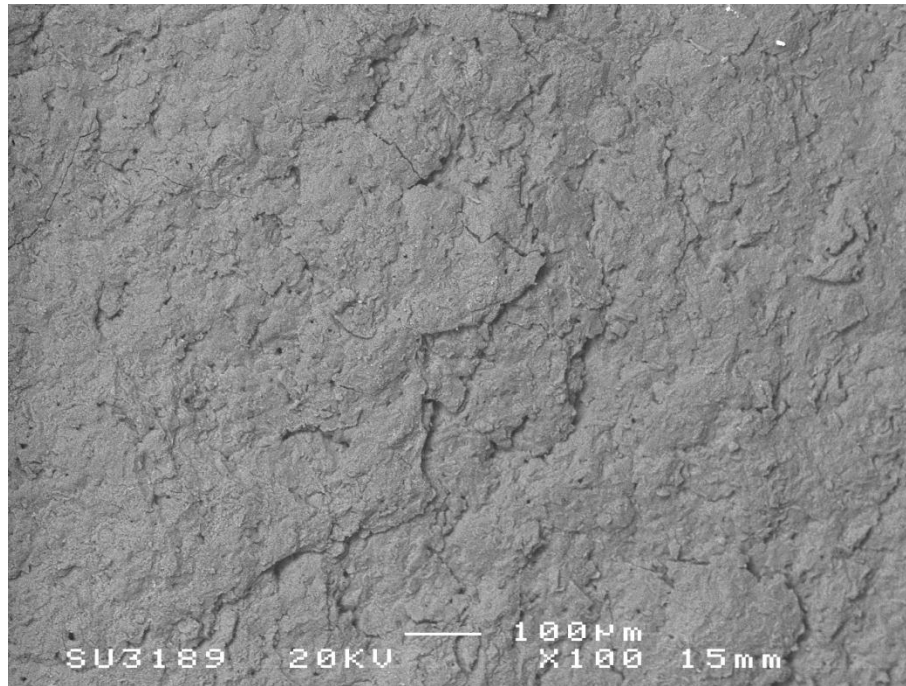


Figure A. 18 SEM BEI of the surface of aluminium encapsulated in CAP 1 for 180 days (x100)

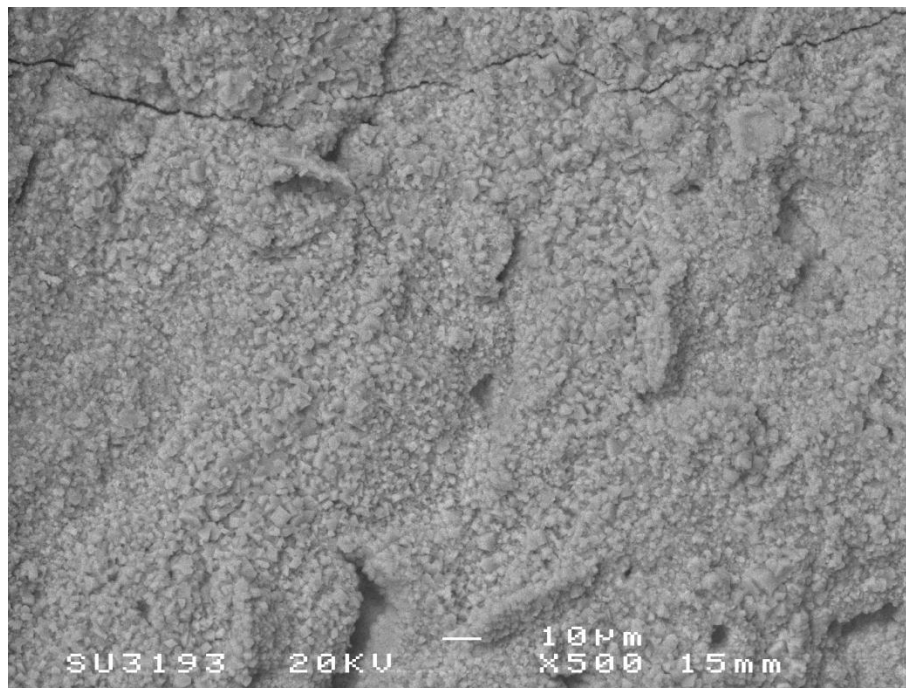


Figure A. 19 SEM BEI of the surface of aluminium encapsulated in CAP 1 for 180 days (x500)

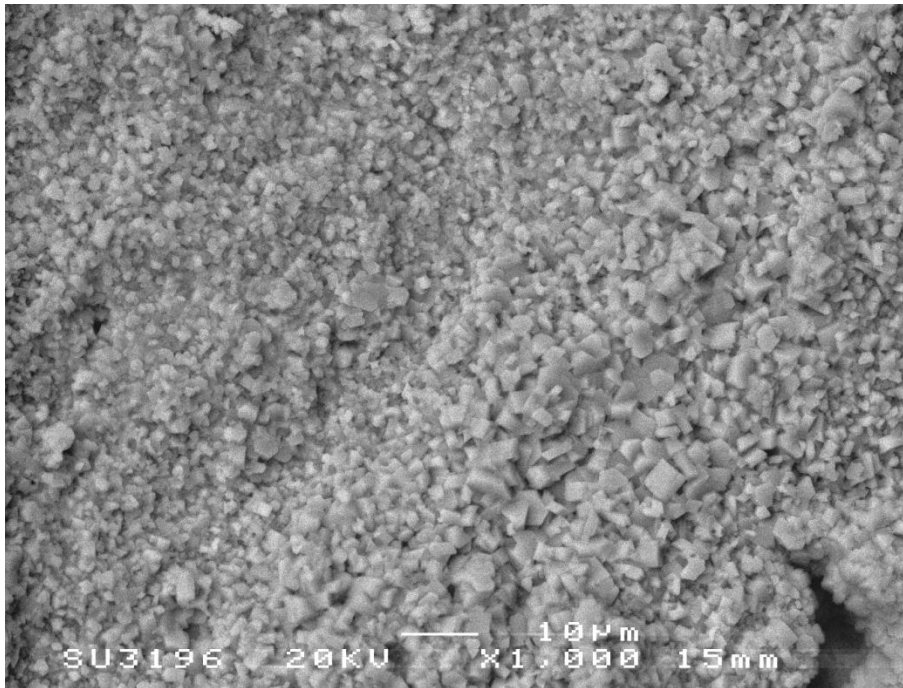


Figure A. 20 SEM BEI of the surface of aluminium encapsulated in CAP 1 for 180 days (x1000)

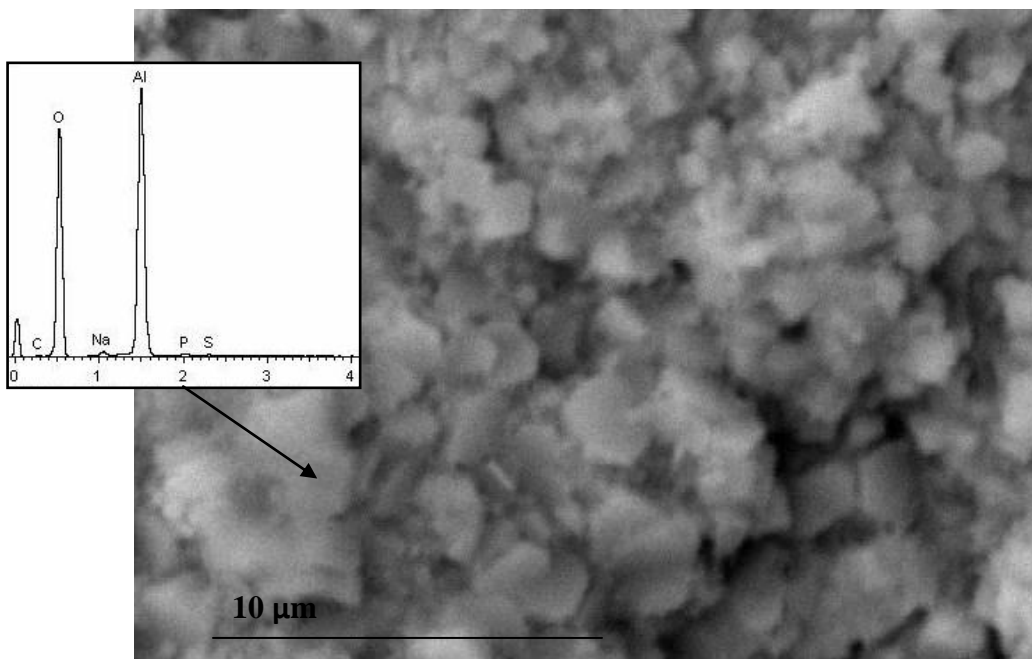


Figure A. 21 SEM BEI and EDX point spectra of the surface of aluminium encapsulated in CAP 1 for 180 days (x5000)

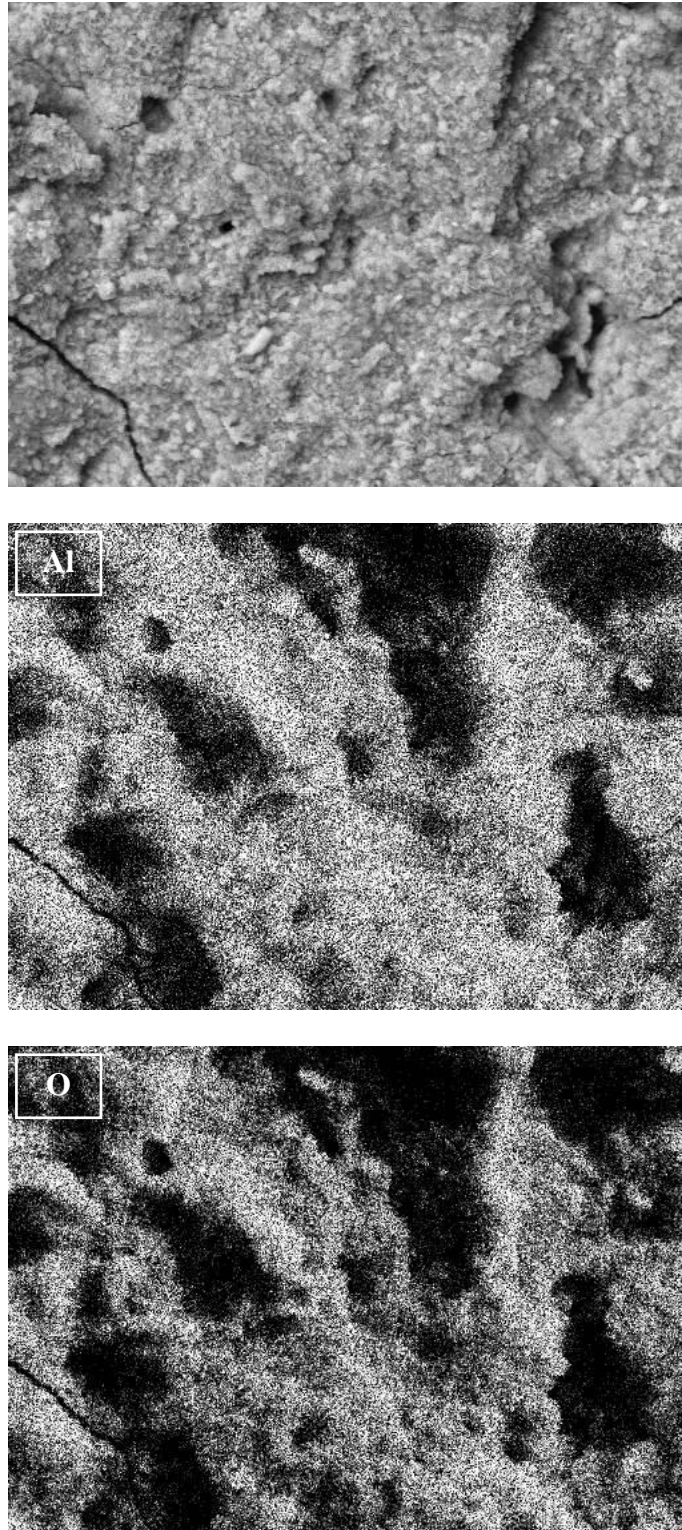


Figure A. 22 EDX elemental mapping of surface of aluminium encapsulated in CAP 1 for 180 days (x1000)

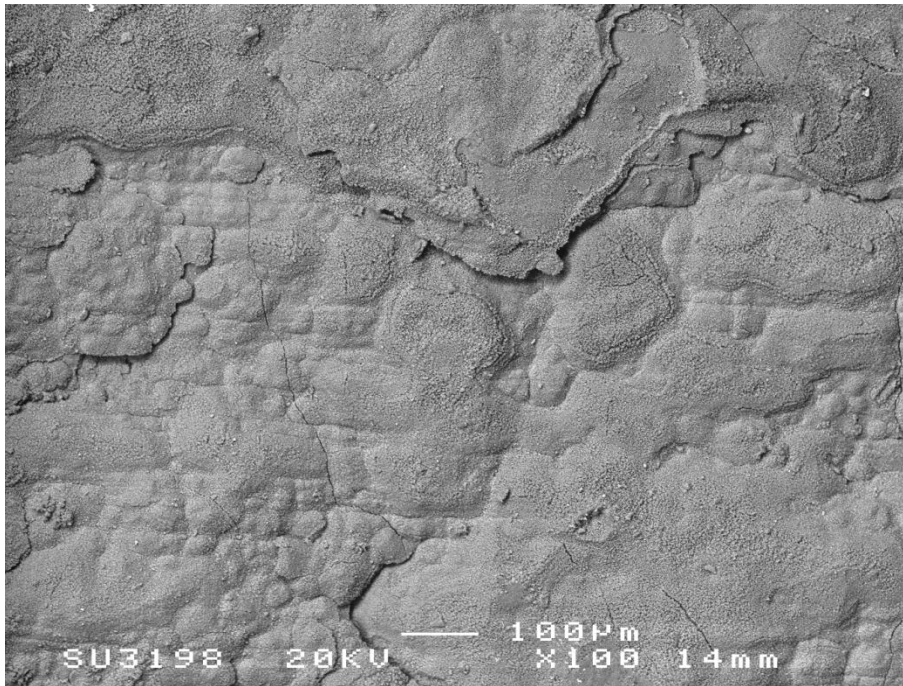


Figure A. 23 SEM BEI of the surface of aluminium encapsulated in CAP 1 for 360 days (x100)



Figure A. 24 SEM BEI of the surface of aluminium encapsulated in CAP 1 for 360 days (x500)

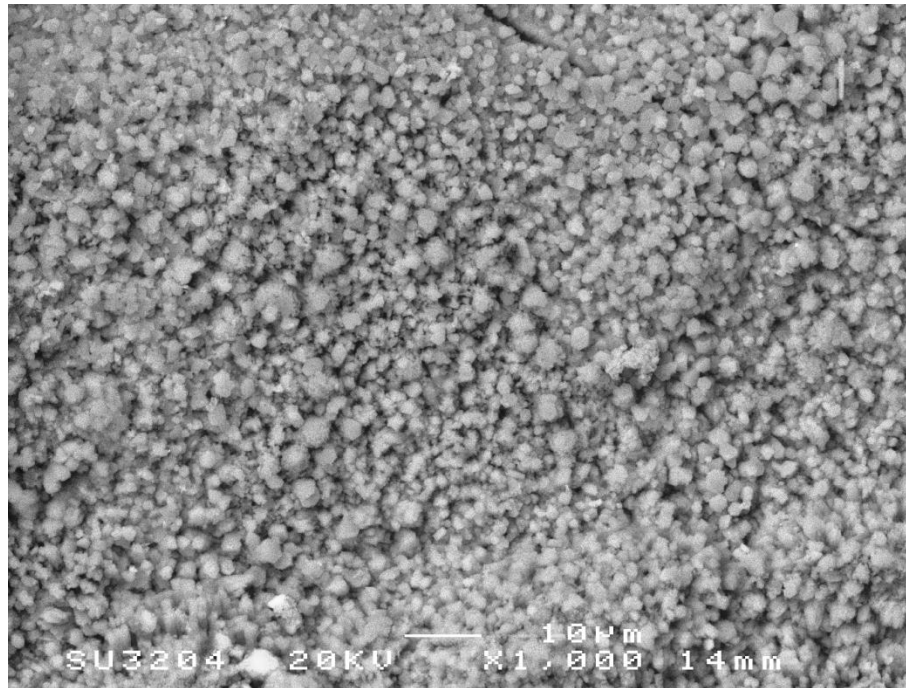


Figure A. 25 SEM BEI of the surface of aluminium encapsulated in CAP 1 for 360 days (x1000)

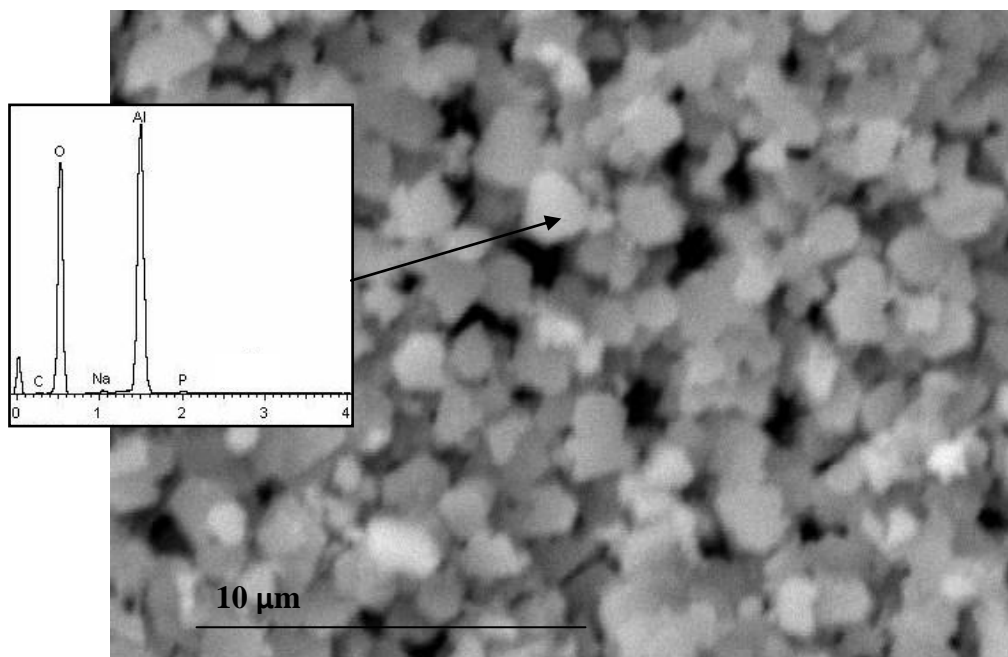


Figure A. 26 SEM BEI and EDX point spectra of the surface of aluminium encapsulated in CAP 1 for 360 days (x5000)

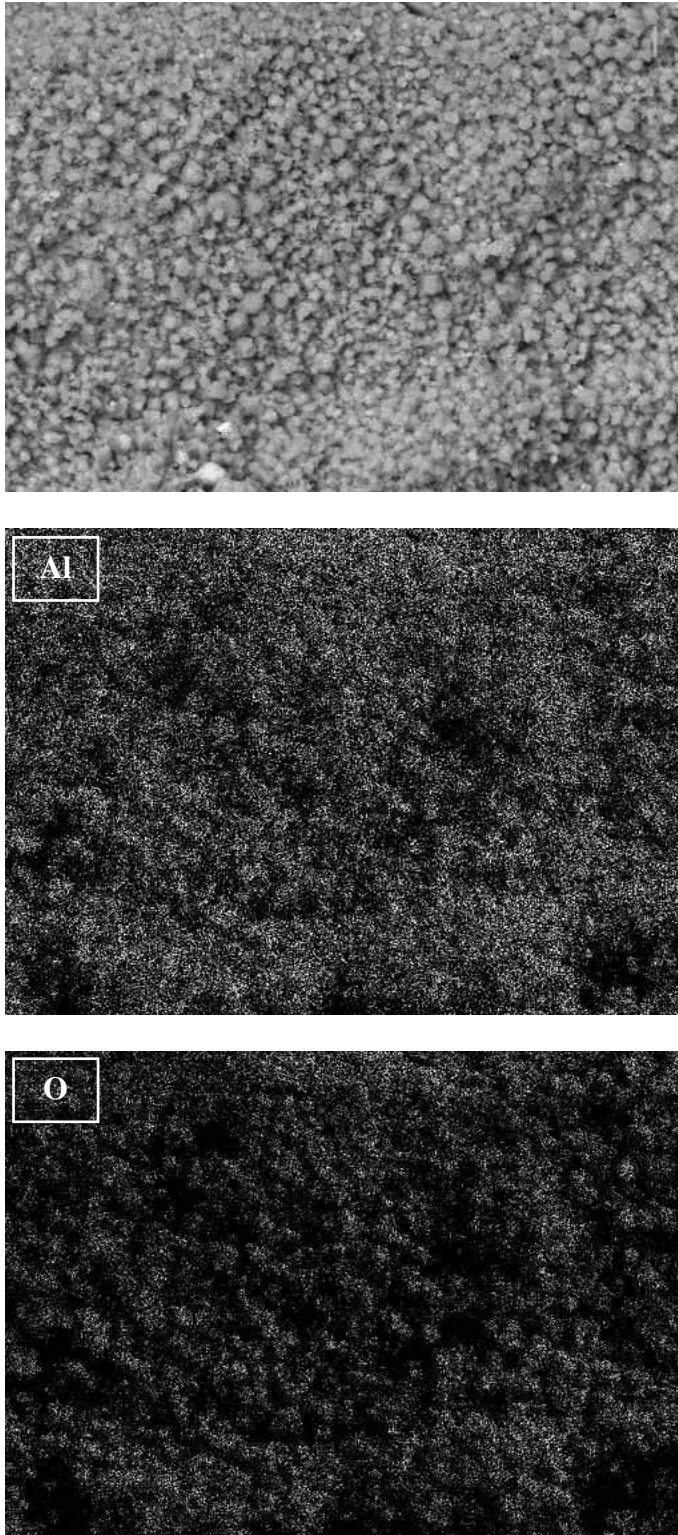


Figure A. 27 EDX elemental mapping of surface of aluminium encapsulated in CAP 1 for 360 days (x1000)

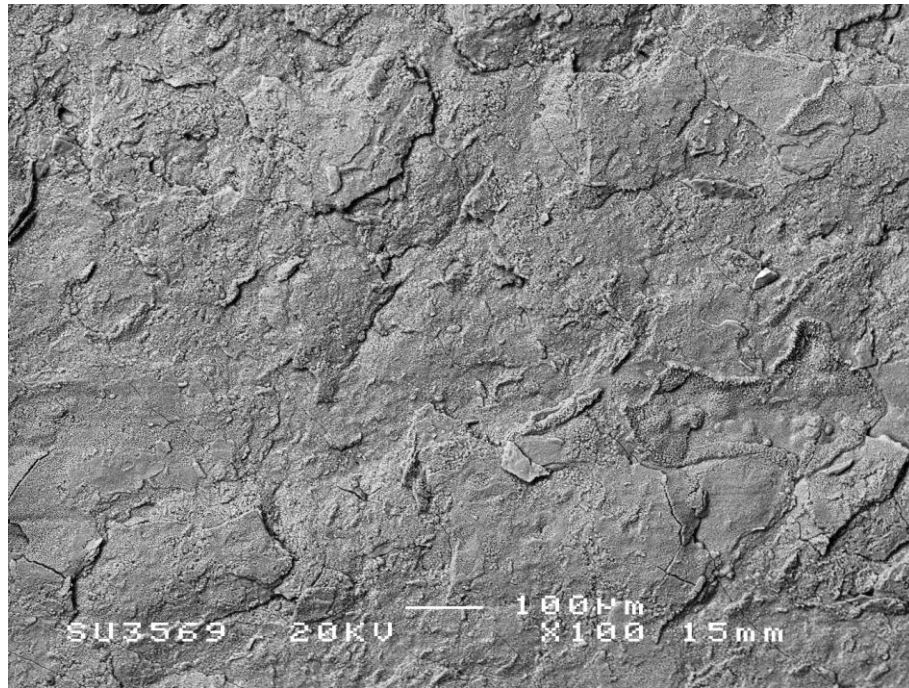


Figure A. 28 SEM BEI of the surface of aluminium encapsulated in CAP 2 for 90 days (x100)

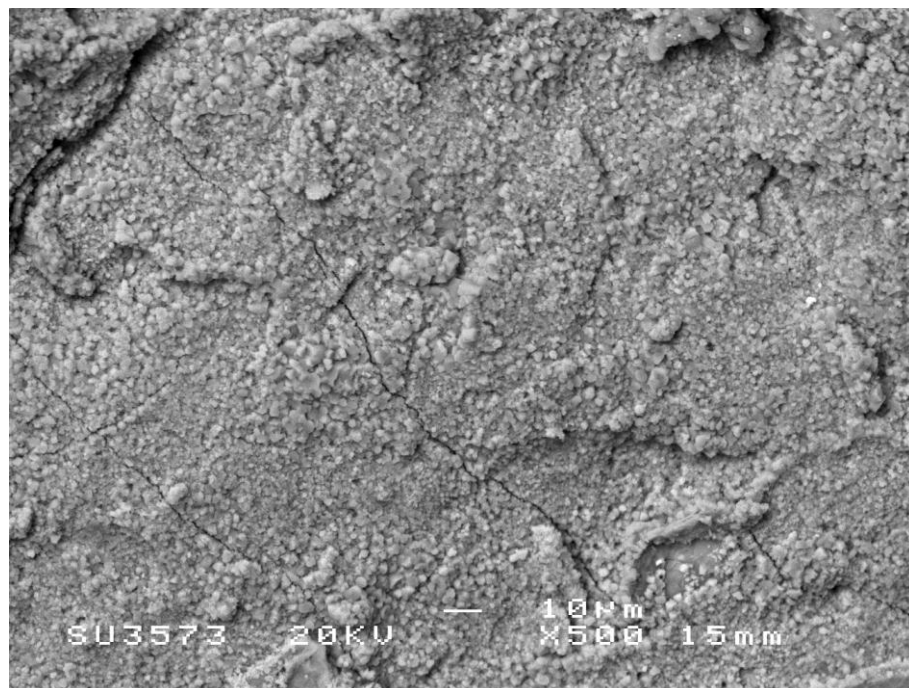


Figure A. 29 SEM BEI of the surface of aluminium encapsulated in CAP 2 for 90 days (x500)

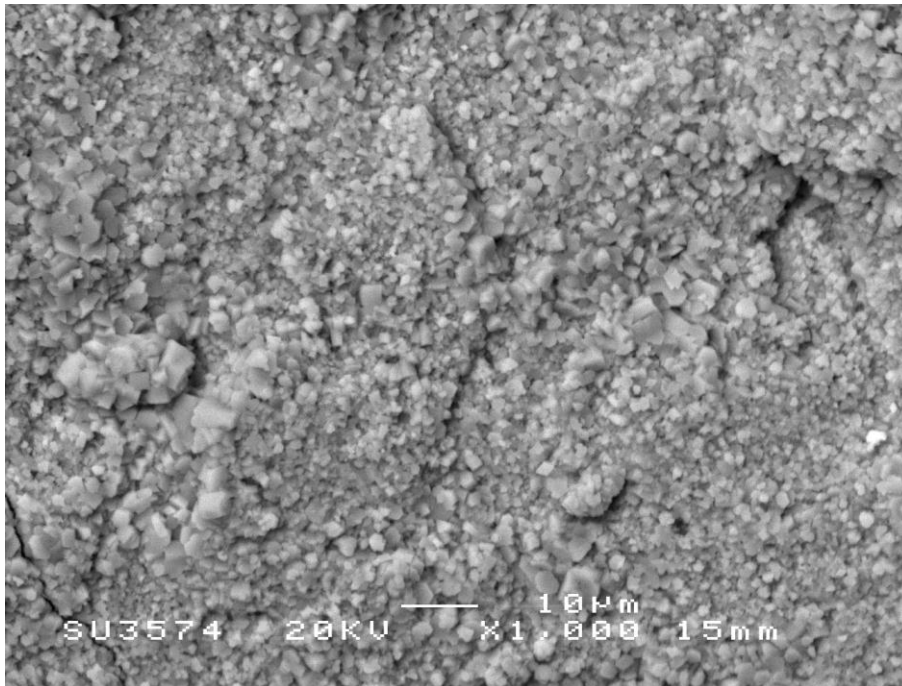


Figure A. 30 SEM BEI of the surface of aluminium encapsulated in CAP 2 for 90 days (x1000)

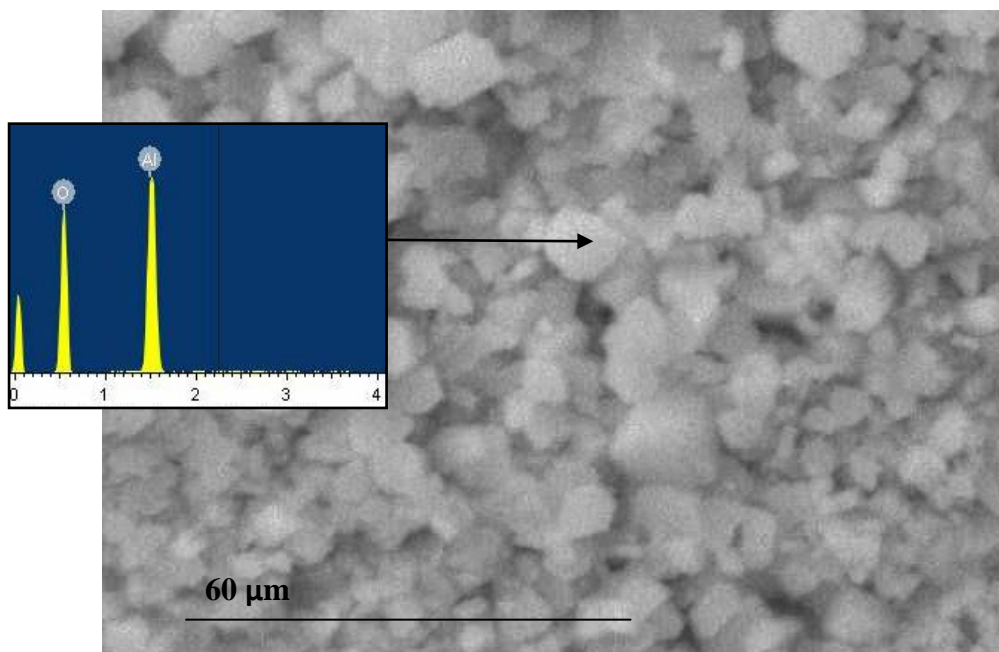


Figure A. 31 SEM BEI and EDX point spectra of the surface of aluminium encapsulated in CAP 2 for 90 days (x2500)

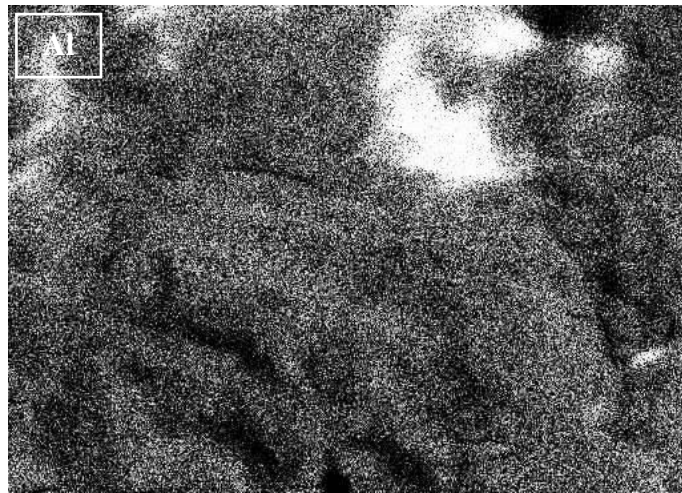


Figure A. 32 EDX elemental mapping of surface of aluminium encapsulated in CAP 2 for 90 days (x1000)

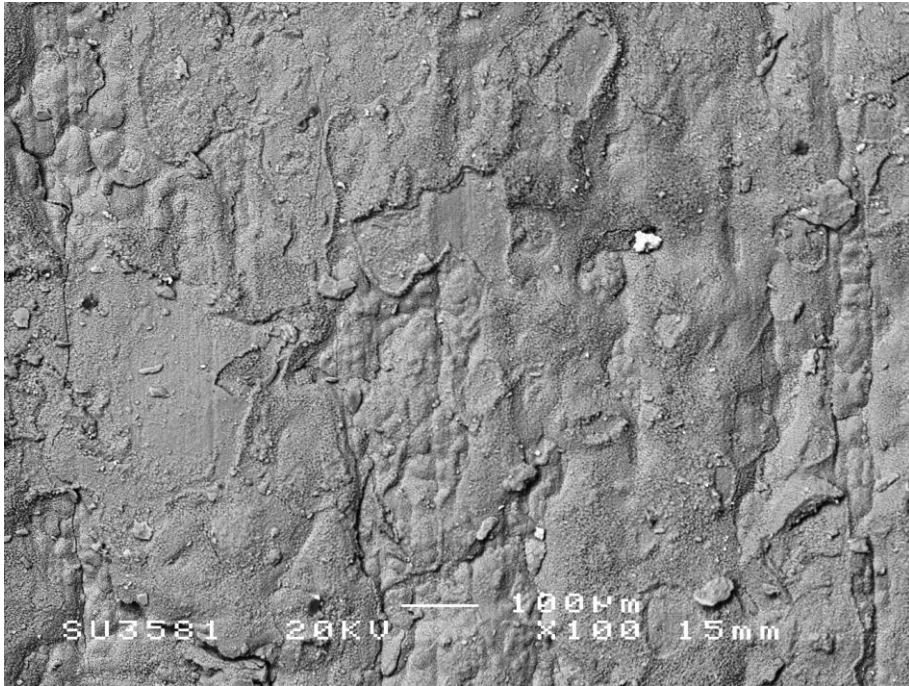


Figure A. 33 SEM BEI of the surface of aluminium encapsulated in CAP 2 for 180 days (x100)

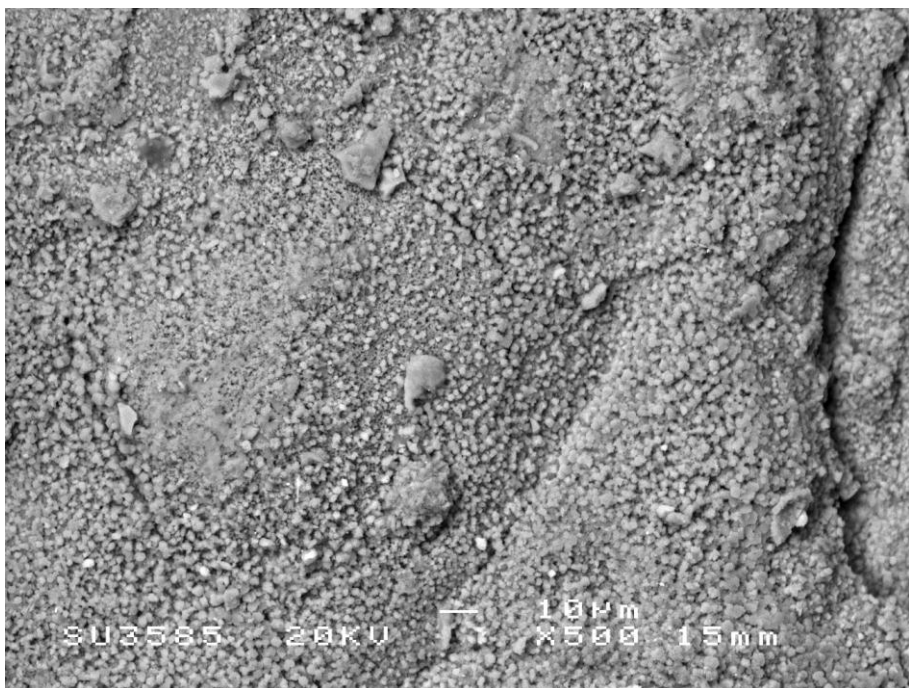


Figure A. 34 SEM BEI of the surface of aluminium encapsulated in CAP 2 for 180 days (x500)



Figure A. 35 SEM BEI of the surface of aluminium encapsulated in CAP 2 for 180 days (x1000)

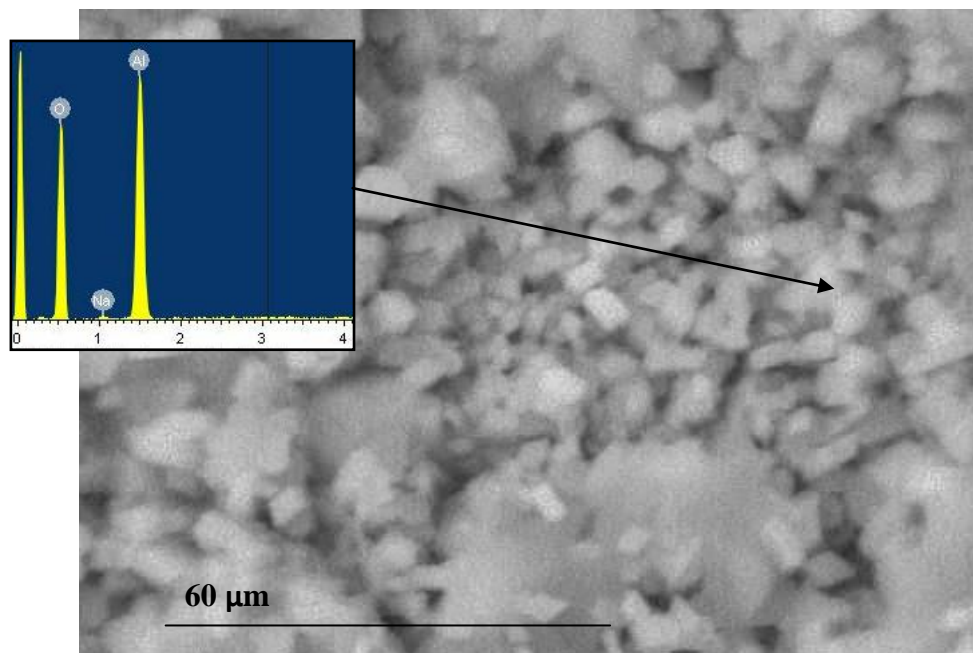


Figure A. 36 SEM BEI and EDX point spectra of the surface of aluminium encapsulated in CAP 2 for 180 days (x2500)

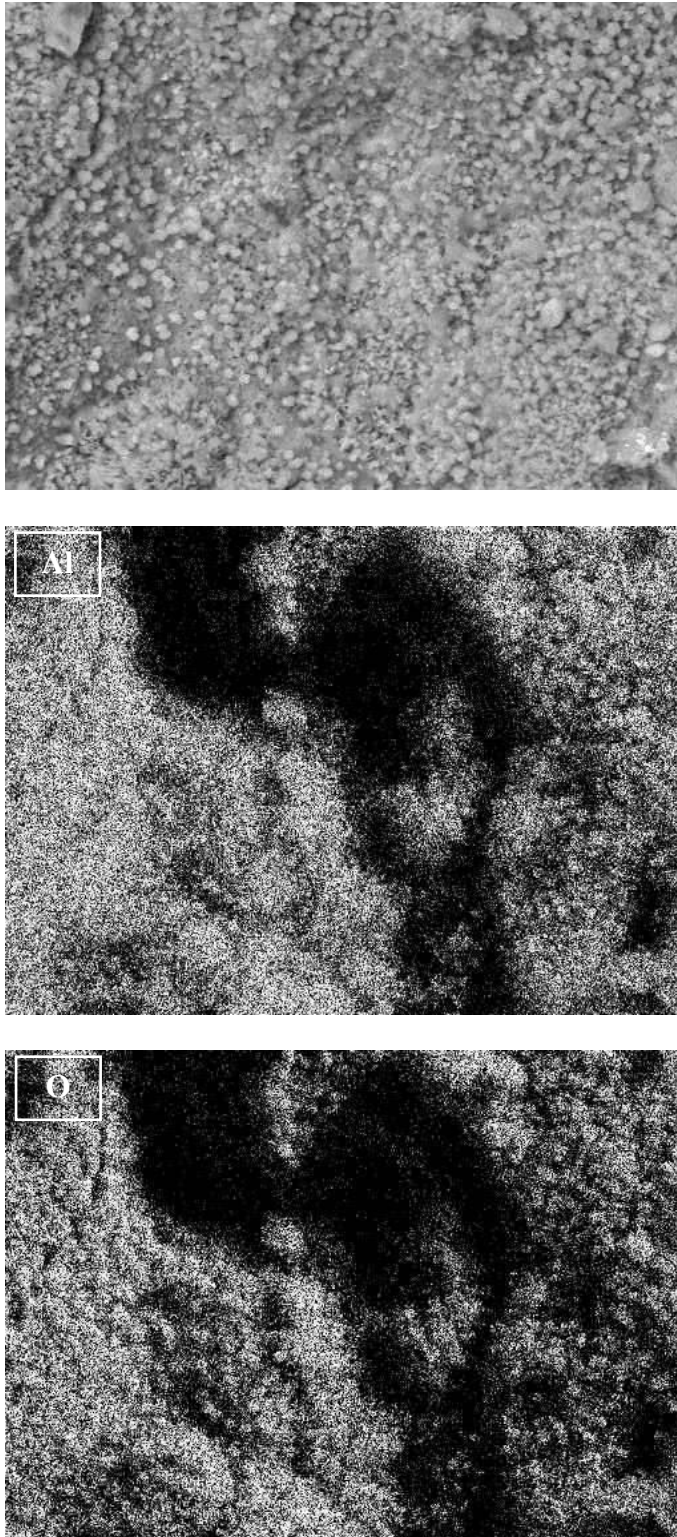


Figure A. 37 EDX elemental mapping of surface of aluminium encapsulated in CAP 2 for 180 days (x1000)

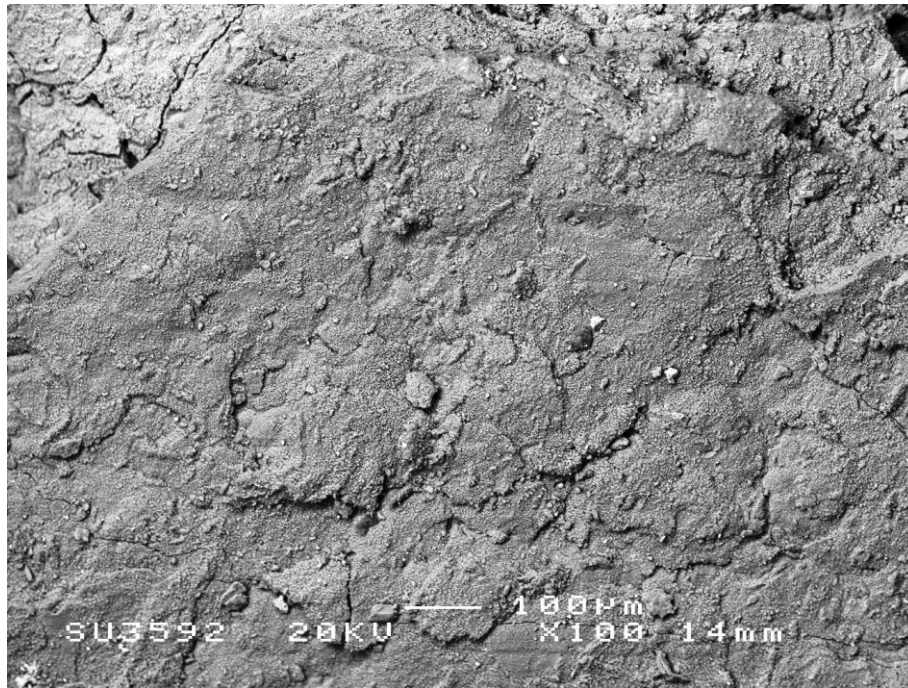


Figure A. 38 SEM BEI of the surface of aluminium encapsulated in CAP 2 for 360 days (x100)

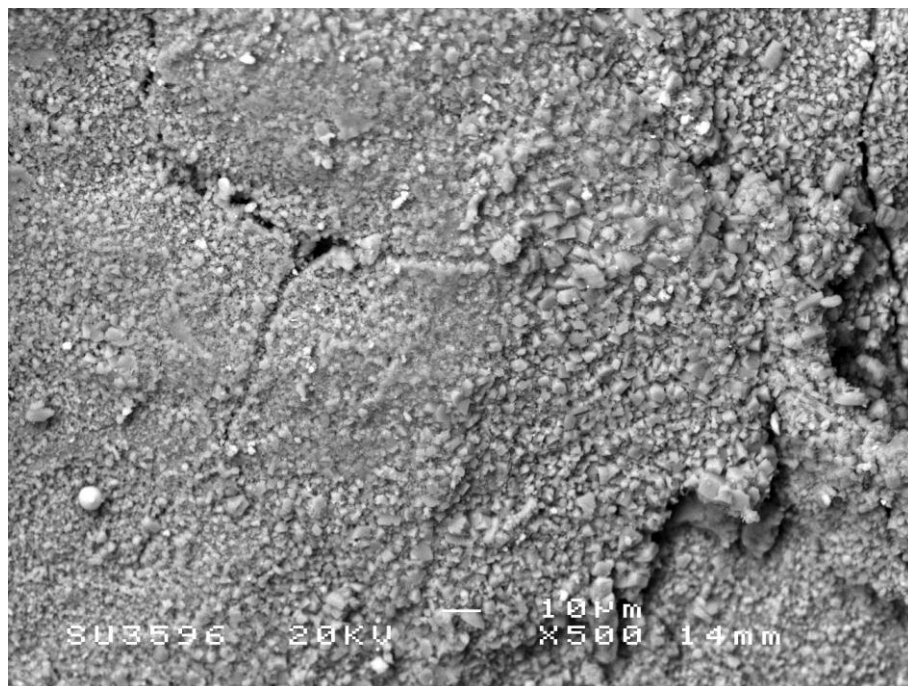


Figure A. 39 SEM BEI of the surface of aluminium encapsulated in CAP 2 for 360 days (x500)

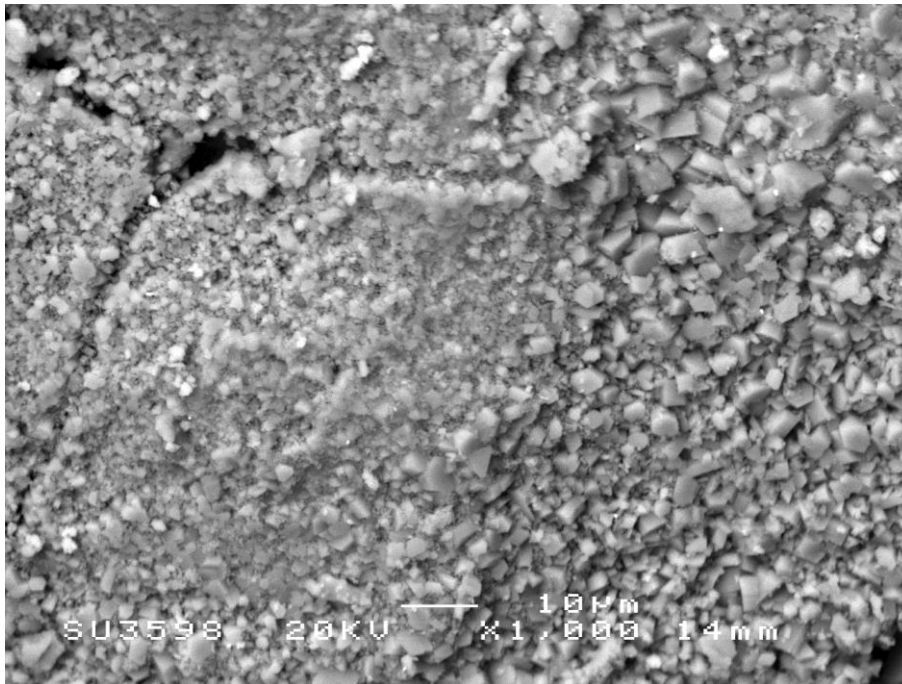


Figure A. 40 SEM BEI of the surface of aluminium encapsulated in CAP 2 for 360 days (x1000)

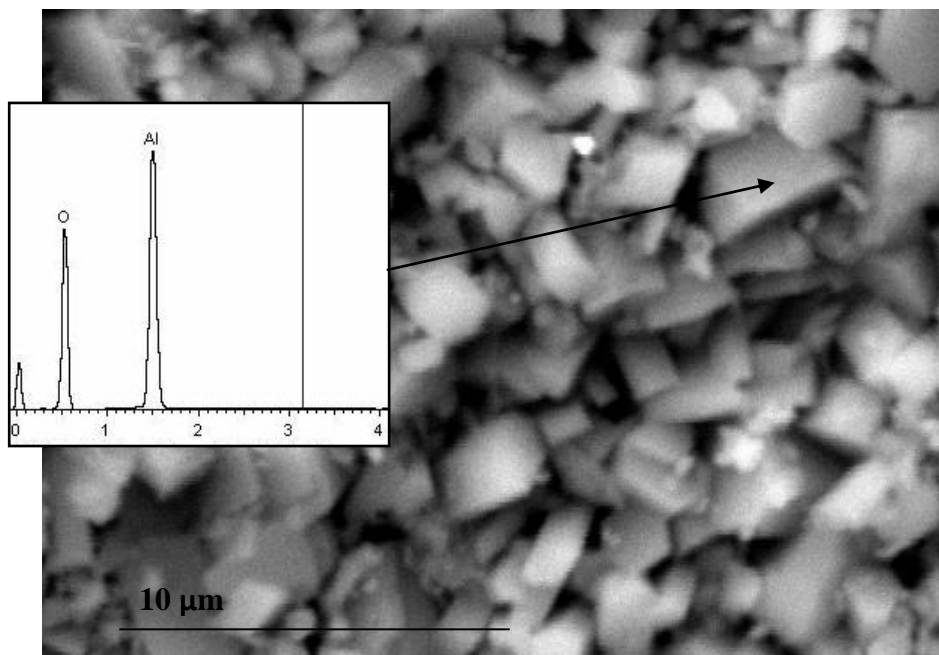


Figure A. 41 SEM BEI and EDX point spectra of the surface of aluminium encapsulated in CAP 2 for 360 days (x5000)

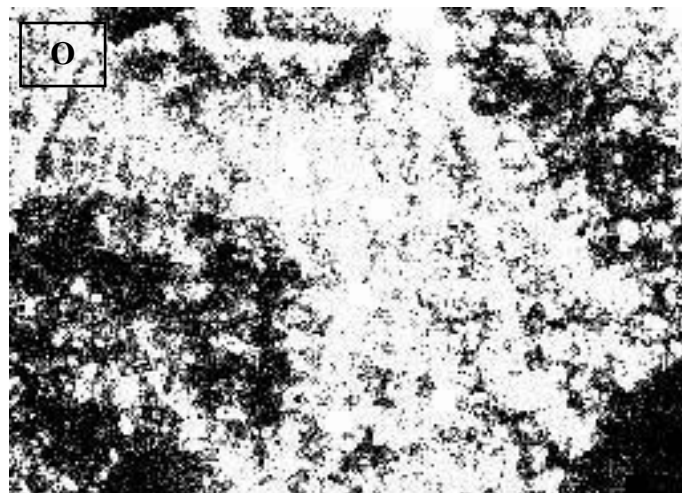
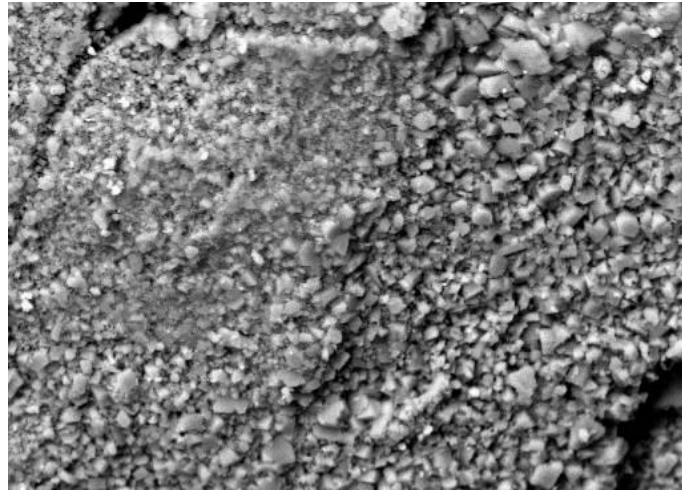


Figure A. 42 EDX elemental mapping of surface of aluminium encapsulated in CAP 2 for 360 days (x1000)

Appendix 4 – Relevant Publications

Journal Papers

Swift, P., Kinoshita, H., Collier, N. C., Utton, C. A., *Phosphate modified calcium aluminate cement for radioactive waste encapsulation*. Advances in Applied Ceramics, Vol. 112 (1), p. 1-8, 2013

Kinoshita, H., Swift, P., Utton, C. A., Carro-Mateo, B., Marchand, G., Collier, N. C., Milestone, N. B., *Corrosion of aluminium metal in PC- and CAC-based cement matrices*, Cement and Concrete Research, Vol. 50 (0), p. 11-18, 2013

Book Chapters

Swift, P., Kinoshita, H., Collier, N. C., *The Effect of Supplementary Pulverised Fuel Ash on Calcium Aluminate Phosphate Cement for Intermediate-Level Waste Encapsulation*, in Cement-Based Materials for Nuclear Waste Storage, Chapter 19, pp. 215-224, 2013

Conference Proceedings

Swift, P., Kinoshita, H., Collier, N., *Phosphate-Modified Calcium Aluminate Cement for Radioactive Waste Encapsulation*, Cement and Concrete Science Conference, 13th-15th September 2010, University of Birmingham, Birmingham, UK

Swift, P., Kinoshita, H., Collier, N. C., *The effect of supplementary pulverised fuel ash on calcium aluminate phosphate cement for intermediate-level waste encapsulation*, NUWCEM – 1st International Symposium on Cement-based Materials for Nuclear Wastes, 11th-13th October 2011, Avignon, France

Swift, P., Kinoshita, H., Collier, N. C., *The Development and Application of Calcium Aluminate Phosphate Cement for the Encapsulation of Low- and Intermediate-Level Radioactive Waste in the UK*, GLOBAL2011, 11th-16th December 2011, Chiba, Japan